CONSTITUTIVE MODELING OF JOINING MATERIALS IN ELECTRONIC PACKAGING

by

Manu Dube

A Dissertation Submitted to the Faculty of the

DEPARTMENT OF CIVIL ENGINEERING AND ENGINEERING MECHANICS

In Partial Fulfillment of the Requirements
For the Degree of

DOCTOR OF PHILOSOPHY
WITH A MAJOR IN ENGINEERING MECHANICS

In the Graduate College

THE UNIVERSITY OF ARIZONA

2004

INFORMATION TO USERS

The quality of this reproduction is dependent upon the quality of the copy submitted. Broken or indistinct print, colored or poor quality illustrations and photographs, print bleed-through, substandard margins, and improper alignment can adversely affect reproduction.

In the unlikely event that the author did not send a complete manuscript and there are missing pages, these will be noted. Also, if unauthorized copyright material had to be removed, a note will indicate the deletion.

ProQuest Information and Learning Company
300 North Zeeb Road
P.O. Box 1346
Ann Arbor, MI 48106-1346

THE UNIVERSITY OF ARIZONA ®
GRADUATE COLLEGE

As members of the Final Examination Committee, we certify that we have read the dissertation prepared by MANU DUBE

entitled CONSTITUTIVE MODELING OF JOINING MATERIALS IN ELECTRONICS PACKAGING

and recommend that it be accepted as fulfilling the dissertation requirement for the Degree of Doctor of Philosophy

Tribikram Kundu	01/20/04 Date
Dinshaw Contractor	10/3/03 Date
Georgel Frantziskonis	5/29/03 Date
	Date
	Date

Final approval and acceptance of this dissertation is contingent upon the candidate's submission of the final copy of the dissertation to the Graduate College.

I hereby certify that I have read this dissertation prepared under my direction and recommend that it be accepted as fulfilling the dissertation requirement.

Dissertation Director Tribikram Kundu	01/20/04 Date

STATEMENT BY AUTHOR

This dissertation has been submitted in partial fulfillment of requirements for an advanced degree at The University of Arizona and is deposited in the University Library to be made available to borrowers under rules of the Library.

Brief quotations from this dissertation are allowable without special permission, provided that accurate acknowledgment of source is made. Requests for permission for extended quotation from or reproduction of this manuscript in whole or in part may be granted by the copyright holder.

SIGNED: _____

ACKNOWLEDGEMENTS

My deepest gratitude goes to my advisor, Prof. T. Kundu, for his crucial help in making this dissertation possible. I have been privileged to have him as my advisor. I have also been fortunate to have an esteemed committee. Major committee members, Prof. D. N. Contractor and Prof. G. N. Frantziskonis provided their valuable time and help for the dissertation. The expertise of the minor committee members, Prof. K.A. Jackson, Prof. J.L. Prince and Prof. H.G. Parks, is greatly appreciated.

Dean D. Horgan and Prof. J.B. Valdes, Dept. Head, offered much encouragement and assistance as I worked through the dissertation process, as did Dean T.W. Peterson, for which I will be forever grateful.

Mr. G.A. Townsend, Mr. J. Wiggins and Mr. S. Albanese in the Department of Civil Engineering and Engineering Mechanics were a great asset during my stay at Arizona, as were Ms. O. Hanson Ms. A. Stilwell, Ms. B. Graham and Ms. J. Gibson of the Department Office.

The support and friendship of my colleagues, Dr. H. Li, Dr. Z. Wang, Dr. C. Shao and Mr. A. Khajeh, and the companionship of Mr. D. Cohen, Dr. S. Pradhan, Dr. M. Nickerson and Mr. Whitenack will be cherished. The help and advice of Dr. T.J. Dishongh was instrumental in my enrolling at the University of Arizona. Mr. S. Ottesen of ExxonMobil provided kind and straightforward advice on details pertaining to my Curricular Practical Training at the University.

This dissertation differs, in both its philosophy and content, from the original dissertation plan intended for me when I came to the University of Arizona. Nevertheless the contribution of Prof. C. Desai in terms of time and resources towards the prior dissertation plan must be acknowledged.

Many thanks are due to Dr. D.L. Dahl and Dr. D.K. Link for their generous and invaluable advice. In the end, the incredible support of Sema and the unconditional love of our families, Prof. G.P. Dube, Mrs. R. Dube, Mr. A.I. Cakici, Mrs. M. Cakici, Mr. D. H. Ilgun, Prof. J.P. Dube, Mrs. M. Dube, Shalu, Amit, Apurv, Murat and Onder have meant everything.

To

Sema and our parents

TABLE OF CONTENTS

TABLE OF CONTENTS - *Continued*

TABLE OF CONTENTS - *Continued*

TABLE OF CONTENTS - *Continued*

LIST OF FIGURES

LIST OF FIGURES - *Continued*

LIST OF TABLES

ABSTRACT

Modeling simplifications for complex material behavior may lead to unanticipated errors under generalized loading conditions, which are difficult to detect in finite element analyses. This work analyzes existing models under simple loading conditions where the nature of the results is known a priori, and proposes new models to overcome the limitations detected. Elastic and elastoplastic formulations for loading-dependent material parameters are generalized, and limitations of the rate-dependent elastoplastic simulation and the Perzyna viscoplastic formulation are discussed. A yield function that provides continuous yielding irrespective of the direction of loading and does not generate spurious plastic strain increments under temperature change is developed. A thermomechanical model based on the concept of superposition of asymptotic phases is also proposed, with generalized stress-strain-temperature relationships that intrinsically predict the variation of the coefficient of thermal expansion and elastic constants with temperature, and is validated for aluminum, lead, tin and solder. A plastic yield criterion shown to be in general agreement with hardening based on dislocation density and a preliminary empirical creep equation for lead-tin eutectic solder are developed as part of the thermomechanical model. Finally an approximate dissipated-work based formulation for the Disturbed State Concept of Desai (2001) is developed and limitations of DSC assumptions are discussed. Validations are conducted for the eutectic lead-tin data of Wang et al. (2001), with prior parameters being shown to require recomputation.

1. INTRODUCTION

Unanticipated failure of electronics systems may lead to severe consequences in defense, aerospace, medical and financial applications. Existing techniques for in-situ anticipation of imminent failure may be unreliable (Pecht et al., 2001), or may require additional instrumentation and interruption of operation (Constable and Lizzul, 1995; Dascher, 1996). Use of redundant systems increases the cost, while still being suspect to common-mode failures. It is crucial that reliability requirements under the expected operating conditions be incorporated within the design phase of a system.

The fast expanding range of application environments, use of innovative materials and processes, and lack of sufficient feedback from field failure data[1] have implied that available design standards may not always be sufficient or cost-effective for ensuring reliability. Increased reliance on off-the-shelf commercial components for military use, due to cost and availability concerns, has also led to the need for effective qualification procedures. Shortened design cycles have led to increased reliance on accelerated laboratory testing for field reliability predictions, both for design and for qualification.

[1] The difficulty in detecting and isolating faults, especially related to transient failures, in complex systems along with the high cost of post-failure analysis implies that up to 85% of field failures may not be traced back to their root cause (Williams et al., 1998; Dube, 1998).

1.1 Background

Identification and modeling of the fundamental, dominant failure mechanisms is an essential component towards design of reliable systems, aided by rational design and interpretation of accelerated tests (Tribula et al., 1989). It would also facilitate qualification of existing systems for enhanced operating envelopes and implementation of cost-effective potential techniques for in-situ prediction of imminent failure (Kelkar et al., 1996; Natishan and Dube, 1997).

Pecht and Ramappan (1992) report that enhancement in inherent component reliability may lead to system-level failures being the predominant cause of field failures. Miniaturization due to surface mount technology has enabled improved performance at reduced cost, size and weight. Solder joints have provided the chip-component and component-board connections in surface mount technology due to their electrical conductivity, ease of manufacture as well as relative compliance (Harper, 2000). However, reliability of the increasingly smaller joints has been of concern under low-cycle thermomechanical fatigue at least as early as Wild (1975). Vibration-related high-cycle damage may also be significant due to the typically high frequency of such loads (Barker et al., 1990). Ensuring solder joint reliability is a key concern in electronics packaging, reinforcing the need for accurate solder modeling.

1.1.1 Solder Modeling

Solder degradation depends on creep-fatigue interactions (Stone, 1990; Attarwala et al., 1992) governed by the size (Stone, 1990) and the strain-time-temperature history of the material (Dasgupta et al., 1992). This includes the processing history which determines the initial microstructure (Mei and Morris, 1992; Conrad et al., 1999), residual strains, defects, pad metallurgy (Lau and Pao, 1997), intermetallics (Chan et al., 1997; Choi et al., 1999) and other trace or dissolved elements (Ross, 1991; Vaynman et al., 1998). It also depends on the atmospheric composition (Konetzki et al., 1990; Frear et al., 1994).

Fatigue predictions typically suffer from inherent scatter in experimental data. Studies may also be difficult to compare due to the definition of failure used (Wilcox et al., 1990). For electrical systems, mechanical degradation of solder must be correlated with failure defined in an electrical sense. This may be system, or even application, specific.

A system may be exposed to a wide range of environmental conditions as part of its service cycle, or may need to be designed for several operating conditions for various applications and the joint response relevant to each need to be modeled. Generalized models for solder degradation typically correlate degradation to internal quantities such as plastic strain or dissipated work (Lee et al., 2000). This requires accurate constitutive models valid under general loads and temperature histories.

Classical mechanics and thermodynamics provide only general limits on the range of possible material behaviors, while direct application of quantum mechanics to macroscopic bodies with an astronomical number of particles may be difficult. Development of constitutive equations for engineering materials has mainly been an empirical effort, and is challenging for solders due to the high homologous temperature under typical operating conditions.

Solder deformation includes a combination of elastic, plastic, creep and viscoelastic modes[2]. The as-cast joint microstructure is unstable, and shows recrystallization (Mei et al., 1991) and coarsening (Hacke et al., 1997, 1998; Vianco et al., 1999) under typical joint operating conditions. Results of Igoshev and Kleiman (2000) for silver-tin solder also indicate that it may be essential to incorporate the effects of microcracks and micropores formed during creep, to properly model solder constitutive behavior. Bulk behavior may not adequately represent the behavior of thin joints (Bonda and Noyan, 1996) and bonded joints may be subjected to both shear and normal stresses during nominal shear cycling, involving different modes of crack propagation (Yamada, 1992).

Purely empirical material-specific equations require substantial time and effort for validation, and are difficult to generalize. The complexity of the problem necessitates

[2] For instance, see Rafanelli (1992) for plastic, Tribula and Morris (1991), Mei et al. (1991), Guo et al. (1992), Hare and Stang (1995) for creep and Tien et al. (1991) for viscoelastic behavior

significant modeling simplifications. Even basic parameters such as the elastic modulus may need to be interpreted with care, depending on the particular simplification used. For instance elastoplastic formulations require rate-dependent elastic parameters for simulating time-dependent behavior, unlike viscoplastic models which are inherently capable of modeling time-dependent response.

Models developed based on simple test configurations and restricted load paths, under test conditions that lead to accelerated failures, must be validated for real joints under field conditions. Results from numerical solutions such as Finite Elements (FE) are complex enough that gross errors in commercial FE software may remain undetected (Anderson et al., 2000). Even the small size of electronics structures may introduce errors in FE simulations conducted using commercial code (Dube and Sahay, 1996).

1.1.2 The State of the Art

A variety of models have been proposed in literature for solder modeling and fatigue predictions (Lee et al., 2000; Desai and Whitenack, 2001). Ju et al. (1996) and Qian et al. (1999) have provided the advantages of the continuum damage approach in that unlike fracture mechanics, explicit modeling of the distribution and growth of microcracks, the behavior of individual cracks and the corresponding requirements of adaptive mesh refinements are not required.

The continuum approximation has been extremely useful in characterizing the constitutive behavior of materials. However as materials are loaded, various discontinuities arise, resulting in deviation from the assumed continuum behavior. The nucleation and growth of such discontinuities has been treated in fields such as fracture mechanics. The potentially large number of microcracks and their random distribution suggests that it might be feasible to 'smear' the behavior of such discontinuities over a small region, thereby maintaining the continuum approximation.

Desai and Whitenack (2001) concluded that The Disturbed State Concept (DSC) developed by Desai (2001) provides a comprehensive model that improves upon the classical damage formulation of Kachanov (1958, 1986) and provides a unified and hierarchical scheme for modeling the constitutive response as well as damage growth. The DSC formulation assumes observed material response to be a weighted superposition of the responses of two hypothetical phases. The relative intact (RI) phase is the hypothetical state of the material free of all defects and can be modeled as elastic, elastoplastic, or elastoviscoplastic as required. The fully adjusted (FA) phase is the phase corresponding to the maximum feasible degradation under laboratory or field conditions. The relative proportion of the two phases is given by the disturbance function.

The DSC approach is extremely general, especially when used in conjunction with the Hierarchical Single Surface (HiSS-δ_0) yield function, applicable to a variety of materials including geotechnical, metals and ceramics (Desai, 2001). This is advantageous, as a

single package may be comprised of a large number of materials including several metals, semiconductor chips, as well as ceramics and plastics. Substantial research has been conducted on solder modeling based on the HiSS-δ_0 model in conjunction with DSC for both elastoviscoplastic modeling, as well as simplified rate-dependent elastoplastic modeling (Chia, 1994; Basaran, 1994; Dishongh, 1997; Wang, 2001).

1.2 Statement of Problem

All models for solder simulation are based on simplifications necessitated by expedience to some extent, and have corresponding limitations as to their validity. Determination of the limitations on the range of validity of models is essential, given the reliance on accelerated testing and the trend towards enhanced operating envelopes. This is especially important for solder as even the interpretation of basic parameters such as the elastic modulus may depend on the simplification employed. It also provides avenues for further development of more generalized models.

For the HiSS/ DSC scheme, the elastic incremental equations are shown to require generalization when the elastic parameters depend on temperature and strain-rate. Elastoplastic and elastoviscoplastic formulations are also modified by the generalization. For plastic deformations, the consistency condition and the convexity conditions used require generalization. The simplified elastoplastic formulation is shown to be restricted

in applicability. The Perzyna viscoplastic formulation used in prior literature is also shown to be appropriate only under restricted loading conditions.

Both the elastoplastic and Perzyna elastoviscoplastic simulations used in prior work require a yield function. The parameter determination procedure for the HiSS-δ_0 function is seen to require modification due to the presence of a nonzero initial plastic strain trajectory, ξ_0. A yield function is required to be developed for systematic resolution of additional issues related to the nonzero ξ_0, including spurious plastic strains under thermal loading and lack of continuous yield under tensile loads.

Prior solder parameters (Wang et al., 2001) and parameter determination procedures for the Perzyna viscoplastic formulation for the HiSS function (Chia, 1994) are shown to require modification for the requisite viscoplastic modeling. Corrections to parameters of Wang et al. (2001) are significant as prior parameters do not allow for viscoplastic simulation, which is more appropriate than the simplified elastoplastic scheme. Modifications may also be required in the sample preparation techniques of Wang et al. (2001) for consistency with industrial practices.

Desai (1998)[3] has suggested that it may be advantageous to express the disturbance function (D) for modeling material degradation in DSC, in terms of dissipated work

[3] Expressing the disturbance function in terms of dissipated work instead of the deviatoric plastic strain trajectory was investigated at the suggestion, and under the guidance, of Dr. C. S. Desai.

instead of plastic strain trajectory. Significant issues related to work balance are seen to arise due to the simplifying assumption of equality of strain in all phases.

For solder, measurement of elastic modulus from the stress-strain curve may be difficult due to test-machine compliance and significant creep strains at higher temperatures. Published values of elastic constants for solder vary widely in literature even at room temperature. If the formulations are complex enough, two different values of elastic modulus may be assumed and two distinct sets of plastic or viscoplastic parameters may be obtained, both sets providing reasonable backpredictions for tests.

Existing formulations for material modeling typically use purely empirical relationships for describing temperature dependence of parameters and do not provide insight into extrapolation of parameters to temperatures outside of the range of measurements. Further, parameters may also show anomalous behavior with temperature due to limitations of the simplifying assumptions used. Dependence of material parameters on loading conditions may be an indication that the material model is not complete. For instance, the elastoplastic scheme cannot provide time-dependent behavior inherently and requires strain-rate dependent parameters. Temperature-dependent parameters also imply that existing models may provide scope for generalization for predicting thermomechanical response in an integrated manner.

1.3 Research Objectives

The main objectives of the research are to

1. Generalize the elastoplastic formulations for the case of variable material parameters.
2. Develop a continuous-yield plasticity yield function with improved thermal response.
3. Develop integrated stress-strain-temperature relationships for modeling metals.
4. Validate the models developed based on the Pb/Sn test data of Wang et al. (2001).

Additionally, the research aims to develop a dissipated-work based DSC scheme[4], develop improved parameter determination schemes for HiSS-δ_0, correct and improve prior parameters for Pb/Sn test data in literature, investigate convexity criteria for yield functions and the definition of plastic strain trajectory, investigate potential improvements in sample making for test samples as well as investigate the use of Digital Image Correlation for visual monitoring of tests.

[4] Development of dissipated-work based DSC, imaging of the Pb/Sn testing for Wang et al. (2001) and improved sample making procedures for Ag/Sn testing was conducted under the guidance of Dr. C. S. Desai. Ag/Sn results are not reported here.

1.4 Outline of the Dissertation

Chapter 2 provides a brief overview of the existing literature on solder joint behavior and modeling techniques, including the DSC formulation.

Chapter 3 provides an analysis of the basic elastic, elastoplastic and viscoplastic formulations. The incremental stress-strain equations are generalized. The rate-dependent elastoplastic scheme is shown to be of limited utility and the Perzyna viscoplastic model is shown to be potentially limited under certain loading conditions. A dissipated-work based DSC scheme is developed.

Chapter 4 develops a plasticity yield function to avoid the potential problems with HiSS-δ_0. Improved procedures for determination of the hardening parameters for HiSS-δ_0 are also developed.

Chapter 5 presents the development of generalized stress-strain-temperature relationships for a thermomechanical model for metals.

Chapter 6 discusses test procedures and the Pb/Sn data of Wang et al. (2001). Validations are presented for the new theoretical concepts developed.

Chapter 7 summarizes the results of the work and presents the conclusions.

2. LITERATURE REVIEW

This chapter reviews suggested approaches for modeling eutectic lead-tin solder behavior in literature. A brief overview of the relation of solder microstructure to solder behavior is also included.

2.1 Constitutive Modeling

Constitutive modeling aims to predict material response to applied loads under some given thermal environment. This requires the constitutive equation for the material as well as values of the various material-specific parameters in the equation.

Classical mechanics and thermodynamics do not provide sufficient information to develop a constitutive equation fully, serving as very general limits on the range of possible material behaviors. Direct application of quantum mechanics to macroscopic systems with an astronomical number of particles may not be feasible. Development of constitutive equations for engineering materials has mainly been an empirical effort, with several simplifications relevant to the expected loading.

Solder joints typically experience thermomechanical loading cycles. In theory, the thermal and mechanical responses are linked (Nowacki, 1986), with deformations leading to temperature changes, and conversely. Temperature changes are interlinked with elastic equations through thermoelastic effects which have been studied at several levels (Kennedy, 1962; Swalin, 1972; Caglioti and Milone, 1981). Such effects may be ignored for solder, allowing for separation of the thermal and mechanical problems.

The total incremental strain in solder can be divided into elastic (e), plastic (p), anelastic (a), creep (c) parts and the thermal (T) part due to the coefficient of thermal expansion,

$$d\varepsilon = d\varepsilon^{e} + d\varepsilon^{p} + d\varepsilon^{a} + d\varepsilon^{c} + d\varepsilon^{T} \qquad \ldots(2.1)$$

Tien et al. (1991) have indicated the contributions of various components of deformation schematically for stress-controlled loading, as shown in Figure 2.1 (a) for a typical test cycle, where load drop to zero load leads to an immediate drop in elastic strain, followed by a time-dependent slow drop corresponding to anelastic strain. Rate-independent plastic behavior for solder was obtained by Rafanelli (1992), as shown in Figure 2.1 (b) based on dynamic test procedures. Creep is observed at constant stress as shown in Figure 2.1 (c), and is also manifested in the stress-reduction shown in Figure 2.1 (d). For strain-controlled loading, creep leads to dependence of the stress-strain curve on the strain-rate, as shown in Figure 2.1 (e).

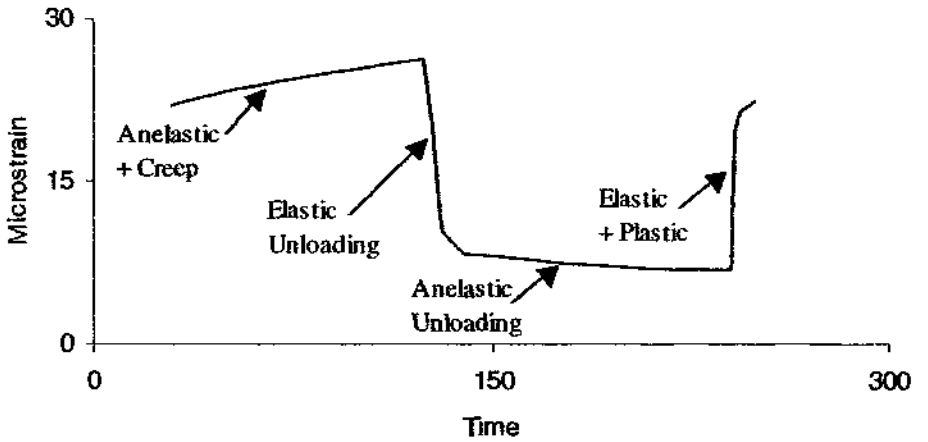

(a) Deformation Modes for Solder (based on data from Tien et al., 1991)

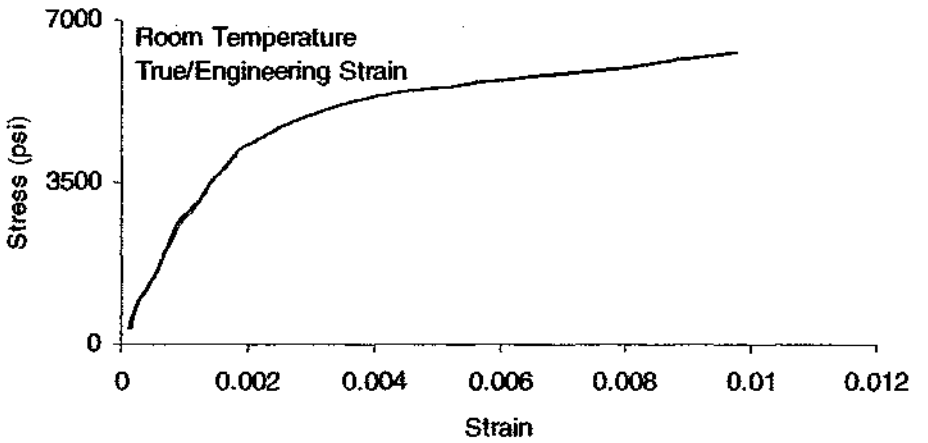

(b) Plastic Stress vs. Strain (based on data from Rafanelli, 1992)

Figure 2.1 Solder Deformation Modes

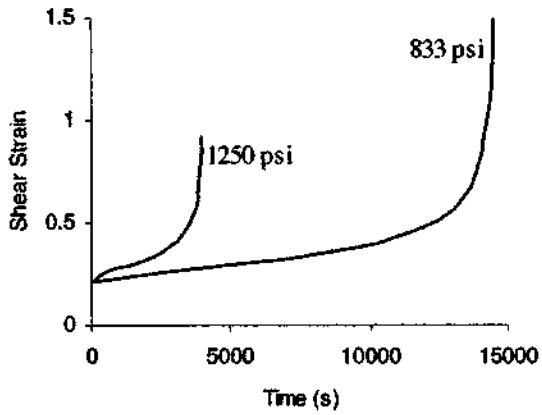

(c) Solder Creep at 65°C (based on Mei et al., 1991).

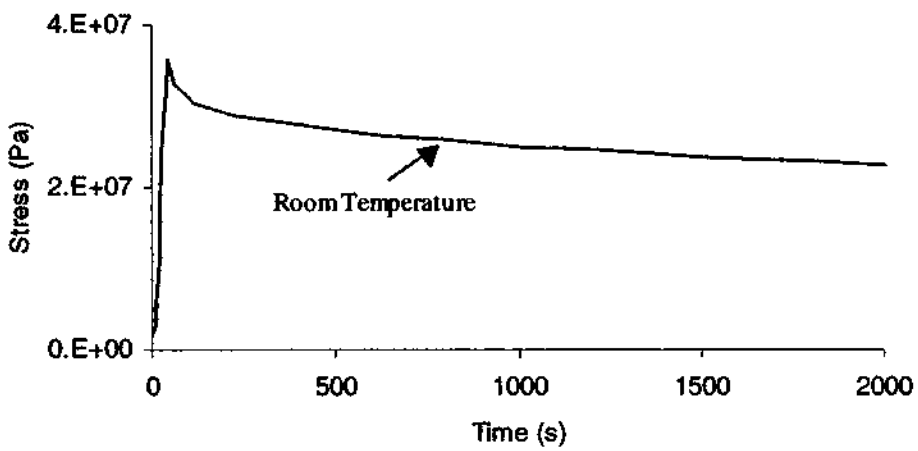

(d) Solder Stress-Relaxation (based on Hare and Stang, 1995)

Figure 2.1 (continued)

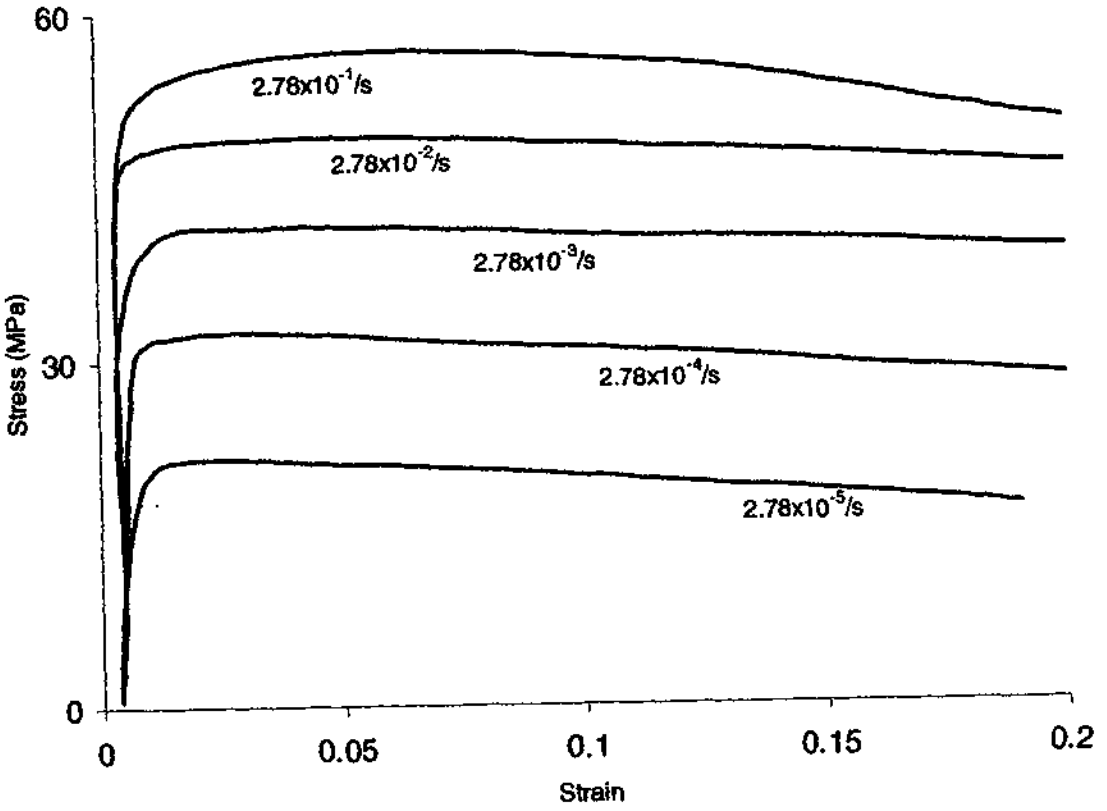

(e) Room Temperature Stress-Strain Curves for Different Strain Rates

(based on Shi et al., 1999)

Figure 2.1 (continued)

Finally, creep also affects the measurement of material parameters. If the elastic modulus is measured as the initial stress-strain slope, the value is found to be rate-dependent as shown in Figure 2.2. This would affect computation of all subsequent parameters.

2.1.1 Elastic Deformation

Elastic strains arise due to stretching of interatomic bonds and are fully recovered if the applied stresses are removed. The theory of elasticity based on the continuum assumption regarding materials is well developed. For isotropic materials only two elastic constants, such as Young's modulus (E) and shear modulus (G), are sufficient to define elastic behavior (Mase, 1970). Elastic strains are assumed to be instantaneous. Most materials may also be assumed to be linear-elastic for small elastic strains, with a constant ratio of stress to elastic strain. For such materials, based on E and G,

$$\sigma_{ij} = 2G\left[\varepsilon_{ij}^{e} + \delta_{ij}\left(\frac{E}{(3G-E)} - 2\right)\frac{\varepsilon_{kk}^{e}}{3}\right] \qquad \ldots(2.2)$$

Desai (2001) has stated that in the tangential form, the incremental constitutive equation may be written as

$$d\underline{\sigma} = \underline{C}_{t}^{e}\, d\underline{\varepsilon}^{e} \qquad \ldots(2.3)$$

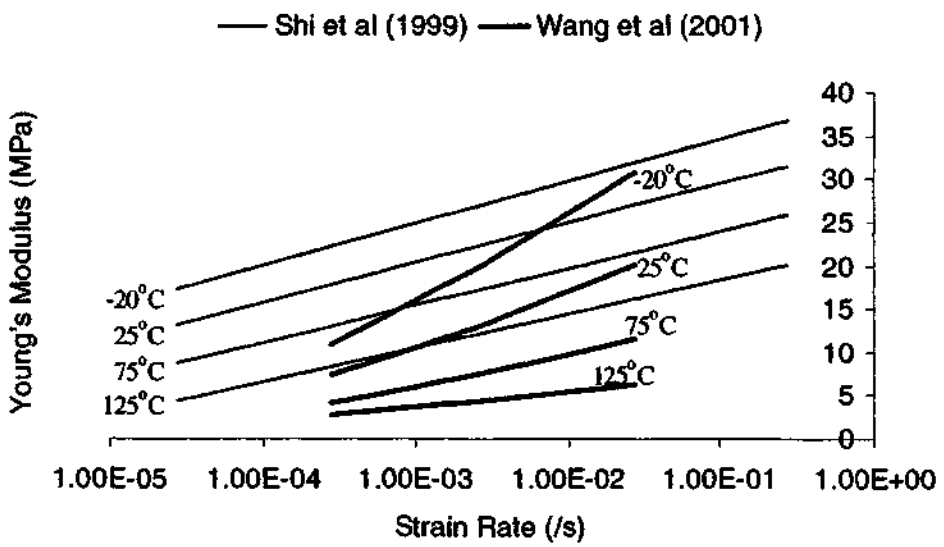

Figure 2.2 Effect of Strain Rate on Elastic Modulus based on

Best-Fit Line from Tensile Data of Shi et al. (1999), Shear Data of Wang et al. (2001)

where the terms of the matrix are variable elastic parameters which may vary from increment to increment, depending on conditions such as the temperature or the strain-rate.

Considerable variation exists in published values of the elastic modulus of solder, ranging from 14.8 GPa to 43.4 GPa (Knecht and Fox, 1991) at room temperature. The variation is caused due to the strong effects of creep and anelastic strains, with a loading rate of at least 80MPa/s required for accurate determination of the elastic modulus at room temperature (Hare and Stang, 1995). Measurement problems also arise due to the compliance of the test equipment (Solomon, 1986; Wilcox et al., 1990; Wang et al., 2001). Visual monitoring such as Moiré interferometry (Guo and Woychik, 1992) can help reveal the realized joint strain. In general, unless the corrections required for creep and machine compliance effects are overestimated, measured values are expected to be smaller than the true value. A comprehensive set of values has been provided by Pan (1991).

Simplified schemes for solder modeling may use a strain-rate dependent elastoplastic formulation to approximate creep behavior. In this case, material parameters are treated as strain-rate dependent and the elastic parameters are obtained from the initial curve of the stress-strain curve. Experimental data for the apparent rate-dependence of elastic parameters along with the temperature dependence has been provided by Shi et al. (1999) and Wang et al. (2001).

2.1.2 Plastic Deformation

Plastic deformation, typically treated as time-independent irreversible deformation, is caused by the motion of dislocations through crystals, with hardening due to generation of additional dislocations which may impede free movement (Dieter, 1961). For modeling purposes, the hardening may be expressed as a function of the plastic strains, or the dissipated plastic work.

The classical theory of plasticity assumes that upon loading, the yielding material always remains on a "yield surface" denoted by the yield function F, which provides the required combination of the state of stress and the hardening in the material (Hill, 1950). The yield function for strain-hardening may be written in the form (Desai, 2001)

$$F(\underset{\sim}{\sigma}, \xi) \equiv 0 \qquad \ldots(2.5)$$

where ξ is the plastic strain trajectory calculated as

$$\xi = \int d\varepsilon_{ij}^{p} d\varepsilon_{ij}^{p} \qquad \ldots(2.6)$$

For an elastoplastic material, with elastic and plastic strain components,

$$d\varepsilon_{ij}^{p} = d\varepsilon - d\varepsilon_{ij}^{e} = d\varepsilon - \left(C_{ijkl}^{e}\right)_{t}^{-1} d\sigma_{ij} \qquad \ldots(2.7)$$

where the subscript t refers to the tangential elastic constitutive matrix. Plastic strains for associated plasticity are assumed to follow the normality condition

$$d\varepsilon_{ij}^{p} = \lambda\left(\frac{\partial F}{\partial \sigma_{ij}}\right)$$

...(2.8)

and incremental stress-strain relationships may be obtained as in Desai (2001).

Yield surfaces used for solder include von Mises, as well as continuous yield surfaces such as the Ramberg-Osgood model (Rafanelli, 1992) which describes the combined elastic-plastic behavior using

$$\varepsilon = \frac{\sigma}{E} + \left(\frac{\sigma}{K}\right)^{\frac{1}{n_p}}$$

...(2.9)

for one-dimensional loading, and using Masing's hypothesis (Dasgupta et al., 1992)

$$\Delta\varepsilon = \frac{\Delta\sigma}{E} + 2\left(\frac{\Delta\sigma}{2K}\right)^{\frac{1}{n_p}}$$

...(2.10)

for cyclic loading. The origin of the stress and strain is at the compressive tip of the hysteresis loop. Rafanelli (1992) did not detect any difference parameters based on true stress-strain curves as against engineering curves. Dynamic testing methods were employed to obtain a time-independent plastic curve.

The HiSS-δ_0 yield function (Desai, 2001) is a general yield function which contains most prior yield functions as special cases, and has been applied to several types of materials including metals, ceramics, sands, rocks, soil and concrete. HiSS-δ_0 has been used for extensively for solder, for elastoplastic as well as viscoplastic modeling under the Perzyna scheme, by Chia (1994), Basaran (1994), Dishongh (1997) and Wang, (2001) to simulate continuous yield of solder.

The HiSS-δ_0 yield function is given by

$$F = \frac{J_{2D}}{p_a^2} - \left(-\alpha \left(\frac{J_1 + 3R}{p_a} \right)^n + \gamma \left(\frac{J_1 + 3R}{p_a} \right)^q \right) (1 - \beta S_r)^{-0.5} \qquad \ldots(2.11)$$

where p_a is the atmospheric pressure, J_1 is the first invariant of stress, J_{2D} is the second invariant of the deviatoric component of the stress tensor, R is the bonding stress, n is the phase change parameter related to the state of stress where the volumetric plastic strain increment vanishes, γ and q are the parameters related to the ultimate yield surface, β is related to the shape of F in the $\sigma_1 - \sigma_2 - \sigma_3$ space, S_r is the stress ratio, and equals $\left(27/\sqrt{2}\right)\left(J_{3D}/J_{2D}^{3/2}\right)$, and α is the hardening parameter, which can be expressed in terms of the plastic strain trajectory ξ as

$$\alpha = \left(\frac{a1}{\xi^{\eta 1}} \right) \qquad \ldots(2.12)$$

where a1 and η1 are material parameters.

Plots of the yield surface are shown in Figure (2.3) for q = 2, which provides a straight ultimate envelope in the $\sqrt{J_{2D}} - J_1$ space. The hardening parameter, α, is infinity at the origin of the yield surfaces (J_1 = -3R) and decreases with hardening, approaching the final value of zero at the ultimate yield surface. The convexity condition for yield functions in the $\sqrt{J_{2D}}$ vs. J_1 plane has been assumed by Chen (1997) to be[4]

$$\frac{\dfrac{\partial^2 \sqrt{J_{2D}}}{\partial J_1^2}}{\left[1+\left(\dfrac{\partial \sqrt{J_{2D}}}{\partial J_1}\right)^2\right]^{\frac{3}{2}}} \leq 0 \qquad \ldots(2.13)$$

which was shown, numerically, to be satisfied for n greater than 2 for $\beta = 0$.

2.1.3 Anelastic Deformation

Anelastic strains are time-dependent, reversible strains arising potentially due to the interaction of the tin and lead phases in solder (Tien et al., 1991). These strains can suppress damage accumulation due to creep strains depending on the loading, requiring a sufficient hold time so as to obviate their effect. Anelastic deformations in general may be due to effects such as bowing of dislocations, and may be a substantial portion of the primary creep deformations (Gittus, 1975).

---

[4] The sign may be reversed in literature depending on whether a convex curve is defined as convex up or convex down. Simple analytical solution is feasible as the denominator is always positive, $n \geq 2$ is required for the square root of J_{2D} to be nonnegative when computed from the yield function.

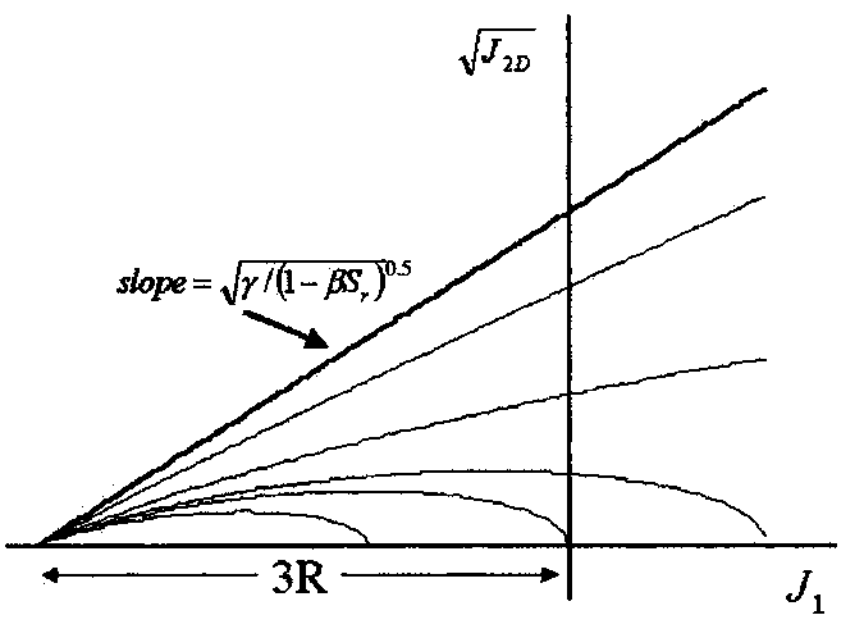

Figure 2.3 The HiSS-δ_0 yield function

2.1.4 Creep Deformation

Creep can be divided into an initial, high-strain rate primary component (2%), a lower-rate, steady state secondary component (10%), and finally, a tertiary phase with an increasing strain rate that consumes at least half the creep file (Tribula and Morris, 1990). Stephens and Frear (1999) report on the temperature-dependence of the relative contribution of primary creep. Dowling (1993) quotes Andrade's results for creep for metals in general to indicate that creep curves at constant true stress might not show tertiary creep. In certain cases, secondary creep may be suppressed and the steady-state creep rate is replaced by the minimum creep rate (Cadek, 1988).

Primary and secondary regions of creep are typically expressed as functions of stress, time and temperature, in terms of separable functions (Ju et al., 1994) in the form

$$\dot{\varepsilon} = f_1(\sigma) f_2(t) f_3(T) \qquad \ldots(2.14)$$

where suggested forms for the stress-dependence for secondary creep include

$$f_1(\sigma) = A\sigma^n$$

$$f_1(\sigma) = Be^{\alpha\sigma}$$

$$f_1(\sigma) = C\left[e^{\alpha\sigma} - 1\right]$$

$$f_1(\sigma) = D\left[\sinh(\beta\sigma)\right]^n$$

$$f_1(\sigma) = A\left[\left(\sigma - \sigma_y\right)/\sigma_y\right]^n$$

$$f_1(\sigma) = e^{[M\langle\sigma-\sigma_y\rangle/\sigma_y]} - 1$$

...(2.15)

For time-dependence of primary creep, functions used include

$$f_2(t) = at^m$$

$$f_2(t) = \left(1 + bt^{1/3}\right)e^{kt}$$

...(2.16)

For temperature dependence, relationships are typically of the Arrhenius type,

$$f_3(T) = e^{-Q/kT}$$

...(2.17)

Steady-state creep deformation has been modeled using the Dorn equation (Guo et al., 1992)

$$\dot{\gamma}_p = AD\mu b\left(\frac{b}{d}\right)^p \frac{1}{kT}\left(\frac{\tau}{\mu}\right)^n$$

...(2.18)

where

$$D = D_0 e^{-\Delta H/kT}$$

...(2.19)

with γ_p being the inelastic shear strain, D the appropriate diffusion coefficient, μ the shear modulus, b the Burgers vector, τ the applied shear stress, d the grain size or interphase spacing, A, n, p being material constants. D_0 is a constant and ΔH is the activation energy for a specific diffusion mechanism, while k is the Boltzmann constant. Similar equations including a back stress may be used, such as

$$\dot{\varepsilon}_C = A\left(\frac{1}{d}\right)^a \frac{1}{kT}\left(\frac{\sigma-\sigma_b}{E(T)}\right)^n e^{-E_a/kT} \qquad \ldots(2.20)$$

At high temperatures and relatively low stresses, the main mechanism for creep is vacancy diffusion. The diffusion may be through the grain boundaries at relatively lower temperatures in this regime, giving rise to Coble creep with a = 3, n = 1, and the activation energy being that for grain boundary diffusion. At higher temperatures, Nabarro-Herring creep with vacancy diffusion through the crystal occurs, where a = 2. At high stresses and intermediate temperatures, dislocation glide involving climb of edge dislocations, with a stress exponent between 3 and 6 is obtained, with the energy of activation being that for vacancies to travel to climb sites. Contrary to the expectation of lack of superplasticity for as-cast joints, Mei et al. (1991) showed that liquid nitrogen quenched joints showed a stress exponent of between 2 and 3.

Both grain boundary and matrix creep may be represented by a Weertman-type equation of the form

$$\dot{\gamma}_p = A\tau^{1/n_c} e^{-Q/kT}$$

...(2.21)

where the constants A and n_c depend on the dominant creep mechanism and Q is the relevant energy of activation. Dasgupta et al. (1992) provide values of 0.5 – 0.7 and 0.08 – 0.2 for n_c, for grain boundary creep and matrix creep respectively, with corresponding values of Q being 0.5 eV and 0.84 eV respectively. Climb-controlled creep has an n_c of 0.14 – 0.2, while the value for superplasticity is 0.5. Yu and Shiratori (1997) have provided temperature dependent values for the stress exponent.

The Perzyna (1966) viscoplastic model, based on the observation that time-dependent behavior is often manifested only at stresses above yield, has been used to simulate time-dependent irreversible deformations in solder (Chia, 1994; Desai and Whitenack, 2001; Wang et al., 2001). The model assumes that at vanishingly small strain rates, the viscoplastic strain due to any load increment is fully manifested, and the material follows a static yield surface which is identical to the hardening surface obtained due to plastic deformations.

The total strain rate at any time is assumed to be the sum of the elastic and the viscoplastic strain rates

$$\dot{\varepsilon}_{ij} = \dot{\varepsilon}^{e}_{ij} + \dot{\varepsilon}^{vp}_{ij}$$

...(2.22)

The corresponding rate of stress increment is

$$\dot{\sigma}_{ij}^{i} = C_{ijkl}^{e} \dot{\varepsilon}_{ij}^{e}$$

...(2.23)

The viscoplastic strain rate is given by

$$\dot{\varepsilon}_{ij}^{vp} = \Gamma \left\langle \phi \left(\frac{F}{F_0} \right) \right\rangle \frac{\partial F}{\partial \sigma_{ij}}$$

...(2.24)

where Γ is the fluidity parameter, F is the static yield function, F_0 is a reference value of F or any constant so as to render dimensionless, and ϕ is flow function, expressible in several different forms such as (Desai, 2001)

$$\phi = \left(\frac{F}{F_0} \right)^{N}$$

...(2.25)

or

$$\phi = e^{\left(\frac{F}{F_0} \right)^{N^*}} - 1$$

...(2.26)

where N and N* are material parameters.

2.2 Degradation Modeling

Several approaches, from the purely empirical to those based on micromechanics, with a corresponding range of simplifications, advantages and limitations have been provided in literature.

Damage accumulation in solder in the field is typically under thermomechanical cyclic loading and is due to creep-fatigue interactions. Comparison across fatigue studies is complicated due to the varying failure criteria used. From a functionality viewpoint, failure occurs when the solder joint does not provide the requisite connection between the component and the board. However, this is not a logical choice for fundamental stress-strain relationships. In general, at small crack lengths, the change in resistance is small, while dramatic increases in resistance may be obtained as the joint approaches final separation (Wilcox et al., 1990).

Wild (1975) indicated that a 10% drop in resistance was obtained subsequent to the first appearance of a crack, while Solomon (1986) showed that a 0.03 mΩ change in resistance corresponded to a load drop of 50% to 90%. Frear et al. (1995) have used resistance spikes of 500 Ω, with a duration of less than 1μs as the criterion corresponding to complete separation, which avoids contamination of results due to pressure from the leads of the joint. A substantial factor of safety may be required in applications, given the scatter in fatigue data.

Alternative criteria include a drop in load to a certain fraction of the original load. Solomon (1989) showed that the fatigue exponent for the Coffin-Manson relationship depended on the fraction selected for defining failure, especially for shear loading, while Wilcox et al. (1990) showed that results of fatigue life under this criterion are sensitive to the compliance of the test equipment. Additional criteria include initiation of a decrement in the ratio of the maximum to the minimum stress in uniaxial loading (Cutiongco et al., 1990), and the critical state of microstructure beyond which further cycling deteriorates the resistance of the material (Zubelewicz et al., 1989).

Initial attempts to describe the behavior of solder under cyclic loads were in terms of the traditional parameters of stress and strain amplitudes, for the Coffin-Manson line, combined at times with the Basquin high-cycle fatigue law as

$$\frac{\Delta\gamma_T}{2} = \frac{\Delta\gamma_e}{2} + \frac{\Delta\gamma_p}{2} = \frac{\tau_f'}{G}(2N_f)^b + \gamma_f'(2N_f)^c \qquad \ldots(2.27)$$

Solomon (1986) indicated that use of plastic strain control instead of total strain control provided a value of 0.52 for the Coffin-Manson exponent for solder, in line with typical metal values of 0.5 – 0.6. The high homologous temperature of solder under typical operating conditions with the resultant dominance of creep indicates that additional parameters such as waveform, ramp rates, hold times could be of crucial importance. Semi-empirical modifications have been provided, such as those by Coffin (1973),

$$\Delta\varepsilon = C\left(N_f \nu^{k-1}\right)^{\beta} + \frac{AC^n}{E} N_f^{-\beta n} \nu^{[-\beta n(k-1)+\alpha]}$$

...(2.28)

where $\Delta\varepsilon$ is the applied strain range, N_f is the number of cycles to failure, ν is the frequency of loading, and the other material parameters are assumed to be temperature dependent, and by Engelmaier (1984)

$$N_f = \frac{1}{2}\left(\frac{\Delta\gamma}{\gamma_f}\right)^{1/c}$$

...(2.29)

with

$$c = -0.442 - 6\times10^{-4}\,\bar{T}_s + 1.74\times10^{-2}\ln(1+360)/t_D$$

...(2.30)

where γ_f = 0.65 for 40/60 and 37/63 lead-tin solder, $\bar{T}_s$ is the mean cycle temperature in °C, and t_D is the high-cycle dwell time in minutes.

Barker et al. (1990) added the effect of elastic strains under high-cycle fatigue using Miner's rule for combined thermomechanical and vibratory loading, while Oyan et al. (1991) have applied the Halford-Manson strain-range partitioning scheme to account for damage due to creep and plastic strains. Creep-strain based damage models have been proposed by Knecht and Fox (1991) and Syed et al. (1998).

Vaynman et al. (1998) showed that energy based criteria may be more appropriate for solder that plastic strain based criteria, as joints which showed lower plastic strains but higher dissipated work relative to other joints were found to fail earlier. Corresponding to strain-range partitioning, Dasgupta et al. (1992) proposed an energy-partitioning scheme, wherein the damage due to the elastic strain energy stored and the inelastic work dissipated per cycle is superposed to predict solder fatigue. Lee et al. (2000) report an energy density based model developed by Akay, and an energy density based fatigue model developed by Gustafsson based on the findings of Darveaux. Zubelewicz et al. (1989) have developed a model based on micromechanical considerations.

2.2.1 Continuum Damage and its Extensions

Ju et al. (1996) have compared the fracture mechanics approach to that of continuum damage, and have stated that fracture mechanics requires assumptions regarding the initial crack and the path of crack growth, along with a fine mesh around the crack-tip as well as adaptive meshing, and modeling of crack failure. Qian et al. (1999) have provided a continuum damage model for solder. Ju et al. (1996) and Zhang et al. (2000) pointed to the lack of a comprehensive continuum damage theory as a drawback for the latter approach.

The classical damage theory of (Kachanov, 1958; 1986) assumes material to be composed of an intact phase and a void like phase of maximum feasible degradation that cannot carry any stress. The Disturbed State Concept (DSC) developed by Desai (2001)

assumes that the material in the state of maximum feasible degradation, which is confined by the intact material, may still carry some load.

DSC assumes that observed material response is a superposition of the responses of a relatively intact (RI) phase and a fully adjusted (FA) phase. The RI phase corresponds to the asymptotic defect-free state of a material, devoid of degradation and micro-cracks. The FA phase is the asymptotic state of the material with the maximum feasible degradation achievable under typical field or the laboratory loading. Each phase may be modeled by a suitable constitutive model. The fraction of the material in the FA phase is defined to be the disturbance, D.

The observed stress (σ^a) is given by a weighted superposition of the RI stress (σ^i) and the FA stress (σ^c),

$$\sigma_{ij}^{a} = (1-D)\sigma_{ij}^{i} + D\sigma_{ij}^{c}$$

...(2.31)

where D is the relative fraction of the phases in the material. Loading may convert a portion of the RI phase into the FA phase. The incremental stress-strain equation is thus

$$d\sigma_{ij}^{a} = (1-D)d\sigma_{ij}^{i} + Dd\sigma_{ij}^{c} + dD(\sigma_{ij}^{c} - \sigma_{ij}^{i})$$

...(2.32)

For simplicity, the strains in the RI and FA phases are assumed to be equal to the observed strain in the material, i.e.

$$\varepsilon_{ij}^{a} = \varepsilon_{ij}^{i} = \varepsilon_{ij}^{c} = \varepsilon_{ij}$$

...(2.33)

Incremental stress-strain equations for the RI and FA phases are then given in terms of the constitutive matrices as

$$d\sigma_{ij}^{i} = C_{ijkl}^{i} d\varepsilon_{kl}$$

...(2.34)

$$d\sigma_{ij}^{c} = C_{ijkl}^{c} d\varepsilon_{kl}$$

...(2.35)

Eqs. (2.31) – (2.34) provide

$$d\sigma_{ij}^{a} = (1-D)C_{ijkl}^{i} d\varepsilon_{kl} + DC_{ijkl}^{c} d\varepsilon_{kl} + dD(\sigma_{ij}^{c} - \sigma_{ij}^{i})$$

...(2.36)

RI behavior under DSC can be modeled as elastic, elastoplastic or elastoviscoplastic depending on the material and the loading. The FA phase may be modeled under one of several simple schemes.

As a void, the FA material is allowed to carry no stress.

$$\sigma_{ij}^{c} = 0$$

...(2.37)

As a constrained liquid, the hydrostatic stress in the FA phase is assumed to equal that in the RI phase while all shear components of the stress are assumed to be zero.

$$\sigma_{ij}^{c} = \frac{J_1^i}{3}\delta_{ij} = \frac{J_1^a}{3}\delta_{ij}$$

...(2.38)

Finally, the FA material may be capable of carrying a shear stress proportional to the mean pressure.

$$J_1^c = J_1^i = J_1^a$$

...(2.39)

$$\sqrt{J_{2D}^c} = \bar{m} J_1^c$$

...(2.40)

The parameter $\bar{m}$ is determined based on the state of stress in the final stages of observed material behavior. For instance, with $D_u = 1$, only FA material remains, providing

$$(J_{2D}{}^c)^{0.5} = (J_{2D}{}^a)^{0.5}$$

...(2.41)

and $\bar{m}$ is determined from the best-fit parameter for the line based on observed stress

$$(J_{2D}{}^a)^{0.5} = \bar{m} J_1{}^a$$

...(2.42)

The disturbance function, D, is the fraction of the material in the FA phase. For computation of growth of degradation, the disturbance function may be represented in terms of all internal variables that affect material behavior, such as the elastic strain, the plastic strain trajectory, the dissipated energy, the entropy, number of loading cycles, temperature and impurities, as well as environmental conditions. For simplicity, under elastoplastic or viscoplastic formulations, the form is typically given by

$$D = D_u\left(1 - e^{-A(\xi_D)^Z}\right)$$

...(2.43)

where A and Z are material parameters, D_u is the ultimate disturbance, usually 0.9 - 1.0, and ξ_d is the plastic or viscoplastic strain trajectory defined as

$$\xi_D = \int \sqrt{de_{ij}^p de_{ij}^p}$$

...(2.44)

where de_{ij}^p are the deviatoric components of the plastic or viscoplastic strain increment. Assuming the mean pressure in the RI and FA phases to be the same, the parameters A and Z are computed from the best-fit line

$$\ln(-\ln(1-D/D_u)) = C_1 + C_2 \ln\xi_D$$

...(2.45)

using

$$A = e^{C_1}$$

...(2.46)

$$Z = C_2$$

...(2.47)

For obtaining the plot, the disturbance at each point may be computed using

$$D = \frac{\sqrt{J_{2D}^{i}} - \sqrt{J_{2D}^{a}}}{\sqrt{J_{2D}^{i}} - \sqrt{J_{2D}^{c}}} = \frac{\sqrt{J_{2D}^{i}} - \sqrt{J_{2D}^{a}}}{\sqrt{J_{2D}^{i}} - \bar{m} J_{1}^{a}}$$

...(2.48)

For computation of ξ_D, either the plastic strain trajectory in the RI phase, or the plastic strain trajectory based on increments of plastic strain in the observed material may be used.

An alternative approach for ductile materials that combines plasticity with the observations of local damage due to the substantial void nucleation and growth has been suggested by Gurson (1977). Needleman and Tvergaard (1984) have extended the method to void coalescence. The plasticity function in the Gurson model is given by

$$F = \frac{\sigma_e^2}{\sigma_M^2} + 2f \cosh\left(\frac{1}{2}\frac{\sigma_{kk}}{\sigma_M}\right) - 1 + f^2 = 0$$

...(2.49)

where f is the void fraction, σ_e is the von Mises equivalent stress and σ_M is the yield stress of the matrix (Planicka et al., 2001). Void evolution is in terms of void nucleation and void growth, as

$$\dot{f} = \dot{f}_{nucleation} + \dot{f}_{growth}$$

...(2.50)

with appropriate models for each, depending on whether or not a critical void fraction has been reached. Matrix strains and continuum variables are related through the equality of plastic work,

$$(1-f)\varepsilon_M^P \sigma_M = \varepsilon^P \sigma$$

...(2.51)

2.3 Joint Microstructure

The macroscopic behavior of a joint depends on the initial microstructure, and its evolution during loading. A fine microstructure is desirable due to its superior creep resistance. Cracks have also been observed to initiate faster in coarser regions (Wild, 1975; Mei and Morris, 1992)[5].

2.3.1 Initial Microstructure

The initial state of a joint is determined by the soldering process and the subsequent cooling rate. The latter depends on the size, composition and configuration of the board, as well as the soldering process.

Slow cooling rates (Conrad et al., 1999) for Pb/Sn eutectic solder result in stable, alternating lamellae of the tin and lead-rich phases, parallel to the direction of growth,

with the fineness of the microstructure increasing with faster cooling (Lau, 1991). Faster cooling rates and the presence of impurities (Jackson, 2002) lead to increasingly finer globular degenerate structures, with quenching leading to a dispersion of the lead-rich phase in a tin-rich matrix (Mei and Morris, 1992).

The excellent solvent properties of molten solder (Ross, 1991) imply that surroundings of the joint determine the presence of impurities, as well as the extent of oxidation. Instabilities such as unfavorably oriented growth and local variation in cooling rates may cause a breakdown in the long-range structure and short-range colonies, with homogenous phase distributions within, may arise. Colonies are separated from each other by a distinct colony boundary which is delimited by a narrow region of enlarged, equiaxed particles (Tribula et al., 1989; Tribula and Morris, 1990).

The microstructure of 60/40 tin-lead solder is similar to that of the eutectic alloy, but coarser and with less distinct boundaries (Summers and Morris, 1990), with pro-eutectic lead rich particles containing plate-shaped tin-rich precipitates dispersed in the eutectic structure (Tribula et al. 1989).

---

[5] Shen et al (2001) argue that the coarsened region is not weaker per se, but is subjected to earlier damage due to higher plastic strains.

2.3.2 Intermetallics

During soldering, molten solder on the substrate, typically copper, instantly forms intermetallic copper-tin compounds and the layer rapidly thickens to a few microns. This forms the bonding layer between the solder and the copper (So et al., 1997).

The intermetallic consists of two phases, a thin layer of Cu_3Sn (ε-phase) at the copper pad, and rod-like hexagonal projections of Cu_6Sn_5 (η-phase) into the solder in contact with the tin. The rods can break off into the molten solder, appearing as intermetallic particles or whiskers in bulk solder (Tribula et al., 1989). Formation of intermetallics may be suppressed in the presence of additional elements. Cooling rates along with the metallization of the connecting pads determines the nature, quantity and distribution of the intermetallics formed.

For Pb/Sn solder, intermetallic growth has also been observed to continue with time depending on the temperature, obeying

$$d = \sqrt{Dt} \qquad \ldots(2.52)$$

where d is the layer thickness, D is the interdiffusion constant and t is the aging time. The dependence of layer growth in terms of temperature can be given by the Arrhenius equation

$$D = D_0 e^{-Q/kT}$$

...(2.53)

where D_0 is the interdiffusion constant, Q is the activation energy for the growth of the intermetallic layer, k is the Boltzmann constant and T is the absolute temperature.

Wassink (1989) reported growth even at room temperature, while So et al. (1997) cite results from literature indicating that the intermetallic thickness is unaffected by up to 13 weeks of heating at 70°C, while heating at 170°C leads to thickening of both phases, as well as conversion of the η-phase to the ε-phase. Intermetallic growth under thermal cycling with no applied mechanical loads has been reported by Pang et al. (2001).

2.3.3 Microstructure Evolution

The as-cast degenerate microstructure of Pb/Sn joints (Mei and Morris, 1991; 1992; Conrad et al., 1999) obtained in the presence of impurities (Jackson, 2002), is unstable (Tribula et al., 1989; Cutiongco et al., 1990; Morris et al., 1991) with respect to coarsening of the lead-rich region due to diffusion of vacancies (Vianco et al., 1999) under aging (Cutiongco et al., 1990; Ross, 1991), thermal cycling (Pang et al., 2001) and especially thermomechanical loading (Hacke et al., 1997, 1998) where the number of vacancies is higher. Equilibrium is attained under isothermal annealing at 100°C after a few days, or a few months at room temperature (Cutiongco et al., 1990; Ross, 1991). Solomon (1986) did not find significant microstructural changes after fatigue at 35°C for a relatively coarse as-cast structure while recrystallization and grain growth were

observed by Wild (1975), especially for long-duration high-temperature tests. Summers and Morris (1990) noted that strains were more homogenous and the coarsening was less pronounced in 60/40 tin-lead solder as compared to the eutectic solder.

Ag/Sn joints, with less than 5% intermetallic Ag_3Sn by volume, show coarsening under aging at higher temperatures only (Yang et al., 1994; 1995). However, a large number of intermetallic particles, while increasing the creep resistance also result in increased sites for microcrack initiation (Igoshev and Kleiman, 2000).

Under shear deformation, inhomogeneous deformations observed in eutectic and near-eutectic solders have been observed to lead to a band of coarsened material slightly offset from the interface. Tribula et al. (1989) ascribed the growth of the band due to the relatively soft coarsened material acting like a Type II crack creating a narrow band of high plastic deformations, with recrystallization leading to propagation at the tip. However, Shen et al. (2001) argue that locally coarsened material may not be weaker than the surrounding region, but is subject to early damage initiation due to accumulation of plasticity.

2.3.4 Damage Accumulation

Cracks were noted in all cyclic loading studies within the coarsened band, and were observed to merge and form thermal fatigue cracks. Faster initiation and propagation of cracks in coarser microstructures has been observed by Wild (1975) and Mei and Morris

(1992). Attarwala et al. (1992) provided experimental confirmation for creep-fatigue interactions under thermomechanical cycling, with the observation of fatigue striations related to crack growth, from cracks initiated mainly in the harder tin region, as well as voids. Mechanistic models for crack initiation and propagation have been proposed by Wong and Helling (1990) and Stone (1990) for crack initiation due to grain-boundary sliding, thermal nucleation at triple points, and subsequent propagation.

Zubelewicz et al. (1989) reported transgranular and mixed fracture modes for high strain ranges, and intergranular for low strain ranges. Tribula et al. (1989) reported formation of coarsened bands under shear loading for unidirectional loading and thermomechanical cycling leading to strain concentrations and thus, crack growth. The band was seen to follow colony boundaries at low strain rates, while at high rates the band was parallel to the direction of shear. Similar results have been obtained for thermomechanical cycling by Frear et al. (1995). Under tensile cycling, failure was obtained at the brittle intermetallic. Failure at this site may also be expected under impact loads. Lee and Stone (1992) reported shear localization and transgranular failure with a dimpled fracture surface for high strain rates, and failure by cavitation at low strain rates due to grain boundary sliding for tensile loading. Under tension-compression fatigue, low frequency and high strain range lead to numerous intergranular cracks at the surface, which propagated along grain boundaries to the interior, while high frequencies at low strains led to transgranular failure.

Cutiongco et al. (1990) reported increased fatigue life after heating at 150°C for up to a week, with a subsequent leveling-off. Vaynman et al. (1998) reported increased ductility and fatigue life for joints aged for seven years. Mei and Morris (1992) showed that quenched joints had about twice the fatigue lifetime for isothermal cycling as compared to furnace cooled joints. Chan et al. (1997) showed a decrease in fatigue life with intermetallic thickness. Summers and Morris (1990) reported that a slight change in microstructure, such as that between 63/37 and 60/40 lead-tin solder, could lead to substantial differences in fatigue lives.

Microstructure and its effects on solder behavior, including constitutive response as well as damage accumulation must be considered in design of accelerated tests, to ensure that the fundamental mechanisms of deformation and damage accumulation being modeled are the one that is expected under field conditions. Frear et al. (1995) have provided guidelines for design of thermomechanical tests for Pb/Sn solder.

3. CONSTITUTIVE FORMULATION

This chapter develops generalized elastic and elastoplastic formulations for the case of temperature and strain-rate dependent material parameters. The range of validity for the rate-dependent elastoplastic formulation and the Perzyna viscoplastic formulation for solder modeling are discussed. An approximate dissipated-work based DSC formulation is also developed.

3.1 Elastic Formulation

Elastic deformations are recovered completely when the applied loads are removed. Thus the relationship between elastic deformation and applied stresses should be history-independent. If the elastic strain and all other relevant conditions[6] such as the temperature and the strain rate are known at any instant, the stress at that instant can be determined independently of the path through which the given values were attained. History-independence is satisfied if a stress-strain relationship in terms of a secant constitutive matrix of the form

[6] The relevant conditions include damage if damaged material is not modeled as a separate phase. For schemes such as DSC (Desai, 2001) history-independence is required for the intact material.

$$\sigma_{ij} = C^{se}_{ijkl}(p_1,...p_n)\varepsilon^e_{kl}$$

...(3.1)

is assumed, where C_{ijkl}^{se} is the secant elastic constitutive matrix which may depend on the instantaneous values of the n loading parameters, $p_1,...,p_n$, such as temperature, strain rate, stress or strain depending on the material, and ε^e_{kl} is the elastic strain tensor.

The incremental stress-strain relationship for elastic deformations is then given by

$$d\sigma_{ij} = C^{se}_{ijkl}(p_1,..., p_n)d\varepsilon^e_{kl} + \left(\frac{\partial C^{se}_{ijkl}}{\partial p_m}\varepsilon^e_{kl}\right)dp_m$$

...(3.2)

where the summation notation is extended to the index for the loading parameters p_m, m varying from 1 to n.

For a strain-dependent secant constitutive matrix, the tangent constitutive matrix may be defined as

$$d\sigma_{ij} = \left(C^{se}_{ijkl} + \frac{\partial C^{se}_{ijmn}}{\partial \varepsilon^e_{kl}}\varepsilon^e_{mn}\right)d\varepsilon^e_{kl} = C^{te}_{ijkl}d\varepsilon^e_{kl}$$

...(3.3)

For a linear-elastic material, the tangent and secant elastic matrices are equal.

For solder, the ratio of the reversible strain to the stress depends on the temperature. The temperature-dependent elastic constitutive matrix provides

$$d\sigma_{ij} = C^{e}_{ijkl}(T)d\varepsilon^{e}_{kl} + \left(\frac{\partial C^{e}_{ijkl}}{\partial T}\varepsilon^{e}_{kl}\right)dT \qquad \ldots(3.4)$$

or incorporating thermal strains,

$$d\sigma_{ij} = C^{e}_{ijkl}(T)d\varepsilon_{kl} + \left(\frac{\partial C^{e}_{ijkl}}{\partial T}\varepsilon^{e}_{kl} - C^{e}_{ijkl}(T)\delta_{kl}\alpha(T)\right)dT \qquad \ldots(3.5)$$

where ε_{kl}, the total strain, is the sum of the elastic and thermal strains and $\alpha(T)$ is the temperature-dependent coefficient of linear thermal expansion.

3.1.1 Rate-Dependent Formulation

For the simplified rate-dependent elastoplastic formulation (Chia, 1994; Shi et al., 1999; Wang et al., 2001) where creep effects are simulated based on strain-rate dependent elastic and plasticity parameters, the incremental equation is

$$d\sigma_{ij} = C^{e}_{ijkl}\left(T, \dot{\varepsilon}^{e}_{pq}\right)d\varepsilon^{e}_{kl} + \left(\frac{\partial C^{e}_{ijkl}}{\partial T}\varepsilon^{e}_{kl}\right)dT + \left(\frac{\partial C^{e}_{ijkl}}{\partial \dot{\varepsilon}^{e}_{pq}}\varepsilon^{e}_{kl}\right)d\dot{\varepsilon}^{e}_{pq} \qquad \ldots(3.6)$$

The rate-dependent formulation predicts a discontinuous jump in stress if the strain-rate changes discontinuously. For instance, the formulation predicts a discontinuous drop or

rise in stress for an elastic material at the corners of a symmetric trapezoidal displacement-controlled cycle, as shown in Figure 3.1.

For an elastoplastic material, the stress drop at Point 2 and the corresponding stress rise at Point 3 can only be greater than that for the elastic case. Any further yielding at Point 2 at the commencement of holding would only serve to decrease the stress further. For Point 3 at the commencement of unloading, the stress-rise is elastic as the material has already been hardened to the maximum value of stress at Point 2 at the loading strain-rate.

Since this behavior is not observed for solder, the rate-dependent elastoplastic scheme may not be useful for solder modeling unless the strain-rate is constant. For isothermal, constant strain-rate tests, Eq. (3.6) degenerates to the prior incremental formulation of Eq. (2.3). However, as shown in Appendix I, Eq.(2.3) does not provide a history-independent relationship when the parameters relevant to the elastic response, such as temperature and strain-rate vary during loading.

The incremental relationship between stress and elastic strains is also assumed to be valid for elastoplastic materials. Modifications in the elastic relationship entail modifications to the incremental elastoplastic equations.

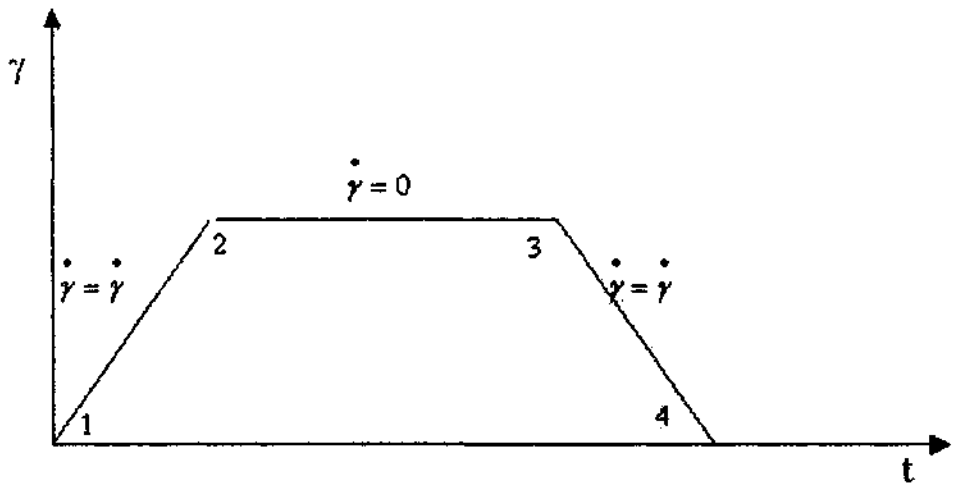

(a) Strain-Controlled Trapezoidal Loading

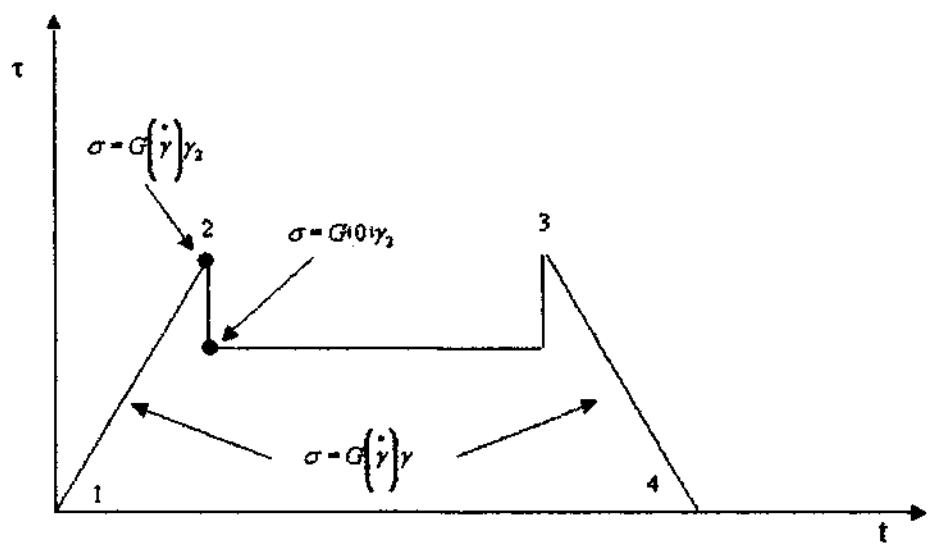

(b) Stress Response

Figure 3.1 Rate-Dependent Elastoplastic Response

3.2 Plasticity Formulation

Plastic deformation refers to the irreversible deformations due to dislocation slip that are rate-independent in that they are virtually instantaneous as compared to the viscous, time-dependent deformation obtained due to creep. For associated plasticity, the plastic strain increments are computed based on the normality assumption

$$d\varepsilon_{ij}^{p} = \lambda\left(\frac{\partial F}{\partial \sigma_{ij}}\right) \qquad \ldots(3.7)$$

where λ is a scalar and F is the yield function that depends on the state of the stress and for hardening materials, either on the plastic strain trajectory ξ defined as

$$\xi = \int d\xi = \int d\varepsilon_{ij}^{p} d\varepsilon_{ij}^{p} \qquad \ldots(3.8)$$

or the dissipated work W^p,

$$W^{p} = \int dW^{p} = \int \sigma_{ij} d\varepsilon_{ij}^{p} \qquad \ldots(3.9)$$

as well as k material parameters, m_k, depending on the yield function under consideration, which govern the material-specific yield behavior, in the form

$$F = F(\sigma_{ij}, \xi, m_1 \ldots m_k) \qquad \ldots(3.10)$$

It may be noted that the definition of plastic strain trajectory in terms of the engineering plastic strain vector (Desai, 2001; Wang et al., 2001)

$$\xi = \int \sqrt{d\varepsilon_i^p d\varepsilon_i^p} = \int \sqrt{(d\varepsilon_1^p)^2 + (d\varepsilon_2^p)^2 + (d\varepsilon_3^p)^2 + (d\gamma_1^p)^2 + (d\gamma_2^p)^2 + (d\gamma_3^p)^2}$$

...(3.11)

where ε_i^p denote components of the engineering plastic strain vector should be avoided as besides being numerically different from the definition of Eq. (3.8), the plastic strain trajectory defined using Eq. (3.11) is not an invariant. Simulation results would demonstrate spurious dependence on the coordinate axes chosen for the problem.

3.2.1 Convexity Condition

In case the yield function F is defined in terms of the invariants of stress, the convexity condition required in the J_1 vs. $\sqrt{J_{2D}}$ plane instead of Eq. (2.13) is

$$\frac{\partial^2 \sqrt{J_{2D}}}{\partial J_1^2}\left[-\frac{J_1}{2}\frac{\partial J_{2D}}{\partial J_1} + J_{2D}\right] \leq 0$$

...(3.15)

for any point on the surface where J_{2D} is not zero. The convexity constraint is obtained based upon the observation that at least for the initial yield surface, the dot product of the position vector to any point on the yield surface with the curvature of the surface at that point should be negative (Figure 3.2). The same constraint is required for all subsequent surfaces which continue to enclose the origin.

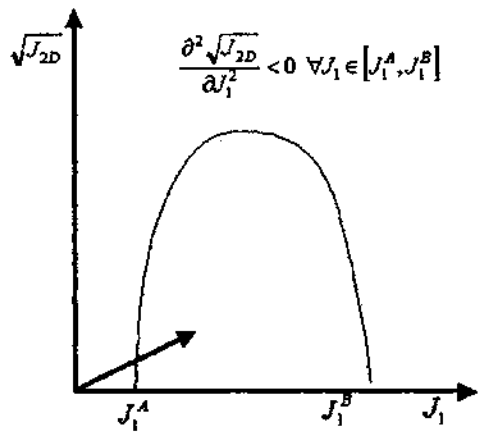

(a) Curve Convex Relative to J_1 Axis

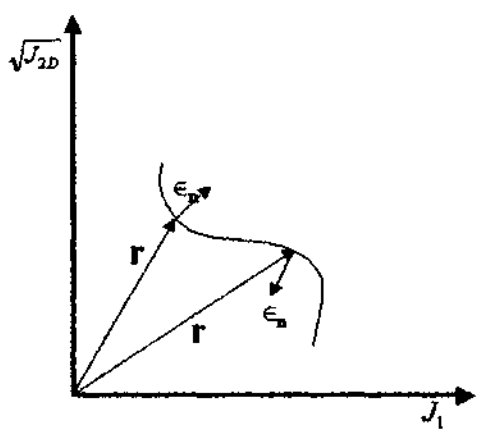

(b) Convexity Relative to Origin

Figure 3.2 Convexity Criteria

3.2.2 Consistency Condition

The elastoplastic formulation assumes that upon loading, the material always remains on the yield surface and that the function F remains zero identically.

$$F \equiv 0 \qquad \ldots(3.14)$$

If the material parameters m_k in Eq. (3.10) depend on r loading conditions $p_1 \ldots p_r$ such as temperature and strain rate, in addition to the stress and the plastic strain trajectory, the consistency condition can be written as

$$\frac{\partial F}{\partial \sigma_{ij}} d\sigma_{ij} + \frac{\partial F}{\partial \xi} d\xi + \frac{\partial F}{\partial p_s} dp_s \equiv 0 \qquad \ldots(3.15)$$

where the summation notation is assumed for the index s, which varies from $1 \ldots r$. This form of the consistency condition has also been provided by Cook et al. (1989).

Since yield behavior for solder is temperature dependent, the consistency condition is that provided by Kachanov (1971)

$$dF = \frac{\partial F}{\partial \sigma_{ij}} d\sigma_{ij} + \frac{\partial F}{\partial \xi} d\xi + \frac{\partial F}{\partial T} dT \equiv 0 \qquad \ldots(3.16)$$

For the simplified elastoplastic scheme with strain-rate dependent plasticity parameters, the consistency condition contains an additional term for the strain-rate.

3.2.3 Incremental Elastoplastic Formulation

The elastoplastic formulation assumes that the total strain is given by the sum of the elastic (e), plastic (p) and thermal (T) strains.

$$d\varepsilon_{ij} = d\varepsilon_{ij}^{e} + d\varepsilon_{ij}^{p} + d\varepsilon_{ij}^{T} = d\varepsilon_{ij}^{e} + d\varepsilon_{ij}^{p} + \delta_{ij}\alpha(T)dT$$

...(3.17)

The incremental stress-strain relationship for temperature-dependent elastic parameters is

$$d\sigma_{ij}^{i} = C_{ijkl}^{e}(T)\left(d\varepsilon_{kl} - d\varepsilon_{kl}^{p}\right) + \left(\frac{\partial C_{ijkl}^{e}}{\partial T}\varepsilon_{kl}^{e} - C_{ijkl}^{e}(T)\delta_{kl}\alpha(T)\right)dT$$

...(3.18)

For the case of temperature-dependent material parameters, the incremental equation based on the generalized stress-strain relationship and temperature-dependent material parameters is

$$d\underset{\sim}{\sigma}^{i} = \left[\underset{\sim}{C}^{e} - \frac{\underset{\sim}{C}^{e}\frac{\partial F}{\partial \underset{\sim}{\sigma}}\left(\frac{\partial F}{\partial \underset{\sim}{\sigma}}\right)^{T}\underset{\sim}{C}^{e}}{\left(\frac{\partial F}{\partial \underset{\sim}{\sigma}}\right)^{T}\underset{\sim}{C}^{e}\frac{\partial F}{\partial \underset{\sim}{\sigma}} - \frac{\partial F}{\partial \xi}\left[\left(\frac{\partial \bar{F}}{\partial \underset{\sim}{\sigma}}\right)^{T}\frac{\partial \bar{F}}{\partial \underset{\sim}{\sigma}}\right]^{\frac{1}{2}}}\right]d\underset{\sim}{\varepsilon} -$$

$$\underset{\sim}{C}^{e}\left[\left(\alpha \underset{\sim}{I}_{0} - \left(\underset{\sim}{C}^{e}\right)^{-1}\frac{\partial \underset{\sim}{C}^{e}}{\partial T}\left(\underset{\sim}{C}^{e}\right)^{-1}\underset{\sim}{\sigma}\right) - \frac{\frac{\partial F}{\partial \underset{\sim}{\sigma}}\underset{\sim}{C}^{e}\left(\alpha \underset{\sim}{I}_{0} - \left(\underset{\sim}{C}^{e}\right)^{-1}\frac{\partial \underset{\sim}{C}^{e}}{\partial T}\left(\underset{\sim}{C}^{e}\right)^{-1}\underset{\sim}{\sigma}\right)\frac{\partial F}{\partial \underset{\sim}{\sigma}} - \frac{\partial F}{\partial T}\frac{\partial F}{\partial \underset{\sim}{\sigma}}}{\left(\frac{\partial F}{\partial \underset{\sim}{\sigma}}\right)^{T}\underset{\sim}{C}^{e}\frac{\partial F}{\partial \underset{\sim}{\sigma}} - \frac{\partial F}{\partial \xi}\left[\left(\frac{\partial \bar{F}}{\partial \underset{\sim}{\sigma}}\right)^{T}\frac{\partial \bar{F}}{\partial \underset{\sim}{\sigma}}\right]^{\frac{1}{2}}}\right]dT$$

...(3.19)

where

$$\frac{\partial \bar{F}}{\partial \sigma_i} = \frac{\partial F}{\partial \sigma_i} \forall i \le 3$$
$$= \frac{1}{\sqrt{2}} \frac{\partial F}{\partial \sigma_i} \forall i > 3$$

...(3.20)

For the strain-rate dependent elastoplastic simulation,

$$d\sigma_{ij}^{i} = C_{ijkl}^{e}(T)\left(d\varepsilon_{kl} - d\varepsilon_{kl}^{p}\right) + \left(\frac{\partial C_{ijkl}^{e}}{\partial T}\varepsilon_{kl}^{e} - C_{ijkl}^{e}\delta_{ij}\alpha(T)\right)dT + \frac{\partial C_{ijkl}^{e}}{\partial \dot{\varepsilon}_{pq}^{e}}\varepsilon_{kl}^{e} d\dot{\varepsilon}_{pq}^{e}$$

...(3.21)

Development of the complete incremental elastoplastic matrix for the strain-rate dependent case is not pursued as it is of limited utility for solder. Issues include an overly complex formulation due to additional terms in the consistency condition of Eq. (3.16) and the incremental elastic stress-strain relationship of Eq. (3.19), potentially inaccurate simulations for variable strain-rate loading as shown in Figure 3.1, and the need for additional iterations in Finite Element simulations as strain-rate is an internally computed parameter. Substantial experimentation may also be required to develop relationships between material parameters and the full strain-rate tensor, as well as to distinguish the effects of the elastic, plastic and total strain rates. For instance, shear strain-rate dependent parameters of Wang et al. (2001) may not be directly comparable to the uniaxial strain-rate dependent parameters of Shi et al. (1999).

3.3 Perzyna Viscoplastic Formulation

The Perzyna formulation was developed based on observations regarding the delayed yielding and time-dependence of post-yield material response under relatively high strain-rate loading, such as for wave propagation and impact loading problems, with strain rates up to 10^4/s (Perzyna, 1966). The formulation assumes all irreversible strain in the material to be viscoplastic and that

$$\dot{\varepsilon}_{ij} = \dot{\varepsilon}^{e}_{ij} + \dot{\varepsilon}^{vp}_{ij} \qquad \ldots(3.22)$$

where

$$\dot{\varepsilon}^{vp}_{ij} = \Gamma \left\langle \phi\left(\frac{F}{F_0}\right)\right\rangle^{N} \frac{\partial F}{\partial \sigma_{ij}} \qquad \ldots(3.23)$$

where F is the plastic yield function in terms of material parameters determined from the "static" yield surface, which governs the material behavior at vanishingly small strain rates. At high strain rates the material behavior becomes increasingly elastic. As the strain rate tends to infinity the initial material behavior is purely elastic and elastic parameters are obtained as

$$E = \left(\frac{d\sigma_1}{d\varepsilon_1}\right)_{\dot{\varepsilon}_1 \to \infty} \qquad \ldots(3.24)$$

$$G = \left(\frac{d\tau}{d\gamma} \right)_{\dot{\gamma} \to \infty}$$

...(3.25)

The Perzyna formulation cannot simultaneously model instantaneous plastic strains and creep strains. If the fluidity parameter, Γ, tends to infinity, material response is elastoplastic corresponding to $F = 0$ at finite strain rates while if the fluidity factor is zero, the behavior is elastic. For finite, nonzero values of the fluidity parameter, all irreversible strain is viscoplastic and thus rate-dependent.

For solder, typical nominal strain rates in accelerated thermomechanical tests may be of the order of 10^{-2}/s – 10^{-5}/s. Under these conditions plastic strains are virtually instantaneous and thus, rate-independent. Rate-dependence of behavior is introduced by creep strains. The relative contribution of plastic and creep deformation depends on the temperature and the strain rate. At –45°C, plastic slip may dominate at higher strain rates while at 125°C, creep dominates. Plastic strains along with multiple creep modes may contribute significantly at intermediate temperatures (Darveaux and Banerji, 1992; Stephens and Frear, 1999). Thus, the appropriate division of strains is

$$d\varepsilon = d\varepsilon^{e} + d\varepsilon^{p} + d\varepsilon^{vp}$$

...(3.26)

where the elastic and plastic strains are the reversible and irreversible instantaneous components of the total strain, while the viscoplastic strain is the time-dependent irreversible part. Viscoelastic strains are assumed to be insignificant.

Observed material response to a stress-step loading is shown in Figure 3.3(a). If fluidity parameters are computed from the strain-response to stress-step loading, only the creep portion of strains is included in computation of viscoplastic strains. However, if a constant strain-rate test is used as shown in Figure 3.3(b), both plastic and creep strains are included in the computation of the viscoplastic strain increments. Thus, fluidity parameters computed based on constant strain-rate tests may be overly large even though the rate-dependent creep effects are small at low temperatures.

In the extreme case of no creep, the viscoplastic strain component from stress-step tests is zero, while the viscoplastic strain component from a constant strain-rate test which includes the plastic strain can be used to determine Perzyna parameters using the procedure of Desai (2001).

For uniaxial modeling of elastic, viscoelastic, elastoviscoplastic and viscoelastic-viscoplastic behavior, various overlay schemes based on combinations of springs, dashpots and sliders can also be used. Examples[7] are presented in Appendix II.

[7] Overlay equations were derived in an unpublished report, as part of assistantship work at University of Arizona, in 2000.

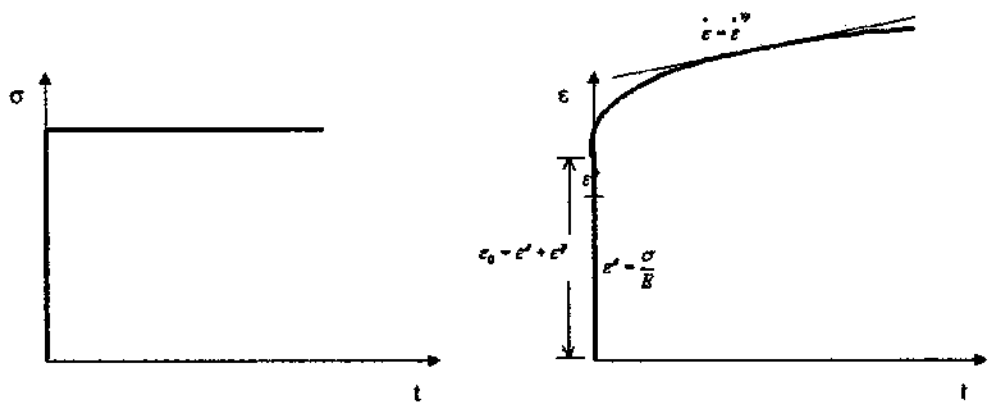

(a) Stress-Step Loading Response

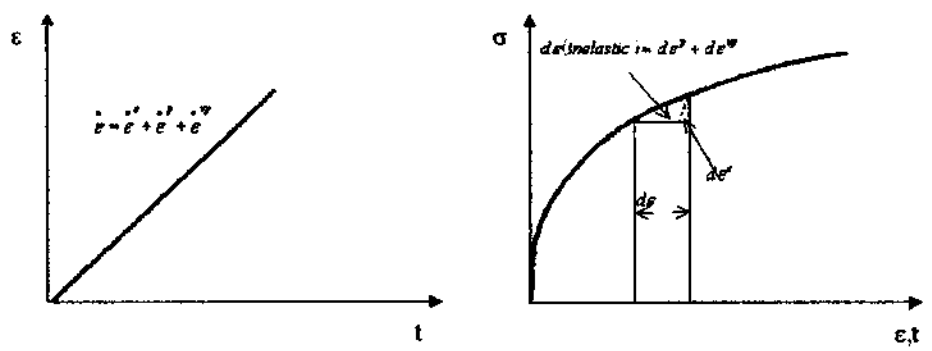

(b) Constant Rate Loading Response

Figure 3.3 Viscoplastic Strain Computations for Different Loadings

3.4 Dissipated-Work based DSC

The formulations developed thus far are relevant to modeling material in the absence of degradation. An approximate dissipated-work based formulation was developed for the Disturbed State Concept of Desai (2001)[8] as an alternative to the strain-based approach for modeling degradation of materials within the constitutive formulation.

The Disturbed State Concept (DSC) of Desai (2001) improves upon the classical damage theory by allowing for the damaged material, which is confined by the intact material, to carry some stress. A hierarchy of deformation modes, including elastic, plastic, viscoelastic and viscoplastic may be modeled as required, along with the growth of damage or healing of a material, and applications have included metals, alloys such as solders, non-metals such as silicon and geo-technical materials including sands, soils, rocks and concrete.

The disturbance function, D, is the fraction of the material in the FA phase. For computation of growth of degradation, the disturbance function may be represented in terms of all internal variables that affect material behavior, such as the elastic strain, the plastic strain trajectory, the dissipated energy, the entropy, number of loading cycles, temperature and impurities, as well as environmental conditions.

---

[8] Expression of the disturbance function in terms of dissipated work was attempted at the suggestion of Desai (1998) as part of research conducted under his guidance.

For simplicity, under elastoplastic or viscoplastic formulations, the form is typically given by

$$D = D_u\left(1 - e^{-A(\xi_D)^Z}\right)$$

...(3.27)

where A and Z are material parameters, D_u is the ultimate disturbance, usually 0.9-1.0, and ξ_d is the plastic or viscoplastic strain trajectory defined as

$$\xi_D = \int \sqrt{de_{ij}^p de_{ij}^p}$$

...(3.28)

where de_{ij}^p are the deviatoric components of the plastic or viscoplastic strain increment.

3.4.1 Dissipated-Work based Disturbance

Formulation of disturbance in terms of work (elastic, plastic and viscoplastic) was attempted at the suggestion of Desai (1998). For simplicity, the disturbance function can be expressed in terms of the dissipated work. As the dissipated work is always positive, the standard equation for disturbance growth, with the plastic strain trajectory replaced by the dissipated work, W^p was suggested by Desai (1998) as

$$D = D_u\left(1 - e^{-A(W^p)^Z}\right)$$

...(3.29)

$$\Rightarrow dD = D_u AZ\left(W^p\right)^{Z-1} e^{-A(W^p)^Z} dW^p = (D_u - D)AZ\left(W^p\right)^{Z-1} dW^p$$

...(3.30)

Derivation of the differential expression inherently assumes that disturbance parameters are not strongly dependent on quantities such as temperature or strain-rate, or that these quantities are held relatively constant.

It is assumed that the observed plastic strain increment equals the RI plastic strain increment. In this case, for a rate-independent material under isothermal loading, using

$$d\underset{\sim}{\varepsilon}^{p} = \frac{\left(\frac{\partial F}{\partial \sigma}\right)\left(\frac{\partial F}{\partial \sigma}\right)^{T} C^{e}}{\left(\frac{\partial F}{\partial \sigma}\right)^{T} C^{e}\left(\frac{\partial F}{\partial \sigma}\right) - \left(\frac{\partial F}{\partial \xi}\right)\left[\left(\frac{\partial \bar{F}}{\partial \sigma}\right)^{T}\left(\frac{\partial \bar{F}}{\partial \sigma}\right)\right]} d\underset{\sim}{\varepsilon} = C^{P}_{ijkl} d\varepsilon_{kl}$$

...(3.31)

provides

$$dD = (D_u - D) A Z (W^{p})^{Z-1} \left((1-D)\sigma^{i}_{ij} + D\sigma^{a}_{ij}\right) C^{P}_{ijkl} d\varepsilon_{kl}$$

...(3.32)

If S denote the current state of strain, then integrating over the strain trajectory,

$$W^{p} = \int_{0}^{S} \sigma^{a}_{ij} d\varepsilon^{p}_{ij} = \int_{0}^{S} \left[(1-D)\sigma^{i}_{ij} + D\sigma^{c}_{ij}\right] d\varepsilon^{p}_{ij}$$

...(3.33)

The final equation is

$$d\sigma_{ij}^{a} = \left(1 - D_u\left(1 - e^{-A\left(W^p\right)^{\gamma}}\right)\right)C_{ijkl}^{i}d\varepsilon_{kl} + D_u\left(1 - e^{-A\left(W^p\right)^{\gamma}}\right)C_{ijkl}^{c}d\varepsilon_{kl}$$
$$+\left(\sigma_{ij}^{c} - \sigma_{ij}^{i}\right)\left(D_u - D\right)A\gamma\left(W^p\right)^{\gamma-1}\left((1-D)\sigma_{mn}^{i} + D\sigma_{mn}^{c}\right)C_{mnkl}^{P}d\varepsilon_{kl}$$

...(3.34)

which is of the form

$$d\sigma_{ij}^{a} = C_{ijkl}^{DSC}d\varepsilon_{kl}$$

...(3.35)

For non-isothermal loading, the plastic strain increment is given by

$$d\underset{\sim}{\varepsilon}^{p} = \frac{\left(\frac{\partial F}{\partial \underset{\sim}{\sigma}}\right)\left(\frac{\partial F}{\partial \underset{\sim}{\sigma}}\right)^{T}\underset{\sim}{C}^{e}}{\left(\frac{\partial F}{\partial \underset{\sim}{\sigma}}\right)^{T}\underset{\sim}{C}^{e}\left(\frac{\partial F}{\partial \underset{\sim}{\sigma}}\right) - \left(\frac{\partial F}{\partial \xi}\right)\left[\left(\frac{\partial F}{\partial \underset{\sim}{\sigma}}\right)^{T}\left(\frac{\partial F}{\partial \underset{\sim}{\sigma}}\right)\right]}d\underset{\sim}{\varepsilon} +$$
$$\frac{\left(\frac{\partial F}{\partial T}\right)\left(\frac{\partial F}{\partial \underset{\sim}{\sigma}}\right) + \left(\frac{\partial F}{\partial T}\right)\underset{\sim}{C}^{e}\left(\alpha \underset{\sim}{I}_{0} - \left(\underset{\sim}{C}^{e}\right)^{-1}\frac{\partial \underset{\sim}{C}^{e}}{\partial T}\left(\underset{\sim}{C}^{e}\right)^{-1}\underset{\sim}{\sigma}\right)\left(\frac{\partial F}{\partial \underset{\sim}{\sigma}}\right)}{\left(\frac{\partial F}{\partial \underset{\sim}{\sigma}}\right)^{T}\underset{\sim}{C}^{e}\left(\frac{\partial F}{\partial \underset{\sim}{\sigma}}\right) - \left(\frac{\partial F}{\partial \xi}\right)\left[\left(\frac{\partial \bar{F}}{\partial \underset{\sim}{\sigma}}\right)^{T}\left(\frac{\partial \bar{F}}{\partial \underset{\sim}{\sigma}}\right)\right]}dT$$
$$= C_{ijkl}^{P}d\varepsilon_{kl} + C_{ij}^{T}dT$$

...(3.36)

For temperature independent DSC parameters, Eqs. (3.30) and (3.36) provide

$$dD = (D_u - D)AZ(W^p)^{Z-1}\left((1-D)\sigma_{ij}^i + D\sigma_{ij}^a\right)\left(C_{ijkl}^P d\varepsilon_{kl} + C_{ij}^T dT\right)$$

...(3.37)

which provides

$$\begin{aligned} d\sigma_{ij}^a = &\left(1 - D_u\left(1 - e^{-A(W^p)^Z}\right)\right)\left[C_{ijkl}^i d\varepsilon_{kl} + C_{ij}^{iT} dT\right] + D_u\left(1 - e^{-A(W^p)^Z}\right)\left[C_{ijkl}^c d\varepsilon_{kl} + C_{ij}^{cT} dT\right] \\ &+ \left(\sigma_{ij}^c - \sigma_{ij}^i\right)(D_u - D)AZ(W^p)^{Z-1}\left((1-D)\sigma_{mn}^i + D\sigma_{mn}^c\right)C_{mnkl}^P d\varepsilon_{kl} \\ &+ \left(\sigma_{ij}^c - \sigma_{ij}^i\right)(D_u - D)AZ(W^p)^{Z-1}\left((1-D)\sigma_{mn}^i + D\sigma_{mn}^c\right)C_{mn}^T dT \end{aligned}$$

...(3.38)

expressible as

$$d\sigma_{ij}^a = C_{ijkl}^{DSC} d\varepsilon_{kl} + Y_{ij}^T dT$$

...(3.39)

Work-based disturbance parameters may be obtained in a manner identical to the standard procedure used for the deviatoric plastic strain trajectory based formulation, except that W^p is substituted for ξ_d.

An alternative formulation may be based upon the observation that in the standard strain-based DSC formulation, disturbance growth may be modeled in terms of the RI plastic strain trajectory instead of the observed plastic strain trajectory. Similarly, it may be postulated that

$$D = D_u\left(1 - e^{-A\left(W^p\right)^Z}\right)$$

...(3.40)

Here, $(W^p)^i$ is the density of work dissipated in the RI phase.

$$\left(dW^p\right) = \sigma_{ij}^i\left(d\varepsilon_{ij}^p\right)$$

...(3.41)

The incremental stress-strain relationships for this assumption may be developed via a procedure similar to that for the assumption that observed plastic strains and RI plastic strains are equal.

3.4.2 Limitations

If disturbance parameters are strongly dependent on loading, clarification is required as to whether the disturbance is to be expressed in terms of Eq. (3.29), or if only the differential form of the equation, Eq. (3.30) is to be used directly as the fundamental relationship. If Eq. (3.29) is the fundamental relationship, variation of parameters requires a generalization of the incremental equation as was the case for incremental elastic equations. Further, disturbance could decrease with change in loading conditions due to variation in parameters. These issues are also relevant for strain-based DSC.

Another approximation is introduced due to the assumption regarding unloading and elastic reloading, where based on the physical interpretation of the RI and FA phases acting in parallel and sharing the load, the unloading and reloading modulus may be expected to decrease with increasing damage. However, in order to match observed behavior, a special assumption is required for unloading (Figure 3.4). This further leads to inconsistencies in the computation of work dissipated, as the total dissipated work does not match the sum of the work dissipated in the RI and FA phases (Appendix III).

While the definition of unloading and reloading is precise for uniaxial deformations, an unambiguous definition is required for multiaxial stress states wherein certain components of the stress may be increasing while others are decreasing. Essentially, what is required is a function that incorporates all components of stress and provides a single value based on which the stress increment may be classified as loading, unloading or reloading.

If the RI material is modeled as elastoplastic, the plastic yield function may be used to define unloading and reloading in terms of the RI stresses. However, this would not be feasible if the RI material is assumed to be elastic. Thus, the flexibility provided in DSC for the assumption of the RI constitutive behavior may require consideration. A Gurson-type formulation explicitly incorporating work-balance may be considered.

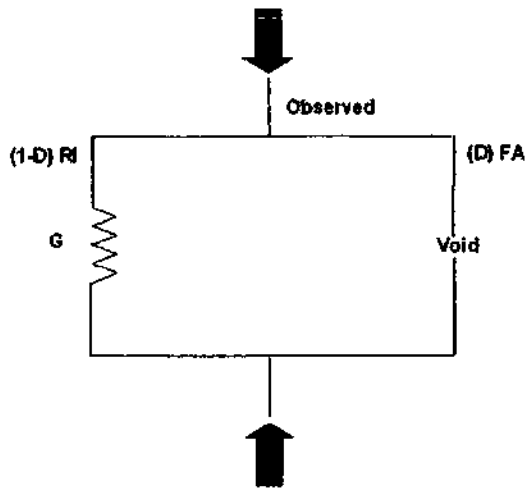

(a) Overlay Schematic of DSC Phases

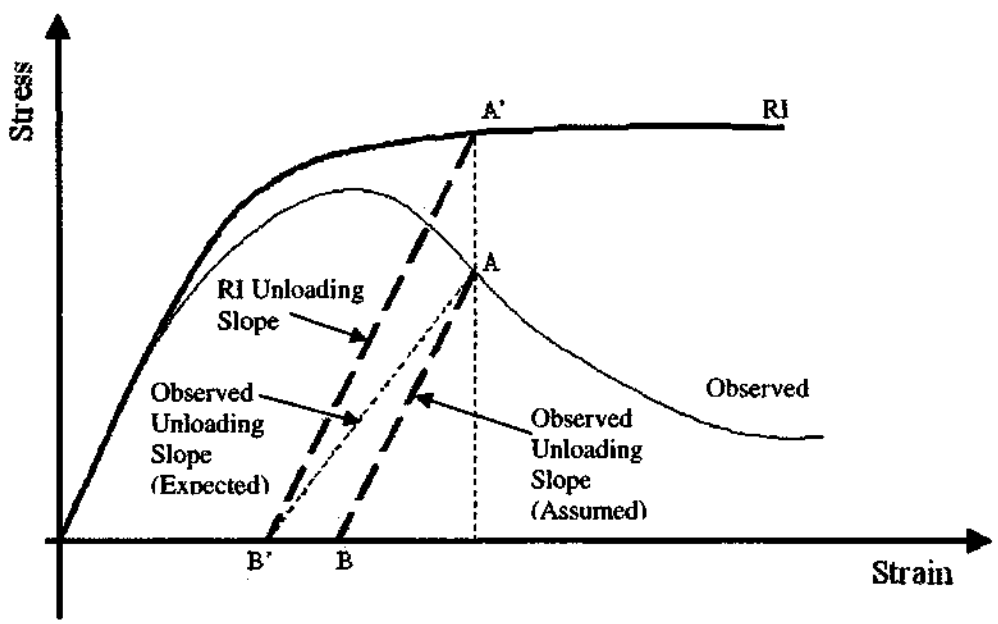

(b) Stress-Strain Curve

Figure 3.4 Unloading Behavior

4. PLASTICITY YIELD FUNCTION

A yield function is proposed for elastoplastic and Perzyna viscoplastic modeling so as to obtain reasonable material response to thermal loads and to simulate continuous yield under both tensile and compressive loads.

4.1 Yield Function

The yield function (Figure 4.1) is given by

$$F = \frac{J_{2D}}{p_a^2} + \gamma\left[\left(1-\alpha\left(\frac{|J_1|}{p_a}\right)^n - \alpha\left(\frac{J_1+3R}{p_a}\right)^q\right)(1-\beta S_r)^{-0.5} \cong 0\right] \qquad \ldots(4.1)$$

where the parameters γ, β, q and R are parameters relevant to the final failure surface as in the HiSS-δ_0 yield function and S_r is the stress ratio. Unlike HiSS-δ_0, the parameter n does not correspond to the phase change parameter, and α, the hardening parameter, is zero when the plastic strain trajectory is zero, and reaches an ultimate value of one when the plastic strain trajectory tends to infinity (Figure 4.2).

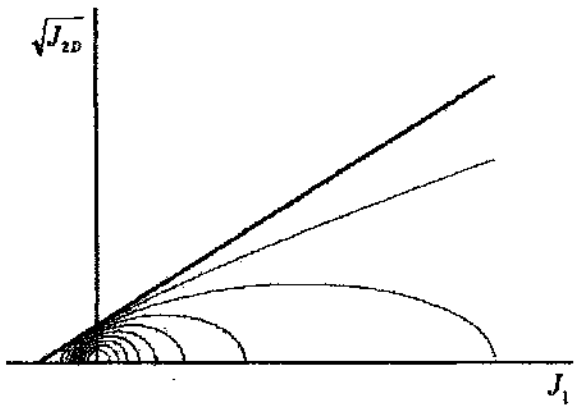

(a) Straight Ultimate Envelop

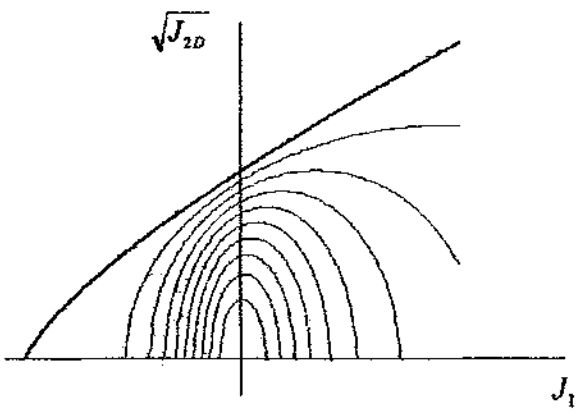

(b) Curved Ultimate Envelop

Figure 4.1 Proposed Yield Function

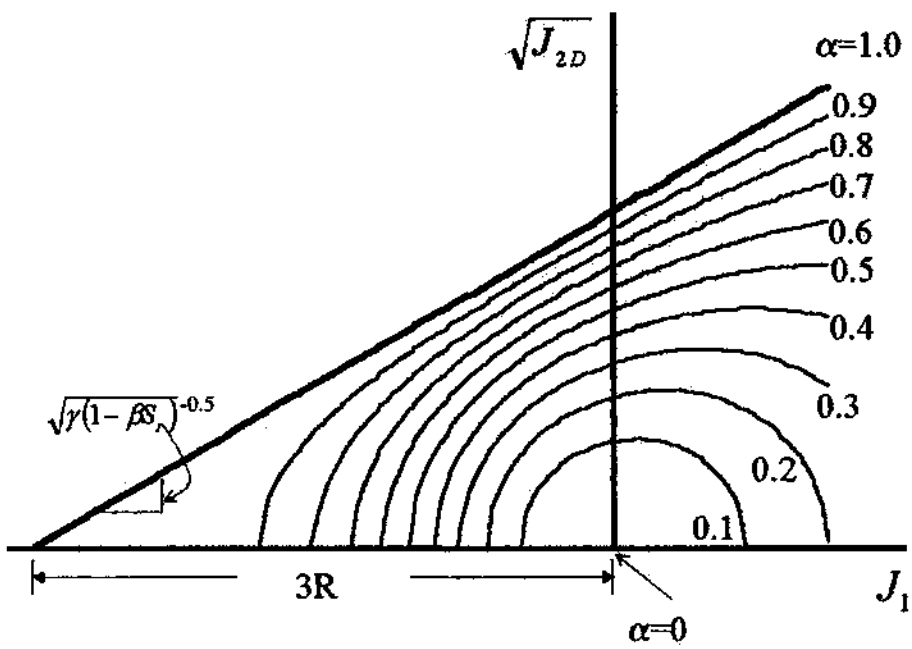

Figure 4.2 Hardening Parameter

4.1.1 Hardening Function

Hardening is assumed to be a function of the plastic strain trajectory, ξ. Since α varies from 0 at $\xi = 0$ to 1 as $\xi \rightarrow \infty$, a modification of the hyperbolic function suggested by Li (2002)

$$\alpha = \left(\frac{\xi^{\eta 1}}{a1 + \xi^{\eta 1}} \right)^2 \qquad \ldots(4.2)$$

was used. In general, the power of 2 may be replaced by some material parameter, θ.

4.2 Parameter Determination

The procedure for determination of the final yield surface parameters γ, β, R and q is the same as the procedure for the HiSS-δ_0 function. The existing procedure of Desai (2001) is sufficient for q = 2. The final yield surface for any stress path, i, is

$$\sqrt{J_{2D}} = J_1 \left[\sqrt{\gamma (1 - \beta S_{ri})^{-0.5}} \right] + 3R \left[\sqrt{\gamma (1 - \beta S_{ri})^{-0.5}} \right] = C_{1i} J_1 + C_{2i} \qquad \ldots(4.3)$$

Thus, if data regarding the final yield surface is available at more than one value of the mean pressure, for two or more stress paths with different values of S_r, the various parameters may be computed using the coefficients for the best-fit line for the stress

paths. For instance, for any stress path *i*, the value of R corresponding to the stress path may be obtained using

$$R = \frac{1}{3}\frac{C_{2i}}{C_{1i}}$$

...(4.4)

And if *i* and *j* be two stress paths,

$$\beta = \frac{\left(C_{1i}/C_{1j}\right)^q - 1}{S_{rj}\left(C_{1i}/C_{1j}\right)^q - S_{ri}}$$

...(4.5)

Finally, for each stress path *i*,

$$\gamma = \frac{C_{1i}}{\sqrt{\left(1-\beta S_{ri}\right)^{-0.5}}}$$

...(4.6)

However, if q cannot be assumed equal to two, the final yield surface equation is

$$\frac{J_{2D}}{p_a^2} = \gamma\left(\frac{J_1 + 3R}{p_a}\right)^q \left(1-\beta S_{ri}\right)^{-0.5}$$

...(4.7)

Since 3R is not known a priori, it is not possible to plot points for the final yield surface expressed in terms of coefficients that can be obtained from a best-fit curve.

An approximate procedure was developed[9] whereby for each stress path, the two points with the minimum algebraic value of the mean pressure, or J_1 are selected. Assuming the yield surface to be a straight line passing through these points, R and β may be obtained approximately using Eqs. (4.4) and (4.5). Next γ and q may be obtained using Eq. (4.7).

Hardening parameters are determined from simple shear tests at zero confining pressure. The hardening parameter α may be computed using

$$\alpha = \frac{J_{2D}}{p_a^2}\left[\frac{1}{\gamma}\right]\left(\frac{3R}{p_a}\right)^{-q} = \frac{\tau^2}{p_a^2}\left[\frac{1}{\gamma}\right]\left(\frac{3R}{p_a}\right)^{-q} \qquad \ldots(4.8)$$

The deviatoric strain component may be computed from shear stress, τ, vs. shear strain, γ tests. The volumetric plastic strain increment ξ_v may be computed for simple shear using

$$\frac{d\xi_v}{d\xi_d} = \frac{3\dfrac{\partial F}{\partial J_1}}{\dfrac{\partial F}{\partial J_{2D}}\dfrac{\partial J_{2D}}{\partial \tau}} = \frac{3\tau q}{2(3R)} \qquad \ldots(4.9)$$

which has a maximum value at the ultimate stress, τ_{ult}, given by

$$d\xi_v = \frac{3\tau_{ult} q}{2(3R)} d\xi_d \qquad \ldots(4.10)$$

[9] The procedure for $q \neq 2$ was developed for HiSS-δ_0 parameters based on discussions with Desai (2001).

For q = 2

$$\frac{\tau_{ult}}{3R} = \sqrt{\gamma}$$

...(4.11)

and thus

$$\left(\frac{d\xi_v}{d\xi_d}\right)_{max} = 3\sqrt{\gamma}$$

...(4.12)

as expected. For materials such as metals with q = 2 and small γ, the volumetric plastic strain during a simple shear test at zero confining pressure may be ignored. Else, the total increment of the plastic strain trajectory can be computed using

$$d\xi = d\xi_d + d\xi_v = d\xi_d\left(1 + \frac{3\pi q}{2(3R)}\right)$$

...(4.13)

Hardening parameters may be obtained using a best-fit line for the equation

$$\ln\left(\frac{1}{\sqrt{\alpha}} - 1\right) = \ln(a1) - \eta 1 \ln(\xi)$$

...(4.14)

while for computation of n, Eq, (4.1) is rearranged to provide

$$\left(\frac{|J_1|}{p_a}\right)^n = \frac{1}{(1-\alpha)}\left[\alpha\left(\frac{J_1 + 3R}{p_a}\right)^q - \frac{J_{2D}}{\gamma(1-\beta S_r)^{-0.5} p_a^2}\right]$$

...(4.15)

Taking the natural log of both sides, and after minor rearrangement of terms, for any test data-point at which J_1 is not zero, n may be determined using

$$n = \frac{\ln\left\{\frac{1}{(1-\alpha)}\left[\alpha\left(\frac{J_1+3R}{p_a}\right)^q - \frac{J_{2D}}{\gamma(1-\beta S_r)^{-0.5}\, p_a^2}\right]\right\}}{\ln\left(\frac{|J_1|}{p_a}\right)} \qquad \ldots(4.16)$$

4.2.1 Convexity Constraints

The ultimate yield surface for the model is the same as the HiSS-δ_0 ultimate yield surface, and so are the limitations on the ultimate parameters β and γ. The convexity condition of Eq. (3.15) can be shown to be satisfied for

$$n > 2 \text{ if } q = 2 \ (3R \neq 0) \qquad \ldots(4.17)$$

which is appropriate for solder.

4.3 Advantages of Proposed Yield Function

Several simplified schemes were developed to ameliorate the issues regarding HiSS-δ_0 yield function, which arise primarily due to the value of the initial plastic strain trajectory being nonzero.

For the state of zero stress, the HiSS-δ_0 function provides[10]

$$\xi_0 = \left[\frac{a1}{\gamma}\left(\frac{3R}{p_a}\right)^{n-2}\right]^{\frac{1}{\eta 1}} \neq 0 \qquad \ldots(4.18)$$

which is inconsistent with the expectation that in the absence of prior loading, the material has not undergone any yielding. Surfaces with $\xi < \xi_0$ do not satisfy Eq. (4.17).

4.3.1 Parameter Determination

If the HiSS-δ_0 model is used as a continuous yield model, the nonzero ξ_0 implies that the incremental stress-strain relationship for the HiSS-δ_0 yield function is not elastic at zero stress. While this is inconsistent with the assumption that the initial stress-strain slope is the elastic modulus, the difference for solder, in practice is not significant (Li, 2002). The proposed yield function provides an elastic constitutive matrix in the limit of initial loading (Appendix IV).

The inconsistency due to nonzero ξ_0 is more severe for determination of hardening parameters. The existing procedure for computation of a1 and $\eta 1$ requires plotting $\ln(\alpha)$ vs. $\ln(\xi)$. This implicitly assumes that ξ_0 to be zero (Appendix IV.1.1) for computing ξ, as only incremental values are obtained based on test data-points. Since ξ_0 cannot be

[10] It is assumed that $1-\beta S_r \neq 0$, even when $S_r = 0/0$ and is undefined. This is reasonable as for all possible stress states other than at the state of zero stress, S_r can be shown to vary between -1 to +1 (Li, 2002) while β is always less than 0.755923 from convexity considerations for the yield surface.

determined before a1 and $\eta 1$ are known, while determination of a1 and $\eta 1$ requires ξ_0, an iterative procedure was developed to provide consistent values of a1, $\eta 1$ and ξ_0.

1. assume ξ_0 to be zero and obtain parameters a1 and $\eta 1$ using the existing procedure
2. recompute ξ_0 using the hardening parameters
3. recompute a1 and $\eta 1$, incorporating the computed ξ_0 in ξ calculations
4. repeat steps 2 and 3 till convergence is achieved

For the proposed yield function, the initial plastic strain trajectory is zero.

4.3.2 Continuous Yield

The HiSS-δ_0 does not provide for continuous yield under tensile loads if compressive stresses are assumed positive (Figure 4.3, Appendix IV.1.3). Reversing the signs creates the same problem for compressive loads while introducing additional issues such as increasing shear strength with increasing tensile mean pressure. Since the same material can be loaded either in compression or tension, a slight modification of the HiSS-δ_0 equation as

$$F = \frac{J_{2D}}{p_a^2} - \left(-\alpha \left(\frac{|J_1| + 3R}{p_a} \right)^n + \gamma \left(\frac{|J_1| + 3R}{p_a} \right)^q \right) (1 - \beta S_r)^{-0.5} \qquad \ldots(4.19)$$

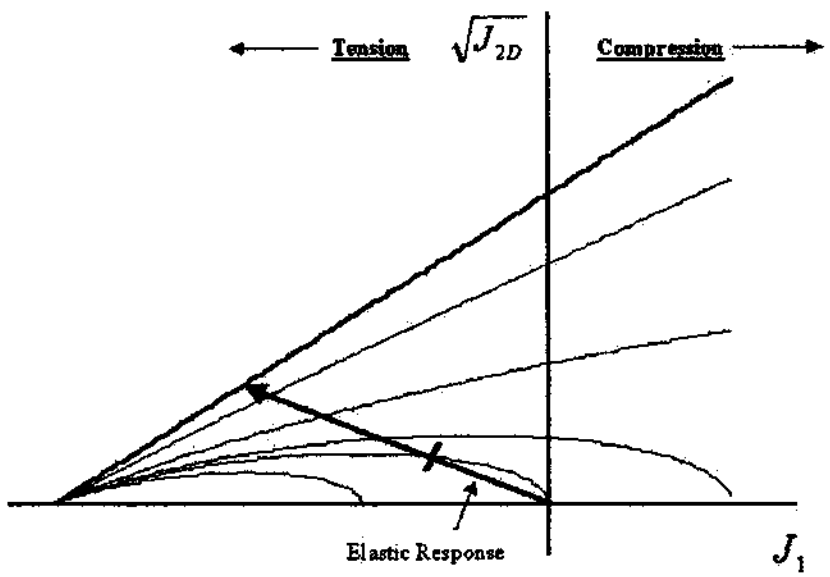

(a) Uniaxial Tensile Loading under Standard Sign Convention

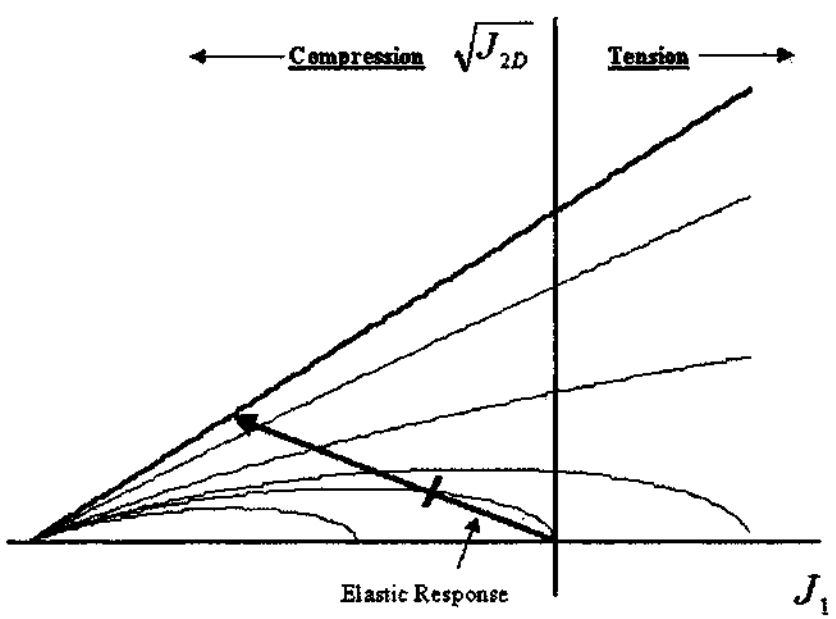

(b) Uniaxial Compression under Reversed Sign Convention

Figure 4.3 Elastic Response under Uniaxial Loading

with yield surfaces as shown in Figure 4.4 was considered. However, the material never fails under either tensile or compressive hydrostatic loads and ultimate failure is delayed with an increasing tensile mean pressure, which is not reasonable. The proposed yield function of Eq. (4.1) provides for continuous yielding under both tension and compression, while maintaining a final yield surface that is reasonable in that hydrostatic tensile forces lead to reduction in shear strength while compressive hydrostatic forces strengthen the material.

4.3.3 Thermal Loading

The HiSS-δ_0 model provides a nonzero linear plastic strain increment under unconstrained heating or cooling (Appendix IV.1.2) due to the temperature-dependence of the initial plastic strain trajectory (Figure 4.5). The proposed yield function provides a temperature-independent value of zero for the plastic strain trajectory, thereby avoiding spurious plastic strains (Appendix IV.2).

The problem of spurious plastic strains under unconstrained heating and cooling for HiSS-δ_0 is especially crucial for materials such as solder, as thermal mismatch is often the driving force for generation of stresses and strains. The variable initial value of the plastic strain trajectory results in a changing datum for measuring plastic strain increments, and thus, plastic strain increments computed even in the presence of applied stresses must be treated with caution. Further, the issue remains valid under the Perzyna

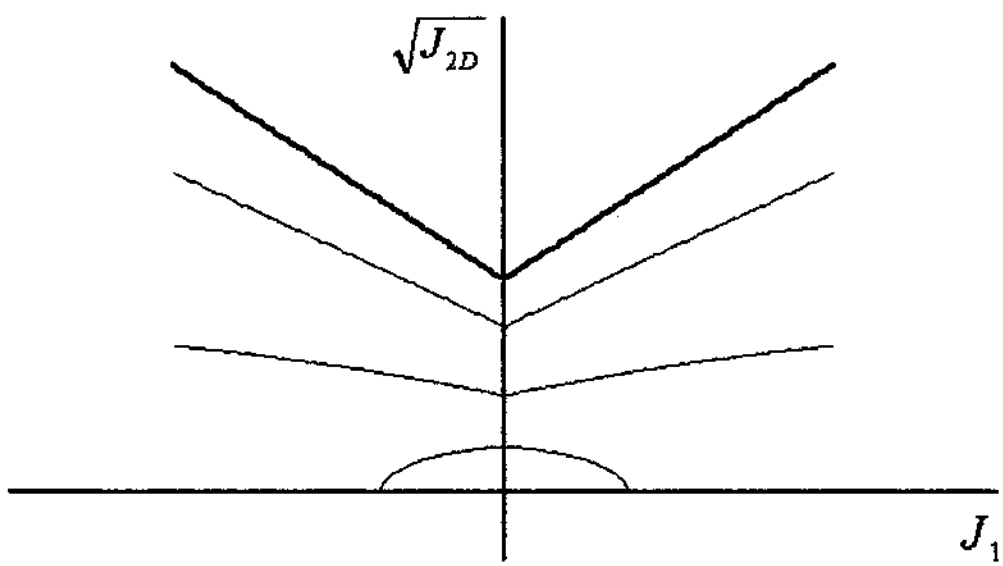

Figure 4.4 Symmetric Yield Surfaces for Tension and Compression

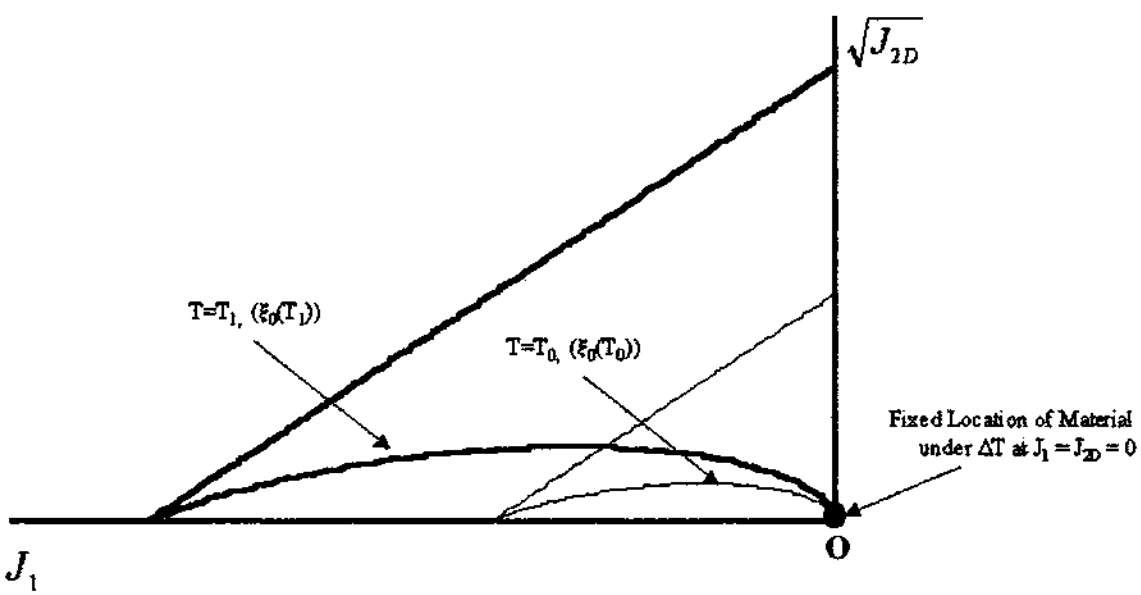

Figure 4.5 Initial Yield Surfaces at Two Temperatures

viscoplastic scheme. Li (2002) has provided a simplified solution to the problem of temperature-dependent initial plastic strain trajectory based on the iterative scheme for determination of hardening parameters developed here.

4.4 Perzyna Viscoplastic Analyses

For both the proposed yield function and HiSS-δ_0, which have a bounded value of the ultimate shear stress for a given mean pressure, it can be shown that for a simple shear test at constant strain-rate, $\dot{\gamma}$ after a sufficiently long time as t $\rightarrow\infty$ if the stress reaches an asymptotic value τ_u, corresponding to the shear rate, the governing equation from the Perzyna formulation provides (Appendix V)

$$\Gamma\left\langle\frac{\tau_u^2}{p_a^2}-\gamma_s\left(\frac{3R_s}{p_a}\right)^2\right\rangle^N\left(\frac{2\tau_u}{p_a^2}\right)=\dot{\gamma} \qquad \ldots(4.20)$$

where the subscript s refers to the static yield surface.Thus, if such shear tests are available at two or more strain rates, the parameters Γ and N can be obtained from a best-fit line for the plot corresponding to

$$N\ln\left\langle\frac{\tau_u^2}{p_a^2}-\gamma_s\left(\frac{9R_s^2}{p_a^2}\right)\right\rangle+\ln\Gamma=\ln\left(\frac{\dot{\gamma}\,p_a^2}{2\tau_u}\right) \qquad \ldots(4.21)$$

5. THERMOMECHANICAL MODEL

This chapter presents a new approach to thermomechanical constitutive modeling based on the concept of superposition of hypothetical phases that represent asymptotic states of material.

5.1 Motivation

The presence of loading-dependent parameters for material modeling may indicate a scope for generalization of the constitutive model used. For instance the elastoplastic scheme requires rate-dependent elastic and plasticity material parameters for solder modeling as it is not inherently capable of predicting creep behavior. Explicit incorporation of viscoplastic deformation modes removes the need for rate-dependent material parameters. Constitutive models used for solder modeling typically utilize temperature-dependent material parameters.

Use of loading-dependent parameters also complicates the incremental constitutive formulation. The strain-rate dependent elastoplastic formulation requires additional terms in the incremental elastic stress-strain relationship and the consistency condition for

plastic strains, making the incremental elastoplastic matrix cumbersome. Measurement of material parameters under various loading conditions may be difficult. At high temperatures, mechanical test devices typically provide overly low values of solder elastic parameters. Error in measurement of elastic parameters may carry over for computation of subsequently determined plasticity or viscoplastic parameters. Extrapolation of parameters may be especially difficult when the limitations of the constitutive formulation result in anomalous behavior of parameters with temperature. For instance the fluidity parameter at low temperatures for the Perzyna formulation may be anomalously high if obtained from constant strain-rate curves.

Continuum damage and DSC have provided one approach for successfully incorporating complex material behavior including degradation into the constitutive formulation in a simple manner. The fundamental assumption behind these approaches is that material behavior may be explained as a weighted-superposition of the behavior of two phases which represent asymptotic states of the material, each phase having a relatively simple constitutive equation. The apparent variation in material response to loading is handled by the variation of the relative ratios of the material phases. The traditional approach and the superposition-of-phases approach are depicted in Figure 5.1.

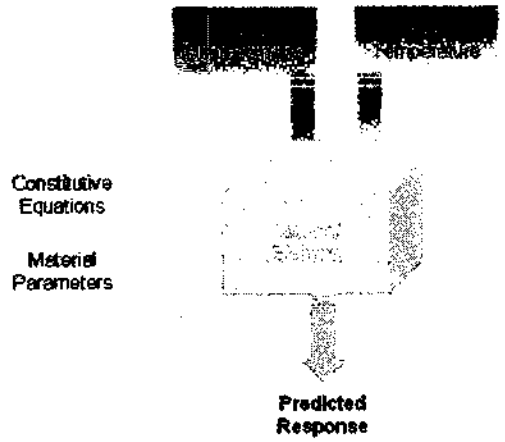

(a) Traditional Material Modeling Approach

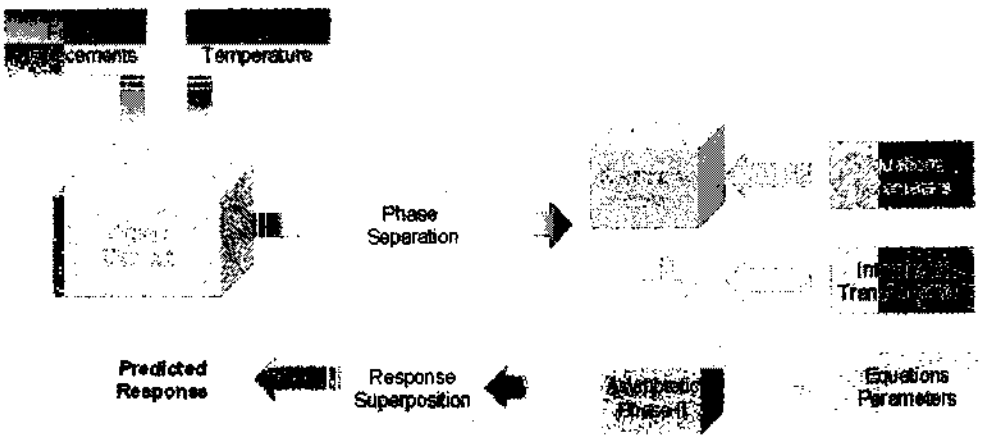

(b) Superposition of Phases Approach

Figure 5.1 Conventional vs. Damage Approach

Damage approaches do not require modeling of the detailed distribution of microcracks and the behavior of individual cracks. The effect of such discontinuities may be assumed to be smeared over a region, thereby maintaining the continuum approach. These approaches have typically considered mechanical loading for defining the asymptotic phases and are based on quantities such as the plastic strain trajectory or dissipated work.

A thermomechanical constitutive model for materials in terms of asymptotic phase behavior that incorporates both temperature and deformation is developed based on the approach of phase superposition. Material behavior is modeled in terms of simplified conceptual models of asymptotic material phases. The phases are separated in a manner so as to ensure energy balance.

The approach is based on temperature-independent material parameters. Variation of material parameters such as the coefficient of thermal expansion, the bulk modulus and the shear modulus with temperature may be computed based on the stress-strain-temperature equations of the model in terms of the basic definitions of these parameters.

5.2 Asymptotic Behavior

The simplistic models of material behavior described herein are used only as guides towards obtaining models for simplified phase behavior. Detailed physical interpretations are not intended and are actually to be avoided here as the approach of superposition would be useful only if it could obviate the need for detailed considerations. Once the final equations are obtained they may be treated as purely empirical relationships, with their validity being determined by the predictions.

Considering a simplistic view of the material comprised of a regular array of atoms bound together by interatomic forces, the internal energy may be considered as the sum of the potential energy due to interatomic interactions and the vibratory kinetic energy due to thermal effects. For nonmagnetic materials[11], the change in the internal energy is the sum of the changes in the thermal energy and the elastic energy (Reed and Clark, 1983).

The internal energy itself cannot be divided into thermal and elastic components. Both the datum of zero elastic energy which is the volume at the stress-free state, and the elastic modulii which determine the elastic energy stored for the given strains, depend on the temperature.

---

[11] For magnetic materials an additional term corresponding to the magnetization must be considered (Reed and Clark, 1983).

At high temperatures and large interatomic spacing, kinetic energy governs behavior, while at low temperatures and at small interatomic spacing near the equilibrium value of minimum potential energy, potential energy increments govern material response to deformation. This permits definition of two asymptotic phases, which are termed here the vapor phase (v) and the condensed phase (c).

5.2.1 Vapor Phase

The vapor phase is assumed to be comprised of the same atoms as the observed material, but with no interatomic forces of attraction. This phase only possesses kinetic energy, K. The pressure applied by this phase is assumed to be given by the relationship for an ideal gas,

$$PV = nRT \qquad \ldots(5.1)$$

where P is the pressure, V the volume of the vapor phase, n the number of moles, R is the universal gas constant, and T is the absolute temperature. For monatomic gases, the kinetic energy for n moles of a gas at temperature T is given by

$$K = \frac{3}{2}nRT \qquad \ldots(5.2)$$

Eqs. (5.1) and (5.2) imply

$$P = \frac{2}{3}\frac{K}{V}$$

...(5.3)

5.2.2 Condensed Phase

Consider a material element in the limiting condition of 0 K in the stress-free state. At this state the kinetic energy is zero and the potential energy is a minimum. Assuming the bulk modulus to be independent of the strain, for small deformations around this state the material constitutive equation may be written as

$$\frac{\sigma_{ii}}{3} = B_0 \varepsilon_{ii}$$

...(5.4)

where B_0 is the bulk modulus at 0K (Appendix VI.1).

5.3 Thermoelastic Volumetric Behavior

Consider a unit volume of a material at 0K in the stress-free state. This is defined to be the state of zero configuration strain (ε^{tc}). Let the energy at this state be given by

$$E = -\frac{U_0}{\eta}$$

...(5.5)

where U_0 is the enthalpy of sublimation and η is an empirical factor (Appendix VI.1).

Let the material be loaded to some state of absolute temperature, T, and volumetric deformation equivalent to the strain ε^{te}_{v} relative to the state of zero configuration strain. The strain includes any volumetric deformation due to thermal expansion. The small-strain approximation is assumed to hold for simplicity.

In order to separate the effects of configuration and kinetic energy, a hypothetical path may be chosen wherein the material is held at 0K, and volumetric strains are imposed first. Next, the material is rigidly held at constant volume, and is heated to temperature T.

For deformation at 0K no heat is added to the material. The total work done equals the change in configuration energy. At the end of this stage, the stress is given by Eq. (5.4) and the configuration energy density in the material (U), which equals the total energy density (E), is

$$E = U = -\frac{U_0}{\eta} + \frac{1}{2} B \left(\varepsilon_v^{te}\right)^2 \qquad \ldots(5.6)$$

If the material is now held at constant volume and heated to temperature T, the heat input, assuming the specific heat to be independent of deformation is

$$Q = \int_0^T N_0 C_v(T) dT$$

...(5.7)

where $C_v(T)$ is the molar specific heat, and N_0 is the number of moles of the material, per unit volume at 0K.

Since the configuration of atoms does not change as no deformation is permitted, it is assumed that the heat input goes towards increasing the vibratory energy of the atoms, and thus, the kinetic energy per unit volume, K(T), in the material is given by

$$K(T) = Q = \int_0^T N_0 C_v(T) dT$$

...(5.8)

The specific heat may be computed based on the Debye expression (Cottrell, 1957)

$$C_v = \frac{36R}{x^3} \int_0^x \frac{y^3}{e^y - 1} dy - \frac{9xR}{e^x - 1}$$

...(5.9)

where R is the universal gas constant and $x = T_D/T$, with T_D being the Debye temperature of the material. The expression can be evaluated numerically (Appendix VI.2), assuming the Debye temperature for a material to be temperature-independent.

5.3.1 Separation of Phases

If U(ε) be the total configuration energy density given by Eq. (5.6), and K(T) be the kinetic energy density as per Eq. (5.8), the material is assumed to behave as a superposition of a condensed phase and a vapor phase, with the fraction of the vapor phase, E_F, given by

$$E_F = \frac{K}{K - U} \qquad \ldots(5.10)$$

with the observed stress assumed to be given by

$$\sigma_{ij} = (1 - E_F)\sigma_{ij}^c + E_F \sigma_{ij}^v \qquad \ldots(5.11)$$

If K = 0, the material consists of the condensed phase only as expected. As K increases, so does E_F, approaching 1 as K tends to infinity. This shows that at extremely high temperatures, the material will behave like a gas. Finally, as the strain increases, U becomes less negative, thereby increasing E_F. When U becomes zero, the material consists of the vapor phase only, confirming that when the atoms are far enough so that their interaction can be ignored, the material will behave like a gas. At intermediate values of U and K, the material acts as a superposition of the two phases.

The stress in the condensed phase may be obtained from Eq. (5.4), with the bulk modulus being the bulk modulus at 0K and the strain being the volumetric strain including the

thermally generated strain. The vapor phase is constrained within the volume of the solid, and is not the same as the presence of a small amount of vapor which leads to partial vapor pressure even for solids. For computing the stress in the vapor phase based on Eq. (5.3), it is noted that since the vapor phase comprises only a fraction E_F of the total material, and further if ρ_f be the packing fraction, based on a first order correction for gases with atoms of finite volume, the free volume of the vapor phase, V^v, may be given by

$$V^v = E_F\left(1 - p_f + \varepsilon_{ii}^{te}\right) \qquad \ldots(5.12)$$

Thus for the vapor phase, v, Eq. (5.3) provides

$$\sigma_{ij}^v = -\delta_{ij}\frac{2}{3}\frac{K}{E_f\left(1-\rho_f+\varepsilon_{ii}^{te}\right)} \qquad \ldots(5.13)$$

The observed stress-strain relationship for volumetric deformations is then given by

$$\frac{\sigma_{ii}}{3} = (1-E_F)B_0\varepsilon_{kk}^{te} - \frac{2}{3}\frac{K}{\left(1-\rho_f+\varepsilon_{kk}^{te}\right)} \qquad \ldots(5.14)$$

5.3.2 Temperature Dependence of Parameters

Eq. (5.14) can be used to predict the thermal coefficient of expansion, as well as the variation in material parameters with temperature. Consider a material in the stress-free state at 0K, which is heated through a range of temperatures in an unconstrained manner, or under atmospheric pressure, p^a, providing

$$-p^a = (1-E_F)B_0\varepsilon_{kk}^{te} - \delta_{ij}\frac{2}{3}\frac{K}{(1-\rho_f+\varepsilon_{kk}^{te})} \qquad \ldots(5.15)$$

$$\Rightarrow \qquad \varepsilon_{kk}^{te} = \frac{-p^a + \frac{2}{3}\frac{K}{(1-p_f+\varepsilon_{kk}^{te})}}{(1-E_F)B_0} \qquad \ldots(5.16)$$

Assuming that the empirical factor η is known, Eq. (5.16) can be solved in an iterative fashion, to obtain the volumetric strain as a function of temperature. A simple explicit scheme, where the temperature values at which computations are carried out are represented by T_i, i = 1, ... provides

$$\varepsilon_{ii}^{te}|_{T_i} \approx \frac{-p^a + \frac{2}{3}\frac{K|_{T_i}}{(1-p_f+\varepsilon_{ii}^{te}|_{T_{i-1}})}}{(1-E_F|_{T_{i-1}})B_0} \qquad \ldots(5.17)$$

The initial conditions are

$$\varepsilon_{ii}^{te}(T=0)=\frac{-p^a}{B_0}$$

...(5.18)

$$K(0)=0$$

...(5.19)

$$U(0)=-\frac{U_0}{\eta}+\frac{1}{2}\frac{(p^a)^2}{B_0}$$

...(5.20)

$$\Rightarrow E_F(0)=0$$

...(5.21)

5.3.2.1 Coefficient of Thermal Expansion

Once the volumetric strain is known as a function of the temperature, the coefficient of linear thermal expansion may be calculated as

$$\alpha=\frac{1}{3}\left(\frac{1}{1+\varepsilon_{ii}^{te}}\right)\frac{d\varepsilon_{ii}^{te}}{dT}$$

...(5.22)

or, in a numerical fashion as

$$\alpha|_{T_i}\approx\frac{1}{3}\left(\frac{1}{1+\varepsilon_{ii}^{te}|_{T_i}}\right)\frac{\varepsilon_{ii}^{te}|_{T_{i+1}}-\varepsilon_{ii}^{te}|_{T_{i-1}}}{T_{i+1}-T_{i-1}}$$

...(5.23)

5.3.2.2 Bulk Modulus

The temperature-dependent, isothermal bulk modulus, B(T), for a material is defined as

$$B(T) = -V \frac{\partial p}{\partial V}\Big|_T$$

...(5.24)

Isothermal conditions imply that K is a constant, and E_F depends solely on the potential energy. Eq. (5.21) then provides

$$-dp^a = \left[(1 - E_F)B - \frac{\partial E_F}{\partial U}\frac{\partial U}{\partial \varepsilon_{ii}^{te}} B\varepsilon_{ii}^{te} - \frac{2}{3}\frac{K}{(1 - p_f + \varepsilon_{ii}^{te})^2} \right] d\varepsilon_{ii}^{te}$$

...(5.25)

which implies

$$-\frac{dp^a}{d\varepsilon_{ii}^{te}} = \left[(1 - E_F)B - \frac{K}{(K - U)^2}(B\varepsilon_{ii}^{te})^2 + \frac{2}{3}\frac{K}{(1 - p_f + \varepsilon_{ii}^{te})^2} \right]$$

...(5.26)

as

$$\frac{\partial E_F}{\partial U} = -\frac{K}{(K - U)^2}\frac{\partial (K - U)}{\partial U} = \frac{K}{(K - U)^2}$$

...(5.27)

Absolute strains in the model are measured relative to the dimensions at 0 K. For the small strain assumption, with V_0 being the volume of an element at 0 K

$$d\varepsilon_{kk}^{te} = \frac{dV}{V_0}$$

...(5.28)

and

$$V = V_0\left(1+\varepsilon_{kk}^{te}\right)$$

...(5.29)

which provides

$$B(T) \approx \left(1+\varepsilon_{kk}^{te}\right)\left[\left(1-E_F\right)B - \frac{K}{(K-U)^2}\left(B\varepsilon_{kk}^{te}\right)^2 + \frac{2}{3}\frac{K}{\left(1-p_f+\varepsilon_{kk}^{te}\right)^2}\right]$$

...(5.30)

5.3.3 Thermodynamic Considerations

The first law of thermodynamics requires

$$dE = \cancel{dQ} + \cancel{dW} = dU + dK$$

...(5.31)

where E is the total energy and a state variable, Q the heat flow into a system and W the work done on the system, are path dependent, and U and K are the potential energy and the kinetic energy respectively. In the conventional sense due to the interaction of elastic and thermal effects, the total energy at any state cannot be separated into elastic potential energy and thermal energy. However, the computation of U and K in this case specifies a unique value of configuration energy and kinetic energy for each state defined by a configuration strain, ε, and absolute temperature, T, such that

$$E(T,\varepsilon)=U(\varepsilon)+K(T)$$

...(5.32)

The separation of the material into two phases, one with only the potential energy U and one with kinetic energy K implies that the total energy, E^*, of the separated system is given by

$$E^* = (1-E_F)U + E_F K$$

...(5.33)

Substituting for E_F using Eq. (5.10) provides

$$E^* = \left(1-\frac{K}{K-U}\right)U + \left(\frac{K}{K-U}\right)K = \frac{K^2-U^2}{K-U} = U+K = E$$

...(5.34)

Thus, the definition of E_F ensures that the total energy of the separated system always equals the total energy of the material.

Any difference in work done, if deformation is carried out at nonzero absolute temperature is assumed to be made up due to heat transfer, which arises from the thermoelastic effect. The thermoelastic effect which couples the thermal and mechanical problems, involving heating or cooling of a body due to elastic deformation, is a

consequence of the second law of thermodynamics. The second law in conjunction with the first law provides (Swalin, 1972)

$$\left[\left(\frac{\partial E}{\partial V}\right)_T + P\right] = T\left(\frac{\partial P}{\partial T}\right)_V = 3T\alpha(T)B(T)$$

...(5.35)

For the separated phases, the configuration energy depends only on volume while the kinetic energy depends only on the temperature. Thus, Eq. (5.35) implies

$$\left(\frac{\partial E}{\partial V}\right)_T = \frac{dU}{dV} = 3T\alpha(T)B(T) - P$$

...(5.36)

For a material heated in an unconstrained manner,

$$\frac{dU}{dV} \approx B_0 \varepsilon_{ii}(T)$$

...(5.37)

Thus, for the separated phases, the second law requires

$$3T\alpha(T)B(T) - p^a = B_0 \varepsilon_{ii}(T)$$

...(5.38)

This provides a test of the internal compatibility of the model with the second law of thermodynamics, although the second law has not been used directly in the development

of the model. If the predicted values are consistent with Eq. (5.38), the assumption that heat transfer makes up the work difference may be assumed to be valid.

5.4 Elastic Shear Deformations

For shear deformations, the vapor phase is irrelevant as it cannot carry any shear. Thus, only the condensed phase needs to be considered. The potential well for atoms is periodic under shear displacements. If all the atoms in a crystal plane were to slip by a certain distance, ignoring surface effects, the original structure is restored. If the atoms are uniformly displaced in shear to the peak potential energy, no further energy is required to be input into the structure for continued displacement, barring dissipation. Material behavior in this state may approach that of a liquid.

It is assumed that when the total configuration energy density in the condensed phase reaches a value U^L, which may be approximated by the latent heat of fusion, the condensed phase behaves like a liquid. Thus, for shear deformations, the condensed phase is separated into a solid phase (s) which can carry shear

$$\tau^s = G_0 \gamma^{se} \qquad \ldots(5.39)$$

where G_0 is the shear modulus at 0 K, and a liquid phase (l) that can carry no shear stress. Since shear deformation is not induced by thermally generated strains, shear or deviatoric components of the thermoelastic strain tensor are identical to the standard strain tensor.

The energy density in the liquid phase is assumed to be U^L. The solid phase is assumed to be at zero volumetric strain, and has an energy density given by

$$U = \frac{-U_0}{\eta} + U^d = \frac{-U_0}{\eta} + G_0\left(\varepsilon_{ij}^{te}\varepsilon_{ij}^{te} - \frac{1}{3}\varepsilon_{kk}^{te}\varepsilon_{ll}^{te}\right) \qquad \ldots(5.40)$$

If volumetric strains are zero, the condensed phase is assumed to act like a solid, and the fluid fraction is zero. Upon application of the deviatoric components of the configuration strain tensor, the maximum volumetric configuration energy density that can be added to the material before complete liquefaction is given by

$$U^v_{\max} = U^L - G_0\left(\varepsilon_{ij}^{te}\varepsilon_{ij}^{te} - \frac{1}{3}\varepsilon_{kk}^{te}\varepsilon_{ll}^{te}\right) \qquad \ldots(5.41)$$

Thus, if the volumetric component of the configuration strains is imposed next, the fraction of the liquid, F_L, is the ratio of the volumetric configuration energy density, U^v, to the maximum feasible value of the volumetric energy density that can be added to the material before complete liquefaction.

$$F_L = \frac{1}{2}\frac{B\varepsilon_{kk}^{te}\varepsilon_{ll}^{te}}{U^L - G_0\left(\varepsilon_{ij}^{te}\varepsilon_{ij}^{te} - \frac{1}{3}\varepsilon_{kk}^{te}\varepsilon_{ll}^{te}\right)}$$

...(5.42)

The total configuration energy in the condensed phase is given by

$$U = -\frac{U_0}{\eta} + U^d + U^v$$

...(5.43)

while the separated solid-liquid system, wherein the liquid has an energy U^L relative to the equilibrium position at 0K and the solid phase carries the shear stresses only with energy U^d relative to the datum, has the total energy, U^*, given by

$$U^* = (1 - F_L)\left(\frac{-U_0}{\eta} + U^d\right) + F_L\left(\frac{-U_0}{\eta} + U^L\right)$$

...(5.44)

Using Eq. (5.42) for F_L,

$$U^* = \frac{-U_0}{\eta} + \left(1 - \frac{U^v}{U^L - U^d}\right)(U^d) + \frac{U^v}{U^L - U^d}(U^L) = \frac{-U_0}{\eta} + U^d + U^v = U$$

...(5.45)

ensuring that the separation of phases maintains the equality of the total energy in the material and its separated phases. However, there is an inconsistency in that the work done to attain a given state of configuration strain is path dependent.

If the applied strains are assumed small enough that the configuration energy density is much smaller than U^L, the work done for various paths differs only by a second order term (Appendix VI.3). This assumption may not hold for large temperature changes. For instance, near the melting point, the fluid fraction may high indicating that the volumetric configuration energy is comparable to U^L. However, the formulation is retained for simplicity.

The deviatoric component of the configuration energy is always much smaller than U^L, as elastic strains approaching the theoretical maximum value are not typically attained in practice. Thus, F_L is relatively independent of the deviatoric configuration energy.

Since only the solid phase can withstand shear stresses, the relationship between observed stress and the shear strain is given in the form

$$\tau = (1 - E_F)(1 - F_L)G_0\gamma^{te} \qquad \ldots(5.46)$$

For small γ^e, this implies

$$G(T) \approx (1 - E_F)(1 - F_L)G_0 \qquad \ldots(5.47)$$

5.5 Thermoelastic Equation

The overall thermoelastic equation may be written as

$$\sigma_{ij} = (1 - E_F)\left[(1 - F_L)2G_0\left(\varepsilon_{ij}^{te} - \delta_{ij}\frac{\varepsilon_{kk}^{te}}{3}\right) + \delta_{ij}B_0\varepsilon_{kk}^{te}\right] - \delta_{ij}\frac{2}{3}\frac{K}{(1 - \rho_f + \varepsilon_{ii}^{te})}$$

...(5.48)

where the superscript *te* on the strains emphasizes that they are elastic strains relative to the datum of the stress-free state at 0K, and thus, include the volumetric strains due to thermal expansion. The stress is a function of the material parameters at 0K, as well as the absolute temperature T, and the thermoelastic strain tensor, i.e.

$$\sigma_{ij} = \sigma_{ij}(T, \varepsilon_{ij}^{te})$$

...(5.49)

In terms of the thermoelastic strains, the incremental stress-strain-temperature relationships may then be written based on

$$d\sigma_{ij} = \left(\frac{\partial \sigma_{ij}}{\partial \varepsilon_{kl}^{te}}\right)d\varepsilon_{kl}^{te} + \left(\frac{\partial \sigma_{ij}}{\partial T}\right)dT$$

...(5.50)

The elastic strain ε_{ij}^{e} may be computed using

$$\varepsilon_{ij}^{e} = \frac{\varepsilon_{ij}^{te} - \delta_{ij}\int_{0}^{T}\alpha(T)dT}{1+\delta_{ij}\int_{0}^{T}\alpha(T)dT} \approx \varepsilon_{ij}^{te} - \delta_{ij}\int_{0}^{T}\alpha(T)dT$$

...(5.51)

This provides

$$d\varepsilon_{ij}^{e} = d\varepsilon_{ij}^{te} - \delta_{ij}\alpha(T)dT$$

...(5.52)

which is the standard equation for division of total strains into elastic and thermal components. It may be noted that the shear strains are unchanged, as thermal expansion does not lead to shear strains.

5.6 Plastic Deformations

The periodic nature of the potential field for shear deformations implies that if all atoms of a layer in a crystal are displaced by a certain distance relative to an adjacent layer, the original structure is regained, if surface effects are ignored[12]. Thus, the deformation is irreversible.

[12] Surface effects leading to extrusions and intrusions are primarily responsible for fatigue crack initiation in metals (Frost et al., 1999).

Plastic yielding typically initiates at much lower stresses due to the presence of dislocations, which are localized deviations from the regular atomic arrangements. Unlike the homogenous liquid phase (*l*) discussed for elastic shear deformations, the presence of dislocations does not reduce the shear modulus as regions of dislocations are typically extremely small compared to the bulk of the material. These localized deviations are capable of moving through the solid structure, resulting in plastic strain increments acting in series to the elastic strain increments.

The energy of configuration for the continuum is assumed to consist of an additional term, U^P, which includes the energy-density locked in due to the presence of localized strains. The energy due to these may not be fully manifested in the macroscopic strains, and deformations due to several of these may also offset each other partially with regard to the externally measured deformation. Thus, for the condensed phase,

$$U = \frac{-U_0}{\eta} + U^P + U^d + U^v = \frac{-U_0}{\eta} + U^P + G_0\left(\varepsilon_{ij}^{te}\varepsilon_{ij}^{te} - \frac{\varepsilon_{kk}^{te}\varepsilon_{ll}^{te}}{3}\right) + \frac{1}{2}B_0\varepsilon_{mm}^{te}\varepsilon_{nn}^{te} \qquad \ldots(5.53)$$

The deviations are assumed to provide localized areas of liquefaction within the condensed phase, with energy U^L. For metals, U^P may be assumed to be small enough relative to the kinetic energy and the configuration energy, so as to not affect E_F or F_L. This is borne out by the observation that plastic deformation does not lead to any significant change in elastic modulus values.

Considering a unit volume of the solid phase (s) when the shear strain is zero, it is seen that the total energy that can be added to the solid phase before liquefaction is U^L. It is assumed that when the deviatoric strain energy reaches the value U^L, the material yields completely. Thus, if U^P is the locked-in energy density due to local distortions, the fraction of material that slips is U^P/U^L, and the energy required to initiate the slip is assumed to be $(U^P/U^L)\ U^L$ or simply U^P.

$$\frac{J_{2D}}{2G_0} = U^P \qquad \ldots(5.54)$$

or

$$J_{2D} = 2G_0 U^P \qquad \ldots(5.55)$$

which is a vonMises type yield criterion, where the yield stress depends on the energy locked-in due to dislocations. For simple shear, the equation provides for the yield stress, τ_y,

$$\tau_y' = \sqrt{2G_0 U^P} \qquad \ldots(5.56)$$

The equation is not unreasonable as assuming U^P to be solely due to dislocations, the total locked-in energy is proportional to the dislocation density, ρ. Further the energy density of a dislocation varies proportionally to the square of the distortion caused by the dislocation, b, and the shear modulus G. At a temperature of 0 K,

$$U^P \sim \rho G_0 b^2$$

...(5.57)

and thus for a unit volume of the solid phase,

$$\tau_y^s \sim G_0 b\sqrt{\rho}$$

...(5.58)

For observed material behavior, the yield stress is then given by

$$\tau_y = (1-E_F)(1-F_L)\tau_y^s \sim (1-E_F)(1-F_L)G_0 b\sqrt{\rho}$$

...(5.59)

which along with Eq. (5.47) provides

$$\tau_y \sim G(T)b\sqrt{\rho}$$

...(5.60)

This is similar to the relationship between flow stress and dislocation density in literature (Hirsch, 1975) given by

$$\tau = \alpha G b\sqrt{\rho}$$

...(5.61)

where α is a constant of proportionality which is usually determined experimentally. The relationship derived in Eq. (5.60) holds only for the assumption that U^P is insignificant as compared to U^L, or equivalently, that the dislocation density in the material is small.

Further, Eq. (5.56) provides for the observed ultimate stress under plastic deformation

$$\tau_{ult} = (1 - E_F)(1 - F_L)\sqrt{2G_0 U^L}$$

...(5.62)

$$\Rightarrow \tau_{ult} = G(T)\sqrt{\frac{2U^L}{G_0}}$$

...(5.63)

which is in line with the experimental observations (Gittus, 1975)

$$\frac{\tau_{ult}(T_1)}{G(T_1)} = \frac{\tau_{ult}(T_2)}{G(T_2)} = \text{constant}$$

...(5.64)

The constant is approximately 1/20 and the maximum shear strain is ~ 0.1 (Cottrell, 1957).

The ratio E_F is relatively more insensitive to strain. However, Eqs. (5.54) – (5.64) implicitly assume that $U^P << U^L$, so as to not affect the ratio F_L. Thus, the expression for the ultimate stress is seen to be a theoretical extrapolation only. Alternative formulations are feasible, which incorporate softening at higher values of U^P, incorporating damage within the elastoplastic framework.

The formulation is also based on the assumption that typical loadings imposed on the material are at a sufficiently low strain-rate that the plastic strains may be assumed to be

instantaneous. In case strain-rate dependence of plasticity is to be incorporated, the Perzyna formulation may be used instead.

5.6.1 Hardening and Recovery

When a material is deformed plastically in shear, a part of the work done, about 10%, is stored in the material, while the rest of the work is dissipated as heat (Dieter, 1961). This leads to an increase in U^P, and thus, the yield stress.

One possible hardening function may be of the form

$$dU^P = \alpha_h \left(1 - \frac{U^P}{U^L}\right) dW^P \qquad \ldots(5.65)$$

where $\alpha_h \sim 0.1$ and dW^P may be computed as

$$dW^P = \left(\sigma_{ij} - \delta_{ij}\frac{\sigma_{kk}}{3}\right)\left(d\varepsilon_{ij}^{tT} - d\varepsilon_{ij}^{te}\right) = \left(\sigma_{ij} - \delta_{ij}\frac{\sigma_{kk}}{3}\right)\left(d\varepsilon_{ij}^{T} - d\varepsilon_{ij}^{e}\right) \qquad \ldots(5.66)$$

where $d\varepsilon_{ij}^{tT}$ is the total strain increment, which is the sum of the thermoelastic strain increment and the plastic strain increment. Plastic strains are assumed to be deviatoric only, and deviatoric strains are the same for thermoelastic and standard strains. It may be noted that the plastic work done on the solid phase is identical to that for the total material. In terms of the deviatoric components of stresses and strains,

$$\left(s_{ij}^{s} de_{ij}^{P}\right)^{s} = (1-E_F)(1-F_L)s_{ij}^{s} de_{ij}^{P} = s_{ij} de_{ij}^{P}$$

...(5.67)

In this case, the yield function is of the form

$$J_{2D} - 2G(T)(U^{P}(W^{P})) = 0$$

...(5.68)

and plastic strain increments can be computed based on the normality rule and the consistency condition as per the standard procedure.

If the initial yield stress of the material is known, U^{P}_{0} may be computed using Eq. (5.56). Otherwise, for starting the procedure plastic yield, a small initial value of U^{P} is required. If the initial U^{P} is zero, the plastic work done is zero and the material behaves in an elastic fashion. This is in line with observations that no plastic yield is observed in specimen where no dislocations are present. However, even if the initial value of U^{P} is small, the model is not a continuous yield function, in that the slope as the yield stress goes to zero is not the elastic slope.

Recovery effects may be assumed in addition to hardening as

$$dU_{-}^{P} = -\beta\left(\frac{U^{P}}{U^{L}}\right)dW^{P}$$

...(5.69)

$$\Rightarrow \qquad dU^P = \alpha\left(1-\frac{U^P}{U^L}\right)dW^P - \beta\left(\frac{U^P}{U^L}\right)dW^P$$

...(5.70)

If τ_{max} be the observed maximum stress obtained in a material as the plastic strain increases, while τ_{ult} be the theoretical maximum strain from Eq. (5.62),

$$\frac{\alpha}{\alpha+\beta} = \frac{\tau_{max}^2}{\tau_{ult}^2}$$

...(5.71)

5.7 Creep Behavior

The localized regions of deviations represented by the locked-in energy U^P can slip through the solid phase (s). It may also be assumed that these regions can flow through the liquid fraction (l) of the condensed phase in a viscous manner. Thus, a creep formulation may be developed, assuming the flow to be Newtonian, as

$$\dot{\varepsilon}_{ij}^{vp} = \Gamma_f\left[\frac{F_L}{(1-E_F)(1-F_L)}\right]^n\left(\frac{U^P}{U_L}\right)\left(\sigma_{ij}-\delta_{ij}\frac{\sigma_{kk}}{3}\right)$$

...(5.72)

5.7.1 Recovery

A simple recovery law, similar in form to plastic recovery, was assumed as

$$dU^P = -\beta_c \left(\frac{U^P}{U^L} \right) dW^{vp} \qquad \ldots(5.73)$$

6. APPLICATION TO SOLDERS

This chapter applies the theoretical concepts developed to solder modeling based on the test data for eutectic Pb/Sn solder reported by Wang et al. (2001)[13].

6.1 Test Data

A series of unidirectional isothermal strain-controlled simple shear tests of Pb/Sn solder have been reported by Wang et al. (2001) at temperatures of –20°C, 25°C, 75°C and 125°C. At each temperature, three constant strain-rate tests, at $2.78\text{x}10^{-4}$/s, $2.78\text{x}10^{-3}$/s, and $2.78\text{x}10^{-2}$/s were conducted. Test data and the hypothetical RI material response in the absence of degradation are presented in Figure 6.1 (a) – (d). Strains greater than 1.0 were excluded. The ultimate stress was assumed to be 1% higher than the final value of the RI stress attained, as shown in Figure 6.1.

[13] Results of eutectic silver-tin solder testing, conducted under the guidance and financial support of Dr. C. S. Desai, are not reported here.

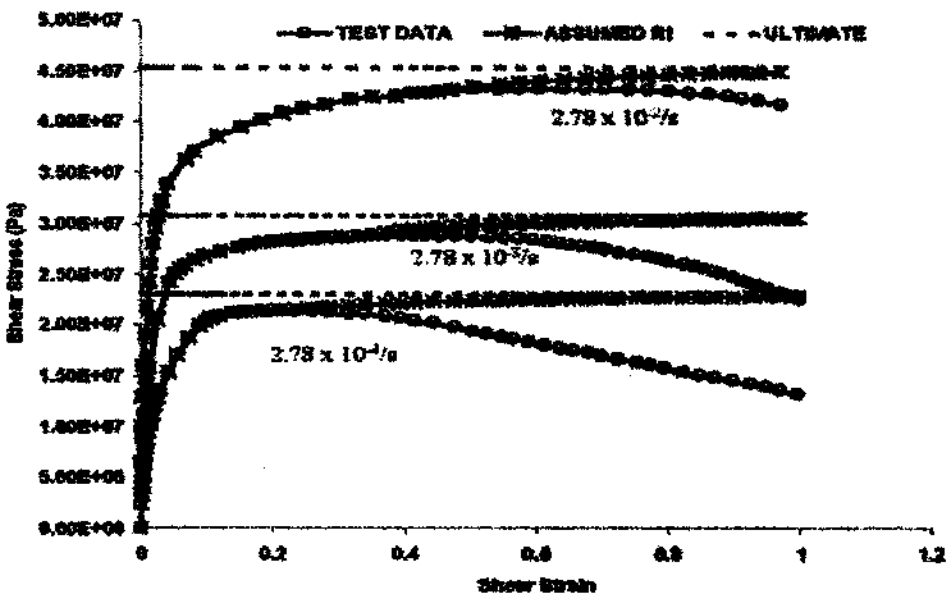

(a) Temperature = -20°C

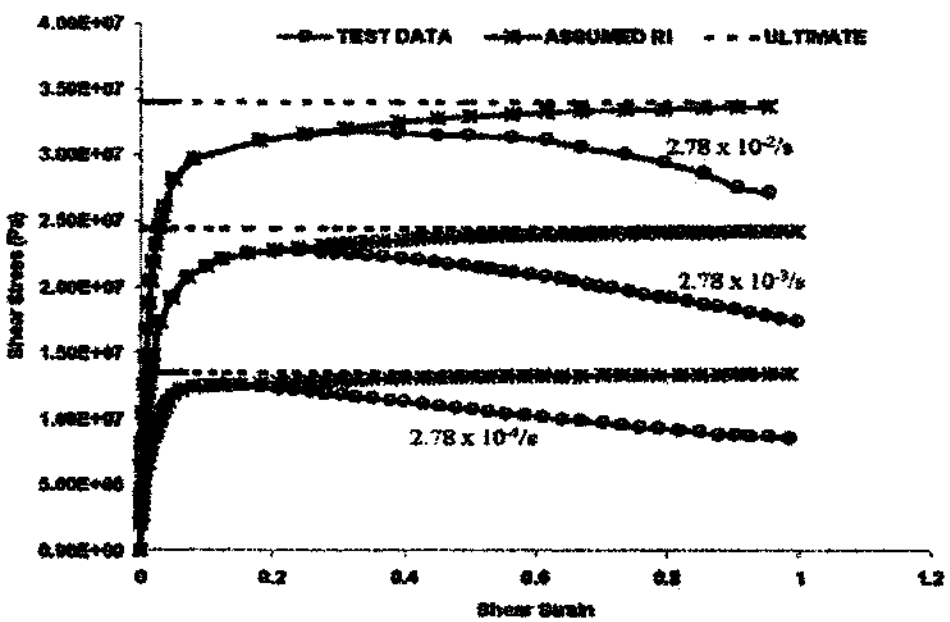

(b) Temperature = 25°C

Figure 6.1 Test Data

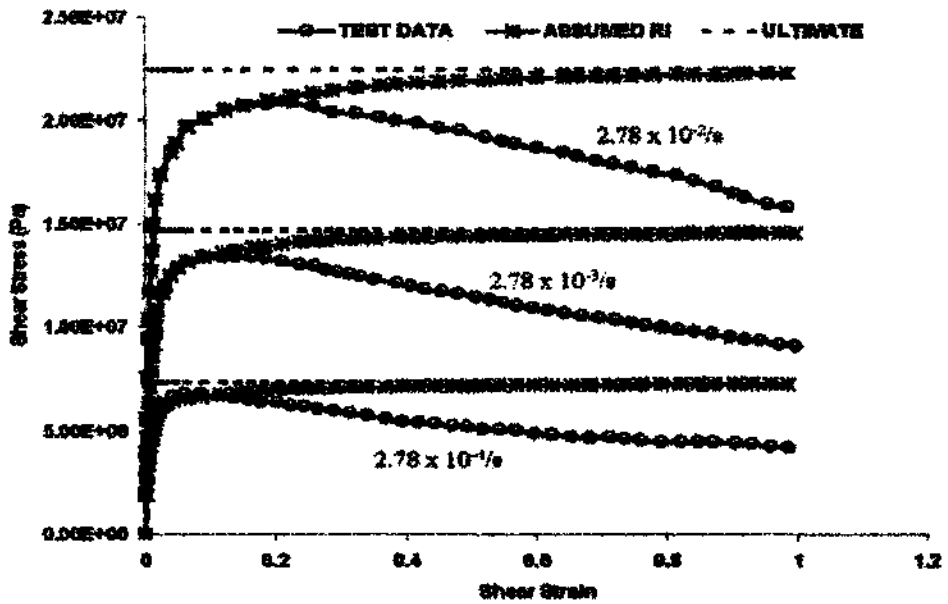

(c) Temperature = 75°C

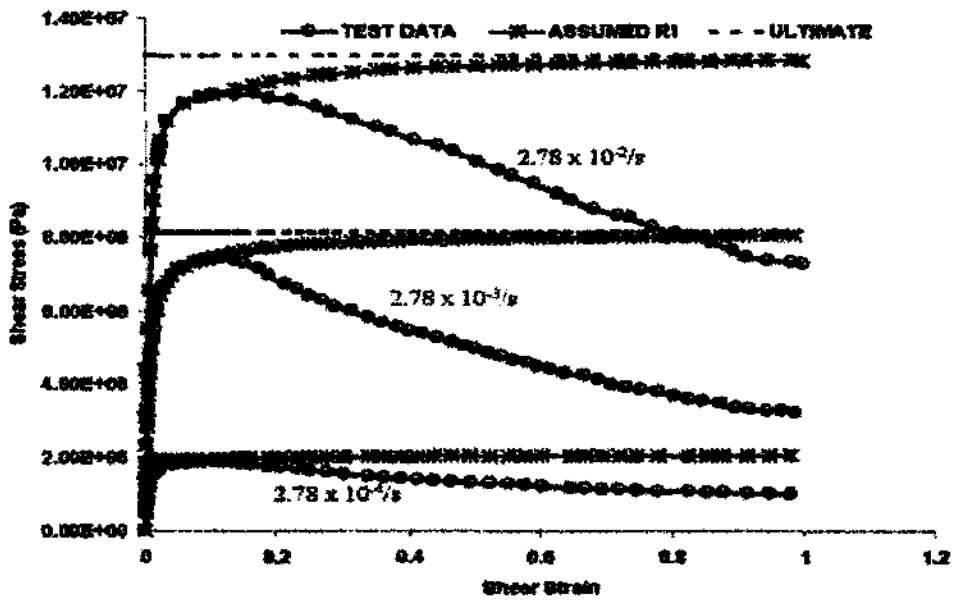

(d) Temperature = 125°C

Figure 6.1 (continued)

6.1.1 Test Procedures

Desai et al. (2001) obtained uniform samples by soldering together two copper bars, separated by spacers, held together with screws. The gap between the bars was filled with solder paste, reflowed in a vacuum chamber, and individual samples were sliced off. Dimensional changes during soldering necessitated post-soldering machining of the faces of the copper bars to achieve final dimensions, with potentially excessive stresses on the solder joints. Lack of adequate heat transfer in the vacuum chamber required heating times of up to 20 minutes, with non-uniform, prolonged and slow bubbling of the flux, and non-uniform melting of the solder. This could potentially lead to localized lack of flux and voids as also excessive copper dissolution (Jackson, 2002). Alternative sample preparation techniques were developed for Ag/Sn testing to avoid these issues[14].

Image acquisition conducted for the testing of Wang et al. (2001) under the guidance of Dr. C. Desai was of significant aid in determining proper test procedures, including sample gripping to prevent rocking upon initial loading (Figure 6.2(a)). It also indicated that high normal-load tests to determine the parameter γ were not appropriate (Figure 6.2(b)). However, use of Digital Image Correlation to determine actual strain distribution attained in the solder was not fully realized primarily due to surface degradation with deformation. Issues of dimensional scaling for zoomed-in pictures and synchronization of test-control and image acquisition computers also require improvements.

[14] A slot of the required joint thickness was machined in a solid copper bar, filled with solder, and heated on a hot-plate in air. Dimensional changes were minimal and soldering was accomplished in 2 – 3 minutes.

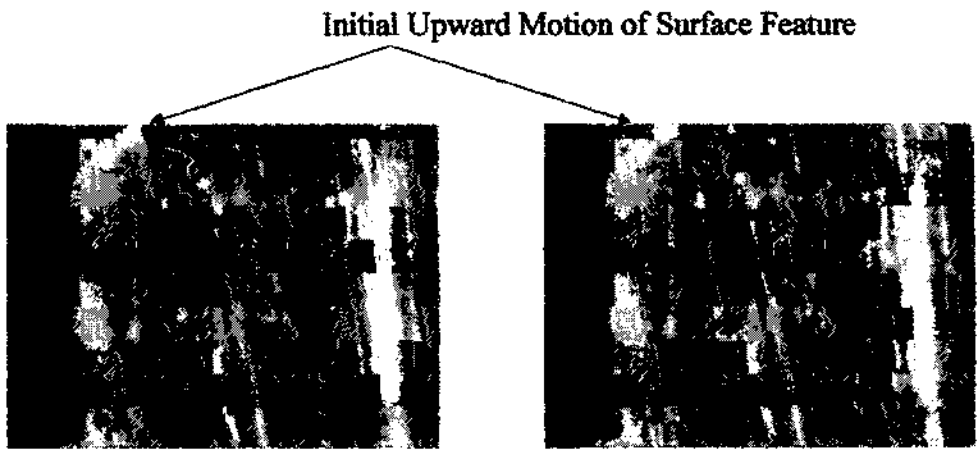

(a) Initial Rocking Motion

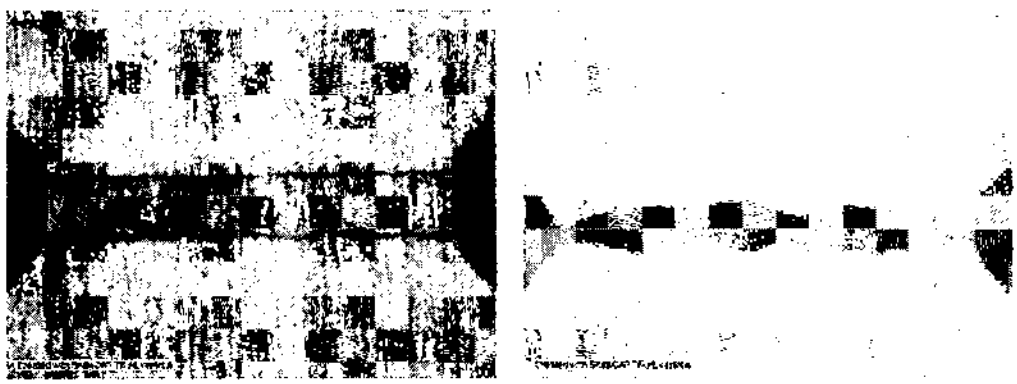

(b) Solder Deformation under High Normal Stresses

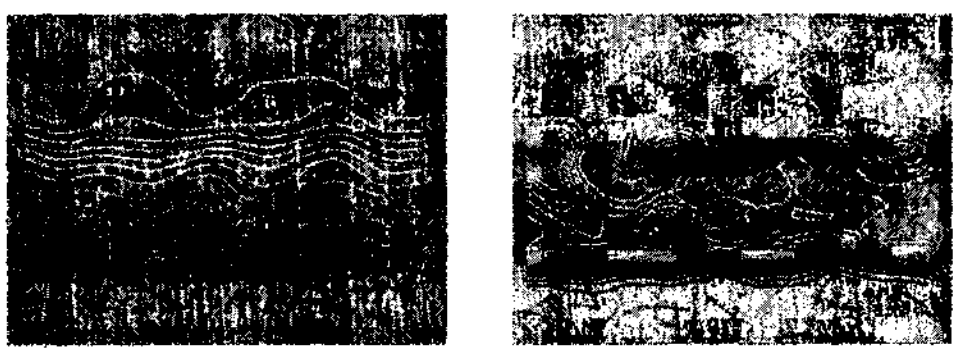

(c) Image Correlation Degradation with Increased Damage

Figure 6.2 Image Acquisition

6.2 Elastoplastic Modeling

The simplified rate-dependent elastoplastic scheme (Wang et al., 2001) was used to model solder material.

6.2.1 Parameter Determination

For the rate-dependent elastoplastic formulation, material parameters depend on the temperature and the strain-rate. Thus, all required parameters were computed from individual tests under given strain-rate and temperature conditions.

6.2.1.1 Elastic Parameters

For each test, the shear modulus, G, corresponding to the test temperature and strain-rate was computed based on the initial slope of the stress-strain curve. The elastic modulus, E, was computed assuming Poisson's Ratio to be 0.4 following Wang et al. (2001). Elastic parameters are presented in Table 6.1. Figure 6.3 provides the apparent variation of the shear modulus with temperature and strain rate.

Table 6.1

Elastic Parameters for Elastoplastic Modeling

v = 0.4 (Wang et al., 2001)

T (°C)	$\dot{\gamma}$ (s^{-1})	G (Pa)	E (Pa)
-20	2.78E-2	1.10E+10	3.08E+10
	2.78E-3	7.22E+09	2.02E+10
	2.78E-4	3.87E+09	1.08E+10
25	2.78E-2	7.20E+09	2.02E+10
	2.78E-3	4.69E+09	1.31E+10
	2.78E-4	2.63E+09	7.36E+09
75	2.78E-2	4.14E+09	1.16E+10
	2.78E-3	2.71E+09	7.59E+09
	2.78E-4	1.49E+09	4.17E+09
125	2.78E-2	2.25E+09	6.30E+09
	2.78E-3	1.53E+09	4.28E+09
	2.78E-4	5.47E+08	1.53E+09

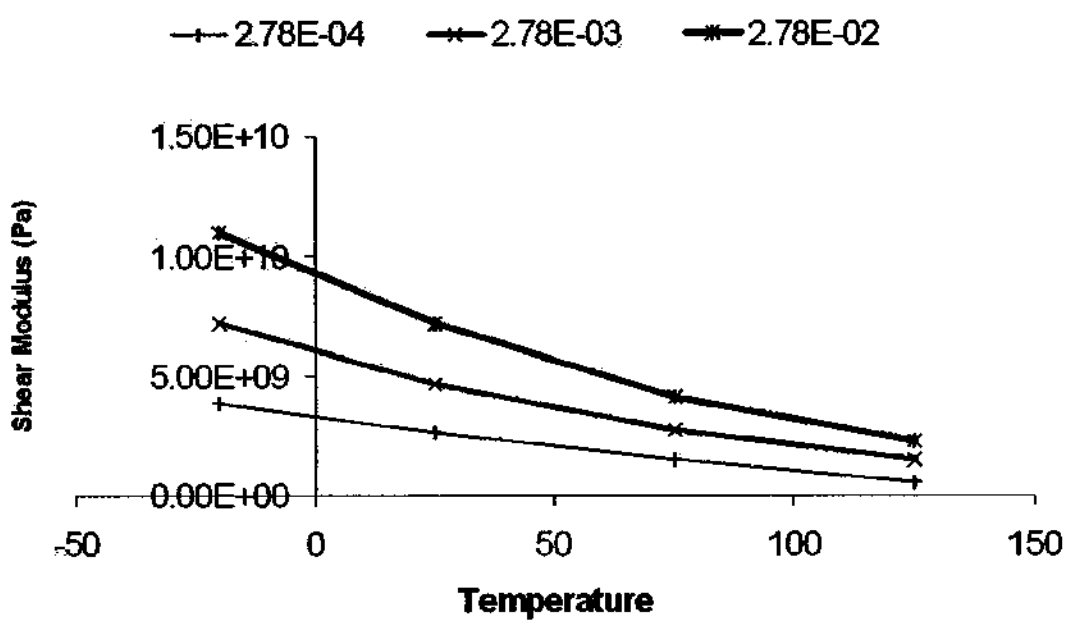

Figure 6.3 Shear Modulus for Elastoplastic Simulation

6.2.1.2 Plasticity Parameters

For the proposed yield function, ultimate parameters γ and β were adopted from Wang et al. (2001). The parameter R was recomputed based on the ultimate stress, τ_{ult}, assumed to be 1% higher than the RI stress reached when the engineering shear strain is 1, based on

$$R = \frac{\tau_{ult}}{3\sqrt{\gamma}} \qquad \ldots(6.1)$$

The hardening parameter α was computed using

$$\alpha = \frac{\tau^2}{p_a^2}\left[\frac{1}{\gamma}\right]\left(\frac{3R}{p_a}\right)^{-2} \qquad \ldots(6.2)$$

Hardening parameters a1 and $\eta 1$ were obtained using a best-fit line for the equation

$$\ln\left(\frac{1}{\sqrt{\alpha}} - 1\right) = \ln(a1) - \eta 1 \ln(\xi) \qquad \ldots(6.3)$$

The parameter n is assumed to be 2 so as to minimize the effects of volumetric stresses on plastic yield. Table 6.2 (a) presents the parameters for the proposed yield function. For comparison, the 3R values of Wang et al. (2001) have been included. The corrected values allow for viscoplastic simulation under the Perzyna scheme, which is crucial considering the limitations of the rate-dependent elastoplastic formulation.

Table 6.2

Rate-Dependent Plastic Parameters

(a) Proposed Yield Function

($\beta = 0$, $\gamma = 0.00112$, $n = 2$, $p_a = 0.1$ MPa)

T (°C)	$\dot{\gamma}$ (s^{-1})	3R (Pa)	3R (Pa) Wang et al. (2001)	a1	η1
-20	2.78E-2	1.36E+09	3.69E+09	0.015933	1.10257
	2.78E-3	9.21E+08	2.53E+09	0.012106	1.17557
	2.78E-4	6.90E+08	1.99E+09	0.011745	1.22619
25	2.78E-2	1.02E+09	2.88E+09	0.013574	0.929229
	2.78E-3	7.32E+08	2.05E+09	0.010962	1.08637
	2.78E-4	4.05E+08	1.22E+09	0.01218	0.9131
75	2.78E-2	6.74E+08	1.90E+09	0.010931	0.858144
	2.78E-3	4.40E+08	1.24E+09	0.00842	0.886948
	2.78E-4	2.20E+08	6.42E+08	0.010993	0.743155
125	2.78E-2	3.88E+08	1.10E+09	0.010412	0.724773
	2.78E-3	2.43E+08	6.97E+08	0.009596	0.807434
	2.78E-4	6.22E+07	1.75E+08	0.009151	0.654864

(b) HiSS-δ_0 Function

($\beta = 0$, $\gamma = 0.00112$, $n = 2.15$, $p_a = 0.1$ MPa)

T (°C)	$\dot{\gamma}$ (s^{-1})	Original Procedure			Iterative (consistent) Procedure		
		a1	η1	ξ_0	a1	η1	ξ_0
-20	2.78E-2	1.05E-05	0.563422	0.003158	6.14E-06	0.798529	0.032424
	2.78E-3	8.33E-06	0.621816	0.003402	5.16E-06	0.849267	0.032923
	2.78E-4	9.54E-06	0.570968	0.002411	4.84E-06	0.877344	0.034728
25	2.78E-2	1.00E-05	0.537183	0.002009	6.04E-06	0.787771	0.016041
	2.78E-3	8.34E-06	0.587933	0.002317	5.11E-06	0.858472	0.023884
	2.78E-4	1.02E-05	0.541749	0.0017	6.21E-06	0.777792	0.013208
75	2.78E-2	7.89E-06	0.57605	0.001817	5.70E-06	0.772274	0.009904
	2.78E-3	6.80E-06	0.615609	0.00193	4.92E-06	0.832342	0.009068
	2.78E-4	9.07E-06	0.542765	0.001171	6.87E-06	0.696568	0.004973
125	2.78E-2	7.78E-06	0.561956	0.001306	6.36E-06	0.710337	0.004395
	2.78E-3	8.25E-06	0.56714	0.001359	6.02E-06	0.757355	0.006561
	2.78E-4	9.51E-06	0.517291	0.000638	7.70E-06	0.675381	0.002168

Plasticity parameters for the HiSS-δ_0 yield function are shown in Table 6.2 (b). Ultimate parameters 3R, β and γ are the same for HiSS-δ_0 as for the proposed yield function. Parameter n is taken to be 2.15 following Wang et al. (2001). Hardening parameters (a1, η1) for the HiSS-δ_0 model were initially determined using

$$\ln(\alpha)=\ln(a1)-\eta 1\ln(\xi)$$

...(6.4)

where α at each data point was computed using

$$\alpha=\left[\gamma-\frac{\tau^2}{(3R)_A^2}\right]\left(\frac{3R}{p_a}\right)^{2-n}$$

...(6.5)

and ξ was computed using the unidirectional shear strain as

$$\xi=\frac{1}{\sqrt{2}}\int\sqrt{d\gamma^p d\gamma^p}=\frac{1}{\sqrt{2}}\gamma^p$$

...(6.6)

to fit

$$\ln(\alpha)=C_1\ln(\xi)+C_2$$

...(6.7)

which provided

$$a_1=e^{C_1}$$

...(6.8)

$$\eta_1=-C_2$$

...(6.9)

Since the initial slope was assumed to be the elastic modulus, the points included in the computation of plastic strain were from the third point of the stress-strain curve. Improved hardening parameters were obtained using the iterative procedure developed in Chapter 4.

Table 6.2(b) additionally provides the value of the initial plastic strain trajectory. It is seen that the values obtained using the scheme that provides for internally consistent values of the hardening parameters and the initial plastic strain trajectory range from 3% at low temperatures to 0.5% at higher temperatures. Thus, cooling from 125°C to –20°C causes an axial plastic strain increment of approximately 1.44%, while assuming the coefficient of linear thermal expansion to be 25 x 10^{-6}/°C over the same region of temperature provides a contraction of 0.36%. Thus, the spurious plastic strain increments may be substantially larger than thermally generated strains, which is not expected for metals.

Variation of plasticity parameters with temperature and strain-rate is provided in Figure 6.4.

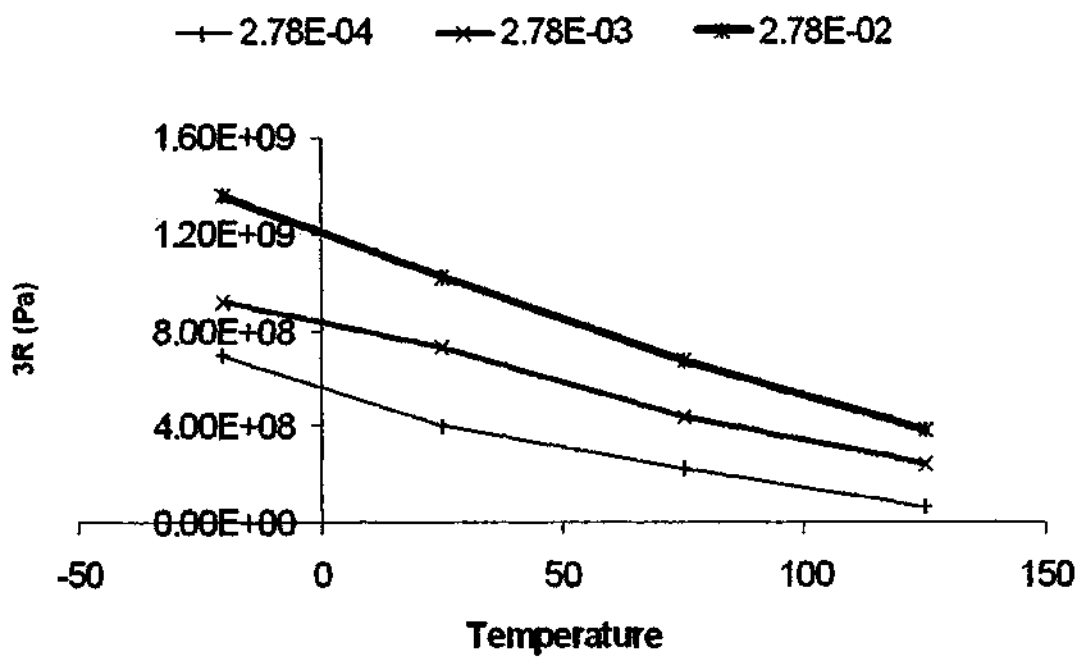

(a) Bonding Stress

Figure 6.4 Plasticity Parameters for Elastoplastic Simulation

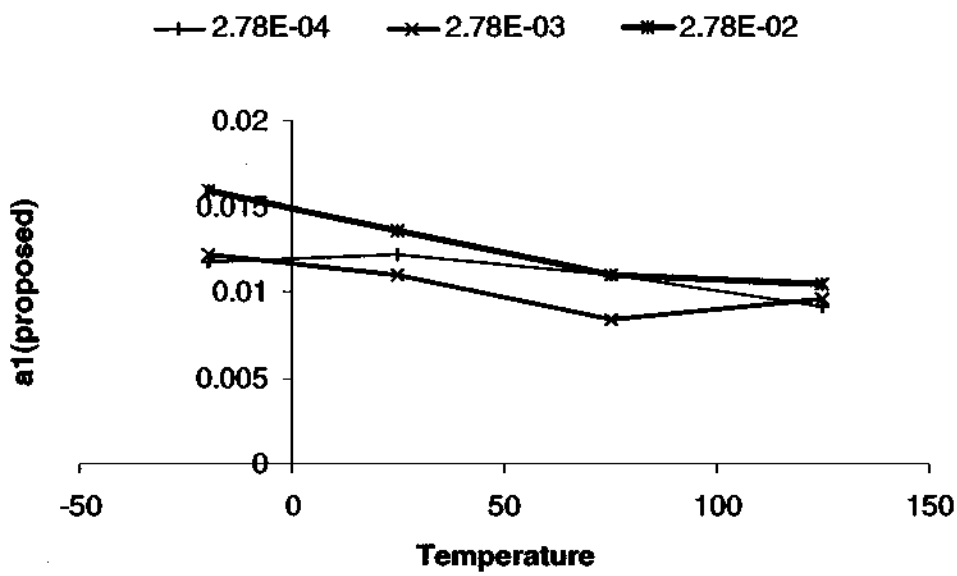

(b) Parameter a1 (Proposed Yield Function)

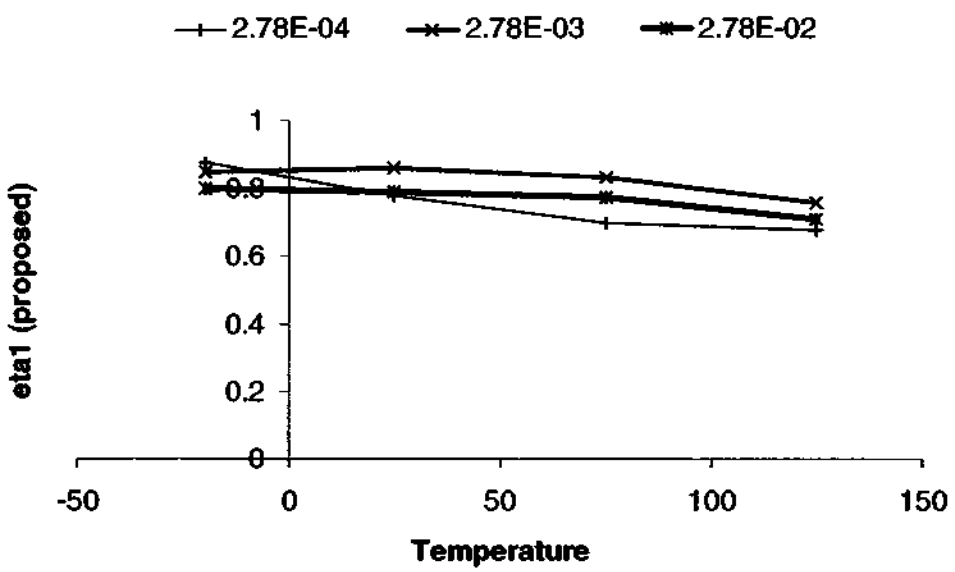

(c) Parameter η1 (Proposed Yield Function)

Figure 6.4 (continued)

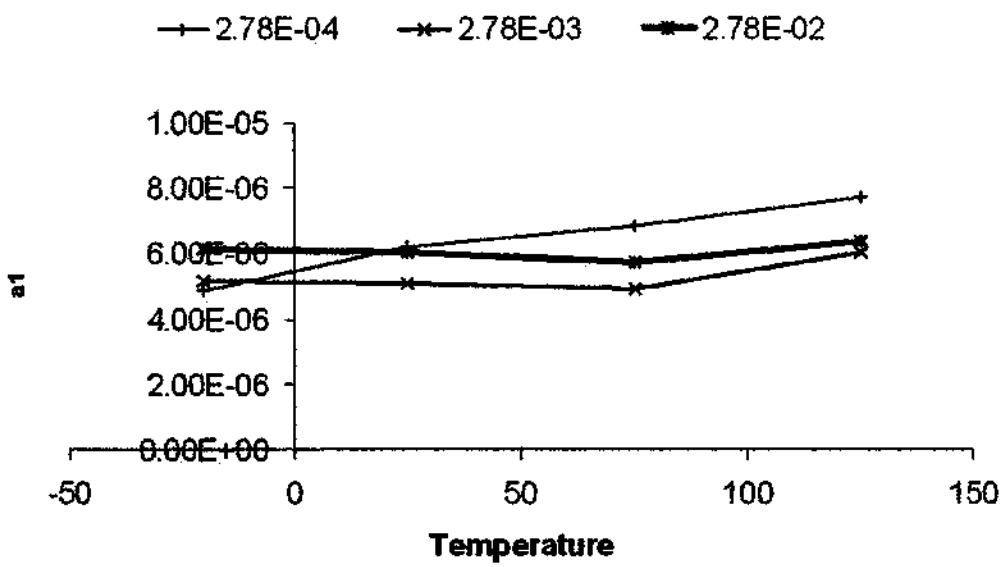

(d) Parameter a1 (HiSS) using Iterative Procedure

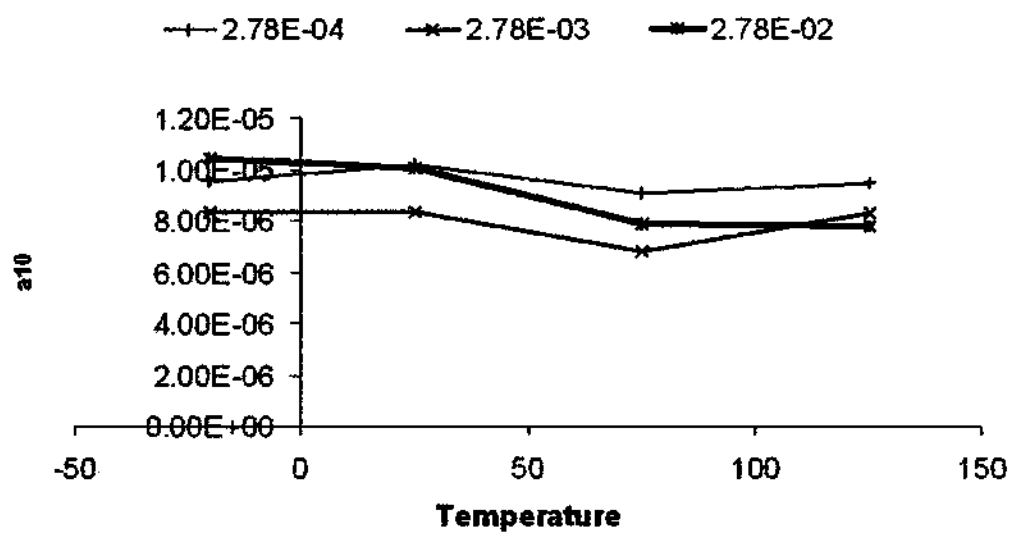

(e) Parameter a1 (HiSS) using Existing Procedure

Figure 6.4 (continued)

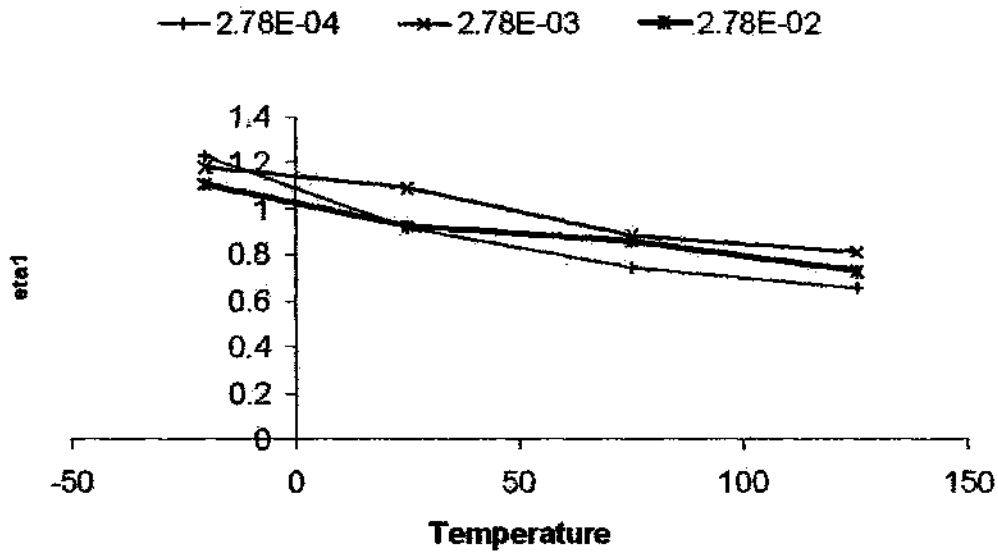

(f) Parameter η1 (HiSS) using Iterative Procedure

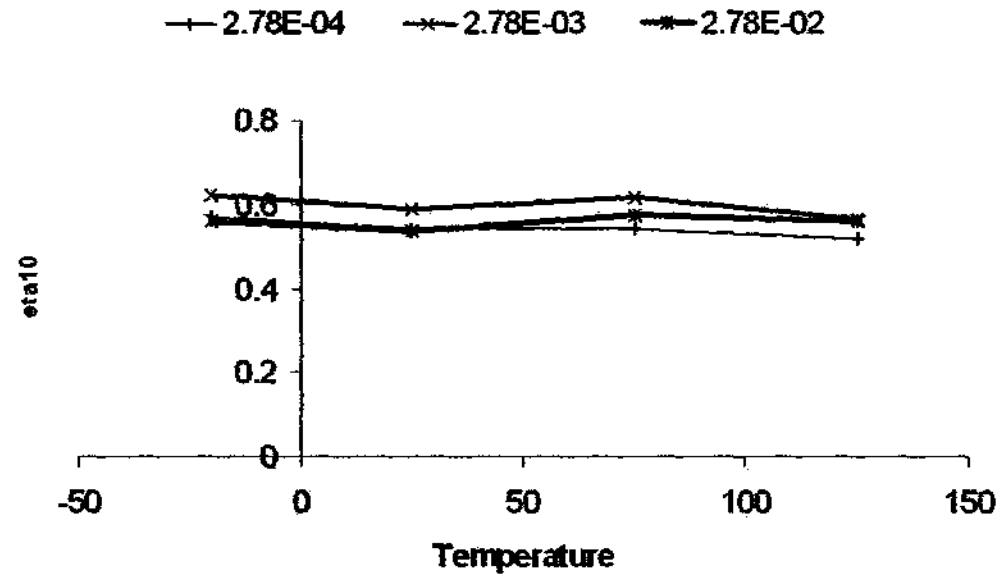

(g) Parameter η1 (HiSS) using Existing Procedure

Figure 6.4 (continued)

6.2.1.3 Disturbed State Parameters

The Disturbed State Concept (DSC) of Desai (2001) was used to model solder degradation. Disturbance was computed in terms of the plastic-strain trajectory, as well as the dissipated-work based schemes developed as part of this work.

For DSC modeling, the fully-adjusted parameter, $\overline{m}$, determined based on the state of stress in the critical state that determines the shear stress that can be carried by the fully adjusted material, is assumed to be zero following Wang et al. (2001). Residual strength is incorporated using the ultimate disturbance, D_u.

The three formulations developed for the disturbance function, including the existing formulation with the deviatoric plastic strain trajectory, the observed dissipated-work formulation, and the RI dissipated work formulation developed in Chapter 3 were investigated. At each relevant point on the test curve, the disturbance, D, is computed using

$$D = \frac{\sqrt{J_{2D}^{i}} - \sqrt{J_{2D}^{a}}}{\sqrt{J_{2D}^{i}} - \sqrt{J_{2D}^{c}}} = \frac{\tau^{i} - \tau^{a}}{\tau^{i}} \qquad \ldots(6.10)$$

D_u for each curve is taken to be 10% higher than the disturbance computed for the highest strain data point considered.

Parameters A and Z corresponding to the relationship

$$D = D_u\left(1 - e^{-A\chi^Z}\right)$$

...(6.11)

where χ can be the deviatoric plastic strain trajectory, the observed dissipated work, or the RI dissipated work depending on the formulation, are obtained from the best-fit line for the plot

$$\ln\left(-\ln\left(1 - D/D_u\right)\right) = \ln(A) + Z\ln(\chi)$$

...(6.12)

following the procedure of Desai (2001) for the deviatoric plastic strain trajectory.

Disturbance parameters A, Z and D_u are reported in Table 6.3 and plotted in Figure 6.5. The parameters for dissipated-work based formulations were not observed to provide any advantage over the deviatoric plastic strain trajectory based disturbance, in terms of temperature or rate-independence, and are more cumbersome to employ because of their magnitude.

Table 6.3

Disturbance Parameters for Elastoplastic Simulation

T (°C)	Rate	D_u	Strain		RI Work		Obs. Work	
			A	Z	A	Z	A	Z
-20	2.78E-02	0.078746	11.1518	4.46484	3.49E-33	4.30093	7.03E-34	4.39609
	2.78E-03	0.286921	5.90212	3.52182	9.29E-26	3.38581	2.88E-27	3.59979
	2.78E-04	0.46435	6.61444	2.82744	2.92E-20	2.71378	1.94E-22	3.03603
25	2.78E-02	0.214613	7.61593	3.08445	2.39E-25	3.33216	2.54E-26	3.47161
	2.78E-03	0.310691	4.8785	2.38449	9.61E-18	2.35479	5.7E-19	2.53607
	2.78E-04	0.398956	5.56024	2.02962	1.07E-14	2.02421	2.77E-16	2.27132
75	2.78E-02	0.321233	4.52662	2.07205	7.07E-16	2.11139	4.38E-17	2.29172
	2.78E-03	0.411774	4.13794	1.63795	3.83E-12	1.64698	2.42E-13	1.83587
	2.78E-04	0.467844	4.84366	1.56173	4.45E-11	1.57486	9.92E-13	1.84703
125	2.78E-02	0.476361	4.86358	1.91448	2E-14	1.9852	4.19E-16	2.24876
	2.78E-03	0.661796	6.13687	1.8759	4.87E-13	1.8569	7.87E-16	2.31634
	2.78E-04	0.561642	6.0296	1.67338	6.61E-11	1.69524	1.64E-12	1.99488

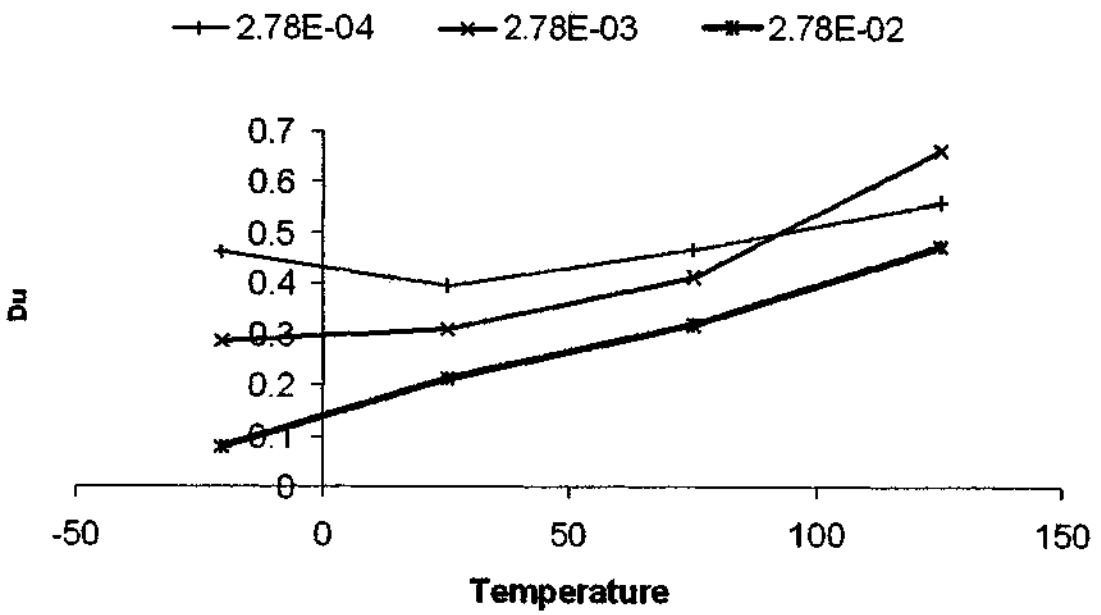

(a) Ultimate Disturbance

Figure 6.5 Disturbance Parameters for Elastoplastic Scheme

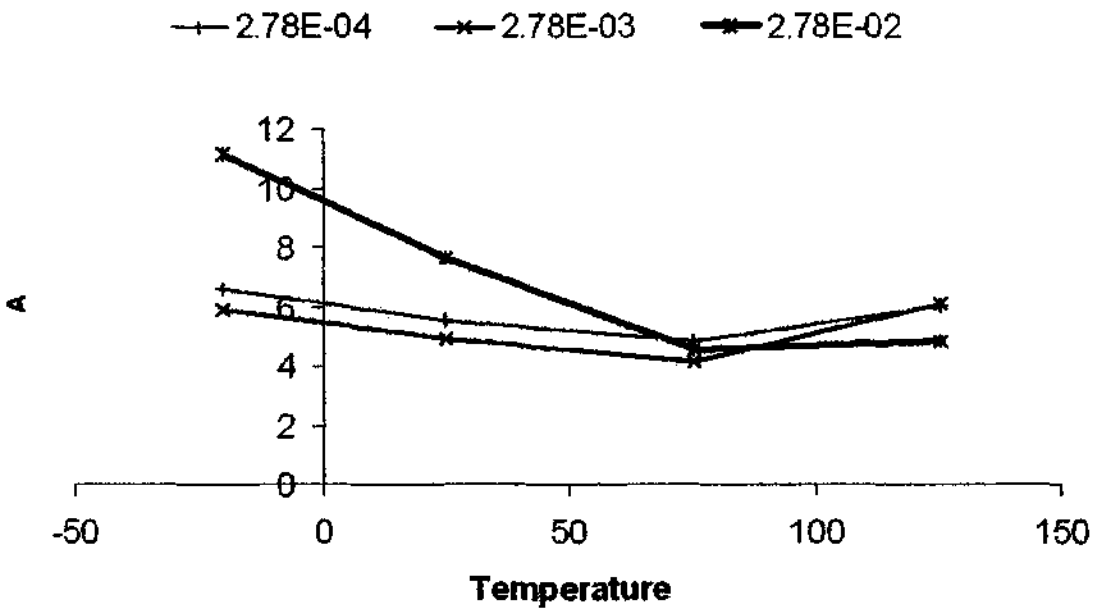

(b) Parameter A

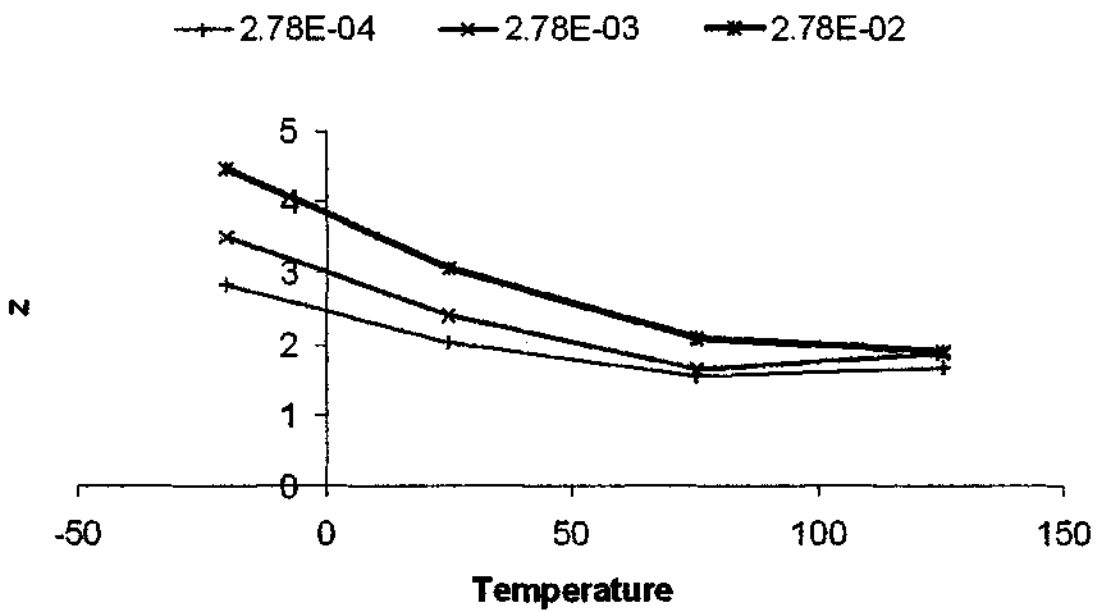

(c) Parameter Z

Figure 6.5 (continued)

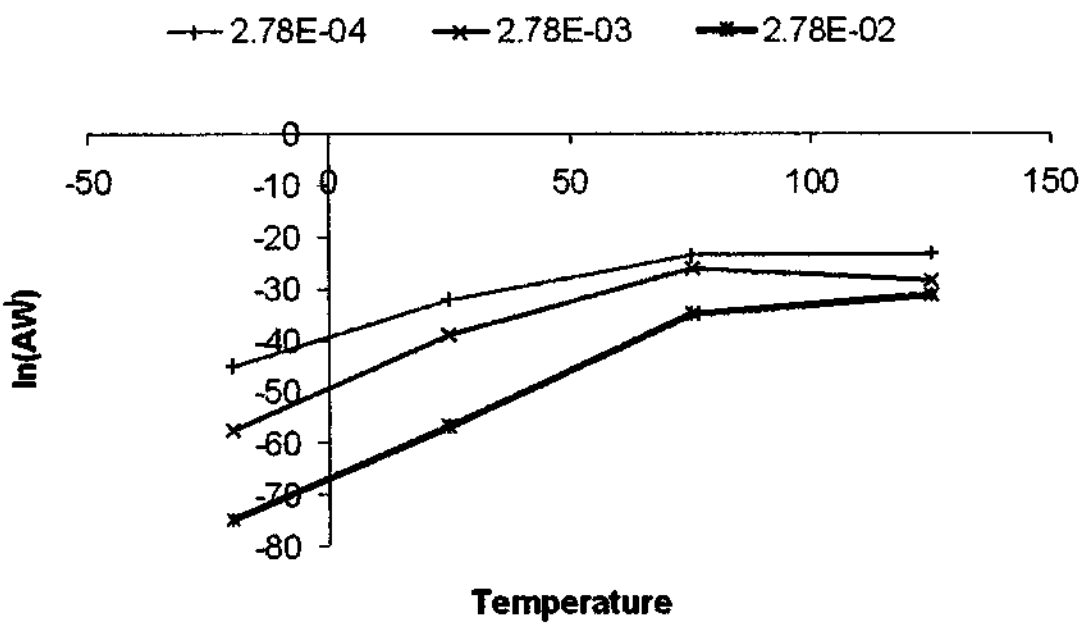

(d) Parameter A (RI Dissipated-Work Formulation)

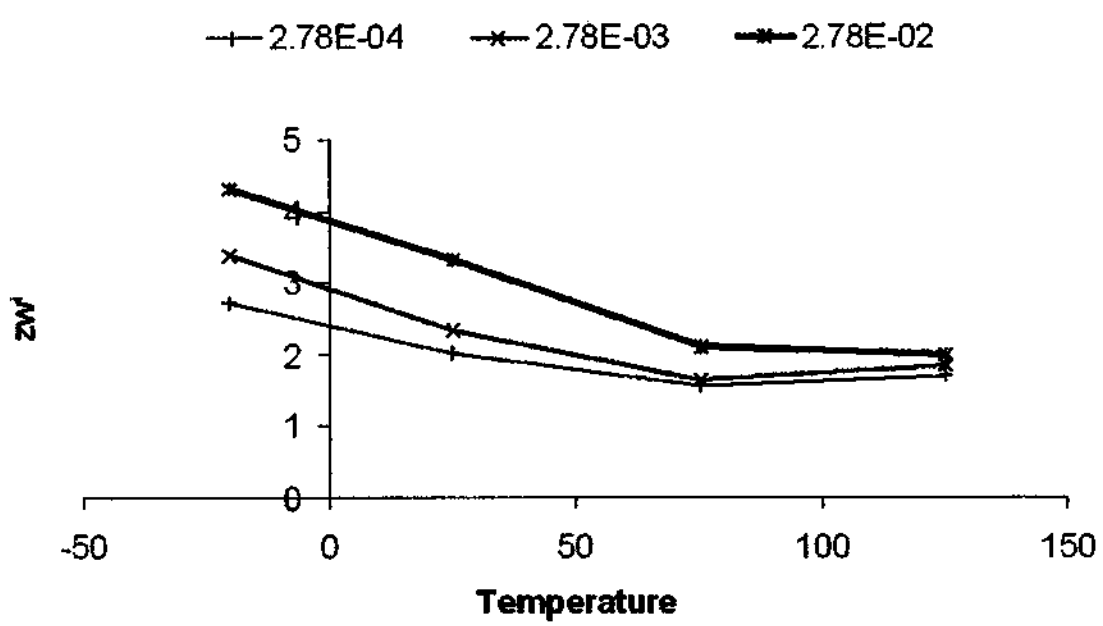

(e) Parameter Z (RI Dissipated-Work Formulation)

Figure 6.5 (continued)

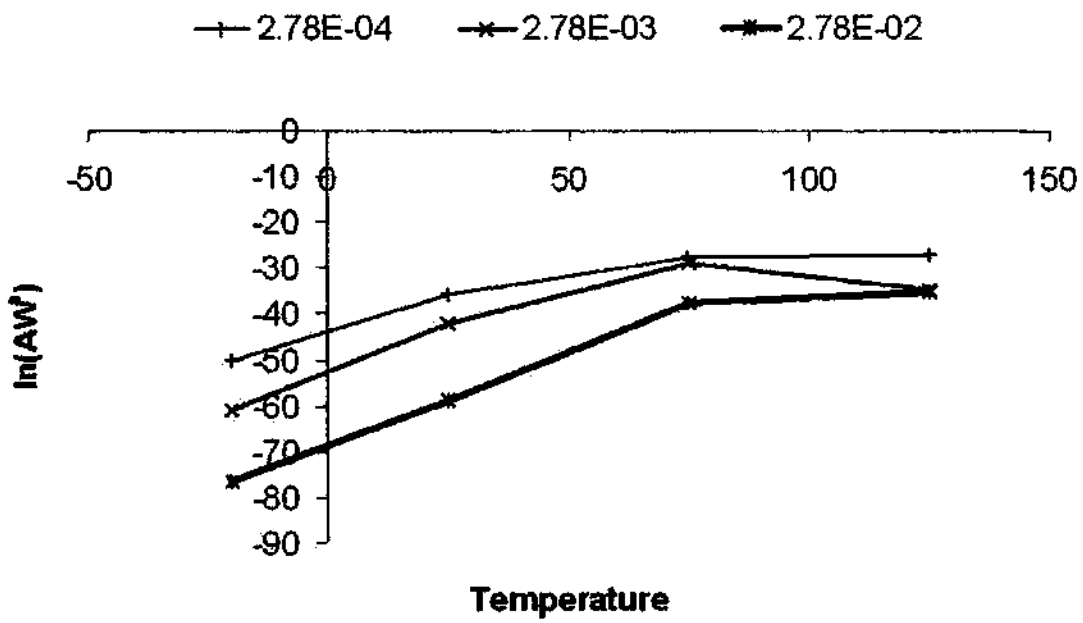

(f) Parameter A (Observed Dissipated-Work Formulation)

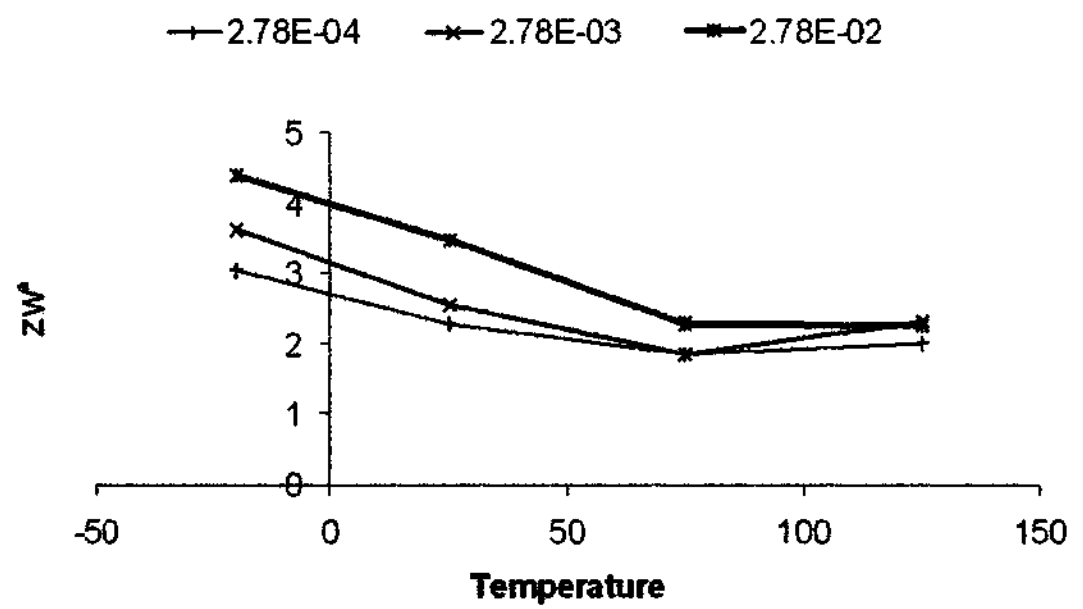

(g) Parameter Z (Observed Dissipated-Work Formulation)

Figure 6.5 (continued)

6.2.2 Backpredictions

Backpredictions were carried out using a simplified one-dimensional scheme wherein the volumetric strains were ignored which is reasonable for metals, and using the full three-dimensional elastoplastic formulation.

6.2.2.1 One-dimensional

Stress-controlled one-dimensional backpredictions were carried out using the RI stress from Figure 6.1. Assuming volumetric plastic strains to be small for simple shear allows for exact computation of the stress-strain curve for stress-controlled backpredictions, and thus, a direct comparison of the plastic yield functions. The procedure used was:

1) For each data point, the stress, τ_i, was used to compute α_i from the yield function, i.e. for the proposed yield function

$$\alpha_i = \frac{\tau_i^2}{p_a^2}\left[\frac{1}{\gamma}\right]\left(\frac{3R}{p_a}\right)^{-2} \qquad \ldots(6.13)$$

and for HiSS-δ_0

$$\alpha_i = \left[\gamma - \frac{\tau_i^2}{(3R)^2}\right]\left(\frac{3R}{p_a}\right)^{2-n} \qquad \ldots(6.14)$$

2) ξ was computed at the point using the α computed above using, for the proposed yield function

$$\xi_i = \left(\frac{a1\sqrt{\alpha_i}}{1-\sqrt{\alpha_i}} \right)^{1/m1}$$

...(6.15)

and for HiSS-δ_0

$$\xi_i = \left(\frac{a_1}{\alpha_i} \right)^{\frac{1}{m_1}}$$

...(6.16)

3) The plastic strain at the point was computed, assuming ξ to be solely due to the shear

$$\gamma_i^p = \sqrt{2}\xi_i$$

...(6.17)

while the elastic strain was computed using

$$\gamma_i^e = \frac{\tau_i}{G}$$

...(6.18)

4) The total strain corresponding to the stress data point was computed using

$$\gamma_i = \gamma_i^e + \gamma_i^p$$

...(6.19)

5) The total deviatoric plastic strain trajectory, and the work done were computed based on the appropriate average stress increments and the increment in plastic strains, and were used to compute the disturbance. From this, the observed stress was computed.

6.2.2.2 Three-dimensional

The RI stress range was divided into 1000 uniform stress increments to allow for a simple explicit numerical integration scheme. Values of all strain components at zero stress were assumed to be zero, and the appropriate value of ξ_0 at zero stress was computed corresponding to the yield function used, to start the procedure. The procedure used was:

1) For each stress data point, *i*, the constitutive elastoplastic matrix was formed using

$$C_i^{EP}(\sigma,\xi) = C^{EP}\left(\sigma_{i-1} + \frac{\sigma_{i-1}+\sigma_i}{2}, \xi_{i-1}\right) \qquad \ldots(6.20)$$

2) The total strain increment was computed using

$$\left(d\underset{\sim}{\varepsilon}\right)_i = \left[C_i^{EP}\right]^{-1}\left(\left(\underset{\sim}{\sigma}\right)_i - \left(\underset{\sim}{\sigma}\right)_{i-1}\right) \qquad \ldots(6.21)$$

3) The plastic strain increment was obtained using

$$\left(d\underset{\sim}{\varepsilon}^{p}\right)_i = \left(d\underset{\sim}{\varepsilon}\right)_i - [C^E]^{-1}\left(\left(\underset{\sim}{\sigma}\right)_i - \left(\underset{\sim}{\sigma}\right)_{i-1}\right)$$

...(6.22)

4) The increment of ξ, $d\xi_i$, was computed from the plastic strain increment based on the tensor definition of ξ.

5) The final strain and ξ for the given stress were obtained using

$$\left(\underset{\sim}{\varepsilon}\right)_i = \left(\underset{\sim}{\varepsilon}\right)_{i-1} + \left(d\underset{\sim}{\varepsilon}\right)_i$$

...(6.23)

$$\xi_i = \xi_{i-1} + d\xi_i$$

...(6.24)

6) Steps 1 – 5 were repeated for the next stress data point.

6.3 Elastoviscoplastic Scheme

The Perzyna viscoplastic formulation was used to model solder behavior following Chia (1994) and Wang et al. (2001).

6.3.1 Parameter Determination

The shear modulus at a given temperature under the elastoviscoplastic scheme is the initial slope of the stress-strain curve as the strain rate tends to infinity. Thus, for each test temperature, the shear modulus was taken to be the highest strain-rate shear modulus.

Hardening parameters for the static yield surface were obtained for the lowest strain rate curve, i.e. 2.78×10^{-4} /s, using the procedure for elastoplastic simulation, but with the appropriate high strain-rate shear modulus for the temperature.

While it is feasible to obtain fluidity parameters Γ and N based on individual test curves that are at a strain rate higher than the static yield surface (Desai, 2001), the alternative procedure of Eq. (4.58)

$$N \ln\left\langle \frac{\tau_u^2}{p_a^2} - \gamma_s \left(\frac{9R_s^2}{p_a^2} \right) \right\rangle + \ln \Gamma = \ln\left(\frac{\dot{\gamma} p_a^2}{2\tau_u} \right) \qquad \ldots(6.25)$$

was followed to obtain average parameters directly. This ensures that parameters obtained for any temperature are from all available test curves, rather than individual test curves. The corrected values of R presented in this work allow for determination of the viscoplastic parameters. Values obtained in prior work provide a negative value for the argument of the logarithmic term, which is the coefficient of N. This is crucial, as elastoplastic formulations have limited validity, as discussed in Chapter 3.

At each temperature, parameters Γ and N were obtained by fitting a straight line for the two strain rates higher than the static yield surface. Viscoplastic parameters for degradation-free material are provided in Table 6.4 and Figure 6.6.

It may be noted that the anomalous behavior of the fluidity parameter, Γ, and the parameter N at low temperature were predicted in Chapter 3, wherein the limitations on the use of the Perzyna viscoplastic scheme for solder were discussed.

Further, the initial value of the plastic strain trajectory for HiSS is seen to be substantial for the static yield surface. Thus, even if the viscoplastic formulation is used, unconstrained heating and cooling would still lead to substantial spurious plastic strain increments.

For DSC simulation, the fully-adjusted parameter was assumed to be zero as for the elastoplastic case. Disturbance parameters (Table 6.5) for each test curve were obtained based on the deviatoric viscoplastic strain trajectory.

Table 6.4

Viscoplastic Parameters for Pb/Sn Solder

(a) Elastic and Fluidity Parameters

$\nu = 0.4$

T(°C)	G (Pa)	Γ	N
-20	1.10E+10	7.54E-08	1.473086
25	7.20E+09	1.29E-11	2.311808
75	4.14E+09	2.17E-08	1.821777
125	2.25E+09	1.32E-07	1.883679

(b) Proposed Yield Function

$\beta = 0$, $\gamma = 0.00112$ (Wang et al., 2001), $n = 2$

T(°C)	3R (Pa)	a1	η1
-20	689665000	0.0104144	0.9623
25	404659000	0.0103873	0.876278
75	220097000	0.0095297	0.794446
125	62191500	0.0080113	0.769286

(c) HiSS-δ_0 Yield Function

$\beta = 0$, $\gamma = 0.00112$, $n = 2.15$, Wang et al. (2001)

T(°C)	a1	η1	ξ_0	a1 (Iterated)	η1 (Iterated)	ξ_0
-20	8.69E-06	0.632395	0.003735	4.711E-06	1.28609	0.039765
25	8.914E-06	0.619121	0.003034	5.991E-06	0.962518	0.015888
75	7.973E-06	0.626245	0.002344	6.492E-06	0.803335	0.006897
125	8.446E-06	0.595122	0.001368	7.016E-06	0.734921	0.003726

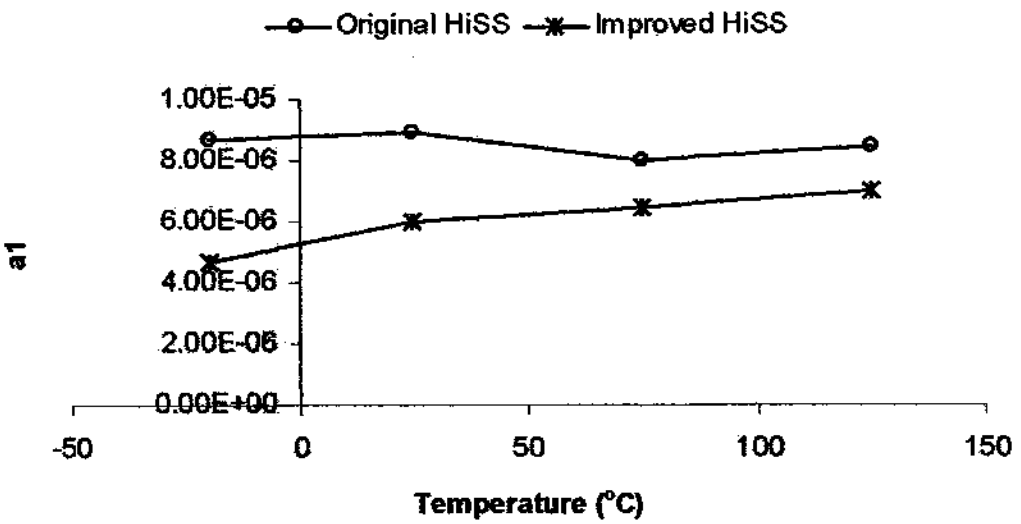

(a) Hardening Parameter a1 for HiSS-δ_0 Static Yield Surface

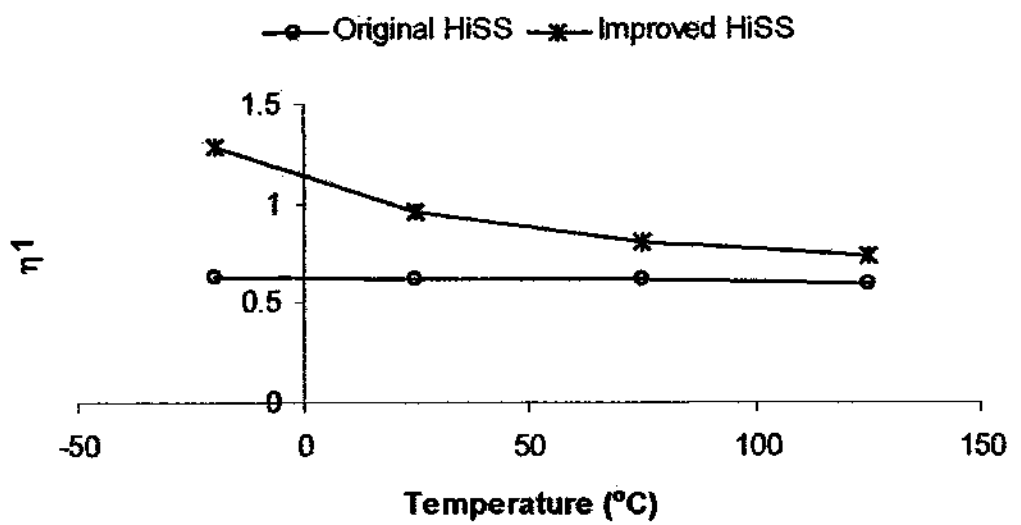

(b) Hardening Parameter $\eta 1$ for HiSS-δ_0 Static Yield Surface

Figure 6.6 Viscoplastic Parameters

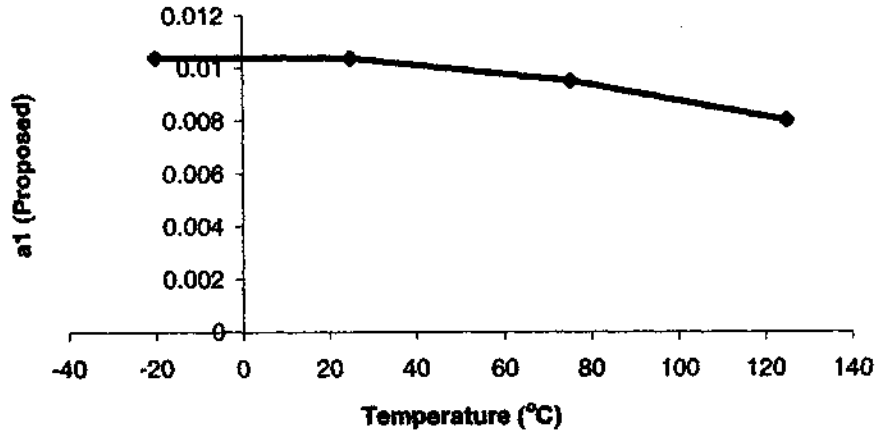

(c) Hardening Parameter a1 for Proposed Yield Function Static Surface

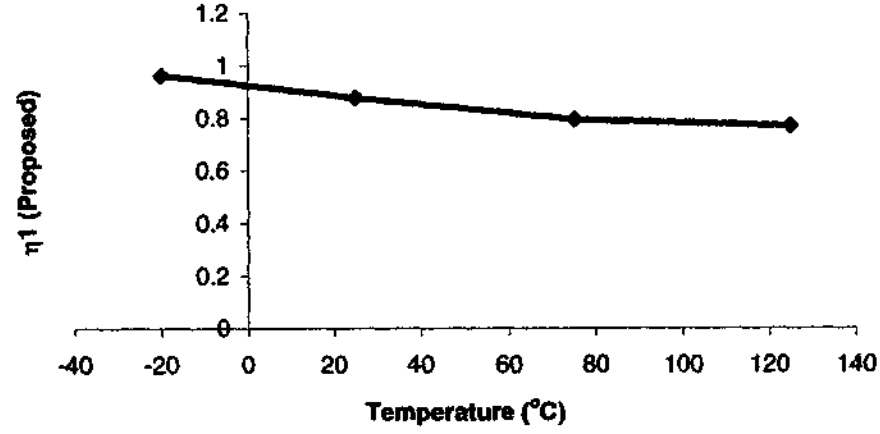

(d) Hardening Parameter η1 for Proposed Yield Function Static Surface

Figure 6.6 (continued)

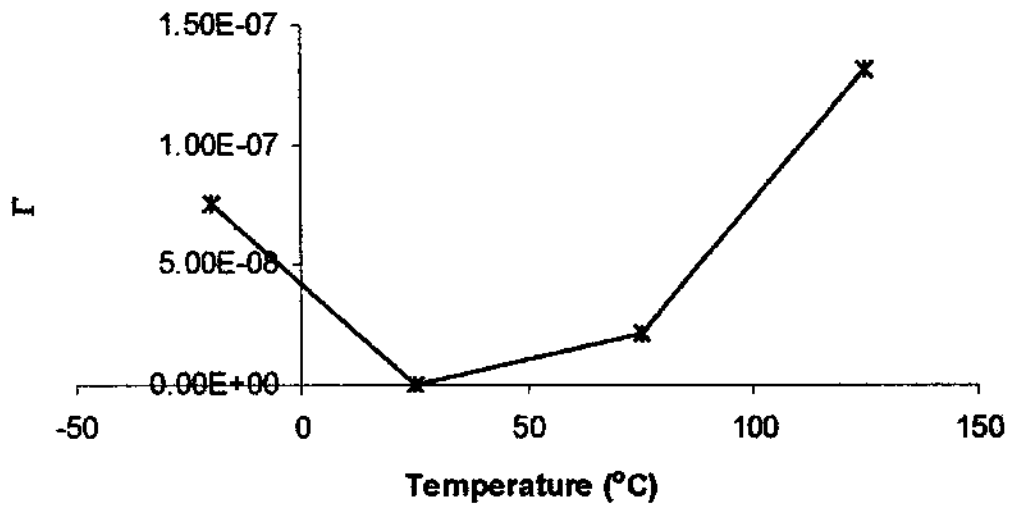

(e) Fluidity Parameter Γ

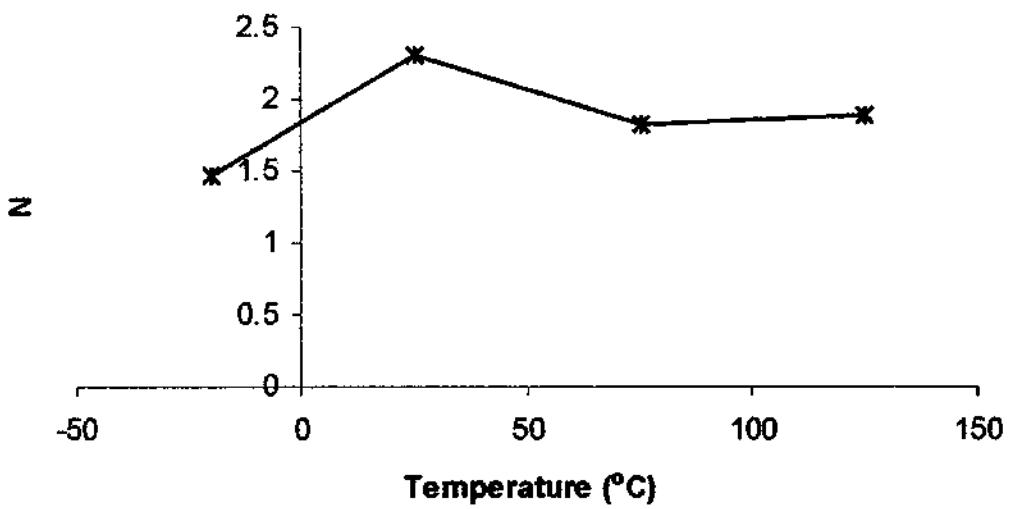

(f) Parameter N

Figure 6.6 (continued)

Table 6.5

Disturbance Parameters for Viscoplastic Formulation

T(°C)	Rate (1/s)	A	Z	Du
-20	2.78E-04	6.62065	2.85124	0.46435
-20	2.78E-03	5.89215	3.53015	0.286921
-20	2.78E-02	11.1518	4.46484	0.078746
25	2.78E-04	5.57672	2.04689	0.398956
25	2.78E-03	4.88202	2.39434	0.310691
25	2.78E-02	7.61593	3.08445	0.214613
75	2.78E-04	4.86257	1.57671	0.467844
75	2.78E-03	4.14931	1.64752	0.411774
75	2.78E-02	4.52662	2.07205	0.321233
125	2.78E-04	6.08405	1.69349	0.561642
125	2.78E-03	6.15168	1.88556	0.661796
125	2.78E-02	4.86358	1.91448	0.476361

6.3.2 Backpredictions

The smoothed test data points were linearly interpolated to provide stress data points at 10^4 uniform strain intervals within the strain range of the data. The initial strain at zero stress was assumed to be zero. The following procedure was used:

1) At any stress data-point, *i*, the initial strain increment was computed using

$$\left(d\underset{\sim}{\varepsilon}\right)_i = \left[C^E\right]^{-1}\left(\left(d\underset{\sim}{\sigma}\right)_i - \left(d\underset{\sim}{\sigma}\right)_{i-1}\right) + \Gamma\left\langle F\left(\left(\underset{\sim}{\sigma}\right)_{av}, \xi_{i-1}\right)\right\rangle^N \left.\frac{\partial F\left(\left(\underset{\sim}{\sigma}\right)_{av}, \xi_{i-1}\right)}{\partial\left(\underset{\sim}{\sigma}\right)}\right|_{\left(\underset{\sim}{\sigma}\right)=\left(\underset{\sim}{\sigma}\right)_{av}}$$

...(6.26)

where

$$\left(\underset{\sim}{\sigma}\right)_{av} = \left(\underset{\sim}{\sigma}\right)_{i-1} + \frac{\left(\underset{\sim}{\sigma}\right)_i + \left(\underset{\sim}{\sigma}\right)_{i-1}}{2}$$

...(6.27)

2) The viscoplastic strain increment was used to compute $d\xi$ corresponding to the given stress increment.

3) Eq. (6.26) was recomputed assuming the average ξ for the stress increment to be

$$\xi = \xi_{i-1} + \frac{d\xi}{2}$$

...(6.28)

4) The sub-iterations were repeated till the average value of ξ converges to the desired accuracy, subject to a maximum of 10^4 iterations.

5) The procedure was then repeated for the next stress data point.

6.4 Results

For basic constitutive modeling without the influence of degradation, elastoplastic simulations were carried out for the simplified elastoplastic scheme using both the simplified 1-dimensional procedure and the full 3-dimensional formulation. It was observed that the simplified one-dimensional and the full three-dimensional elastoplastic schemes provided virtually identical results, thereby confirming that the assumption of zero volumetric plastic strain trajectory is extremely reasonable for metals. Both the proposed yield function backpredictions and the HiSS-δ_0 backpredictions based on improved hardening parameters were similar to each other as expected for shear, and performed consistently better than the HiSS-δ_0 backpredictions based on the existing parameter determination scheme. However, the proposed yield function removes the issues related to spurious plastic strains under unconstrained heating and cooling, as well as provides continuous yielding under both tension and compression.

For DSC simulations, the simplified 1-dimensional scheme showed that backpredictions based on dissipated-work parameters were quite similar to those based on deviatoric plastic strain trajectory. The dissipated-work based disturbance parameters were not found to be advantageous as far as variability of parameters with loading conditions. Thus, the dissipated-work based formulation wherein the deviatoric plastic strain trajectory is simply replaced by the dissipated work in the disturbance equation is not found to be of significant utility. Only strain-based DSC was used for the full 3-D elastoplastic formulation as well as the viscoplastic scheme.

Viscoplastic backpredictions at 2.78×10^{-3} and 2.78×10^{-2}/s have been obtained using the full 3-dimensional formulation. As test data at 2.78×10^{-4}/s has been used as the static yield surface, simplified 1-dimensional elastoplastic backpredictions are provided for the same. The static yield surface backpredictions indicate that if the plasticity model is sufficiently complex, reasonable backpredictions may be obtained for a range of values of the elastic modulus, although the plasticity parameters depend on the value of the elastic modulus selected. Thus, accurate measurement of elastic modulus is crucial to the accurate determination of plasticity parameters.

Backpredictions for the elastoplastic and viscoplastic schemes are presented in Figures 6.7 – 6.18. Each figure includes elastoplastic and viscoplastic simulation results for one set of test conditions.

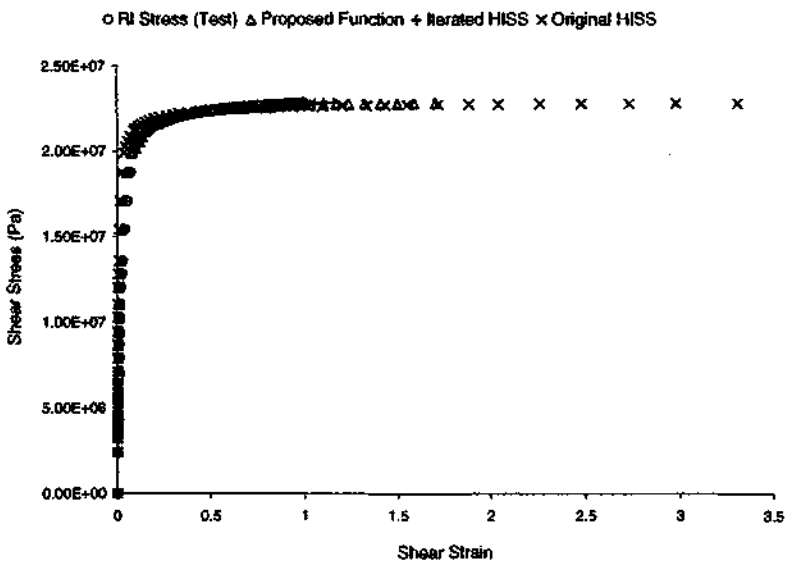

(a) Simplified 1-D RI Elastoplastic Backprediction

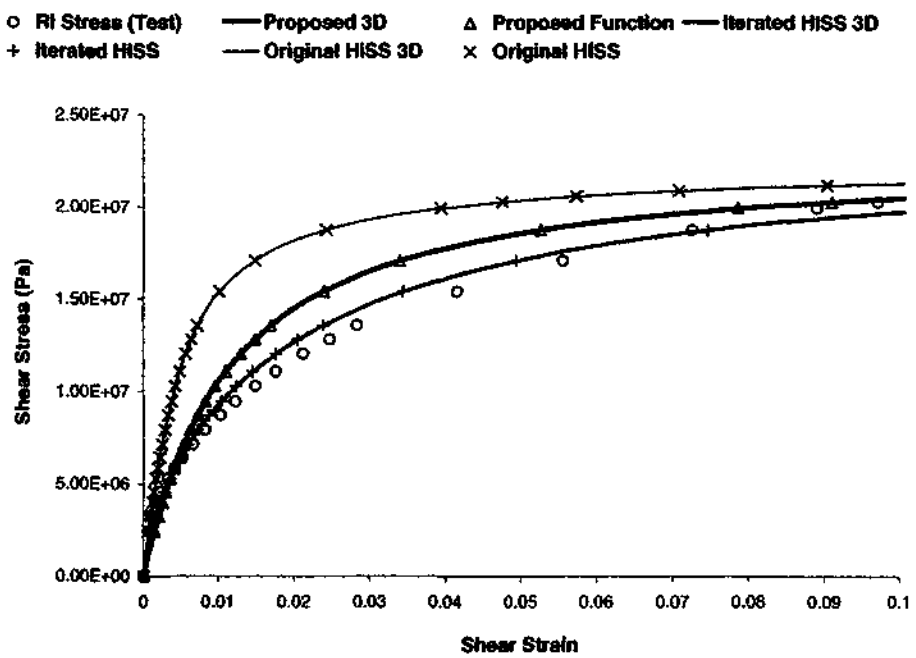

(b) Comparison of 3-D (curves) and 1-D (points) Elastoplastic Backpredictions

Figure 6.7 Temperature = -20°C, Strain Rate = 2.78 x 10^{-4}/s

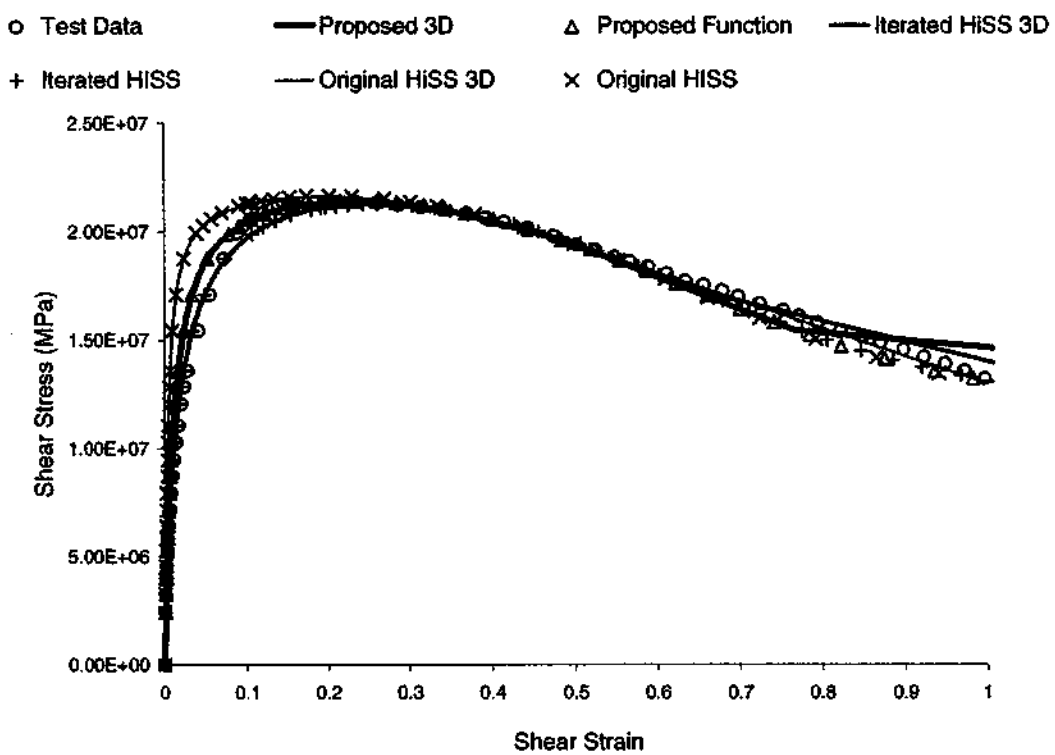

(c) Observed Stress 3-D and 1-D Elastoplastic Backpredictions

Figure 6.7 (continued)

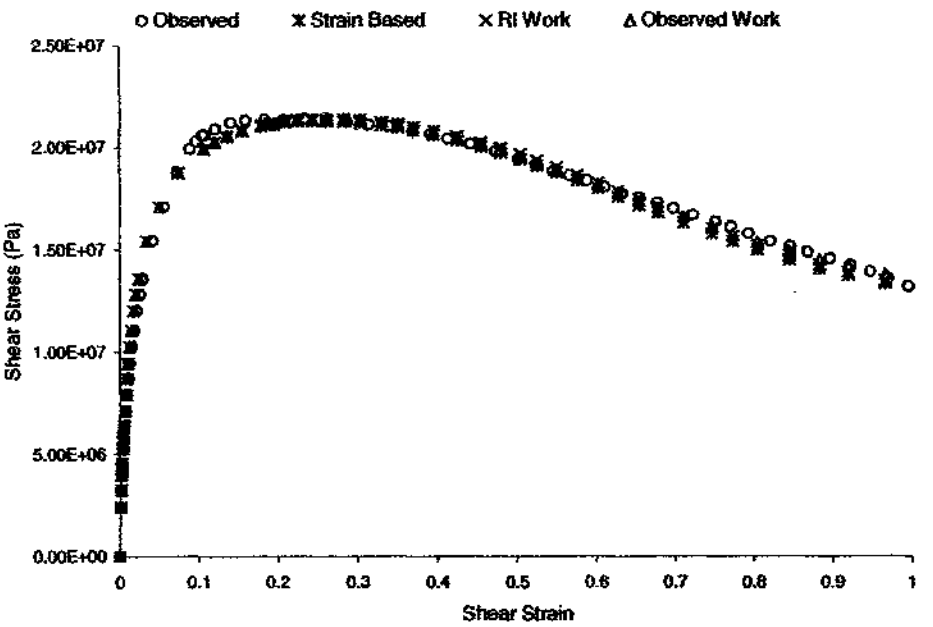

(d) Dissipated-Work DSC for Improved HiSS Parameters

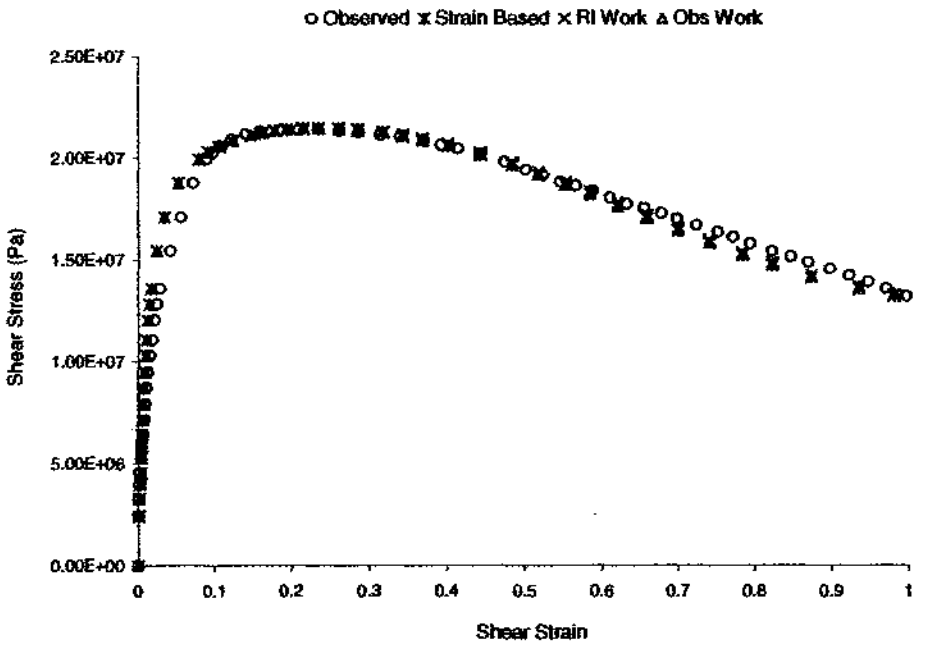

(e) Dissipated-Work DSC for Proposed Yield Function

Figure 6.7 (continued)

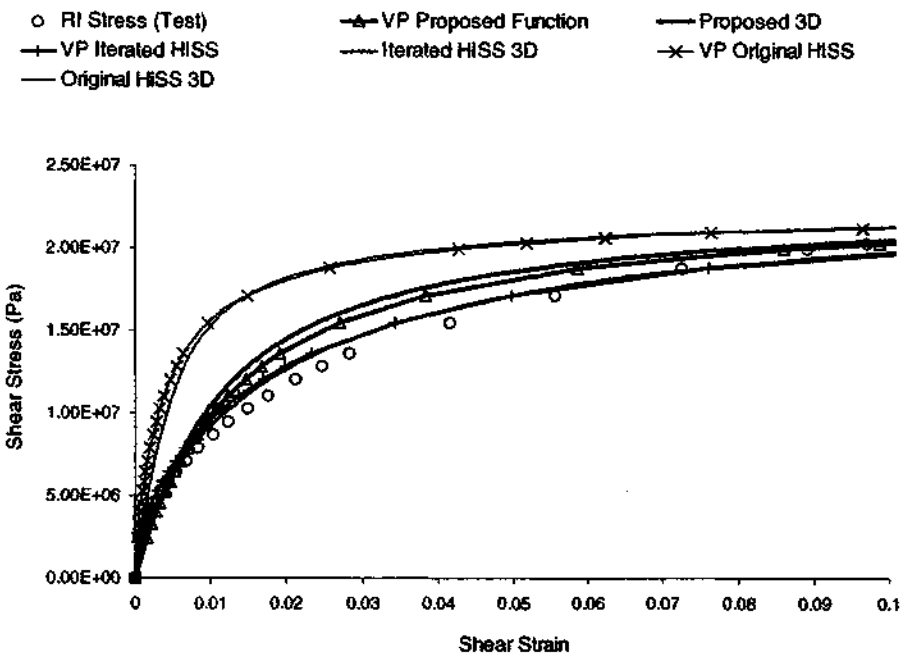

(f) Viscoplastic (Static) and 3-D Elastoplastic RI Comparison

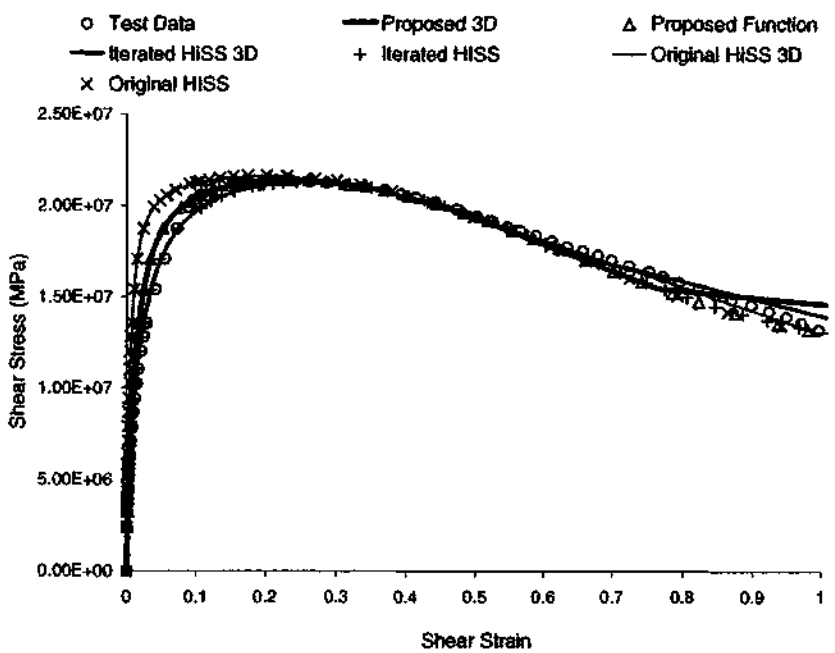

(g) Viscoplastic (Static) Observed Stress

Figure 6.7 (continued)

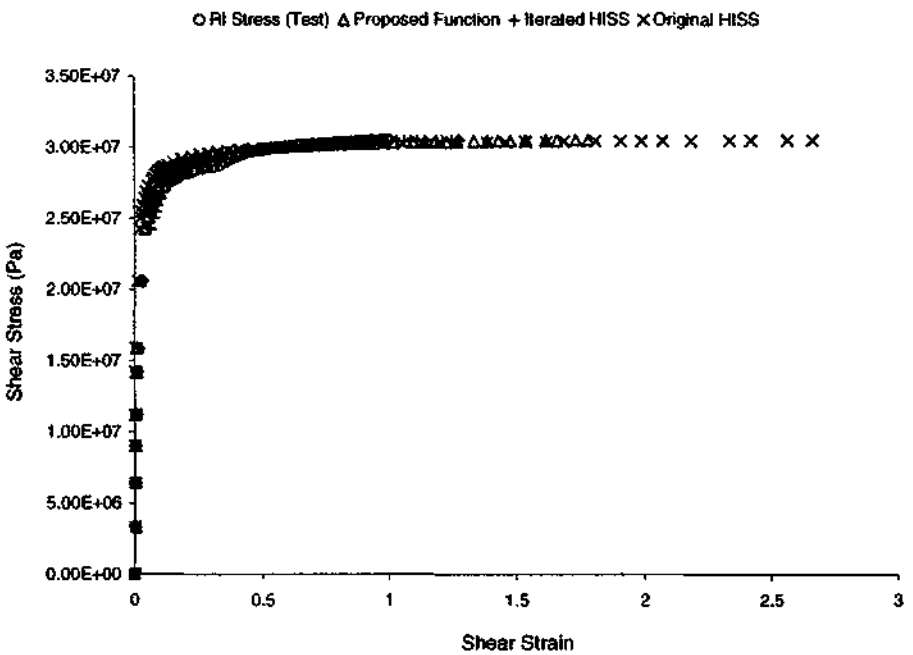

(a) Simplified 1-D RI Elastoplastic Backprediction

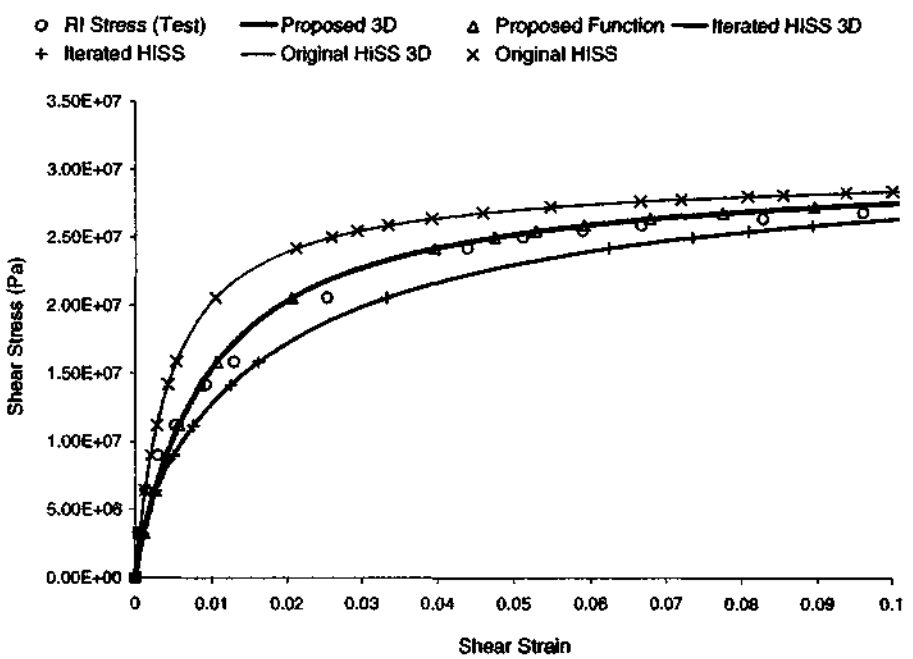

(b) Comparison of 3-D (curves) and 1-D (points) Elastoplastic Backpredictions

Figure 6.8 Temperature = 20°C, Strain Rate = 2.78 x 10^{-3}/s

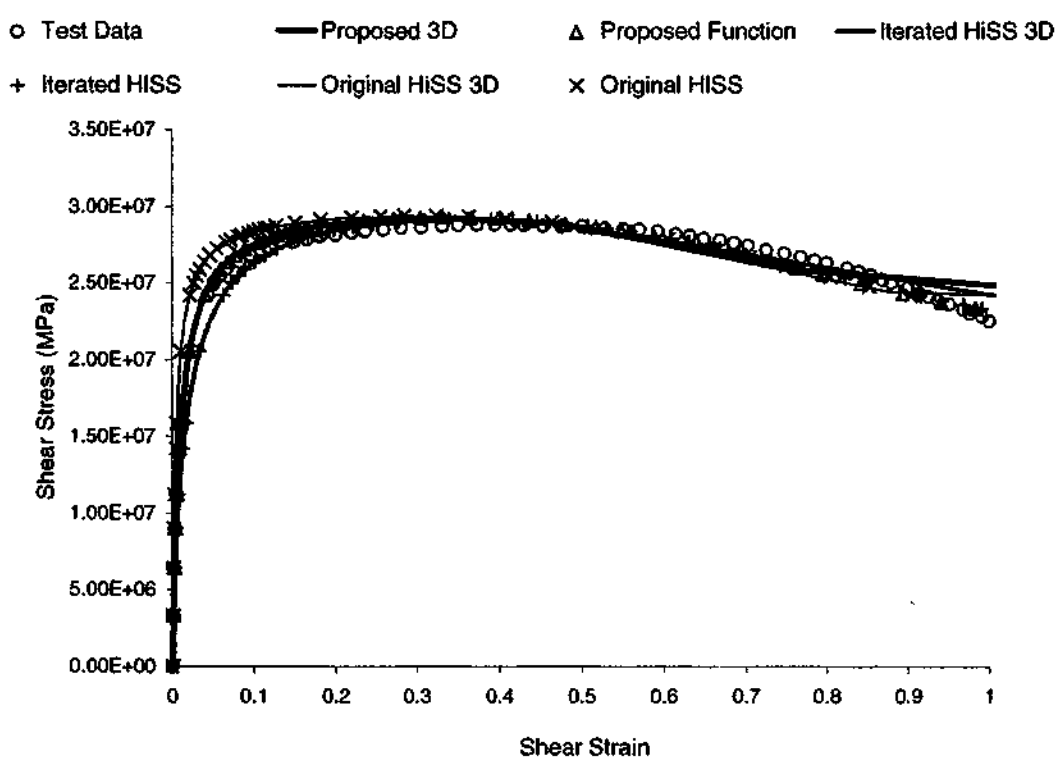

(c) Observed Stress 3-D and 1-D Elastoplastic Backpredictions

Figure 6.8 (continued)

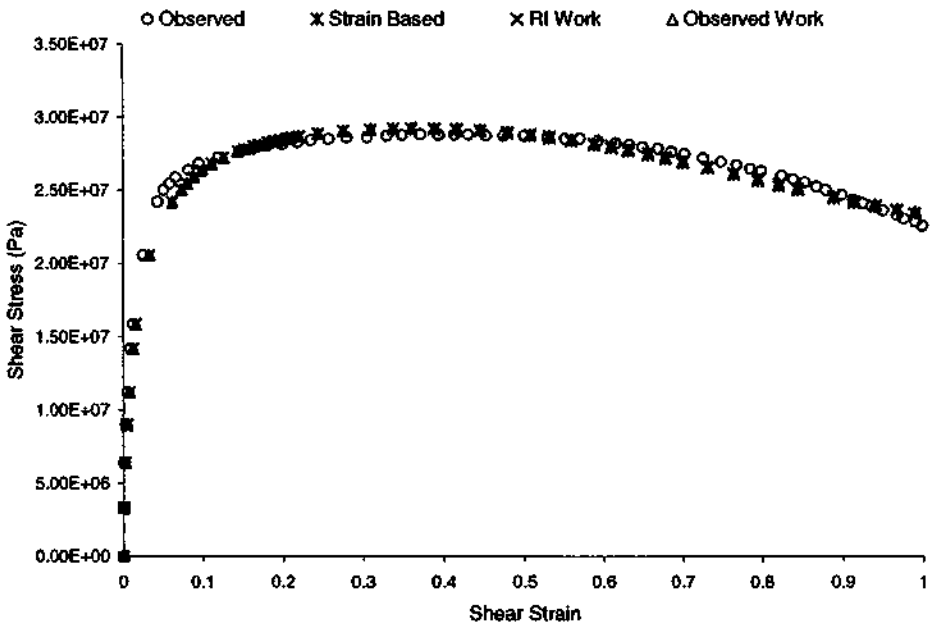

(d) Dissipated-Work DSC for Improved HiSS Parameters

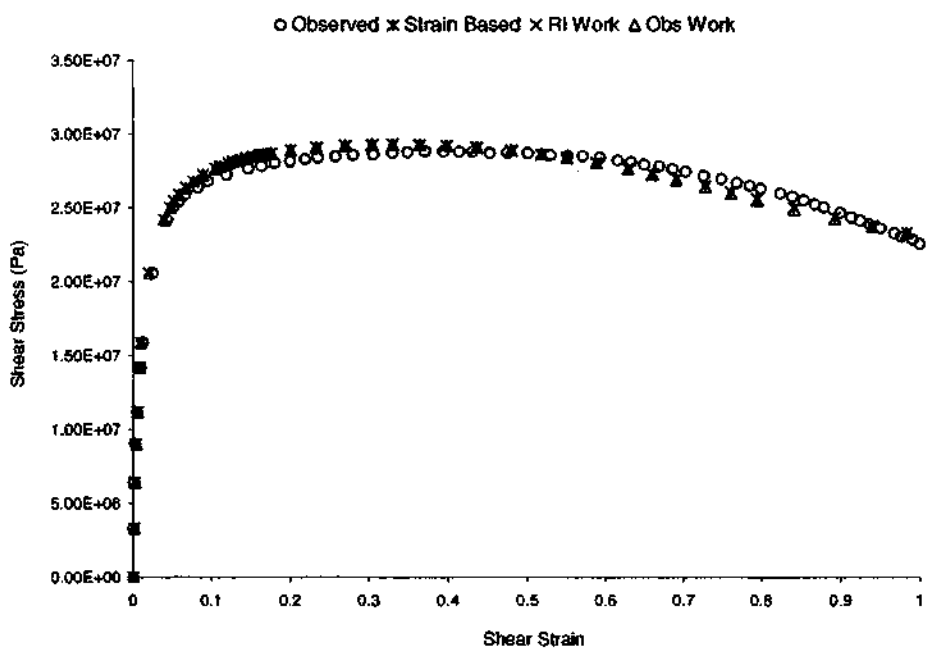

(e) Dissipated-Work DSC for Proposed Yield Function

Figure 6.8 (continued)

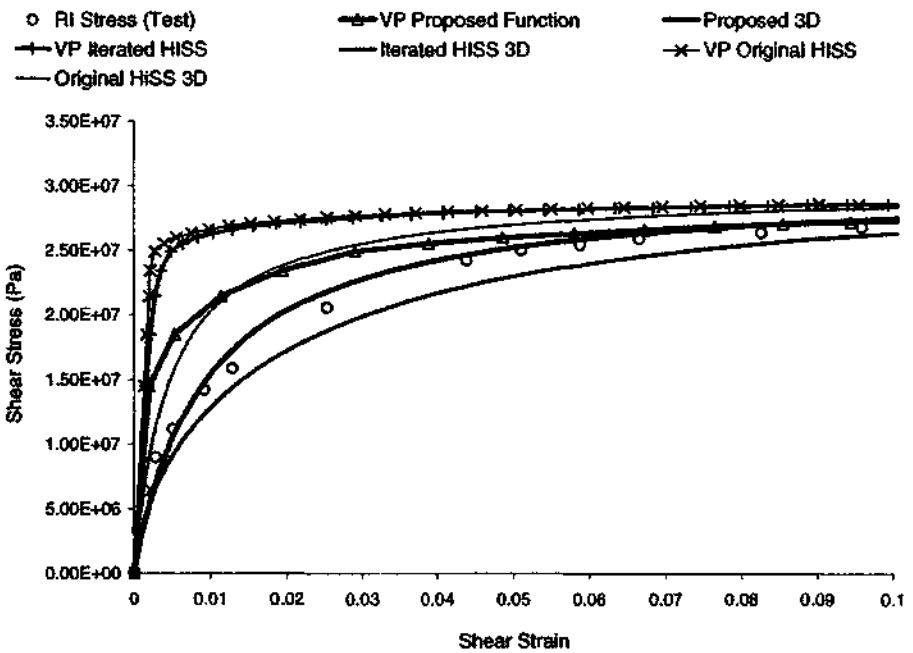

(f) Viscoplastic Backpredictions

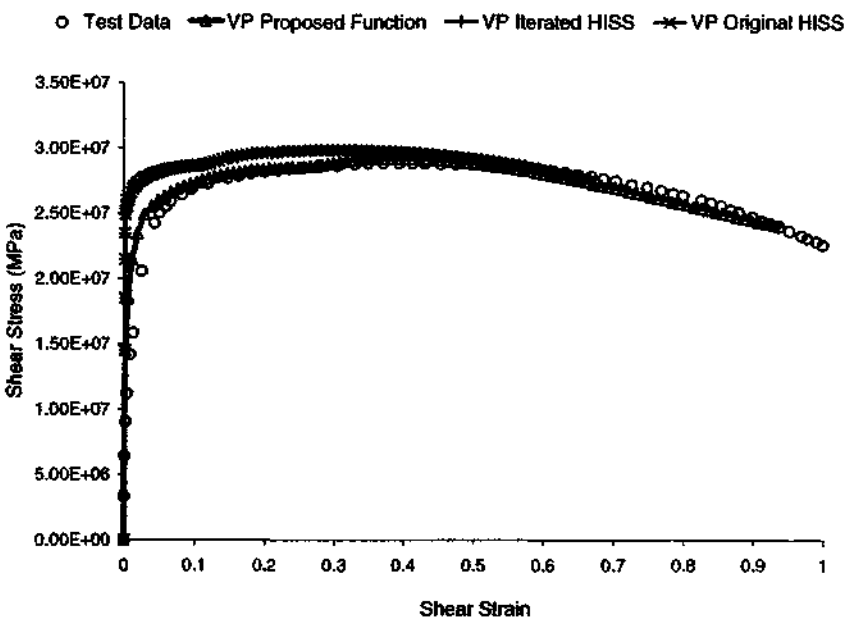

(g) Viscoplastic Observed Stress

Figure 6.8 (continued)

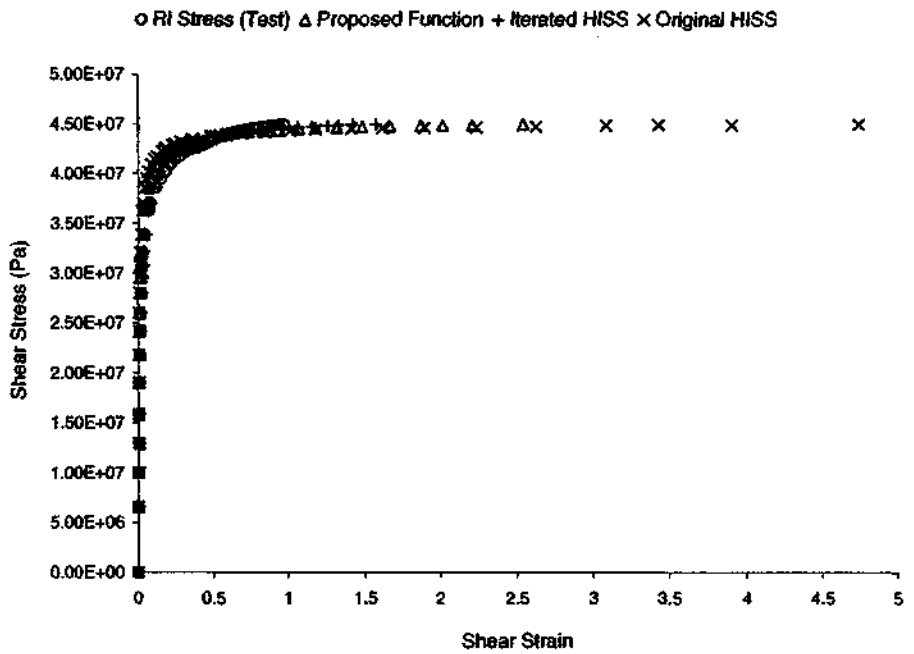

(a) Simplified 1-D RI Elastoplastic Backprediction

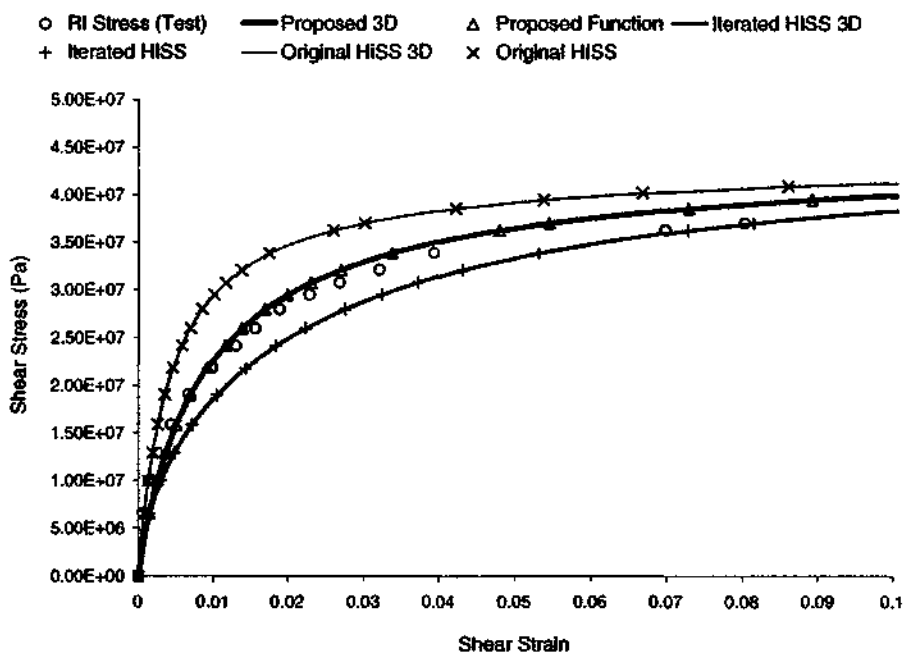

(b) Comparison of 3-D (curves) and 1-D (points) Elastoplastic Backpredictions

Figure 6.9 Temperature = -20°C, Strain Rate ≈ 2.78 x 10^{-2}/s

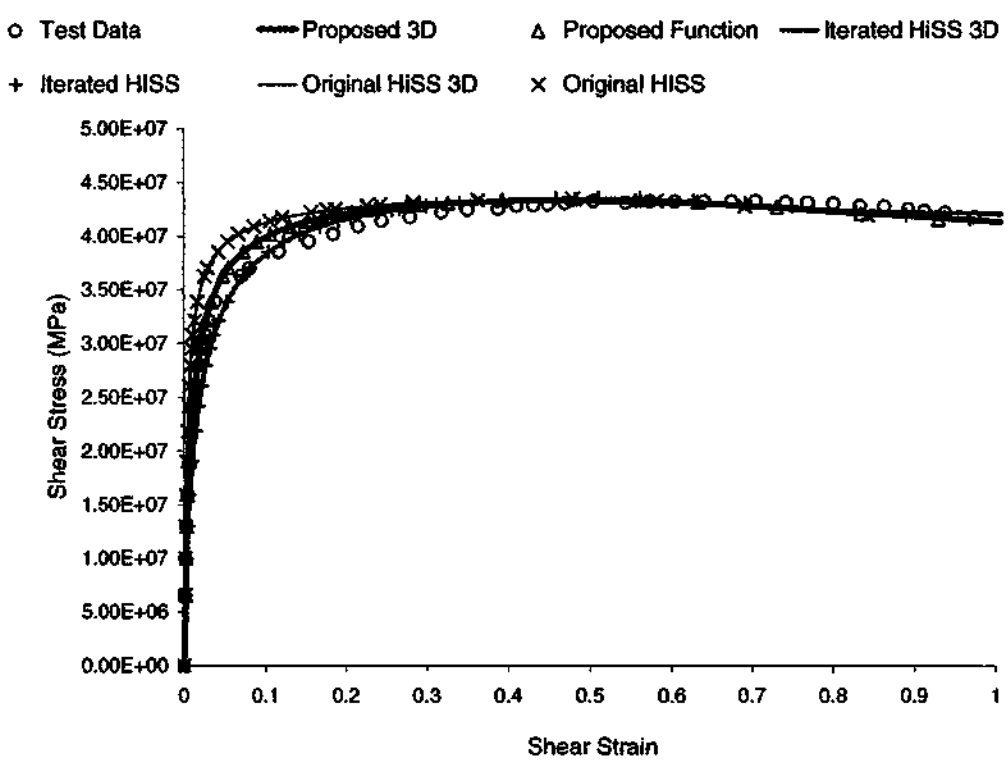

(c) Observed Stress 3-D and 1-D Elastoplastic Backpredictions

Figure 6.9 (continued)

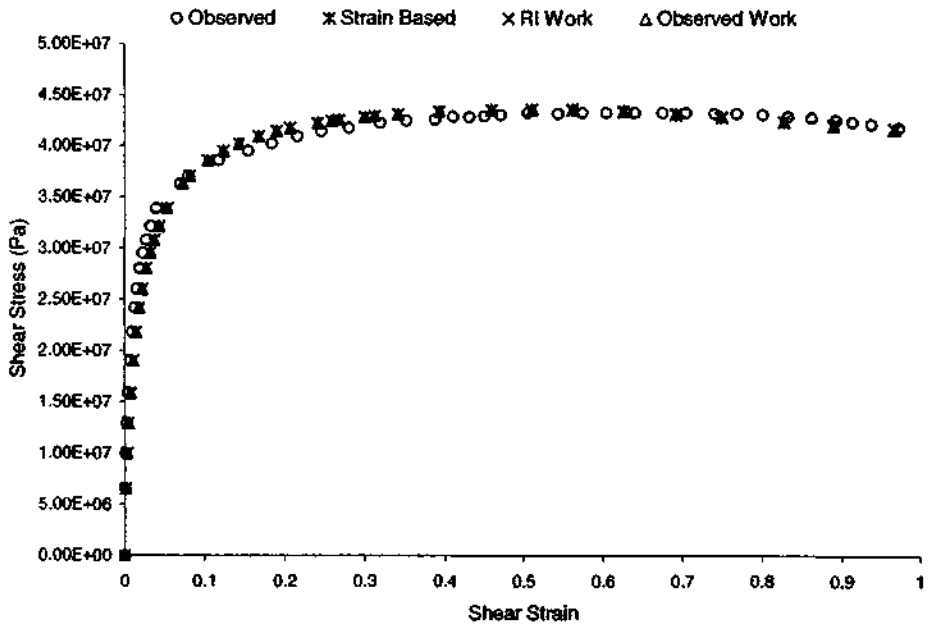

(d) Dissipated-Work DSC for Improved HiSS Parameters

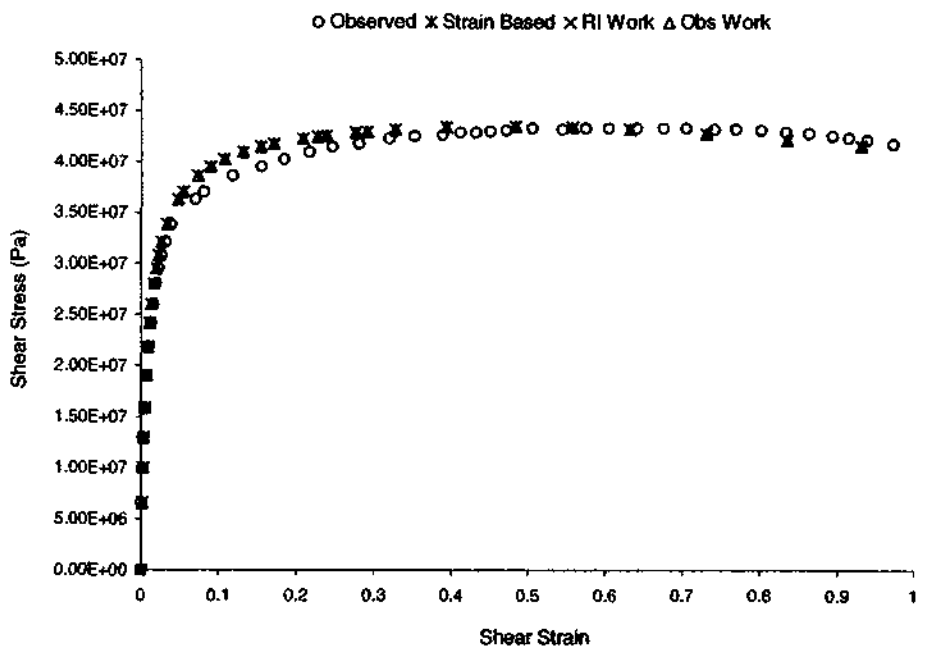

(e) Dissipated-Work DSC for Proposed Yield Function

Figure 6.9 (continued)

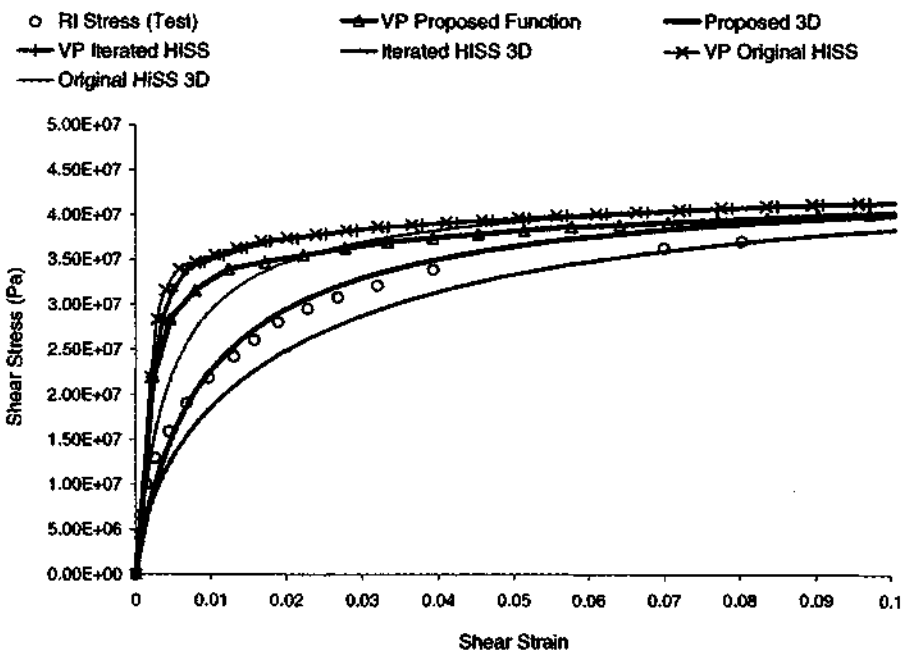

(f) Viscoplastic and 3-D Elastoplastic RI Comparison

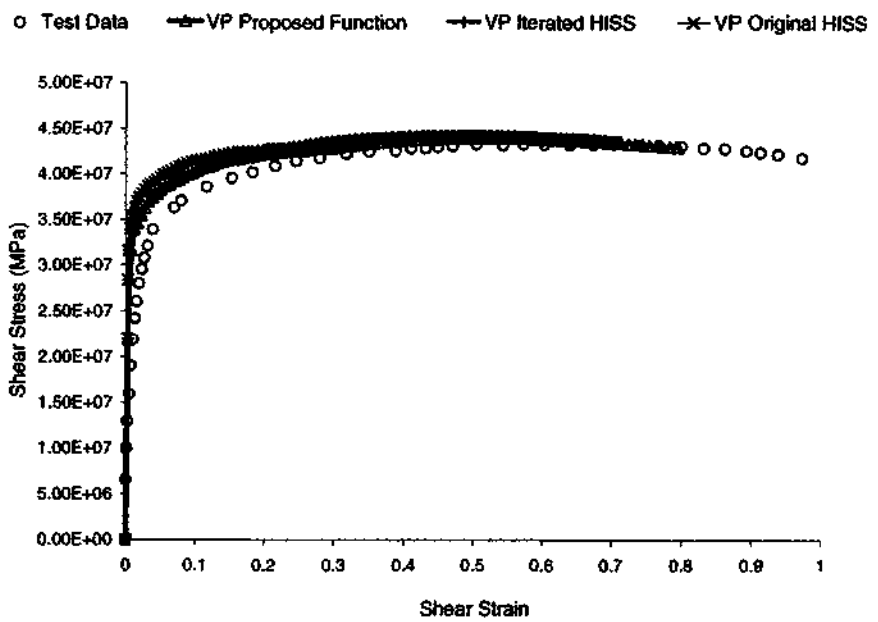

(g) Viscoplastic Observed Stress

Figure 6.9 (continued)

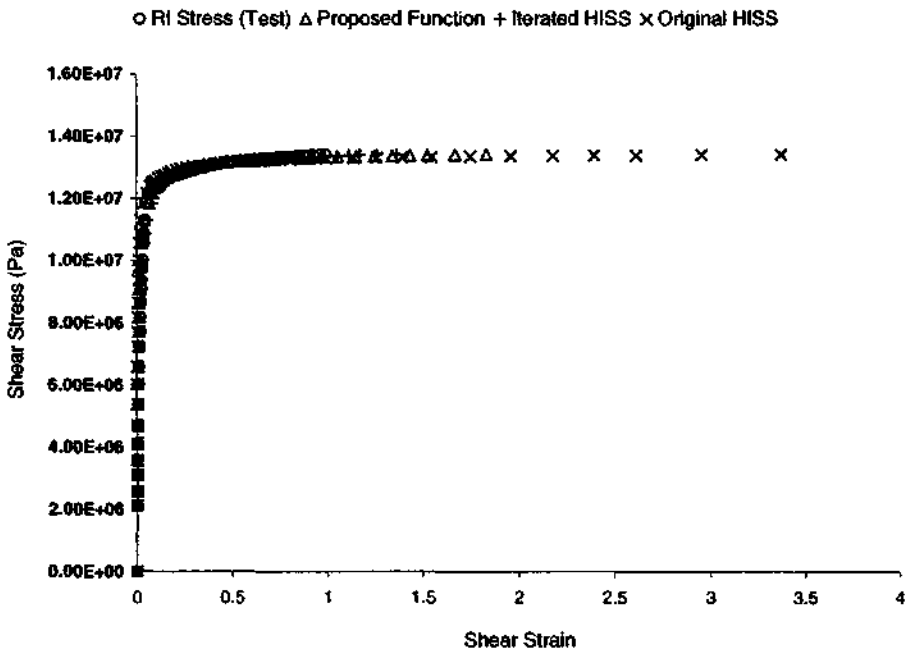

(a) Simplified 1-D RI Elastoplastic Backprediction

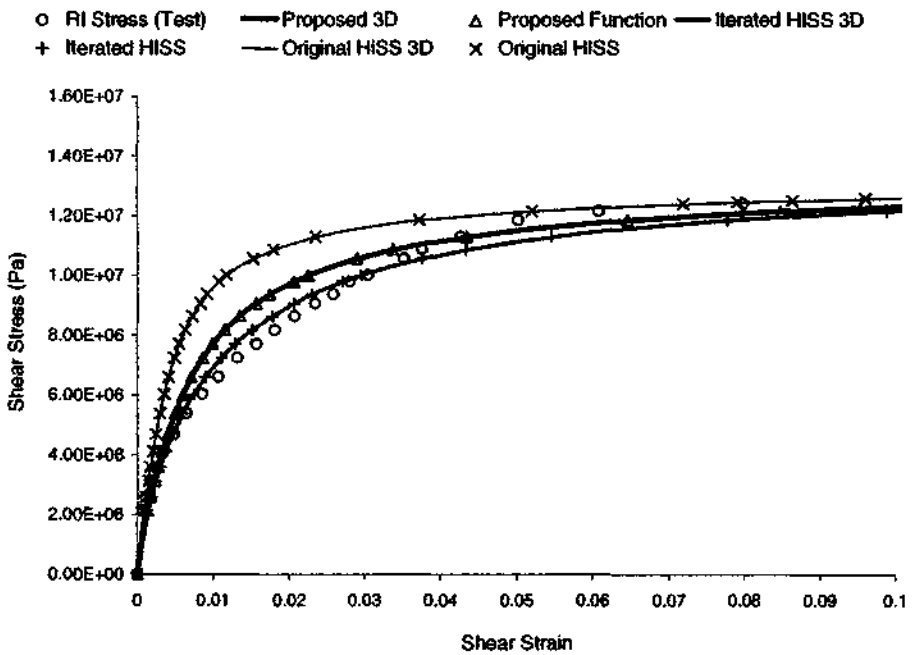

(b) Comparison of 3-D (curves) and 1-D (points) Elastoplastic Backpredictions

Figure 6.10 Temperature = 25°C, Strain Rate = 2.78 x 10^{-4}/s

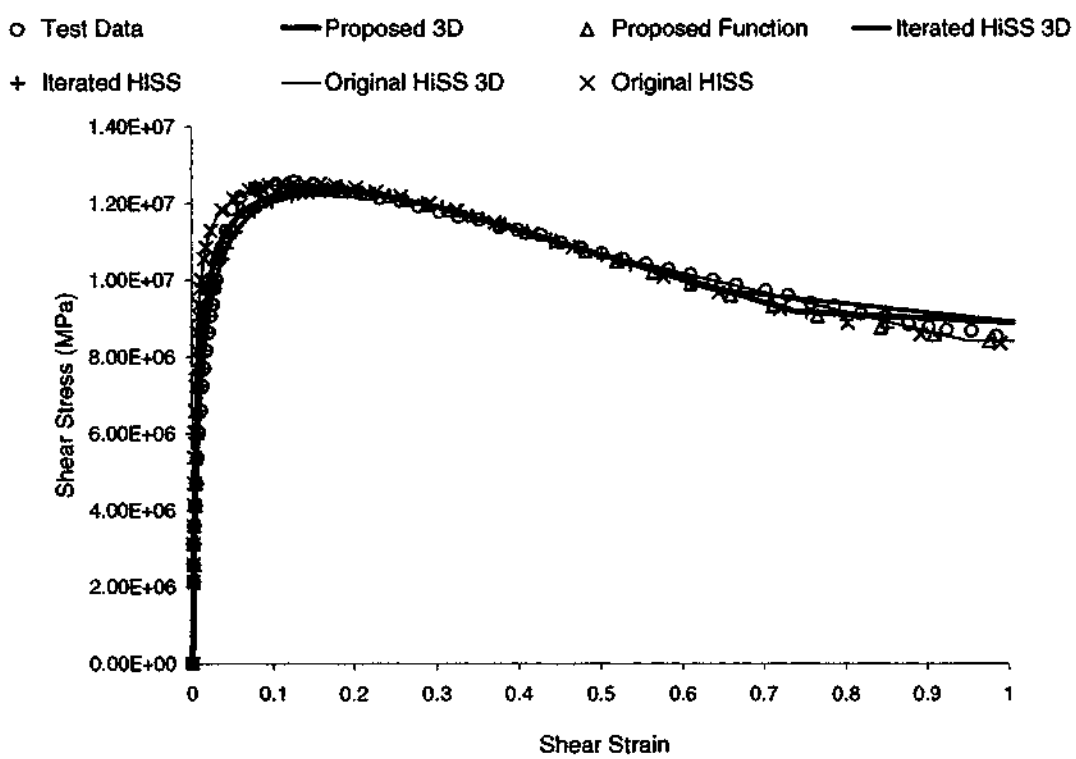

(c) Observed Stress 3-D and 1-D Elastoplastic Backpredictions

Figure 6.10 (continued)

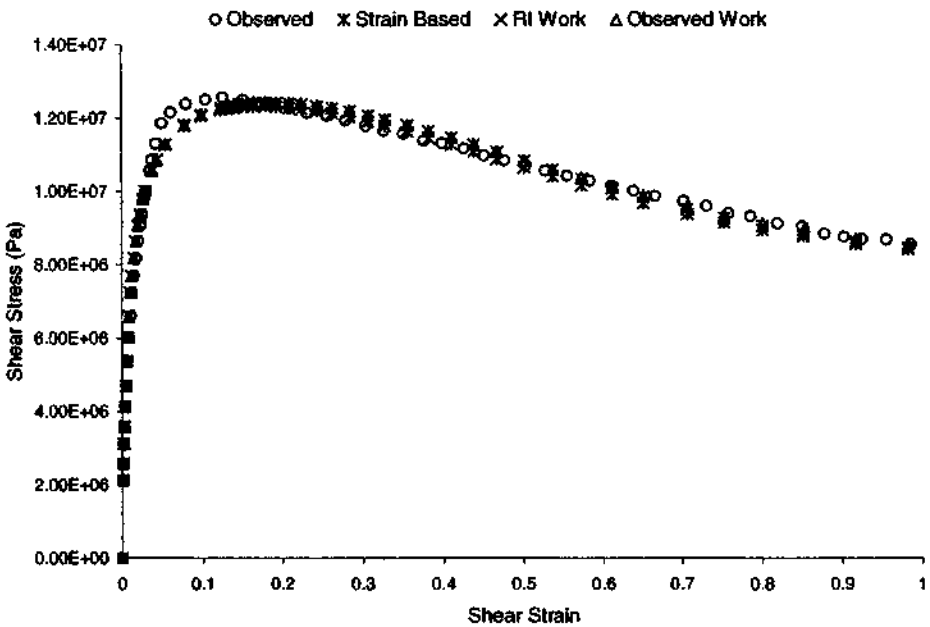

(d) Dissipated-Work DSC for Improved HiSS Parameters

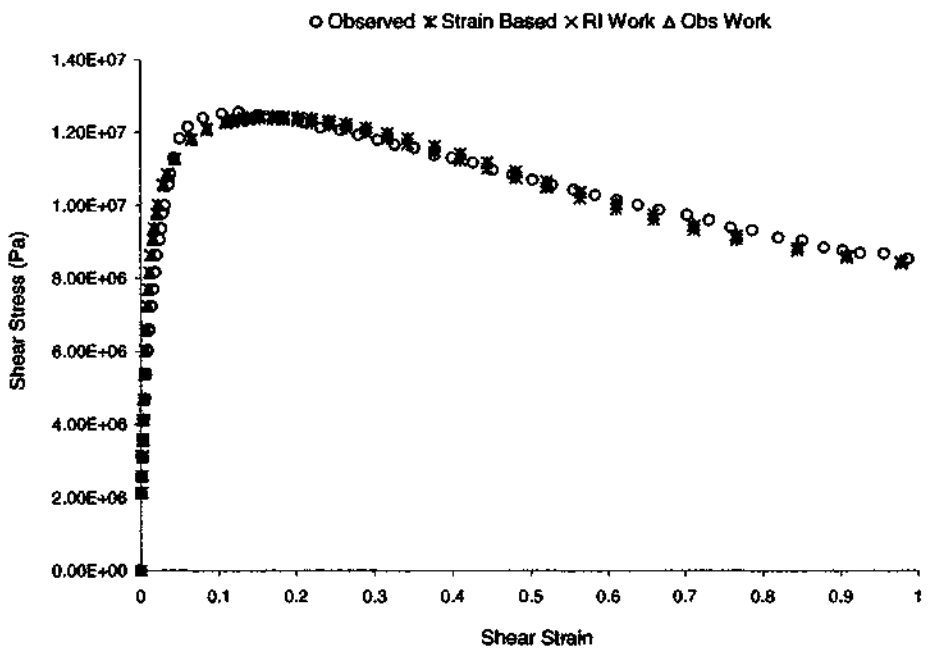

(e) Dissipated-Work DSC for Proposed Yield Function

Figure 6.10 (continued)

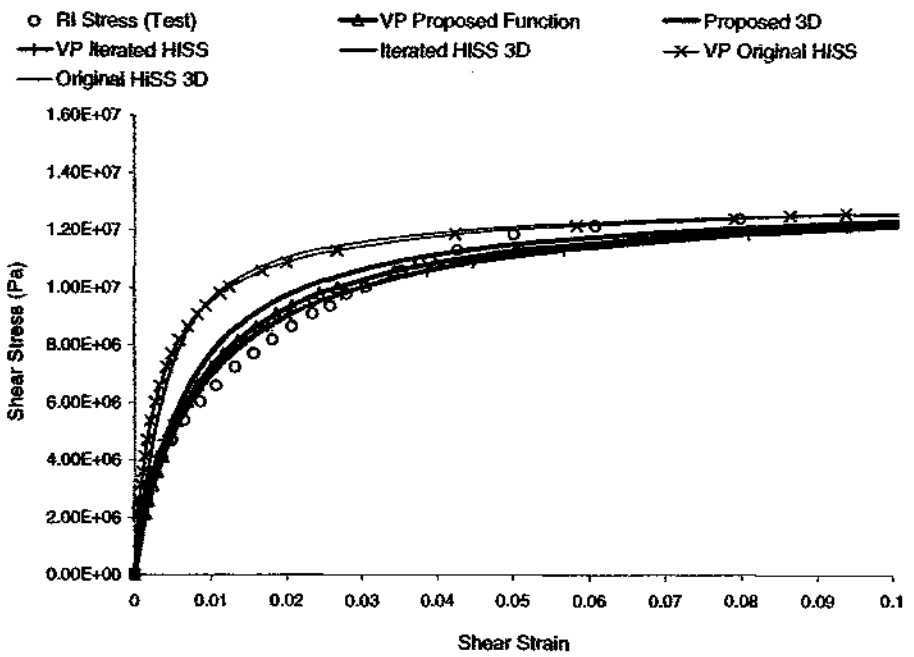

(f) Viscoplastic (Static) and 3-D Elastoplastic RI Comparison

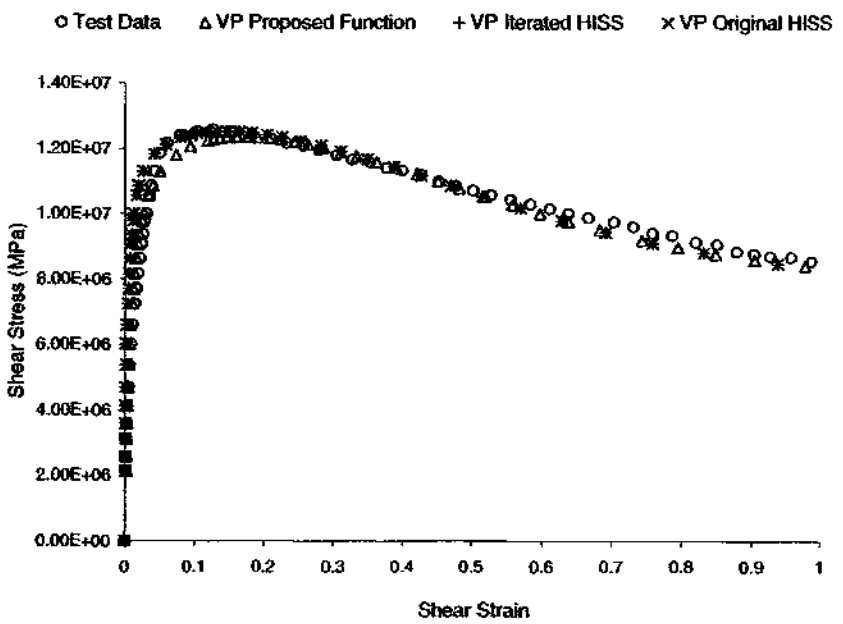

(g) Viscoplastic (Static) Observed Stress

Figure 6.10 (continued)

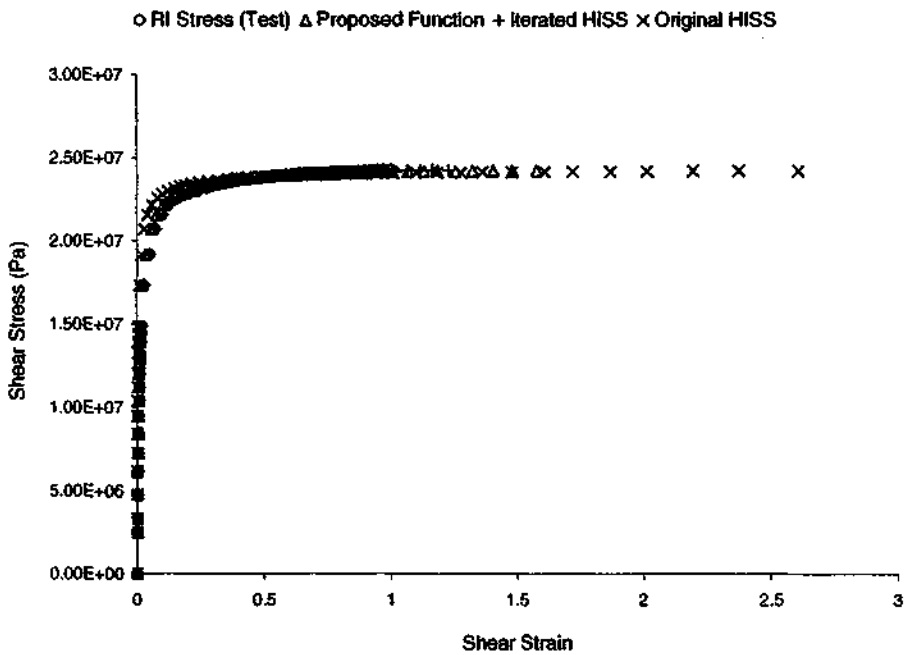

(a) Simplified 1-D RI Elastoplastic Backprediction

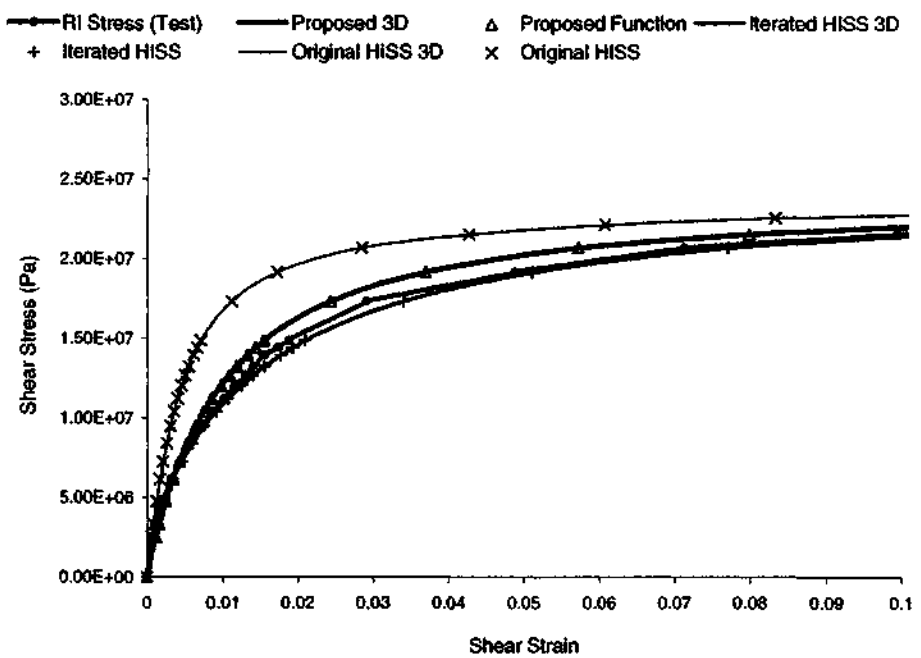

(b) Comparison of 3-D (curves) and 1-D (points) Elastoplastic Backpredictions

Figure 6.11 Temperature = 25°C, Strain Rate = 2.78 x 10^{-3}/s

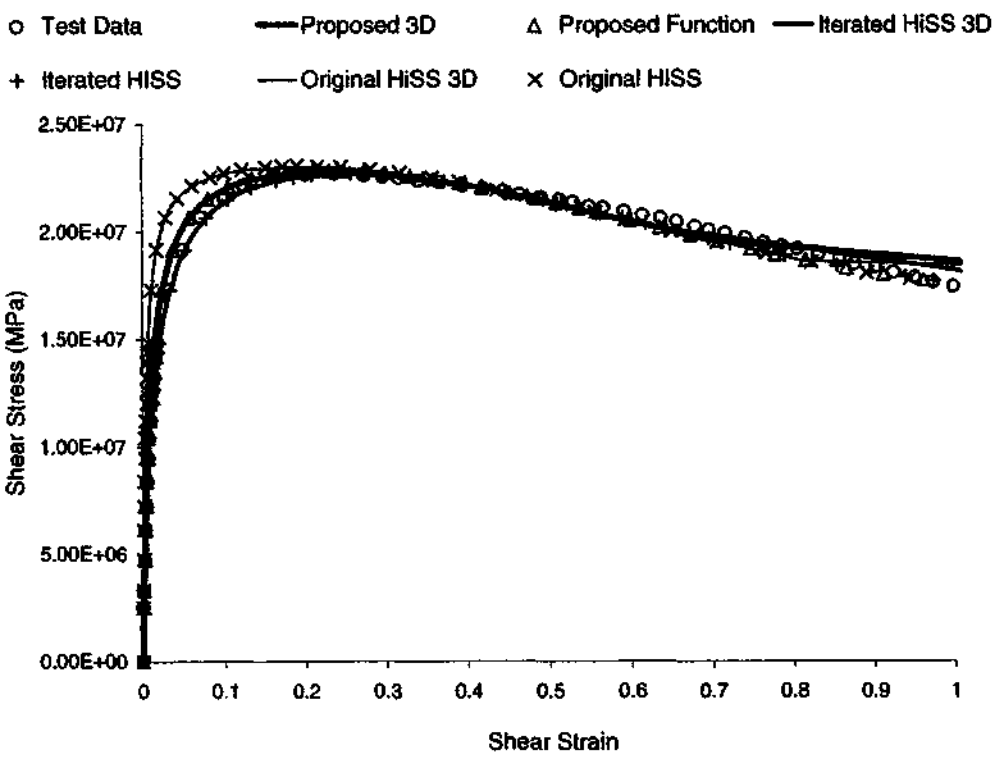

(c) Observed Stress 3-D and 1-D Elastoplastic Backpredictions

Figure 6.11 (continued)

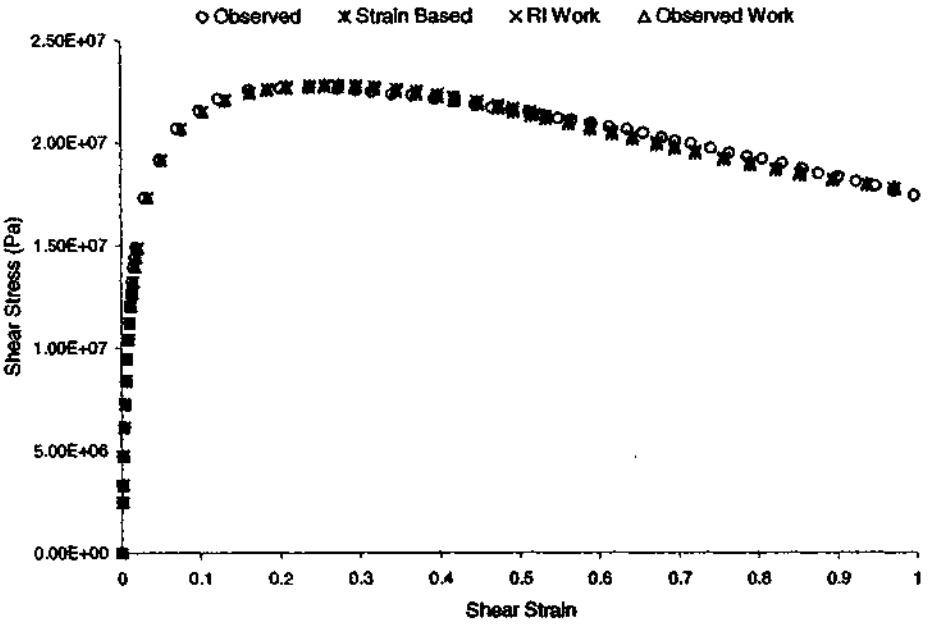

(d) Dissipated-Work DSC for Improved HiSS Parameters

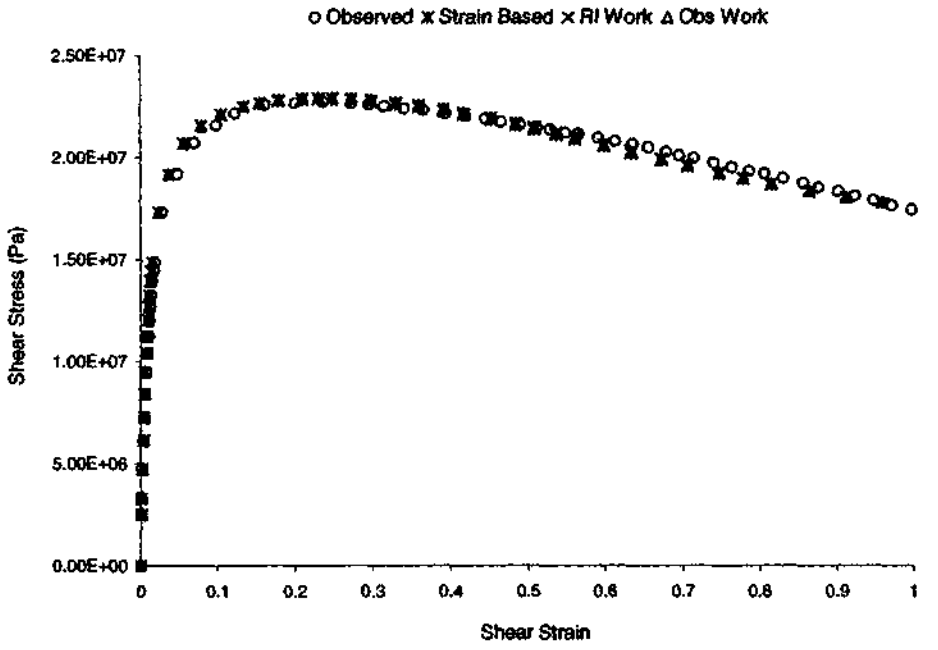

(e) Dissipated-Work DSC for Proposed Yield Function

Figure 6.11 (continued)

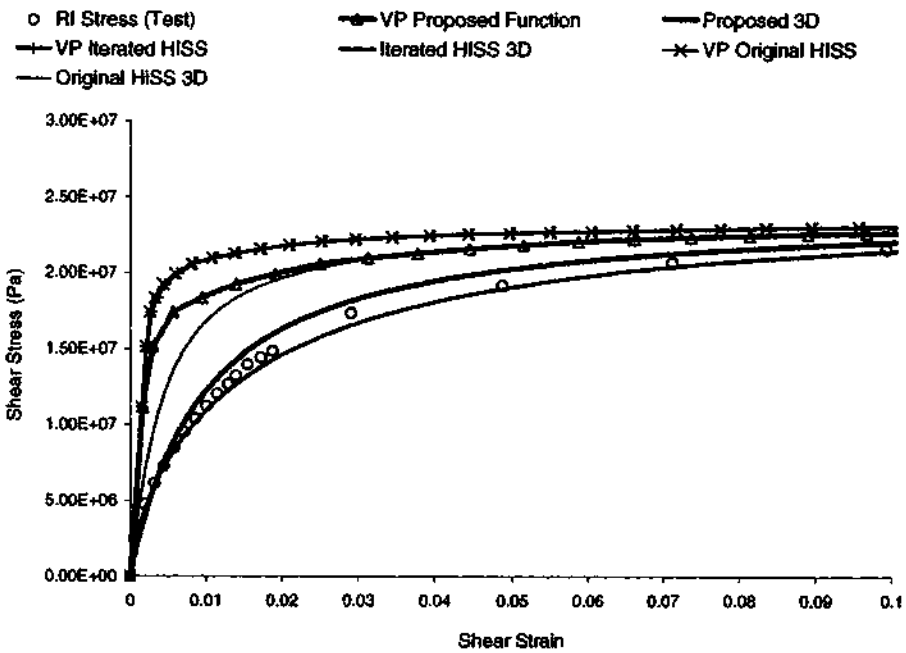

(f) Viscoplastic and 3-D Elastoplastic RI Comparison

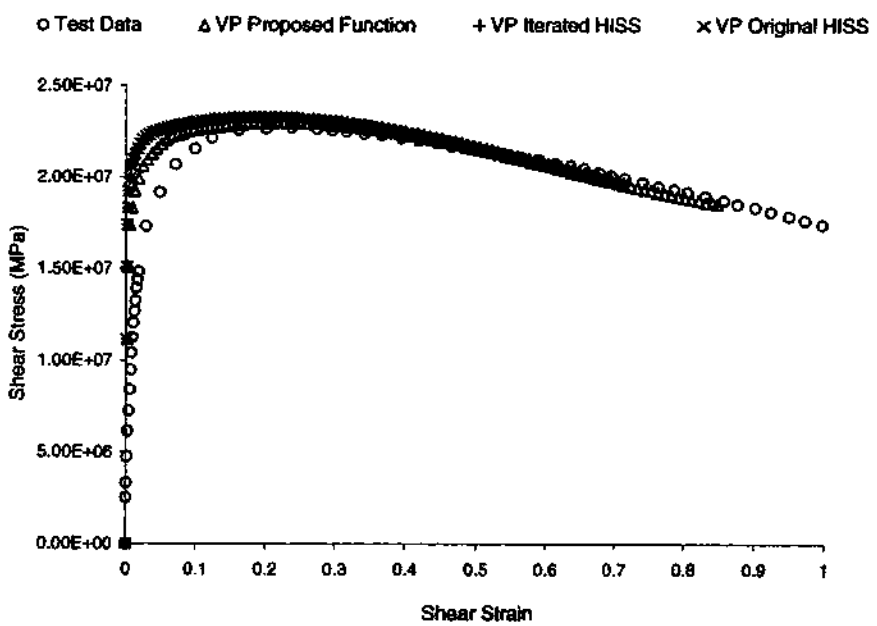

(g) Viscoplastic Observed Stress

Figure 6.11 (continued)

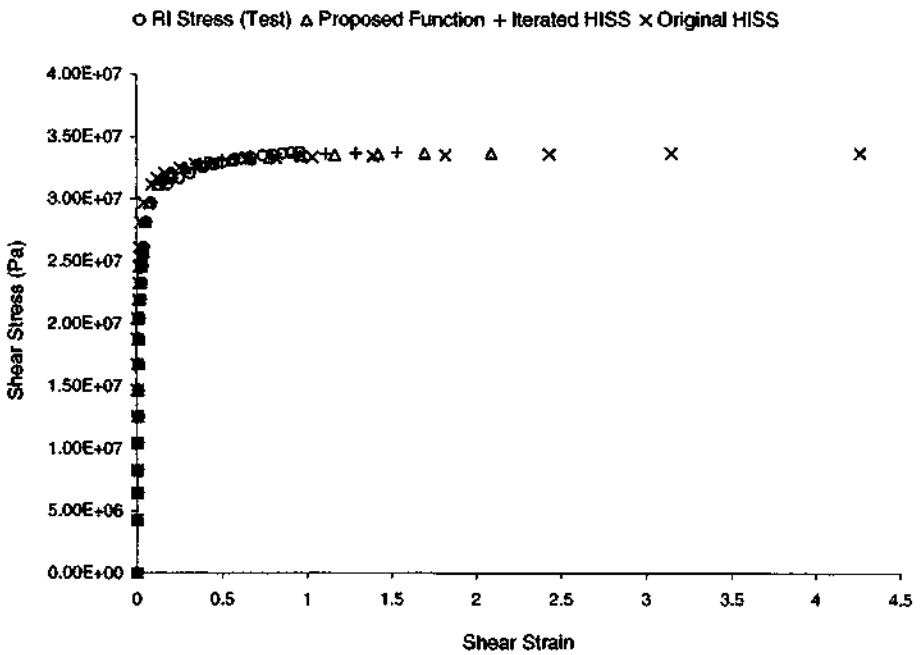

(a) Simplified 1-D RI Elastoplastic Backprediction

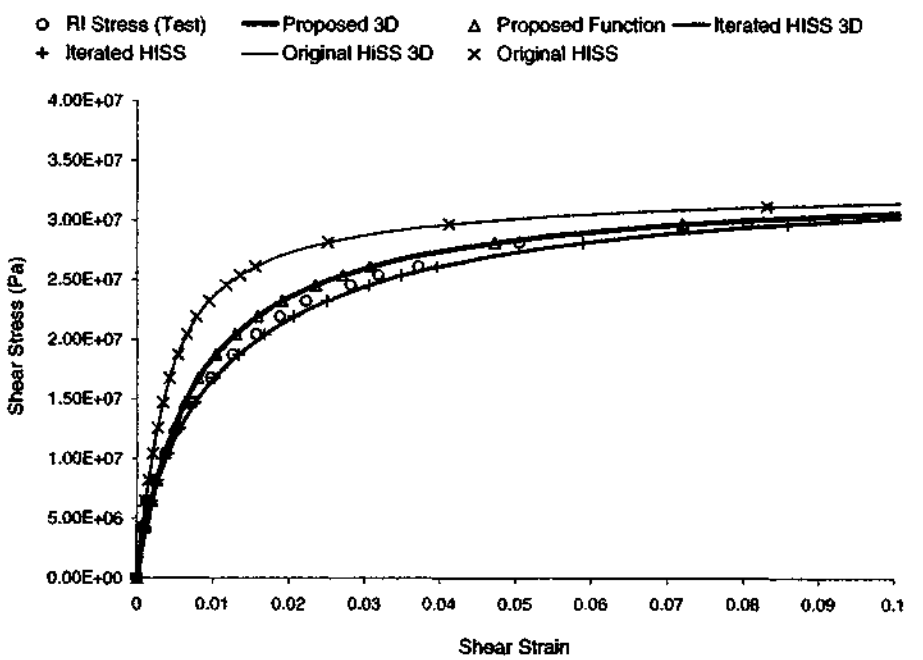

(b) Comparison of 3-D (curves) and 1-D (points) Elastoplastic Backpredictions

Figure 6.12 Temperature = 25°C, Strain Rate = 2.78 x 10^{-2}/s

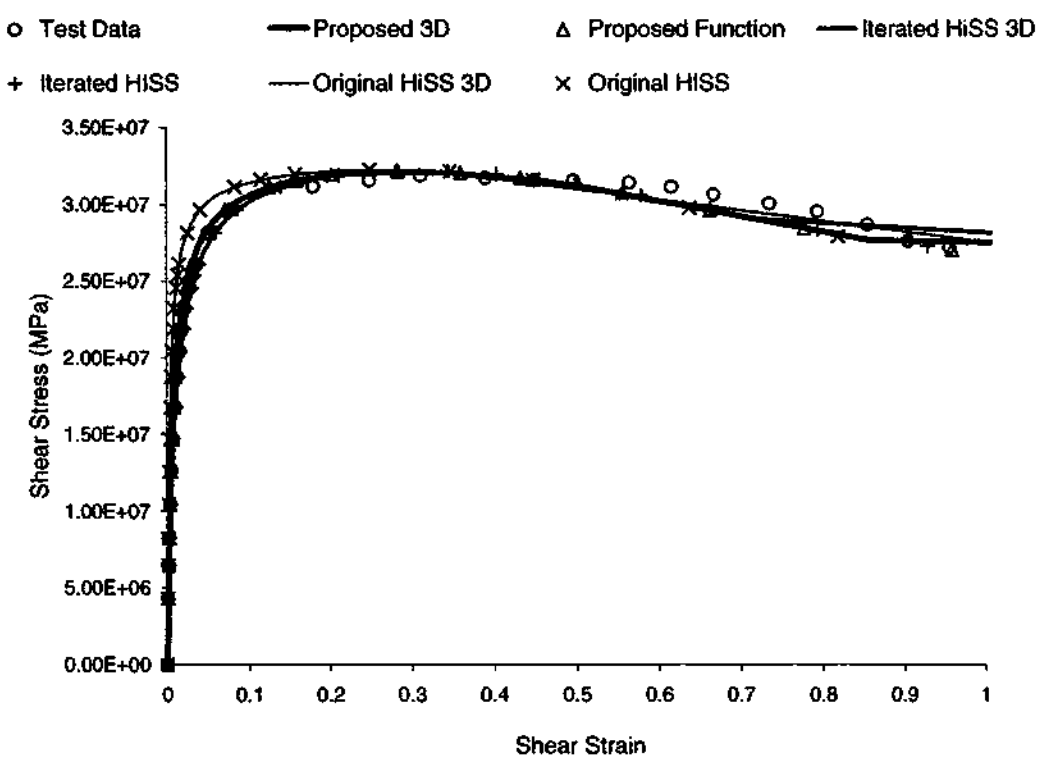

(c) Observed Stress 3-D and 1-D Elastoplastic Backpredictions

Figure 6.12 (continued)

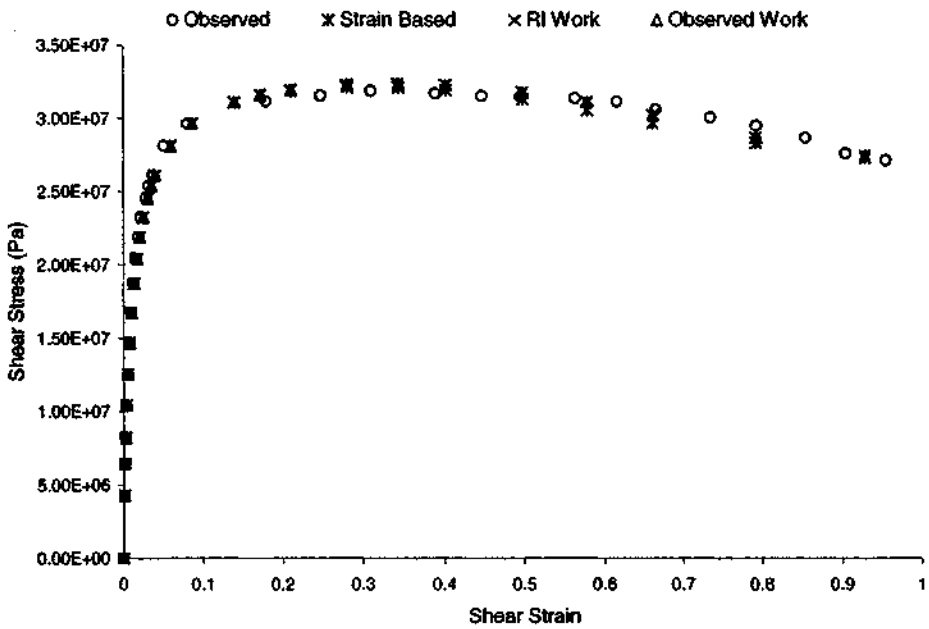

(d) Dissipated-Work DSC for Improved HiSS Parameters

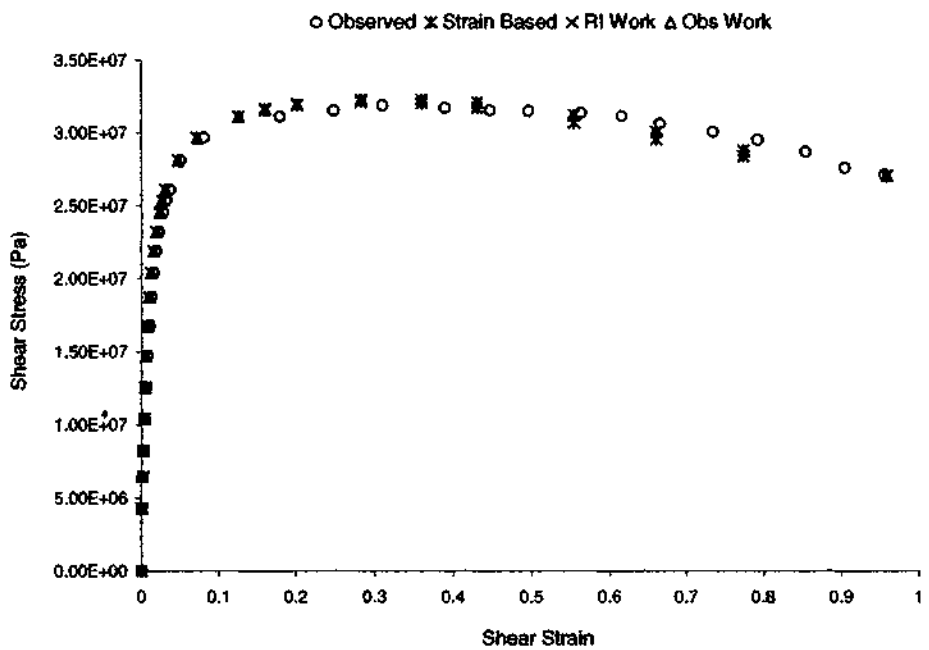

(e) Dissipated-Work DSC for Proposed Yield Function

Figure 6.12 (continued)

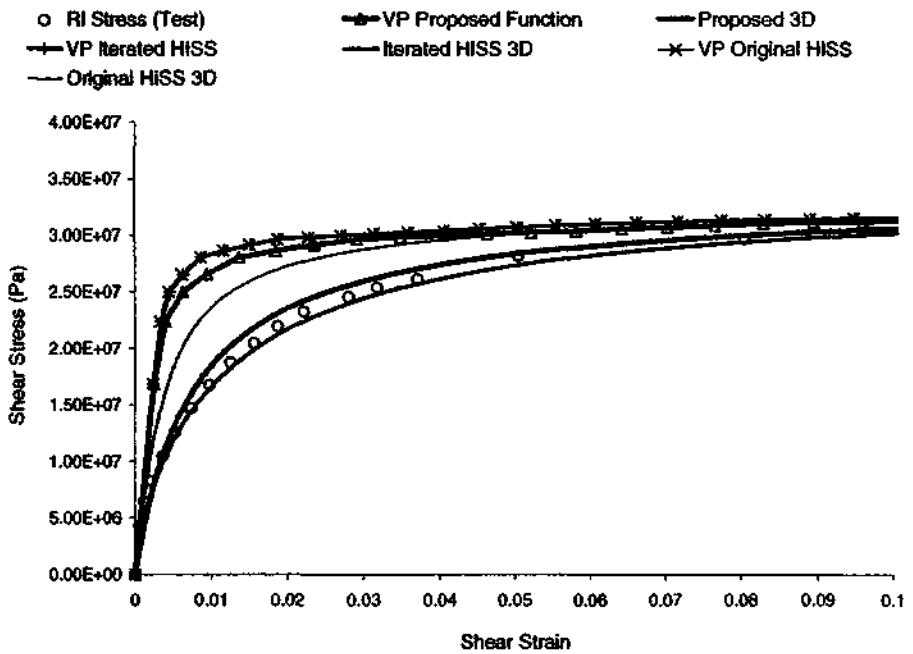

(f) Viscoplastic and 3-D Elastoplastic RI Comparison

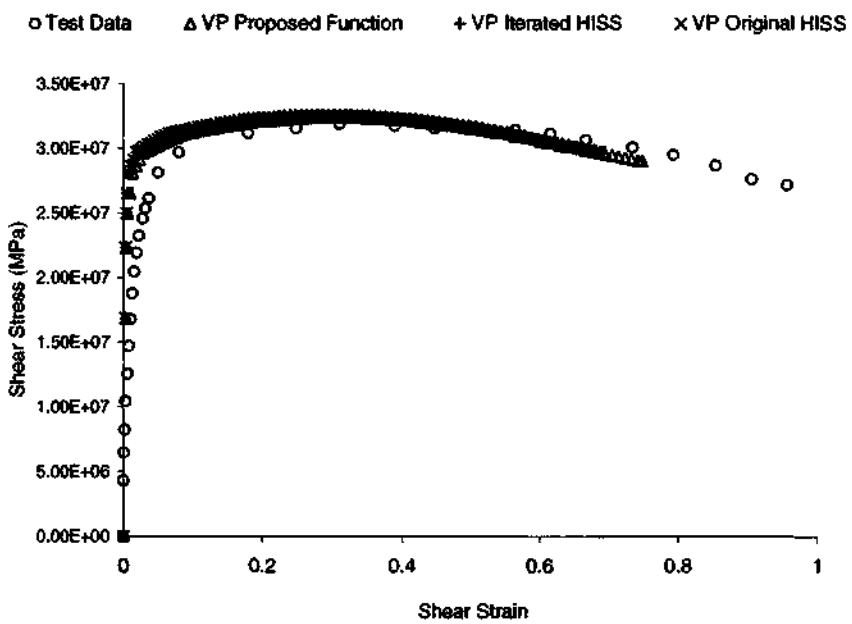

(g) Viscoplastic Observed Stress

Figure 6.12 (continued)

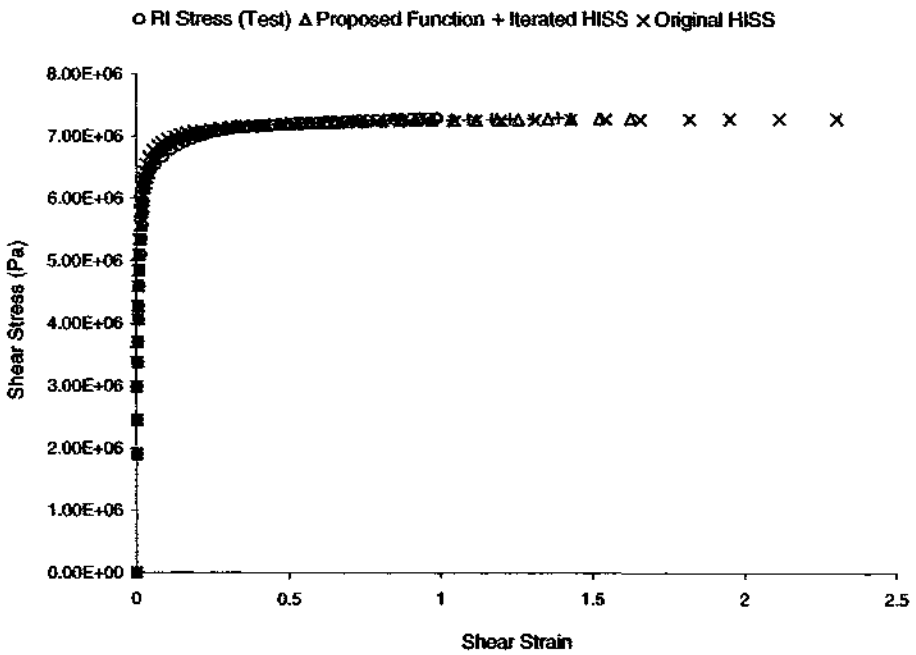

(a) Simplified 1-D RI Elastoplastic Backprediction

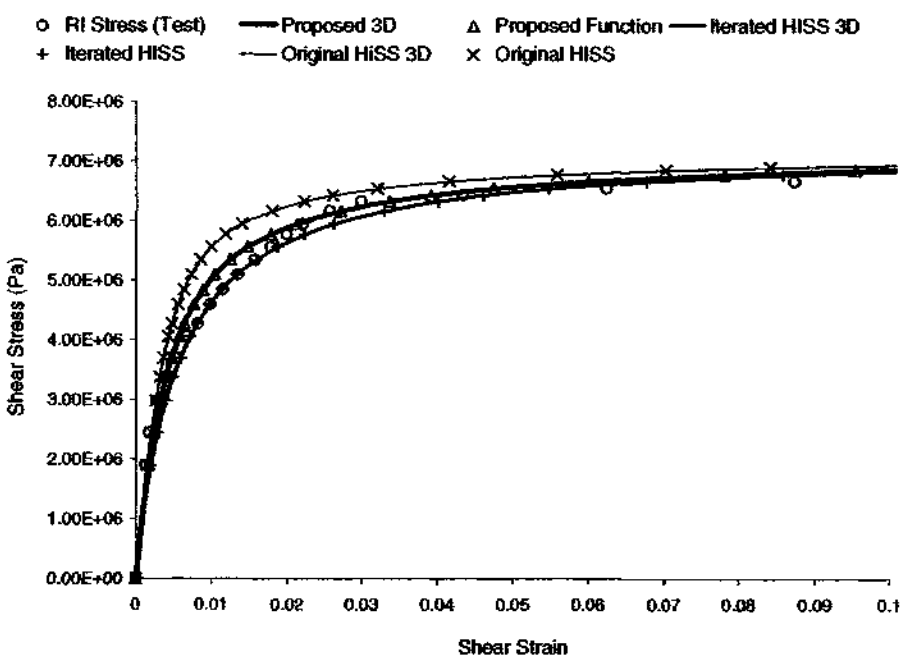

(b) Comparison of 3-D (curves) and 1-D (points) Elastoplastic Backpredictions

Figure 6.13 Temperature = 75°C, Strain Rate = 2.78 x 10^{-4}/s

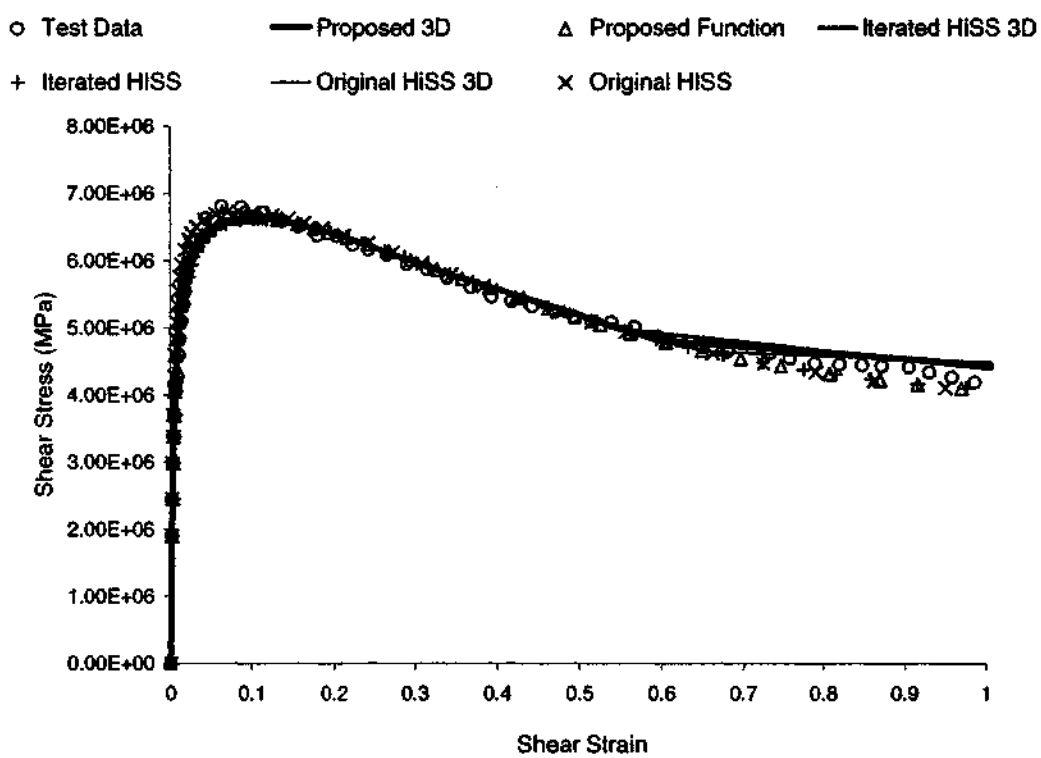

(c) Observed Stress 3-D and 1-D Elastoplastic Backpredictions

Figure 6.13 (continued)

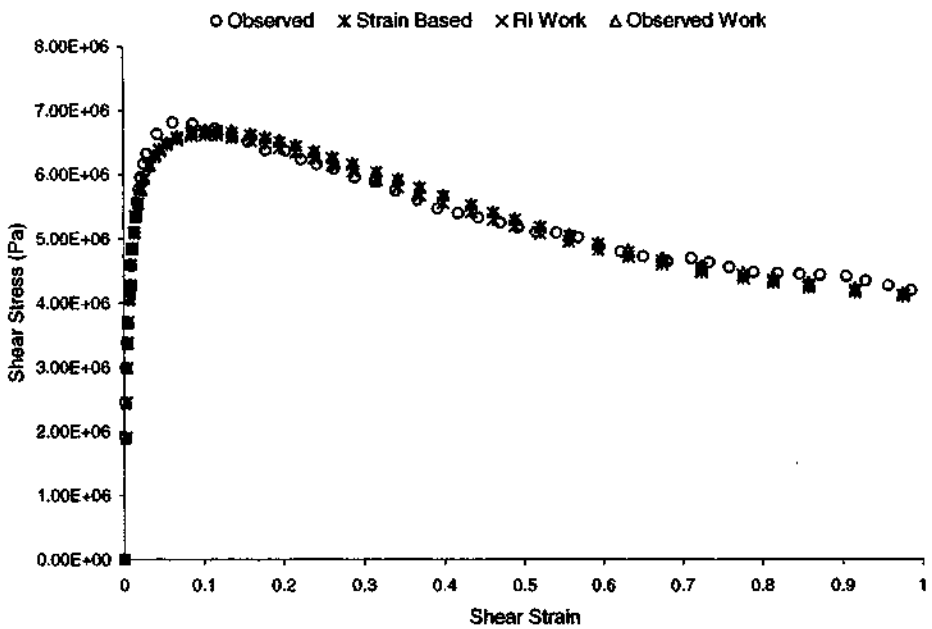

(d) Dissipated-Work DSC for Improved HiSS Parameters

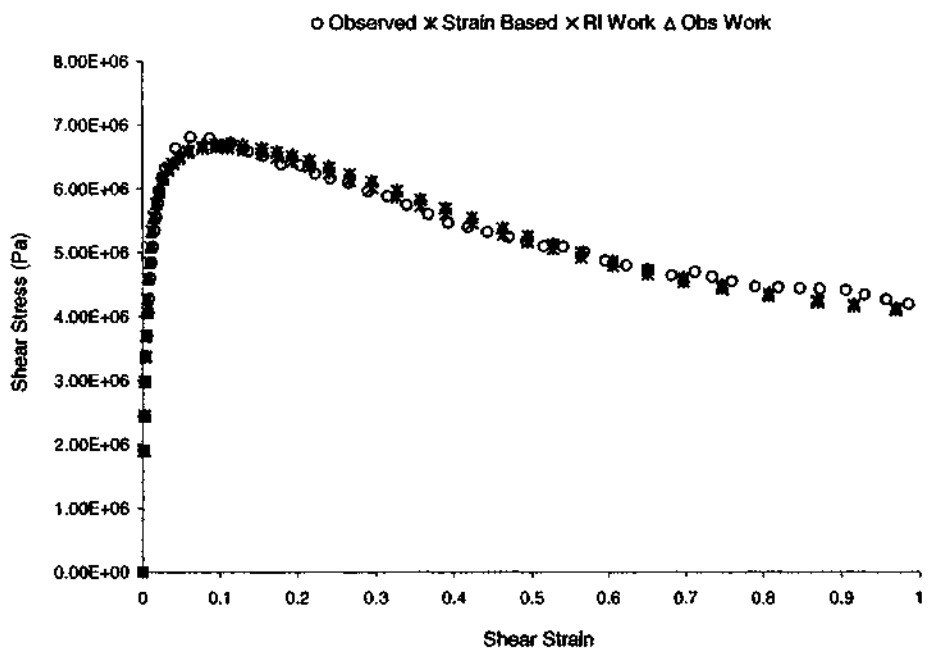

(e) Dissipated-Work DSC for Proposed Yield Function

Figure 6.13 (continued)

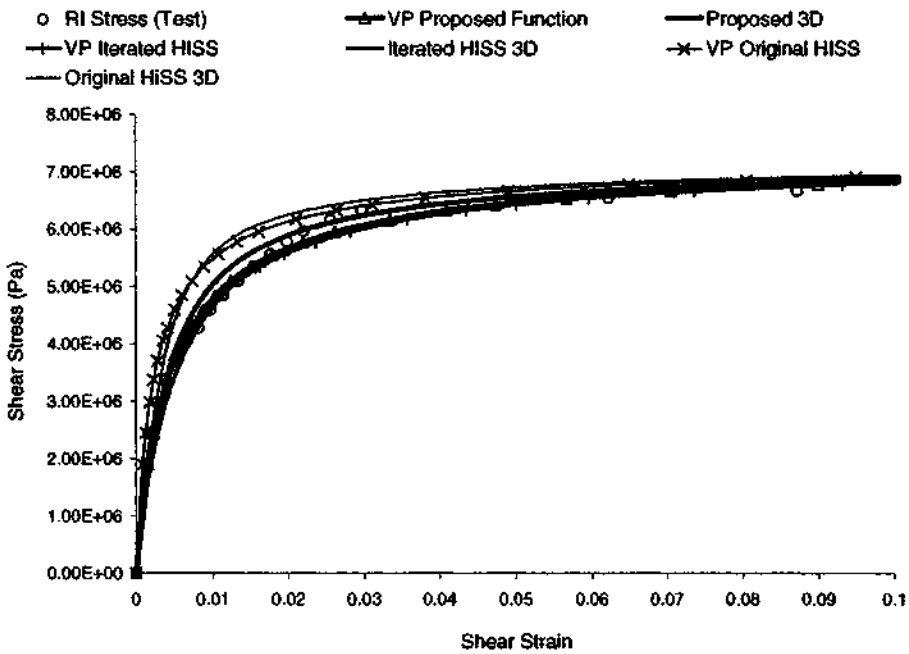

(f) Viscoplastic (Static) and 3-D Elastoplastic RI Comparison

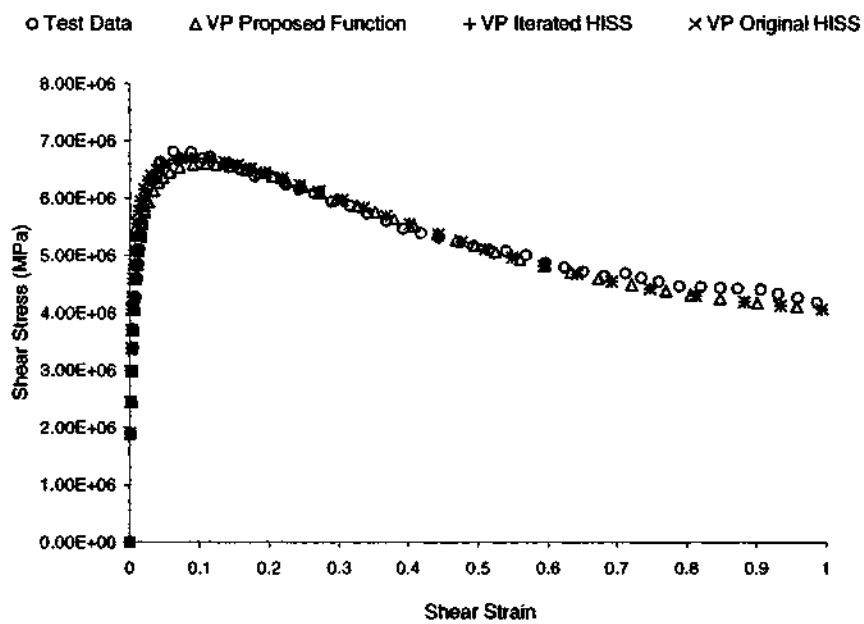

(g) Viscoplastic (Static) Observed Stress

Figure 6.13 (continued)

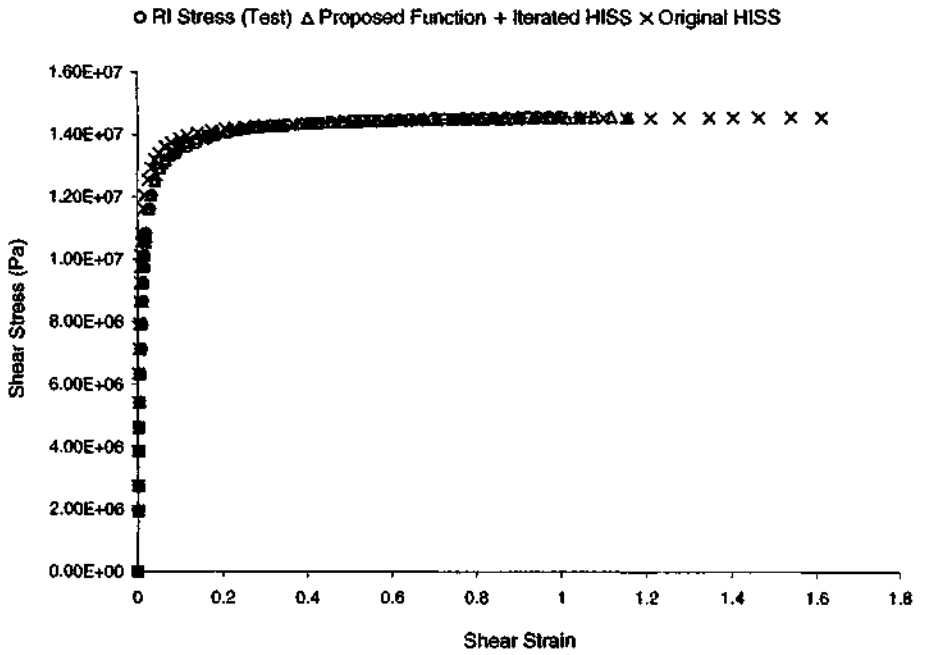

(a) Simplified 1-D RI Elastoplastic Backprediction

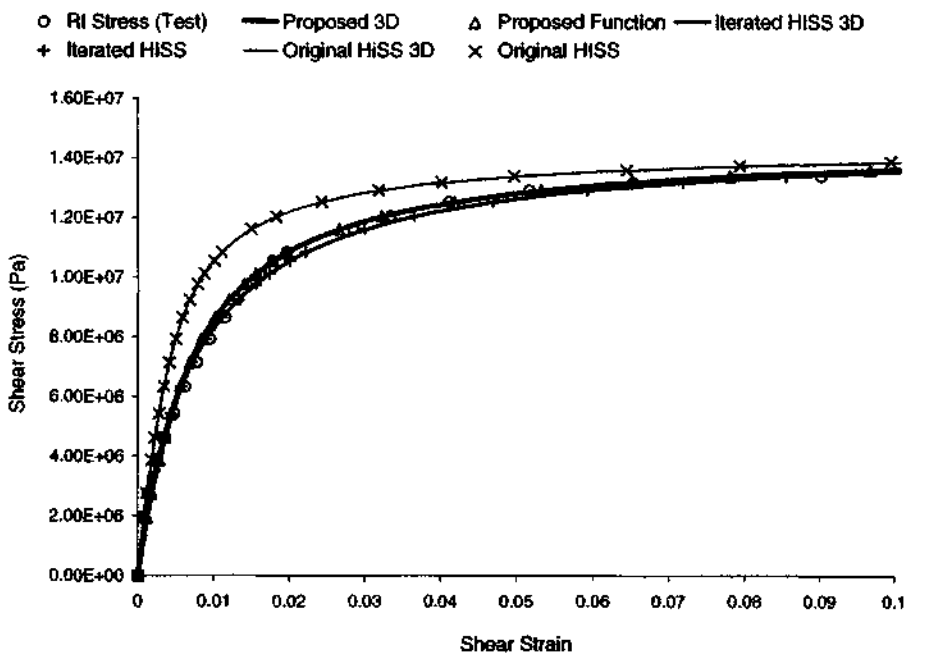

(b) Comparison of 3-D (curves) and 1-D (points) Elastoplastic Backpredictions

Figure 6.14 Temperature = 75°C, Strain Rate = 2.78 x 10^{-3}/s

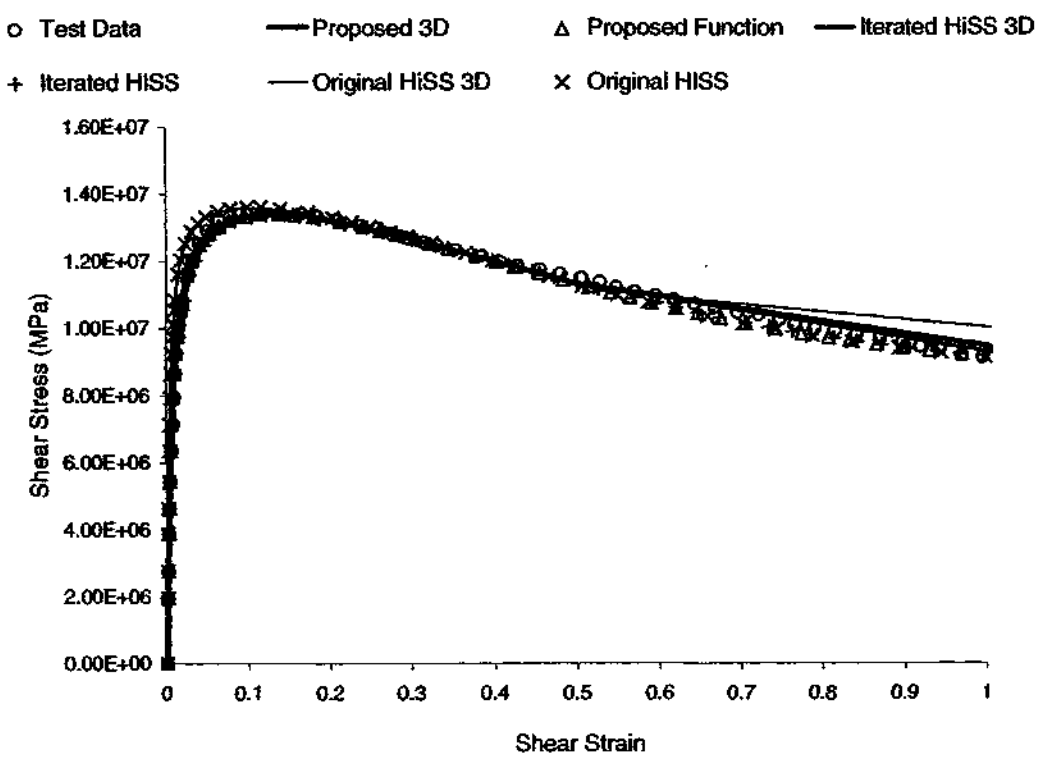

(c) Observed Stress 3-D and 1-D Elastoplastic Backpredictions

Figure 6.14 (continued)

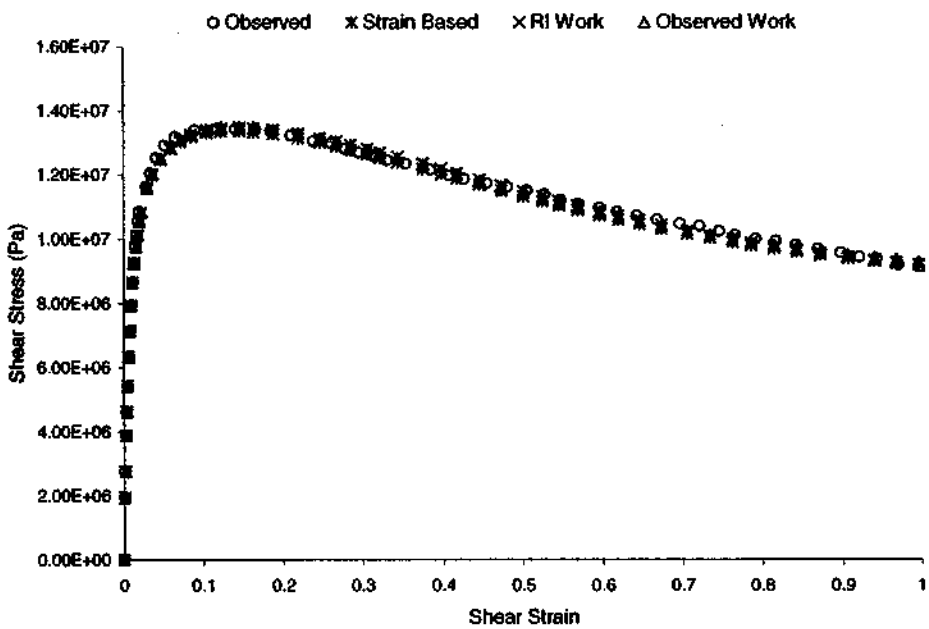

(d) Dissipated-Work DSC for Improved HiSS Parameters

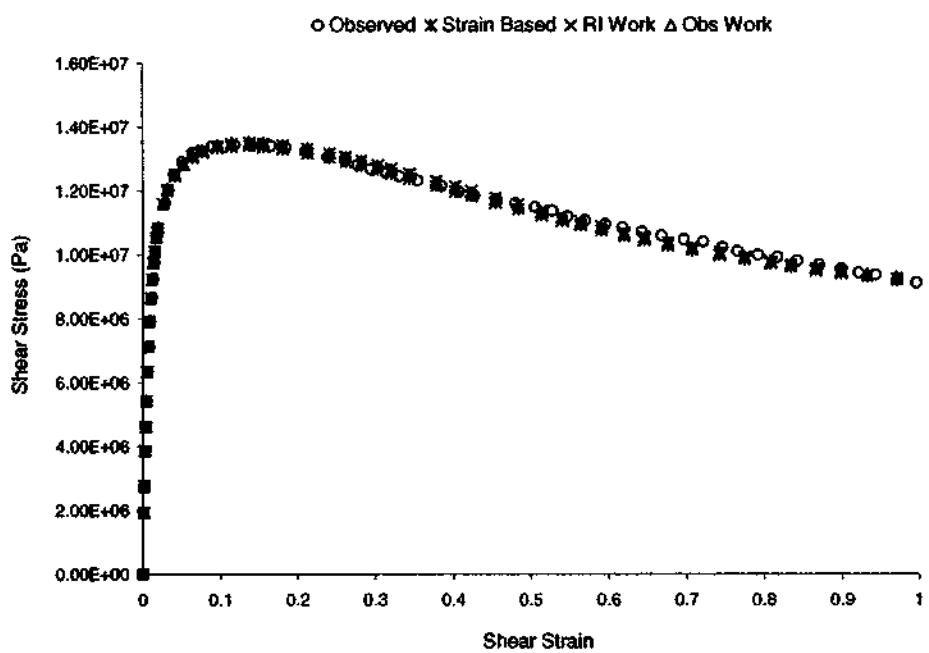

(e) Dissipated-Work DSC for Proposed Yield Function

Figure 6.14 (continued)

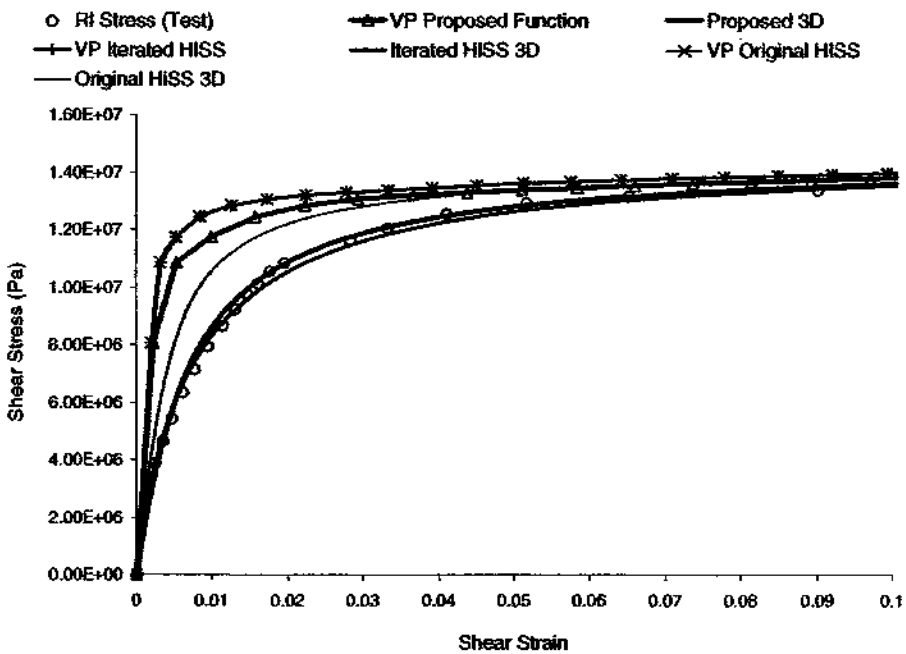

(f) Viscoplastic and 3-D Elastoplastic RI Comparison

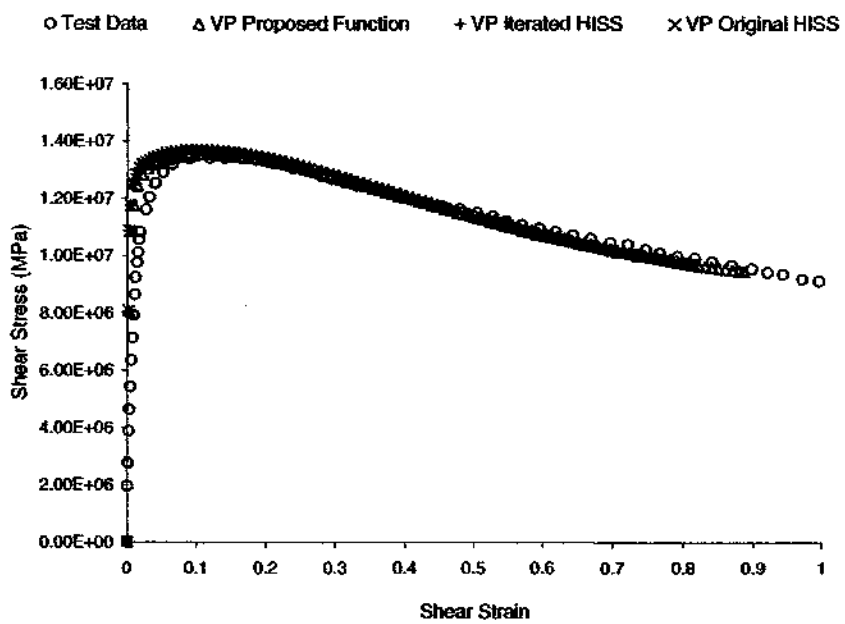

(g) Viscoplastic Observed Stress

Figure 6.14 (continued)

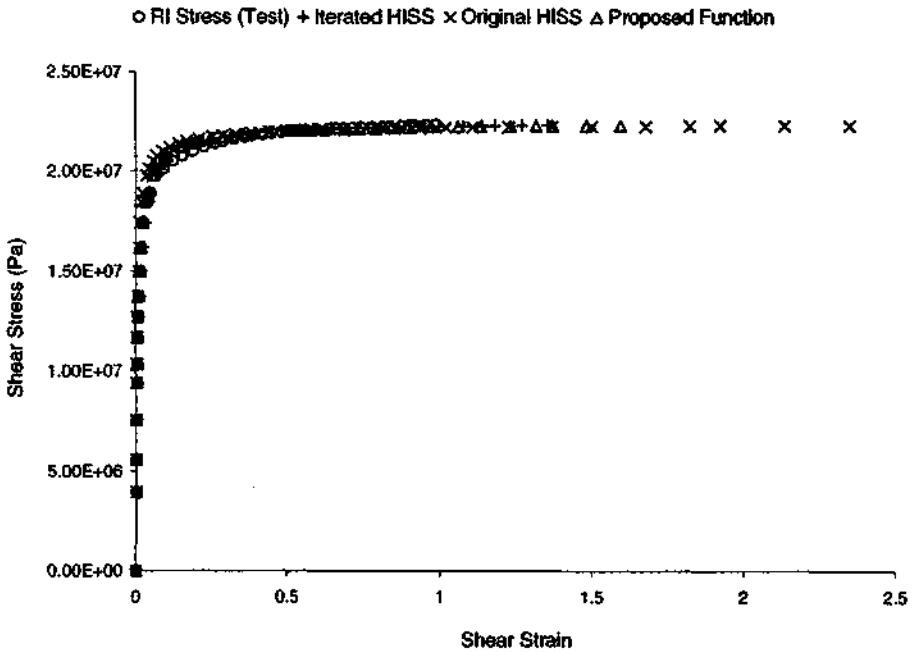

(a) Simplified 1-D RI Elastoplastic Backprediction

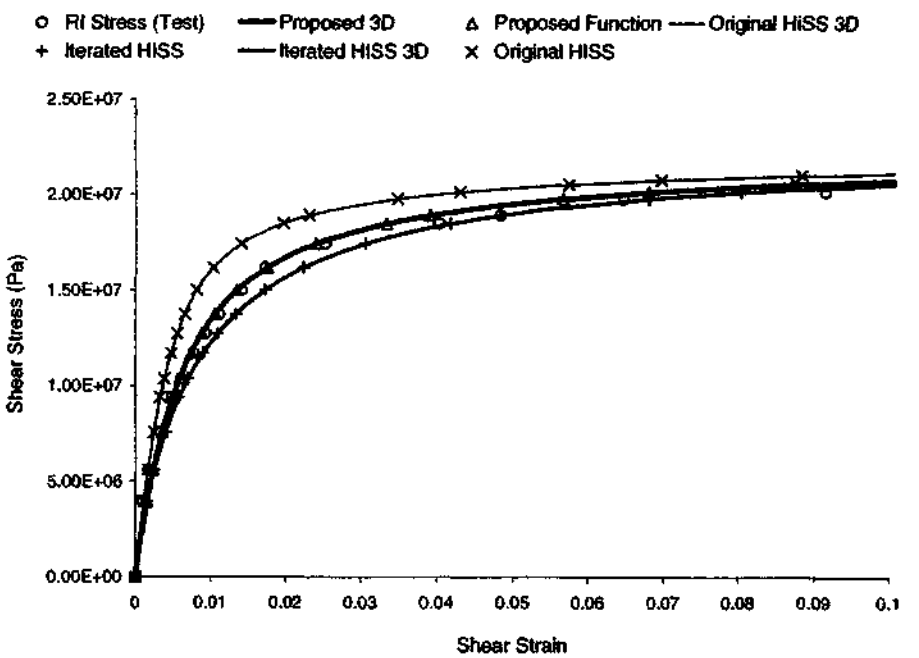

(b) Comparison of 3-D (curves) and 1-D Elastoplastic (points) Backpredictions

Figure 6.15 Temperature = 75°C, Strain Rate = 2.78 x 10^{-2}/s

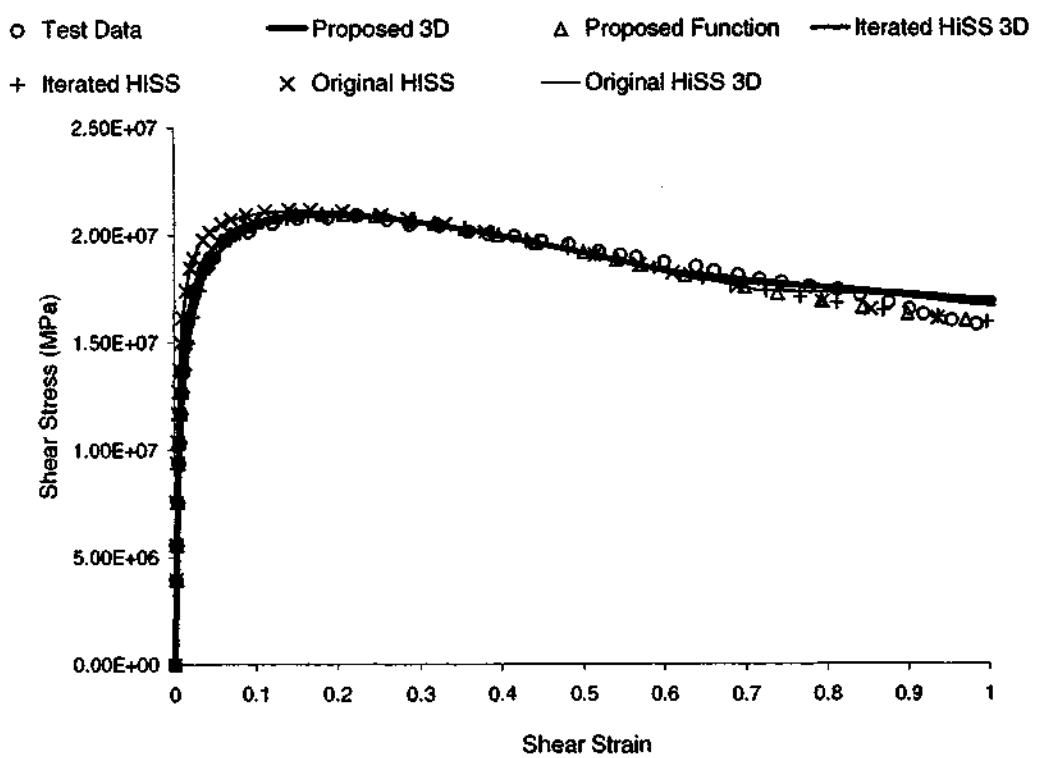

(c) Observed Stress 3-D and 1-D Elastoplastic Backpredictions

Figure 6.15 (continued)

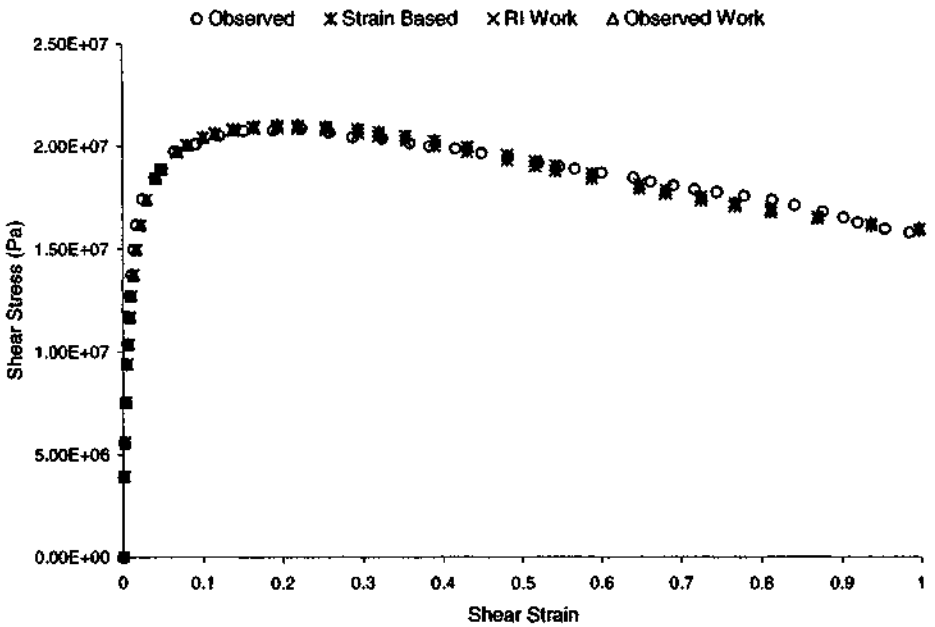

(d) Dissipated-Work DSC for Improved HiSS Parameters

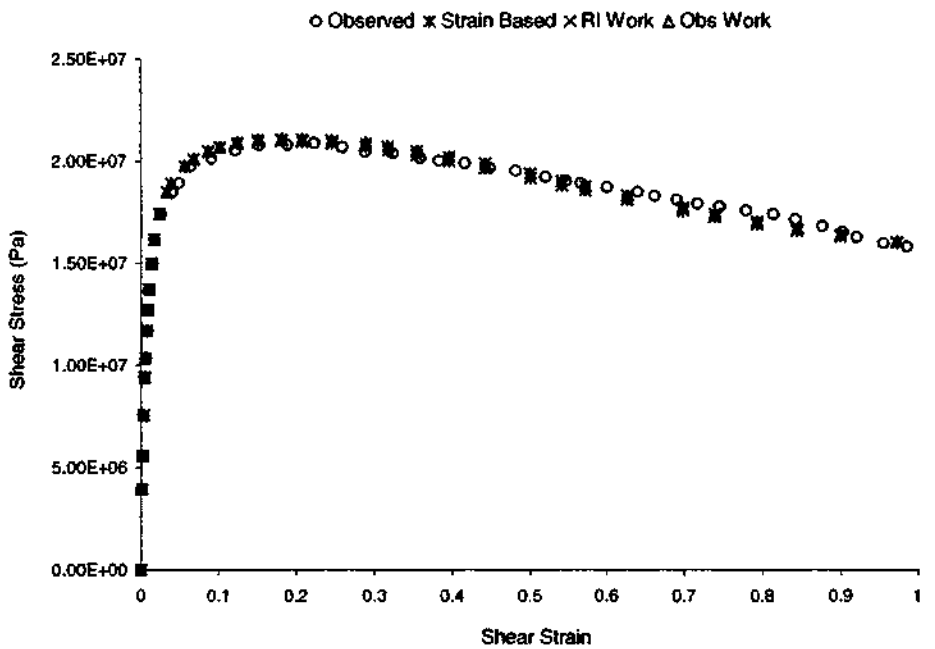

(e) Dissipated-Work DSC for Proposed Yield Function

Figure 6.15 (continued)

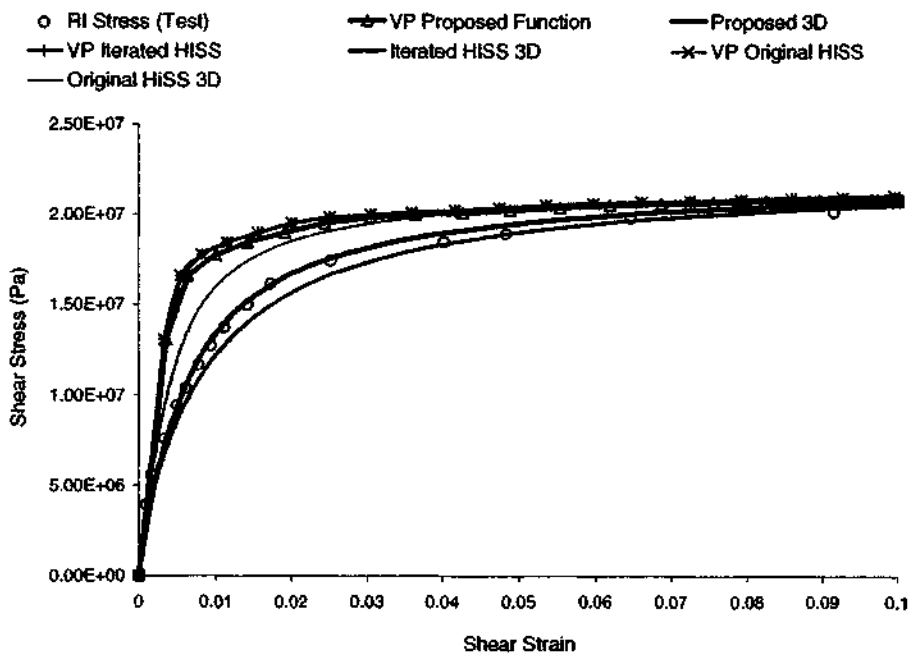

(f) Viscoplastic and 3-D Elastoplastic RI Comparison

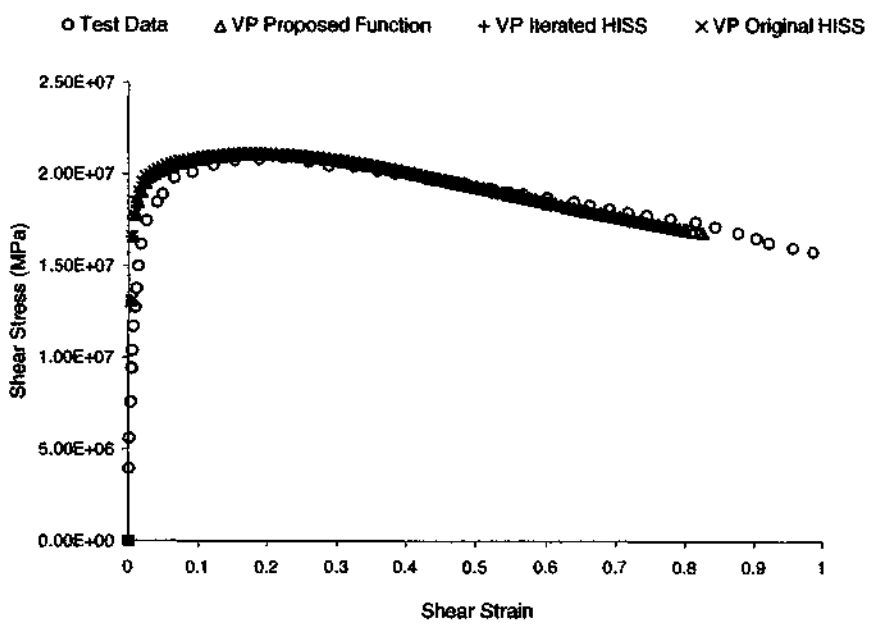

(g) Viscoplastic Observed Stress

Figure 6.15 (continued)

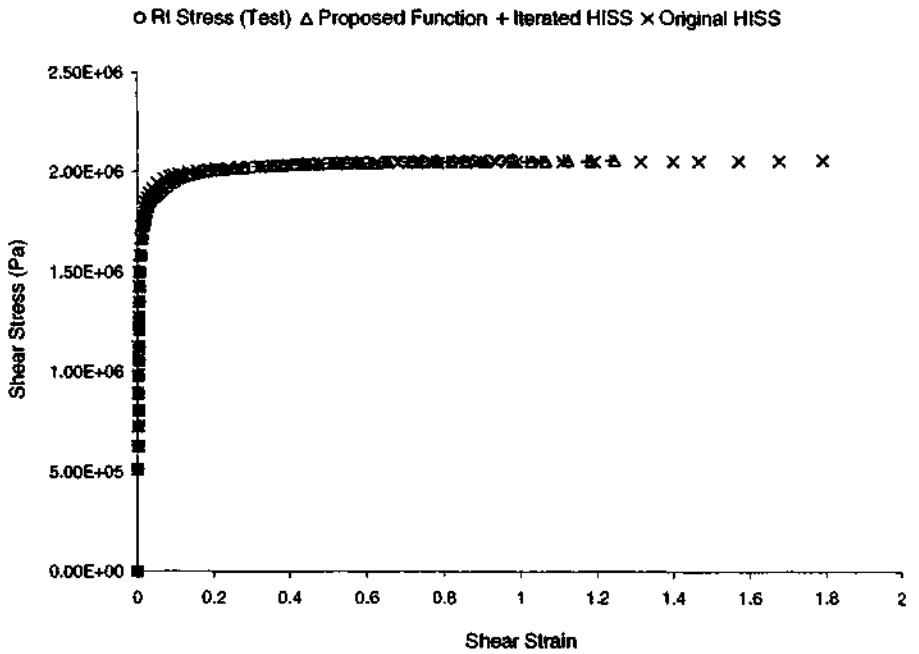

(a) Simplified 1-D RI Elastoplastic Backprediction

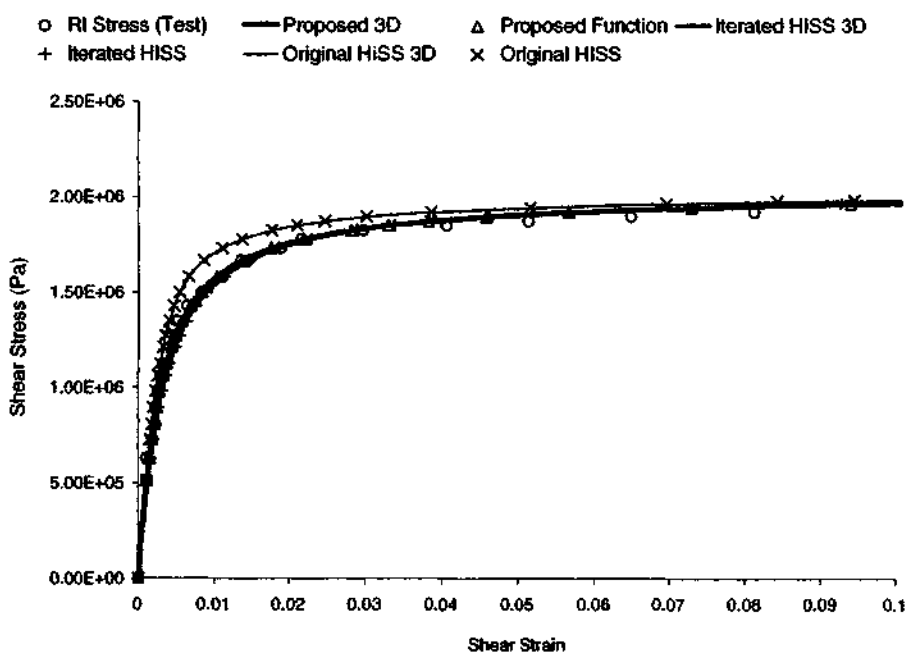

(b) Comparison of 3-D (curves) and 1-D (points) Elastoplastic Backpredictions

Figure 6.16 Temperature = 125°C, Strain Rate = 2.78 x 10^{-4}/s

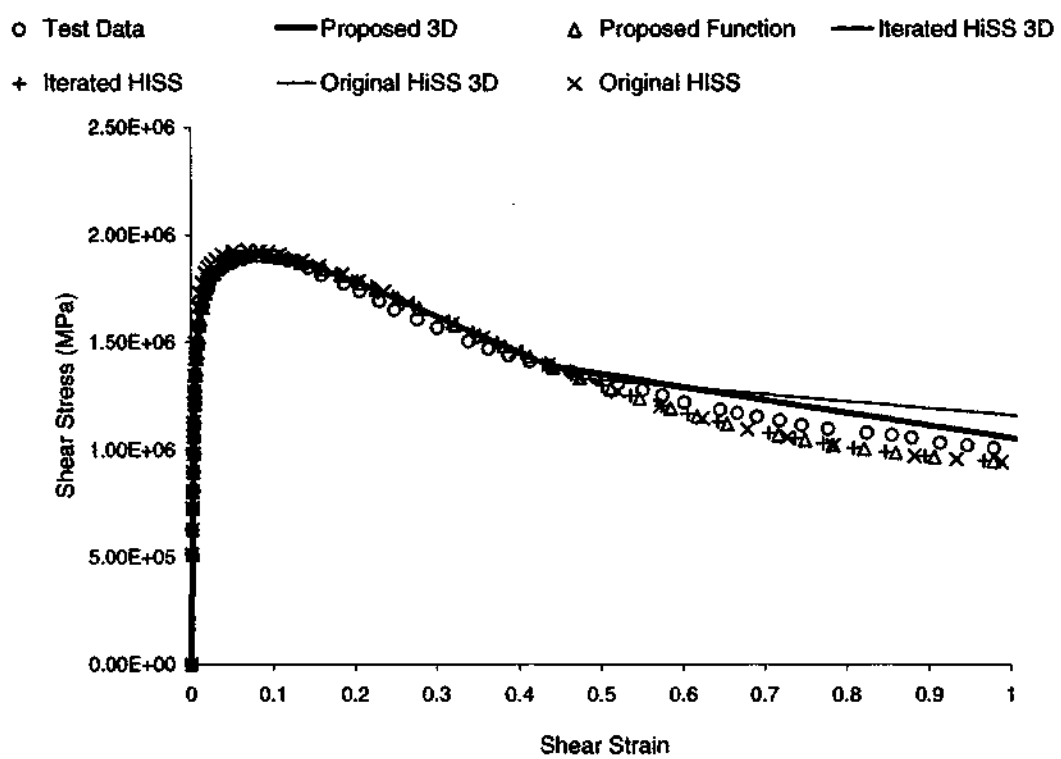

(c) Observed Stress 3-D and 1-D Elastoplastic Backpredictions

Figure 6.16 (continued)

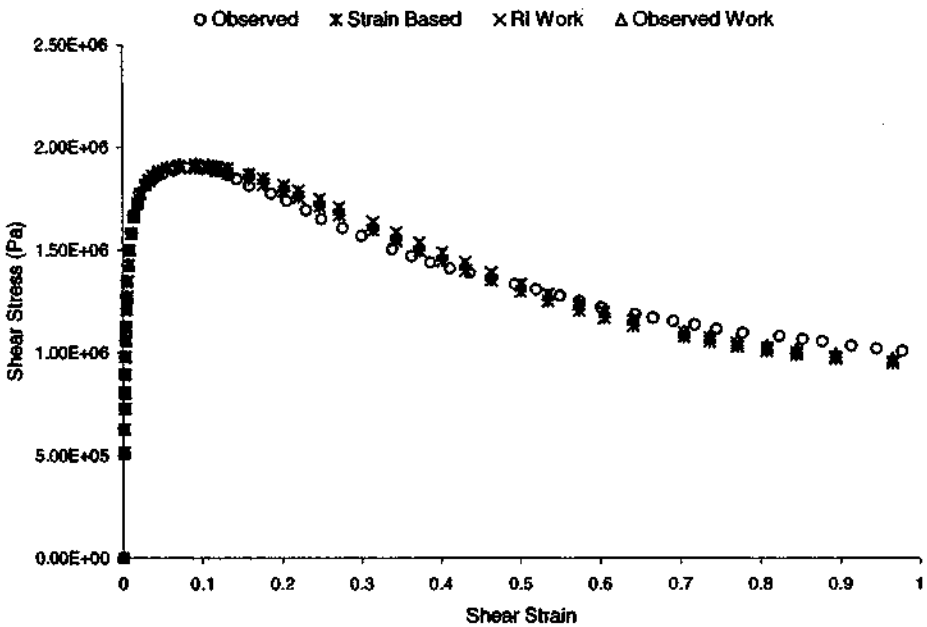

(d) Dissipated-Work DSC for Improved HiSS Parameters

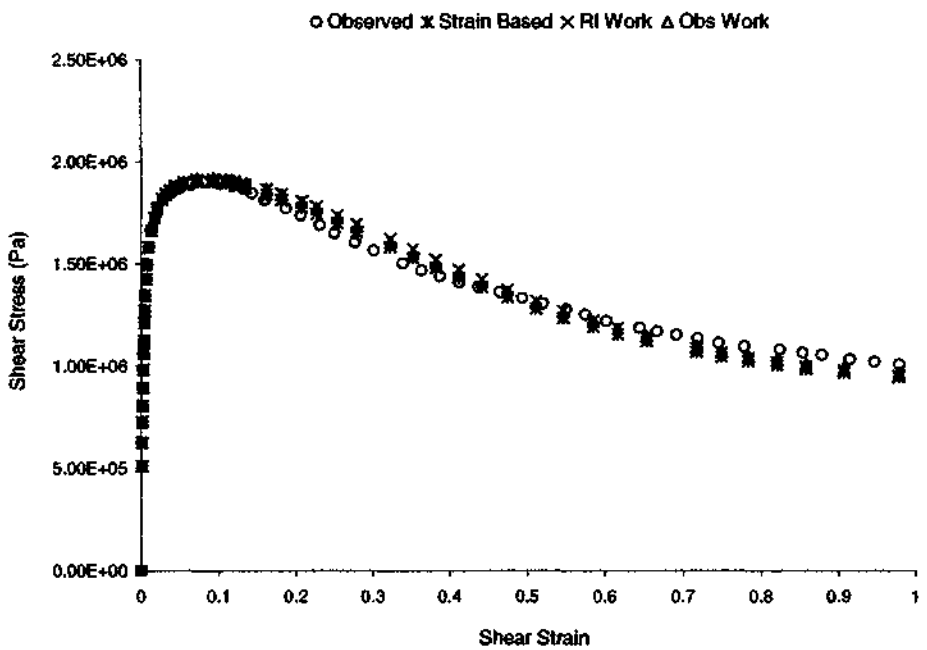

(e) Dissipated-Work DSC for Proposed Yield Function

Figure 6.16 (continued)

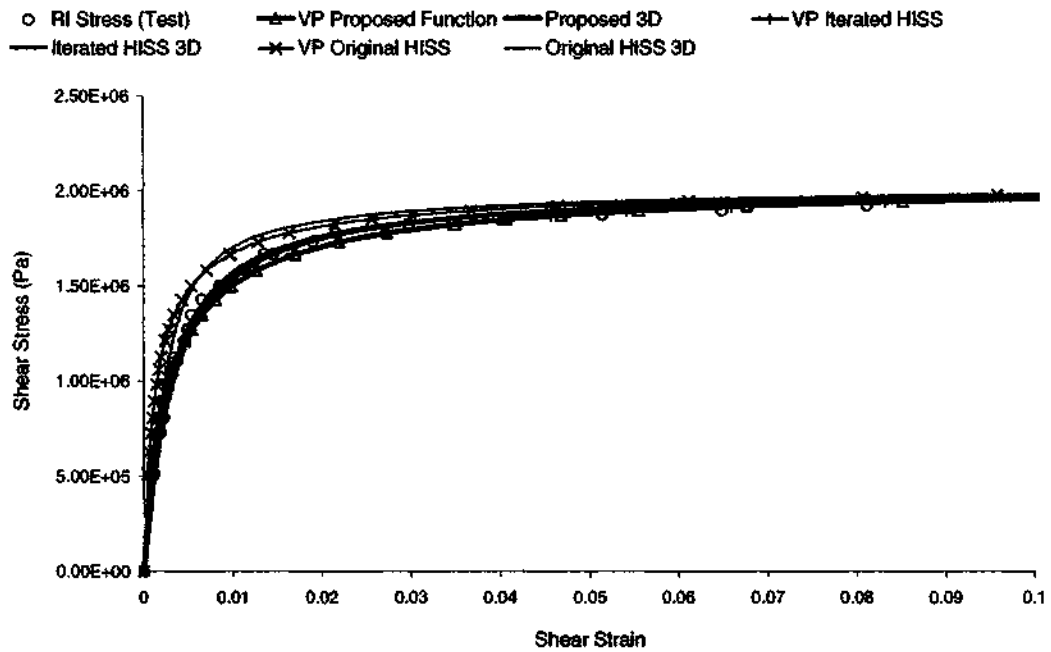

(f) Viscoplastic (Static) and 3-D Elastoplastic RI Comparison

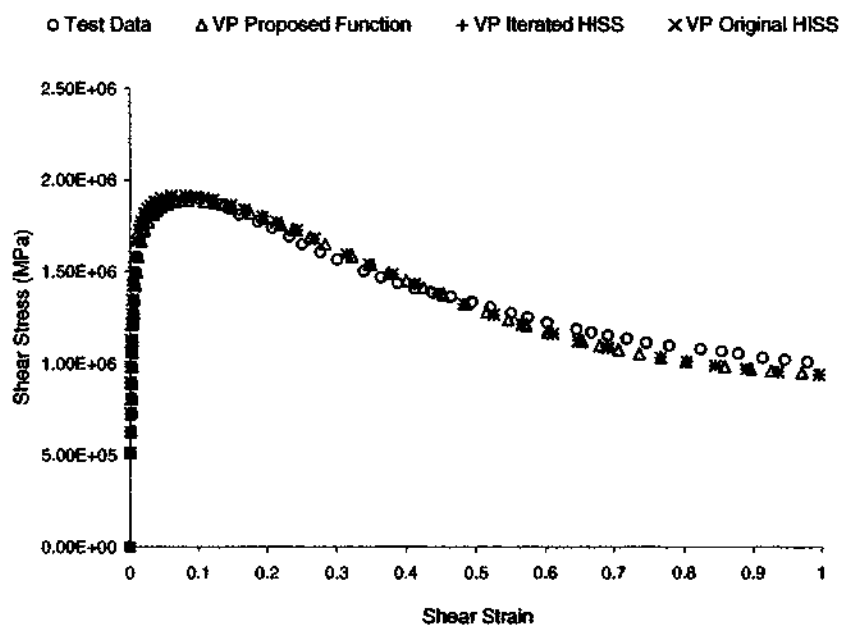

(g) Viscoplastic (Static) Observed Stress

Figure 6.16 (continued)

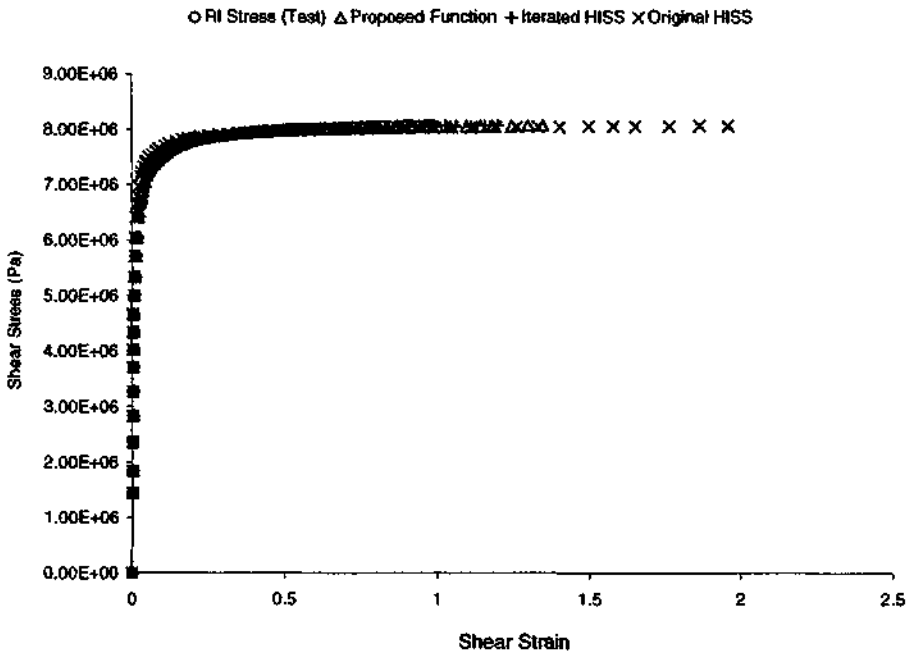

(a) Simplified 1-D RI Elastoplastic Backprediction

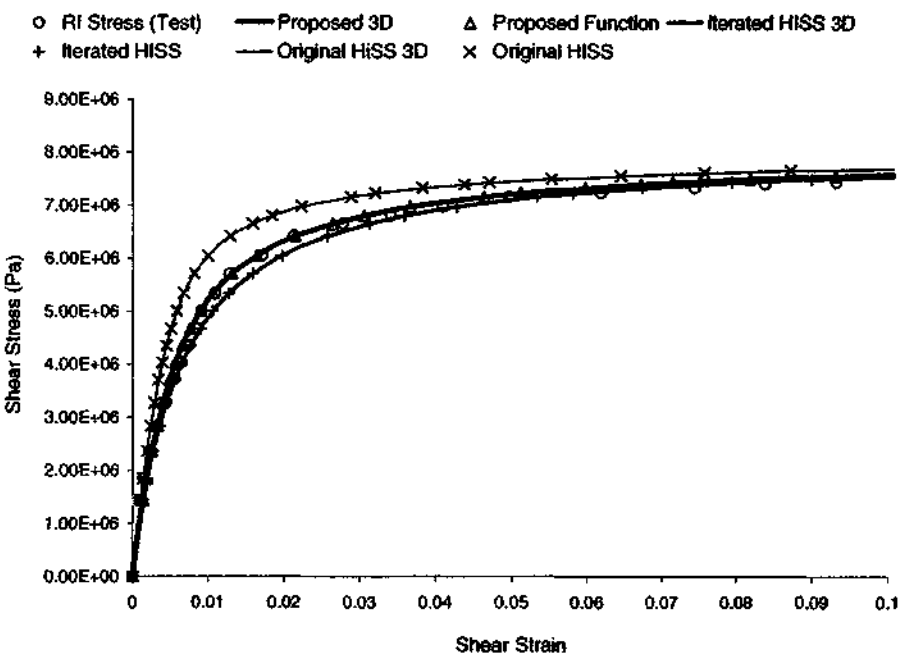

(b) Comparison of 3-D (curves) and 1-D (points) Elastoplastic Backpredictions

Figure 6.17 Temperature = 125°C, Strain Rate = 2.78 x 10^{-3}/s

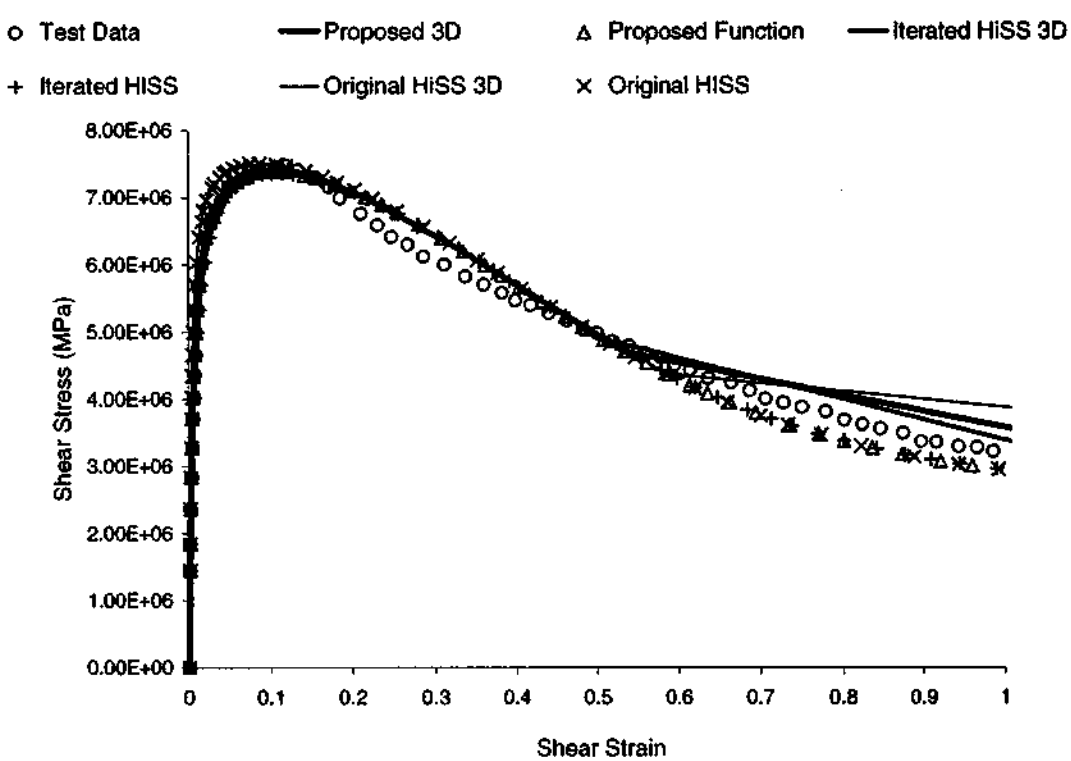

(c) Observed Stress 3-D and 1-D Elastoplastic Backpredictions

Figure 6.17 (continued)

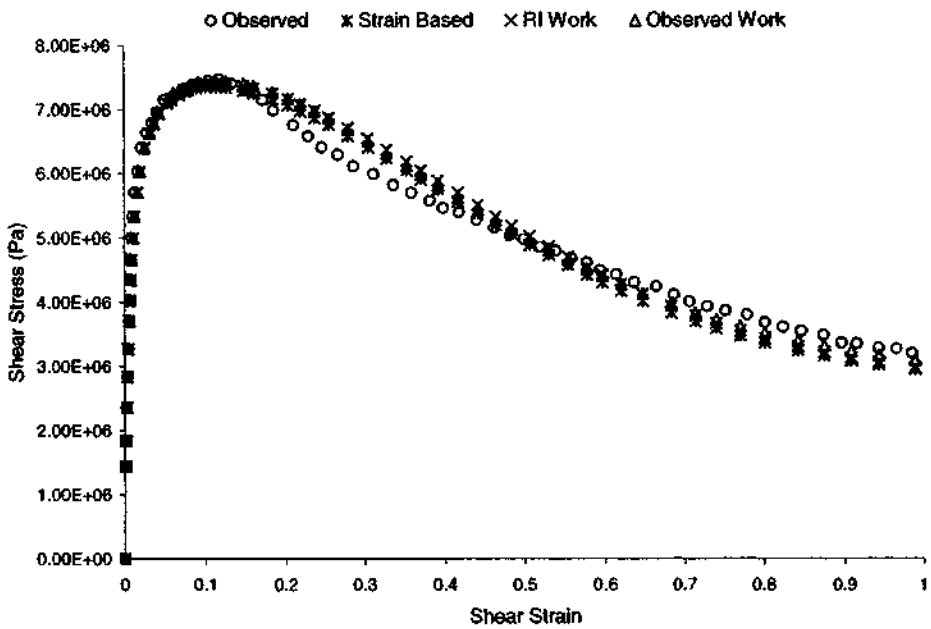

(d) Dissipated-Work DSC for Improved HiSS Parameters

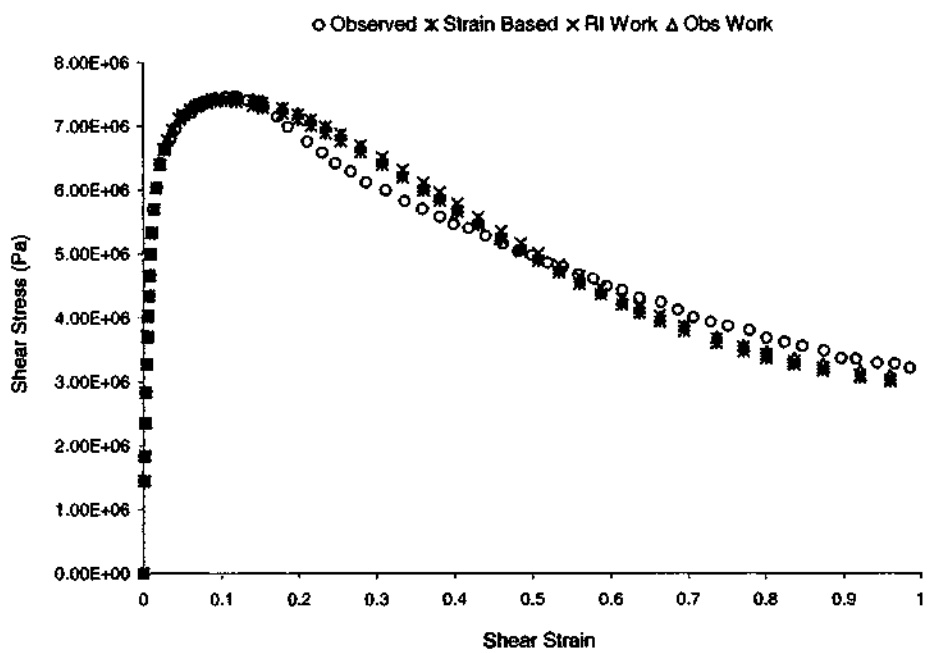

(e) Dissipated-Work DSC for Proposed Yield Function

Figure 6.17 (continued)

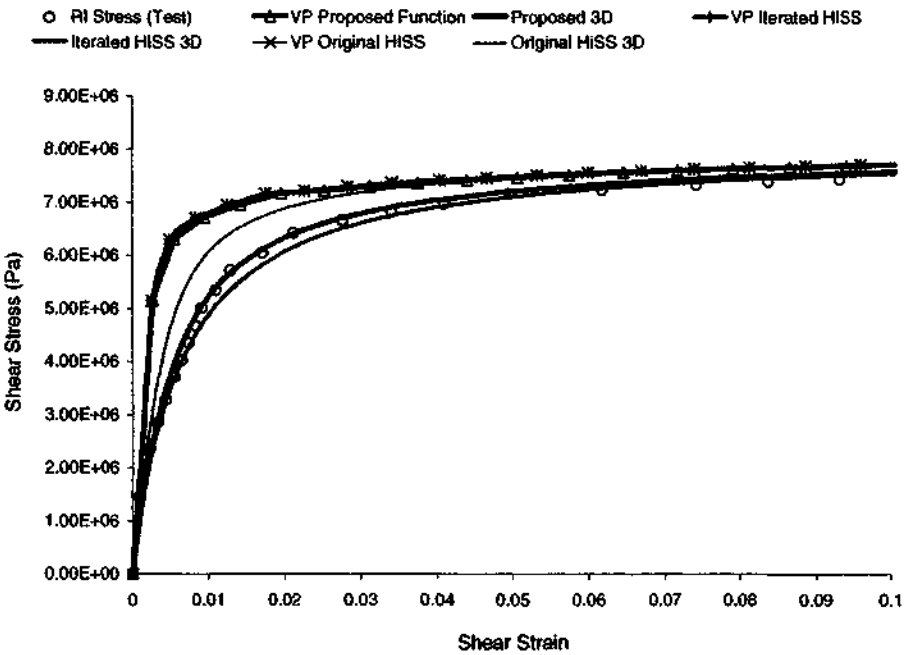

(f) Viscoplastic and 3-D Elastoplastic RI Comparison

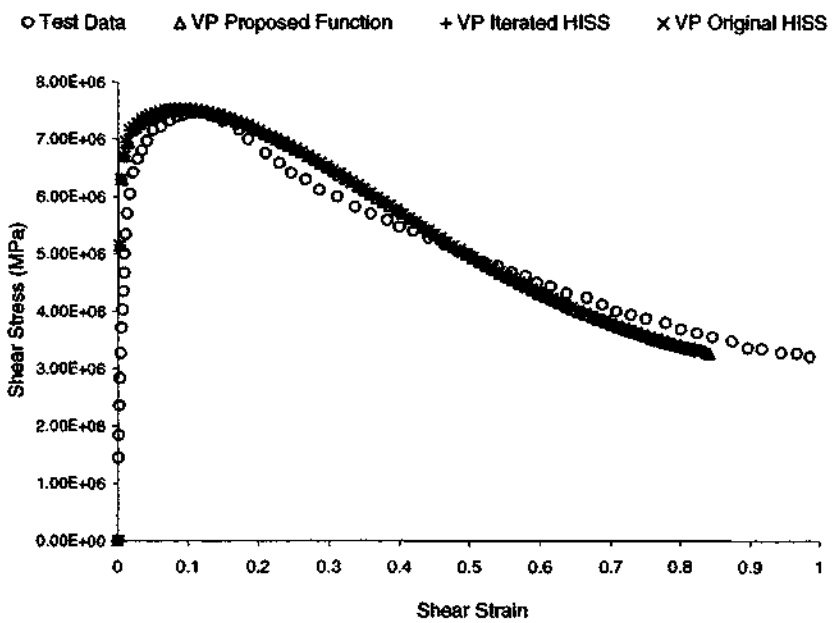

(g) Viscoplastic Observed Stress

Figure 6.17 (continued)

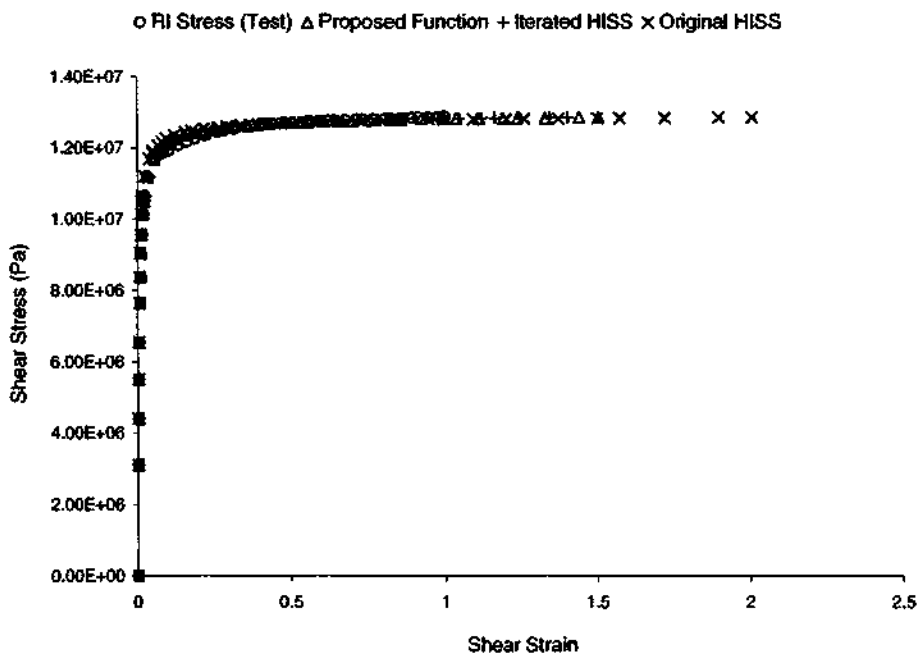

(a) Simplified 1-D RI Elastoplastic Backprediction

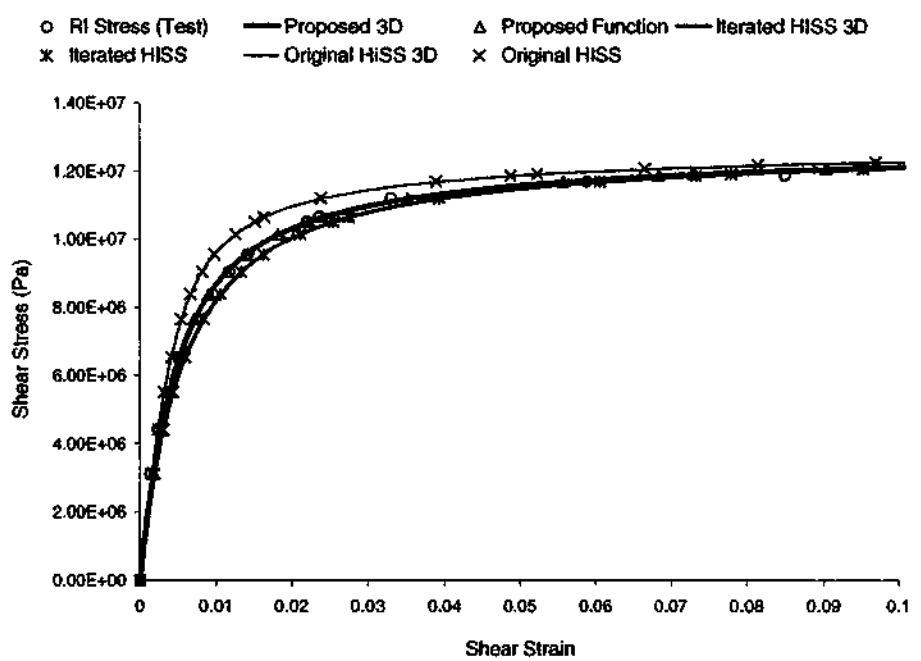

(b) Comparison of 3-D (curves) and 1-D (points) Elastoplastic Backpredictions

Figure 6.18 Temperature = 125°C, Strain Rate = 2.78 x 10^{-2}/s

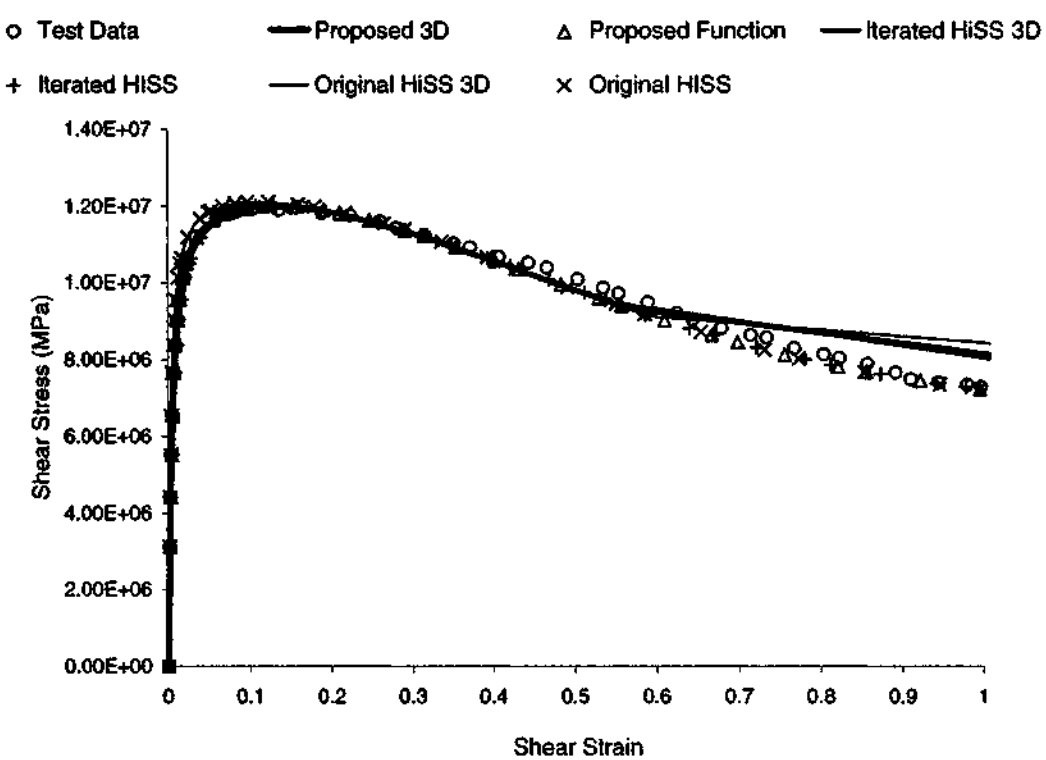

(c) Observed Stress 3-D and 1-D Elastoplastic Backpredictions

Figure 6.18 (continued)

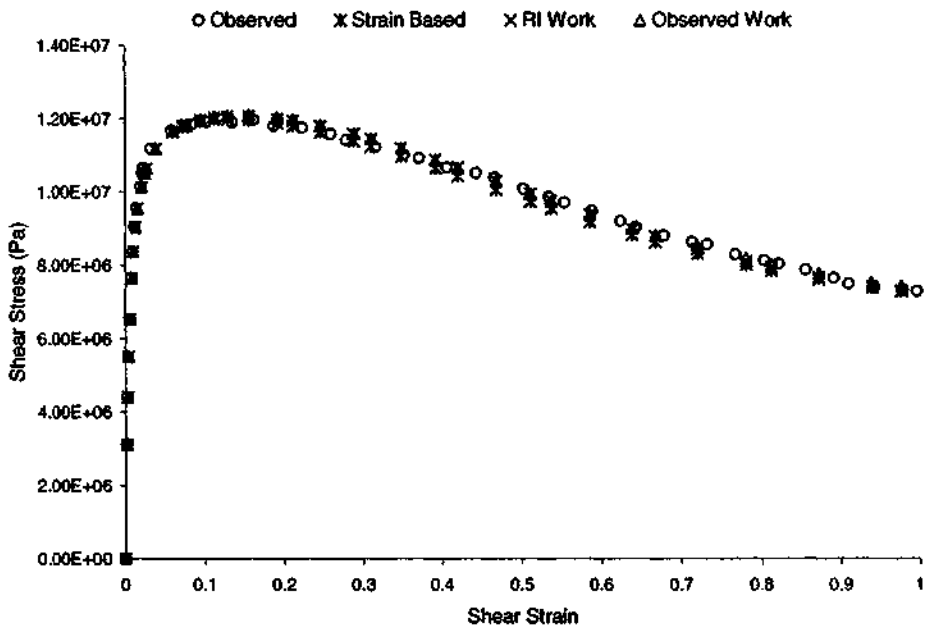

(d) Dissipated-Work DSC for Improved HiSS Parameters

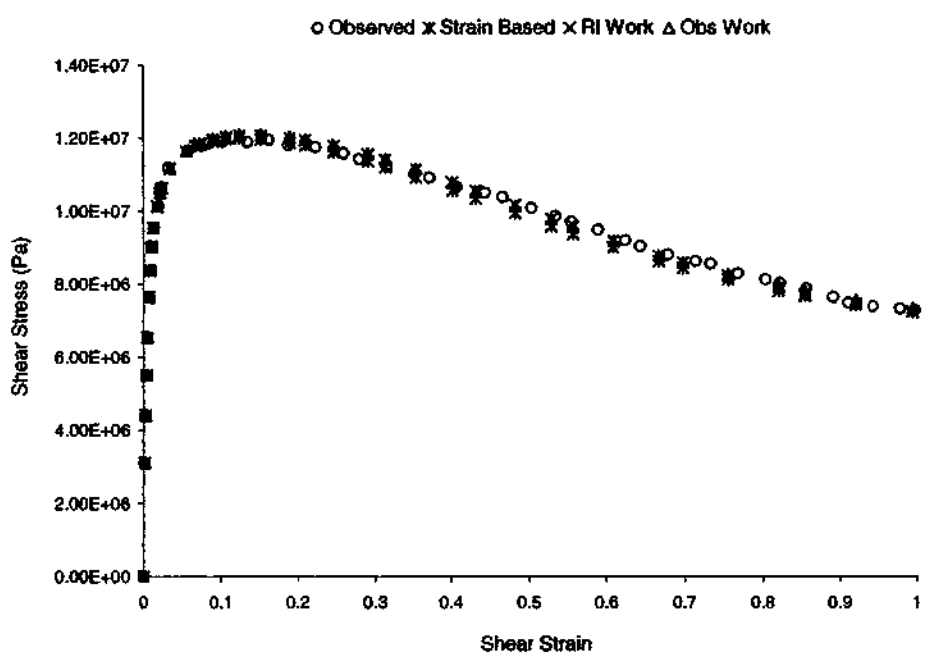

(e) Dissipated-Work DSC for Proposed Yield Function

Figure 6.18 (continued)

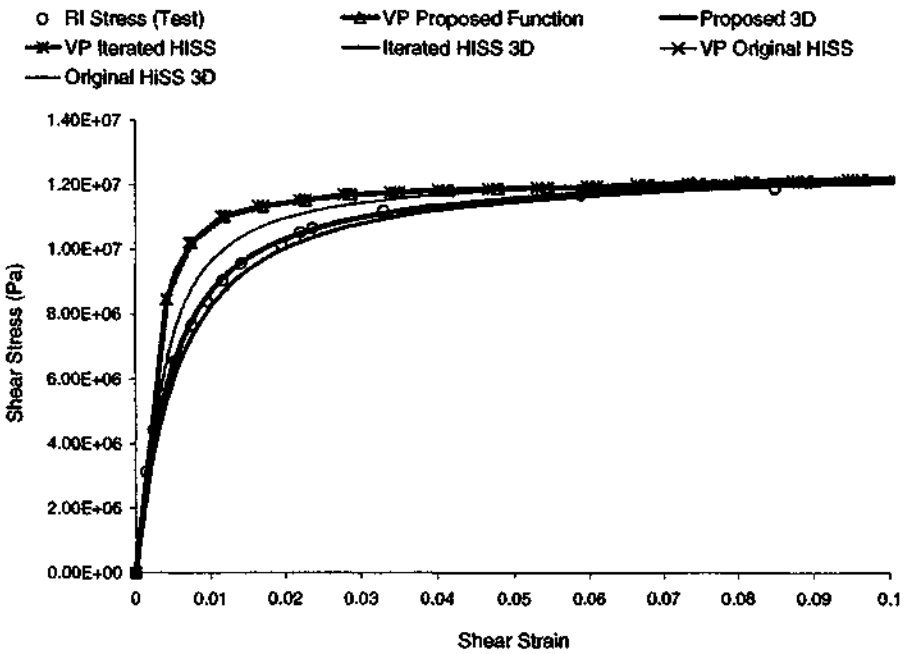

(f) Viscoplastic and 3-D Elastoplastic RI Comparison

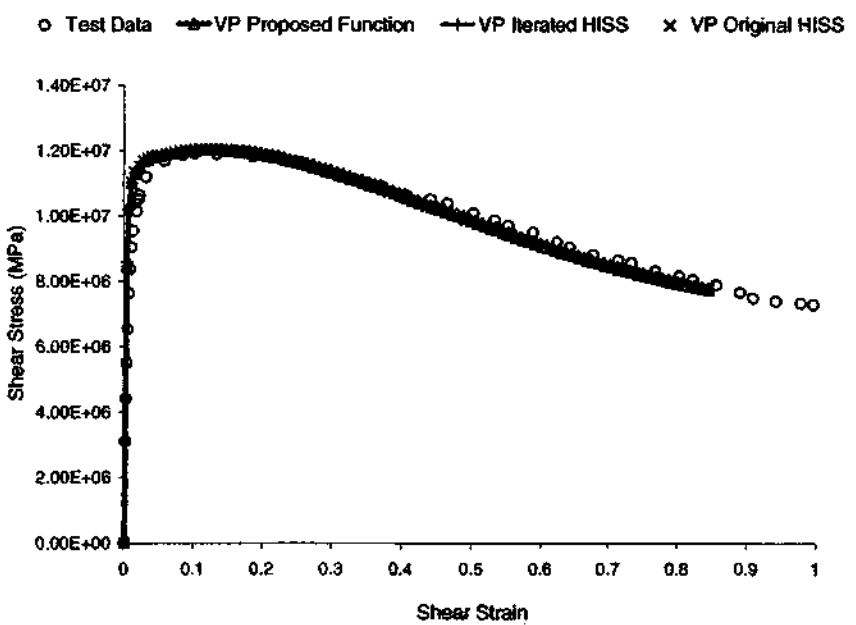

(g) Viscoplastic Observed Stress

Figure 6.18 (continued)

6.5 Thermomechanical Model

Validations for the thermomechanical model are presented for thermoelastic deformations, as well as for plastic and creep deformations.

6.5.1 Thermoelastic Deformations

For application of the model, N_0, the number of atoms per unit volume at 0K is obtained using

$$N_0 = \frac{1000\rho_0}{AW} \times N_A \qquad \ldots(6.29)$$

where ρ_0 is the density at 0K, in kg/m^3, AW is the atomic weight in g/mole, and N_A is the Avogadro Number, 6.023 x 10^{23} atoms/mole. For solder, an equivalent atomic weight may be estimated. The configuration energy density at the stress-free state at 0K, $-U_0$, is estimated using

$$U_0 = 1.602 \times 10^{-19} N_0 \Omega_0 \qquad \ldots(6.30)$$

where Ω_0 is the bonding energy/ atom in eV, and U_0 is in J/m^3. Additional parameters required are the Debye temperature, T_D, bulk modulus at 0K, B_0, and shear modulus at 0 K, G_0, and the density latent heat of fusion, U^L. Latent heat of fusion for elements is from WebElements and Environmental Chemistry websites[15].If latent heat of fusion is in

[15] www.webelements.com, www.environmentalchemistry.com

J/mole, it may be converted to U^L based on N_0. Computations are carried out from 0K to the melting point, *M.P.*. The parameter η is required to be determined empirically.

The thermoelastic equations specialized for the case of unconstrained heating and cooling were applied to Aluminum, Lead, Tin and eutectic Pb/Sn solder, and the variation of material parameters with temperature was computed. Material parameters required for the model are presented in Table 6.6. In case the material undergoes a phase change, the latent heat of fusion requires empirical modification. The explanation for parameters is provided in the section relevant to each material.

6.5.1.1 Aluminum

The density at 0K is taken to be the density at room temperature, as the coefficient of thermal expansion is typically small. If the assumption is not reasonable, an iterative procedure may be used wherein the coefficient of thermal expansion computed by the model may be used to obtain the density at 0K, and the computations repeated till convergence is achieved.

Bulk modulus and shear modulus values at 0 K are provided by Reed and Clark (1983). The Debye temperature and bonding energy is from Marder (2001). Zinovev (1996) has provided the variation in the Debye temperature with temperature for Aluminum. However, the value is assumed to be constant for simplicity.

Table 6.6

Material Parameters for Thermomechanical Model

	Aluminum	Lead	Tin	Solder[3]
ρ_0 (kg/m^3)	2700	11593	7290	8400
AW (g/mole)	27	207.2	118.71	(Av.) 139.94[3]
Ω_0 (eV)	3.34	2.02	3.09	2.8
ρ_f	0.74	0.74	0.74[2]	0.74
$M.P.$ (K)	910	600	505	456
T_D (K)	418	102	200	—
B_0 (Pa)	79.4×10^9	48.79×10^9	61.66×10^9	56.5×10^9
G_0 (Pa)	29.3×10^9	9.71×10^9 [1]	27.57×10^9 [2]	21×10^9
U^L (J/mole)	10670	4799	Used: 2500[2] (Actual: 7030)	Used: 1400 (Actual: 5236)
η	8.70	6.50	7.00	8.00

Notes:

1) See section 6.5.1.2 for estimation of value used.

2) See section 6.5.1.3 for estimation of value used.

3) For all solder properties, see section 6.5.1.4 for estimation of value or equivalent value used. AW and U^L are average values per atom for solder.

The parameter η is estimated iteratively by obtaining the best-fit curve for the variation of the bulk modulus with temperature. The variation of the coefficient of thermal expansion and the shear modulus with temperature is then computed based on the estimated η. Experimental data for the comparison is from Reed and Clark (1983) and Zinovev (1996).

6.5.1.2 Lead

The density of Lead at zero temperature is obtained from Reed and Clark (1983), as is the bulk modulus at 0K. Zinovev (1996) has provided the elastic constants C_{11}, C_{12} and C_{44} for lead as a function of temperature. Thus, for the comparison with experimental data, the bulk modulus at any temperature is obtained using

$$B(T)=\frac{1}{3}(C_{11}(T)+2C_{12}(T)) \qquad \ldots(6.31)$$

At 0K, the value computed using Eq. (6.31) for the data of Zinovev (1996) is identical to the value provided by Reed and Clark (1983).

For obtaining the shear modulus however, an approximation is required. For an isotropic material, the shear modulus may be computed as

$$G(T)=\frac{1}{2}(C_{11}(T)-C_{12}(T))=C_{44} \qquad \ldots(6.32)$$

However, Lead shows a high degree of anisotropy, and the shear modulus based on the constants C_{11} and C_{12} may be less than C_{44} by a factor of 4. While Reed and Clark (1983) have provided means for averaging of shear modulus for anisotropic material, a simplification is made based on the assumption that the zero temperature and room temperature value of the shear modulus for Lead provided by Reed and Clark (1983) is approximately equal to $C_{44}/2$.

Thus, the model is used to predict the variation of $C_{44}/2$, i.e. C_{44} with temperature rather than G. It is simply assumed that for Lead,

$$G(T) \approx \frac{C_{44}}{2} \qquad \ldots(6.33)$$

6.5.1.3 Tin

The model developed is for materials that do not undergo phase change. However, Tin undergoes phase transition from the fcc α–Tin to the bcc β–Tin at 298K with substantial change in specific volume (Zinovev, 1996). Thus, the model is not directly applicable to Tin. Reasonable averaged predictions may still be obtained using the model if the phase transition is ignored, and the packing fraction is assumed to remain 0.74. However, the latent heat of fusion is seen to require empirical modification.

Zinovev (1996) has provided the elastic constants C_{11}, C_{12}, C_{13}, C_{33}, C_{44} and C_{66} for Tin. The bulk modulus is thus estimated as

$$B(T)=\frac{1}{6}(C_{11}(T)+2C_{12}(T)+C_{33}(T)+2C_{13}(T))$$

...(6.34)

while the shear modulus is assumed to be given by

$$G(T)=\frac{1}{2}(C_{44}+C_{66})$$

...(6.35)

The coefficient of thermal expansion depends on the direction and phase. However, average values for polycrystalline material such as those from MatWeb Material Property Database[16] may be used for comparison. Results are not affected if the room-temperature density or the density at 50K is used.

6.5.1.4 Solder

For eutectic lead-tin solder, for consistency of procedure in the code, the number of particles per unit volume was computed by assigning an average weight to the atoms to get an equivalent atomic weight. This is simply an intermediate step in the procedure, and thus, not relevant to the results. The atomic weight was assigned based on the computation that the number of atoms in eutectic solder is approximately 24% Lead and 76% Tin. Similarly, an average bonding energy was assigned to the atoms. The actual

[16] www.matweb.com

value of the bonding energy is not critical as it is used in conjunction with the empirical scale factor η. Finally, since at 0K both Lead and Tin are in the fcc state, a packing fraction of 0.74 was maintained for solder.

Experimental values of the Young's modulus, E, and Poisson's Ratio, ν, have been provided for certain values of the temperature by Pan (1991) from which observed values of bulk modulus and the shear modulus may be obtained.

For estimating the 0K value of the bulk modulus, B_0, along with the empirical scale factor η, predictions for the variation of both the coefficient of thermal expansion and bulk modulus with temperature were curve-fit simultaneously. No formal optimization was required as the variation of material parameters with temperature is quite systematic with the parameters B_0 and η. Similar to the case for Tin, the latent heat of fusion requires empirical modification for solder. The shear modulus at 0K, G_0 and the modified U^L were determined by obtaining the best-fit values for the material parameters to the curve for the variation of shear modulus with temperature. For simplicity, the specific heat used was the weighted-average value for Lead and Tin based on the Kopp-Neumann rule which is frequently assumed to be valid for alloys, although it is intended for compounds (Reed and Clark, 1983).

Results for Aluminum, Lead, Tin and Solder are presented in Figures 6.19 – 6.22, along with experimental values for comparison.

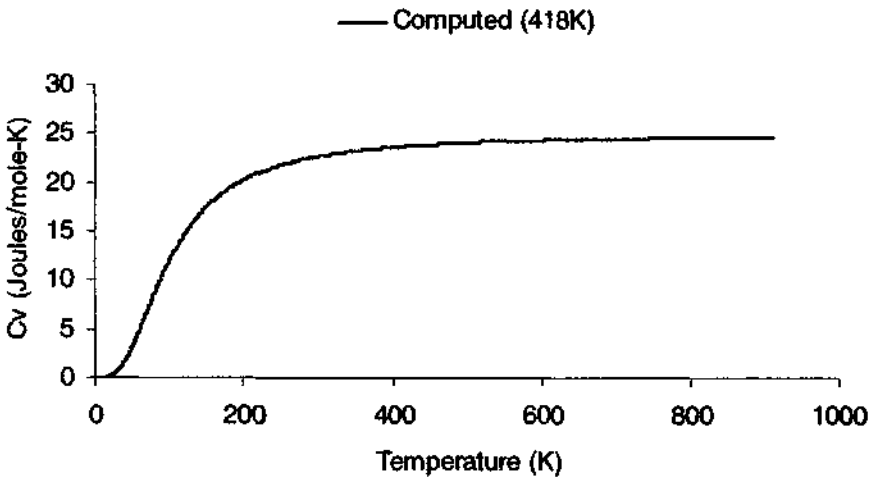

(a) Molar Specific Heat for $T_D = 418K$

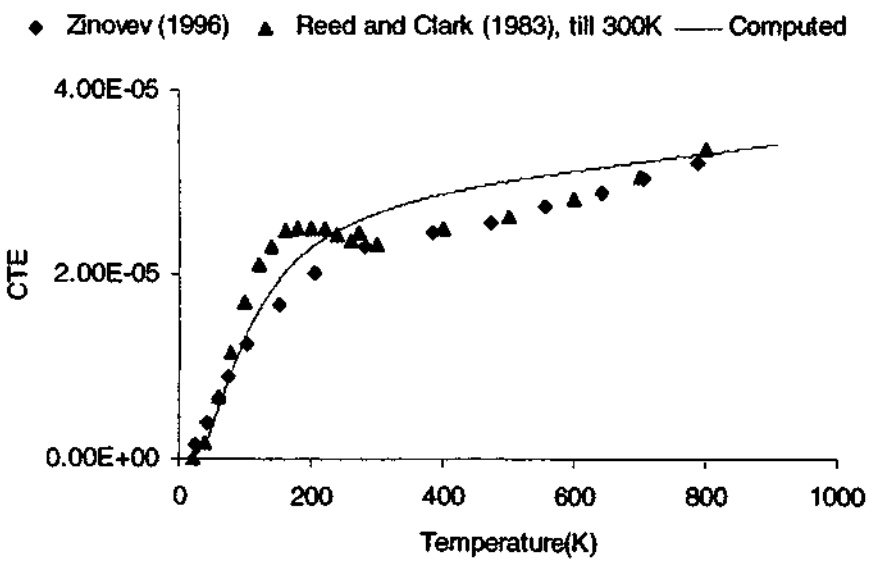

(b) Coefficient of Thermal Expansion vs. Temperature

Figure 6.19 Results for Aluminum

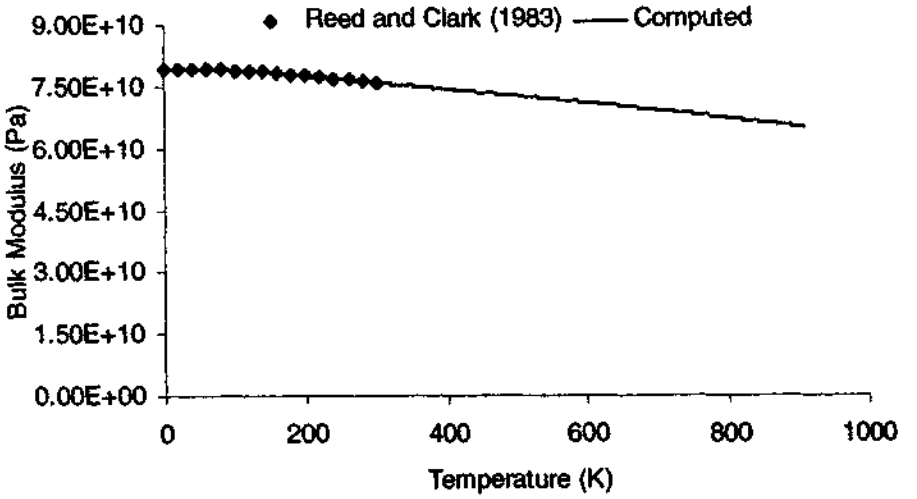

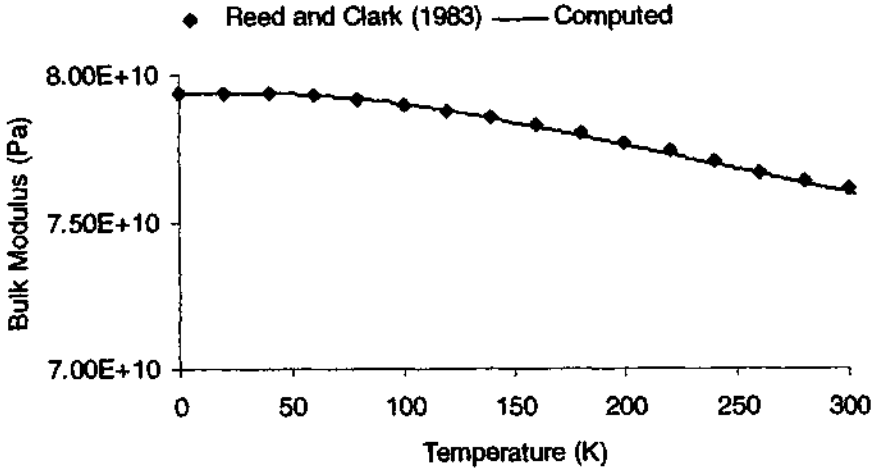

(c) Bulk Modulus vs. Temperature

Figure 6.19 (continued)

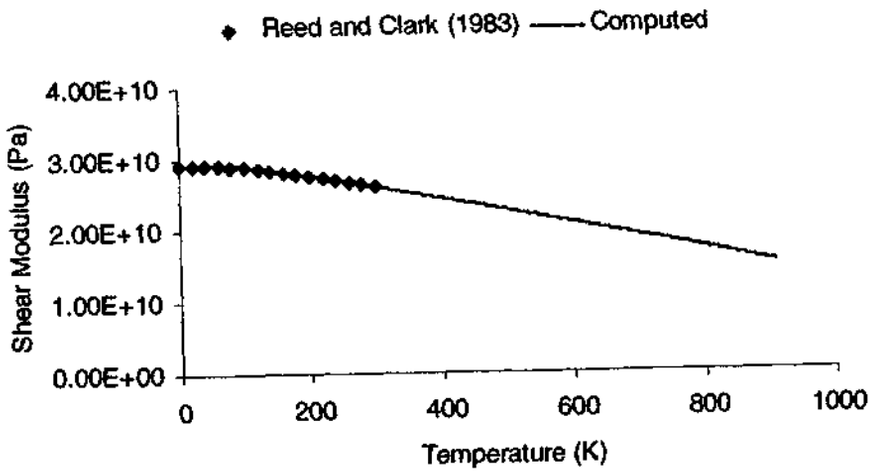

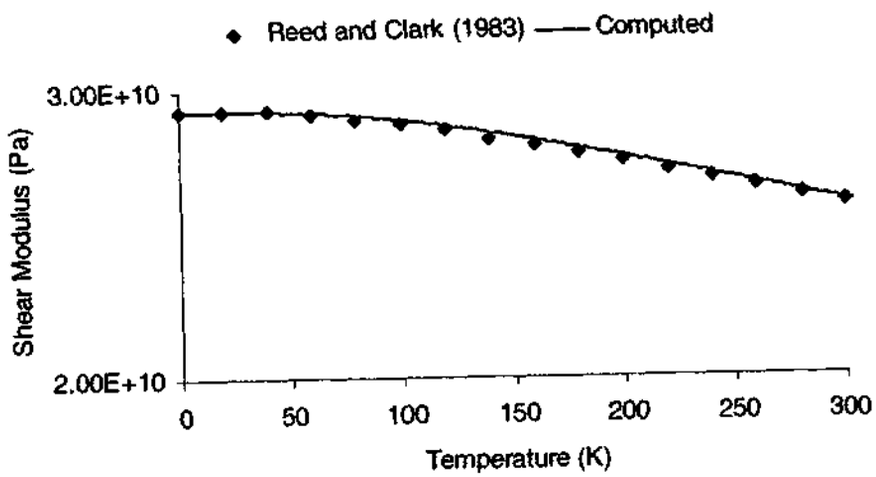

(d) Shear Modulus vs. Temperature

Figure 6.19 (continued)

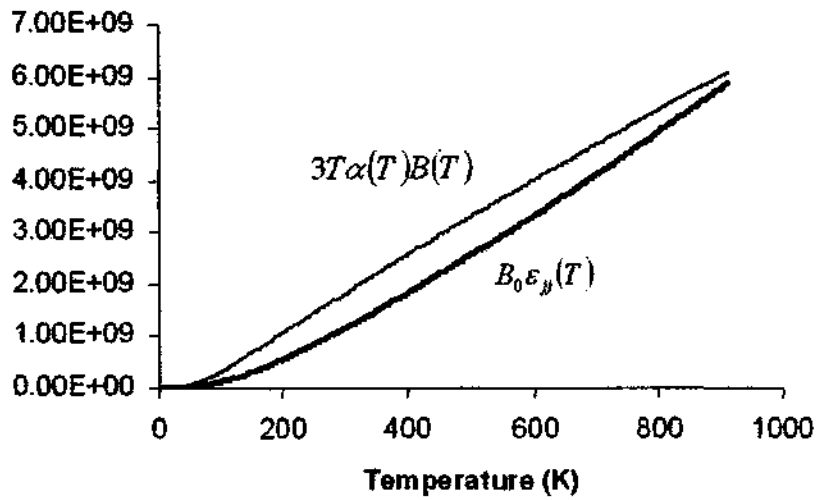

(e) Consistency with Second Law of Thermodynamics

Figure 6.19 (continued)

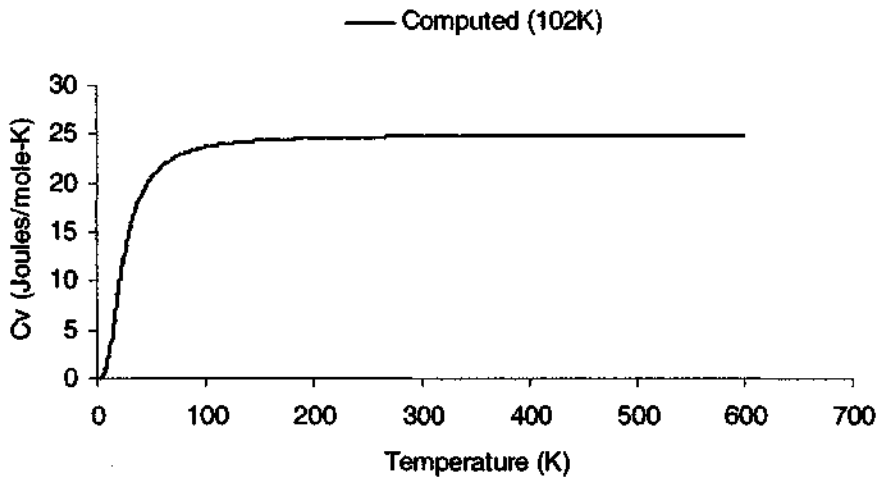

(a) Molar Specific Heat at $T_D = 102K$

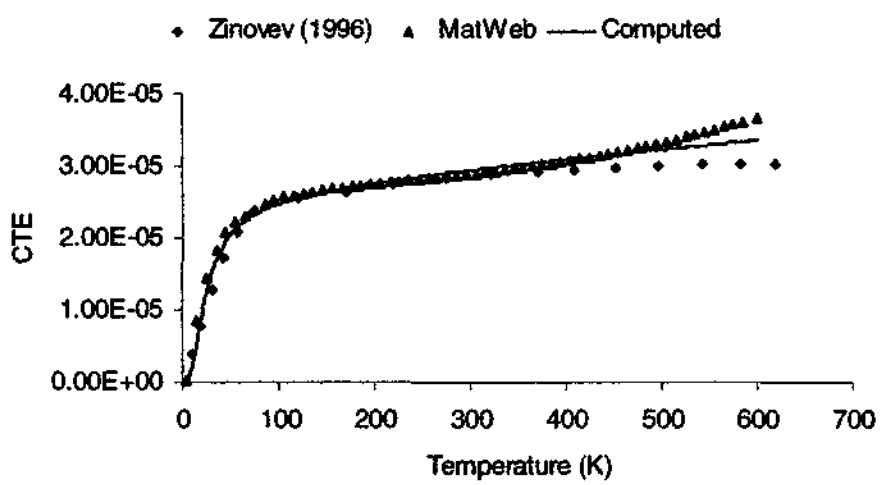

(b) Coefficient of Thermal Expansion vs. Temperature

Figure 6.20 Results for Lead

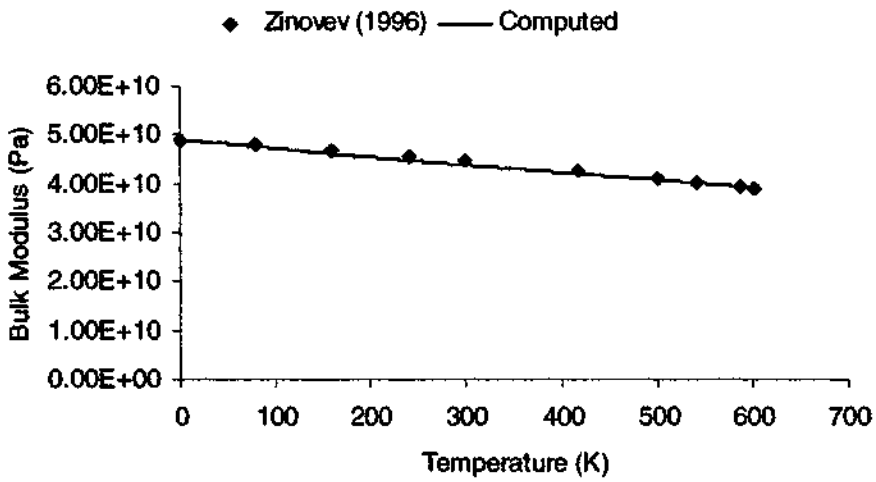

(c) Bulk Modulus vs. Temperature

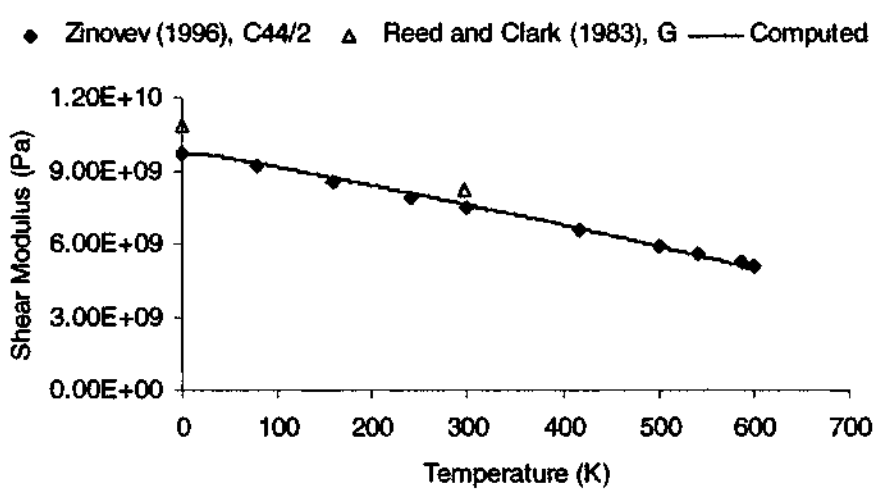

(d) Shear Modulus vs. Temperature

Figure 6.20 (continued)

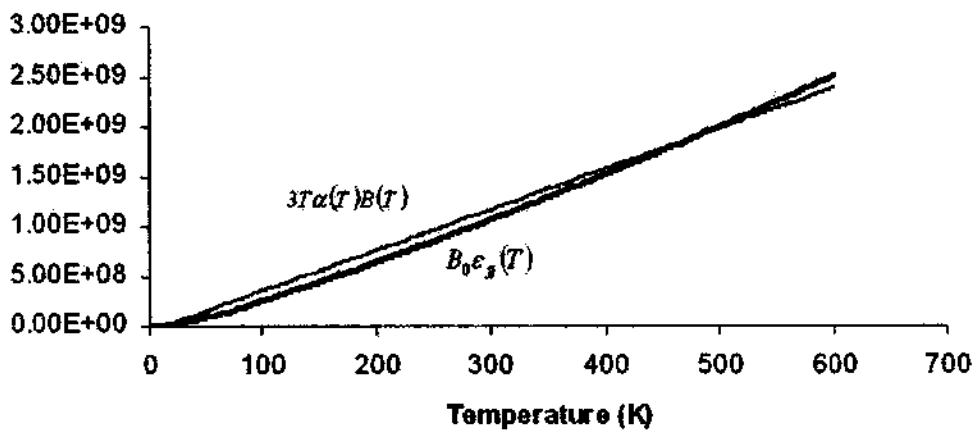

(e) Consistency with Second Law of Thermodynamics

Figure 6.20 (continued)

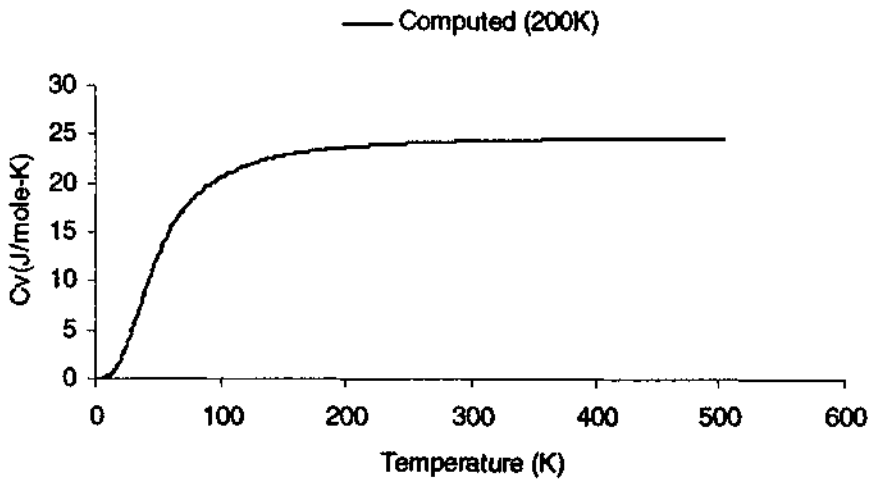

(a) Molar Specific Heat at $T_D = 200K$

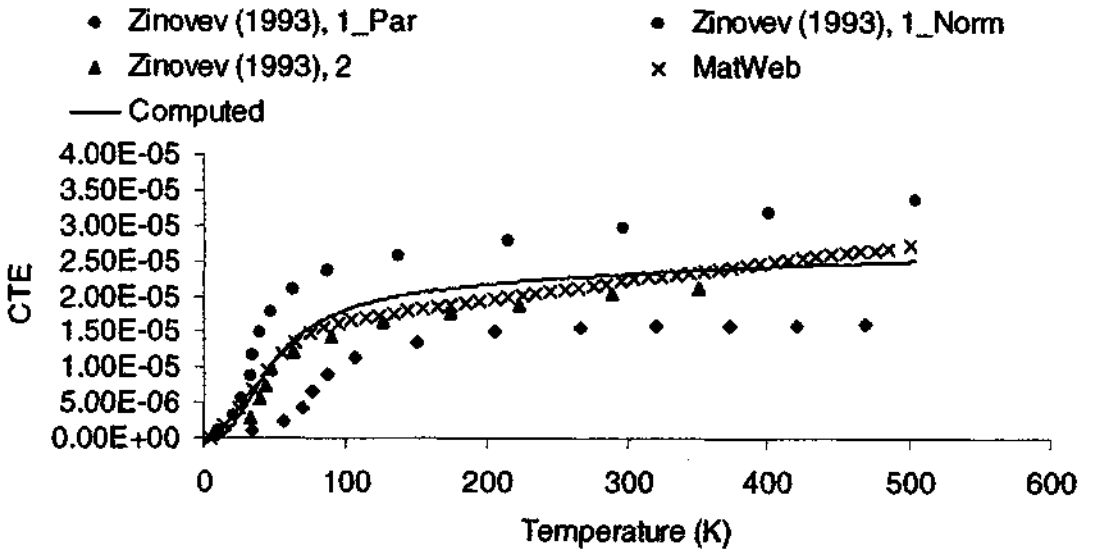

(b) Coefficient of Thermal Expansion vs. Temperature

Figure 6.21 Results for Tin

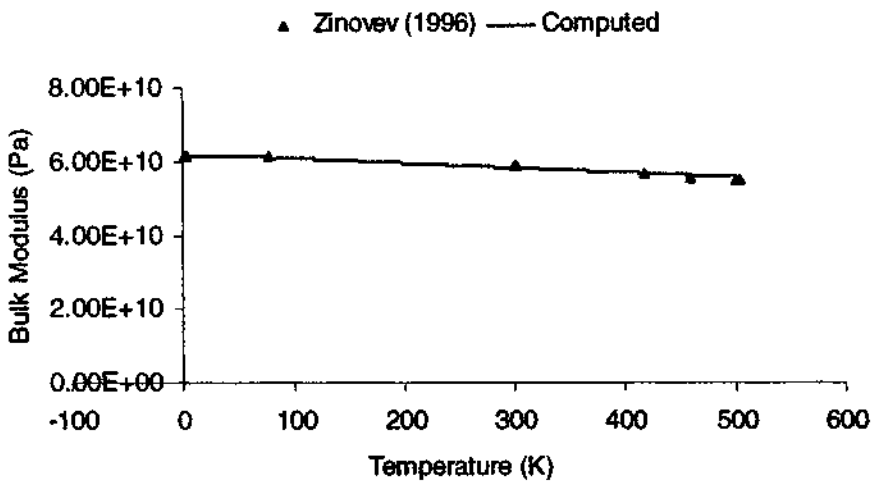

(c) Bulk Modulus vs. Temperature

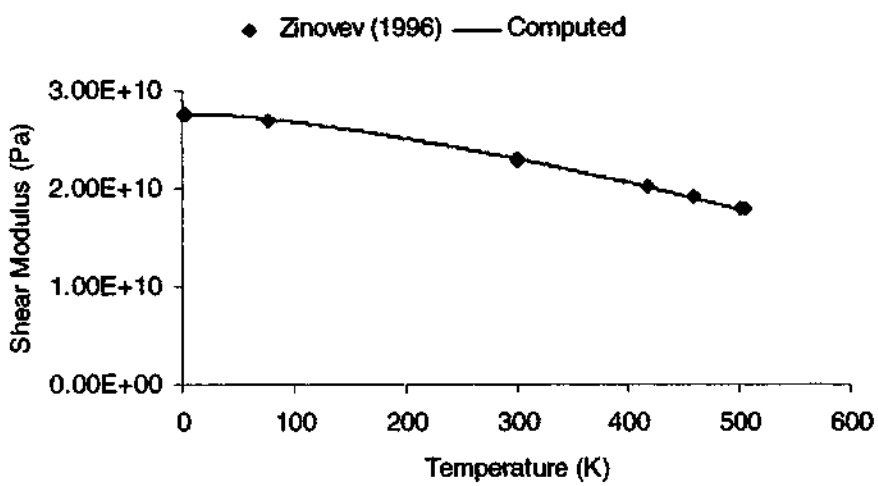

(d) Shear Modulus vs. Temperature (Modified U^L)

Figure 6.21 (continued)

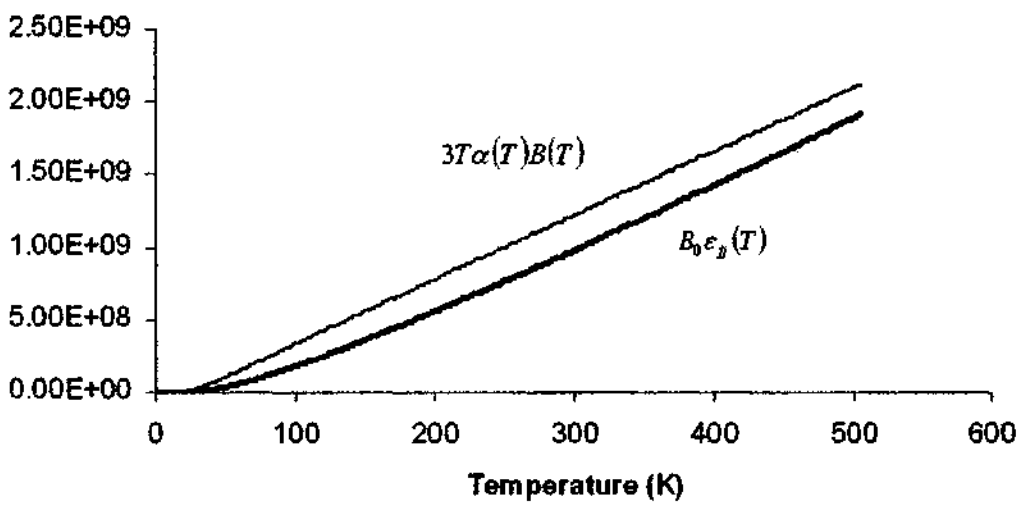

(e) Consistency with Second Law of Thermodynamics

Figure 6.21 (continued)

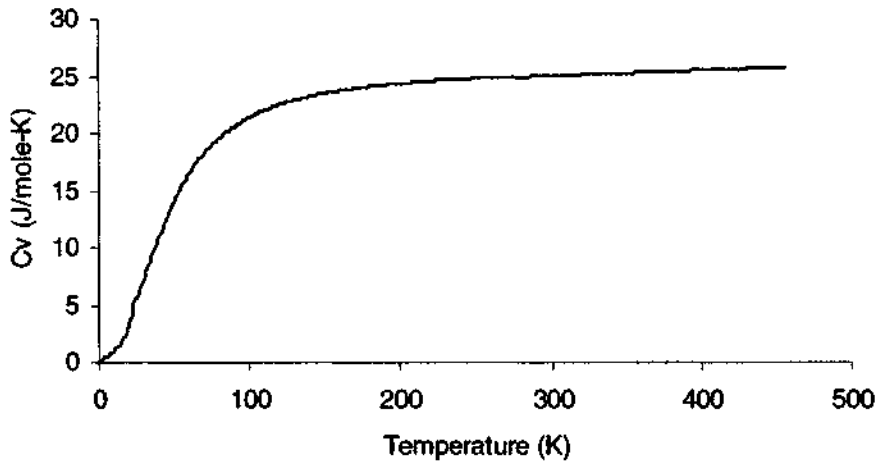

(a) Molar Specific Heat Averaged from Lead and Tin

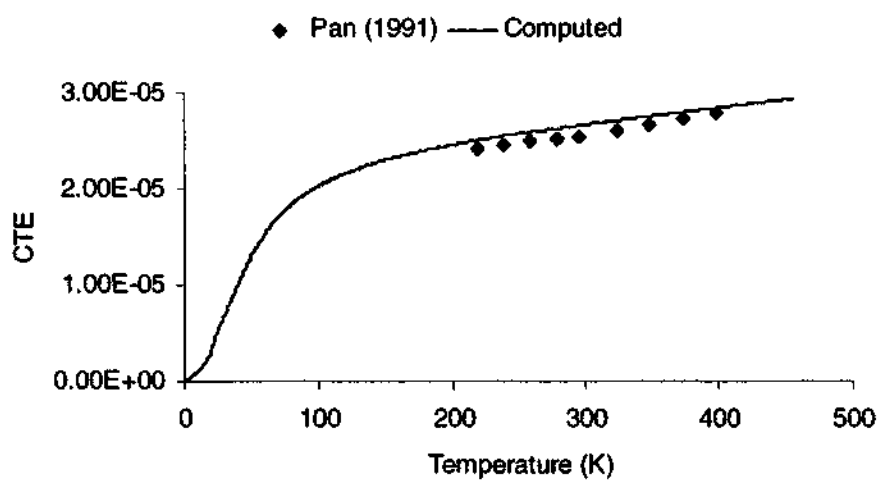

(b) Coefficient of Thermal Expansion vs. Temperature

Figure 6.22 Results for Solder

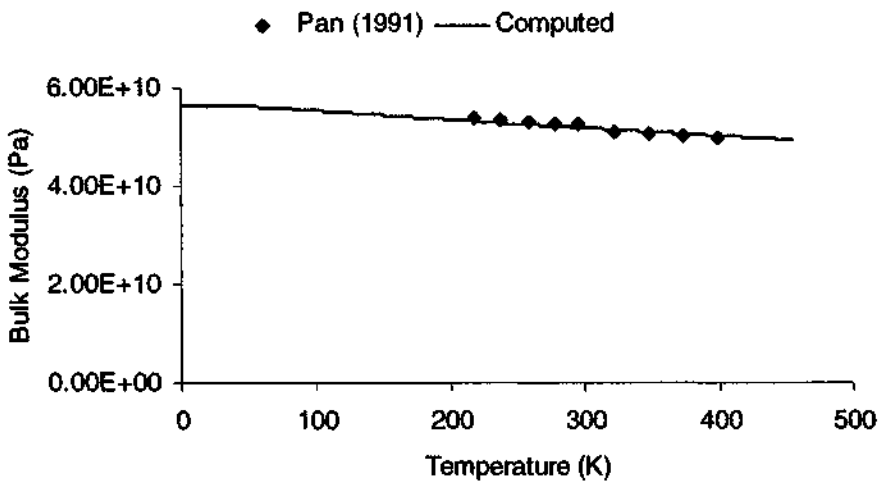

(c) Bulk Modulus vs. Temperature

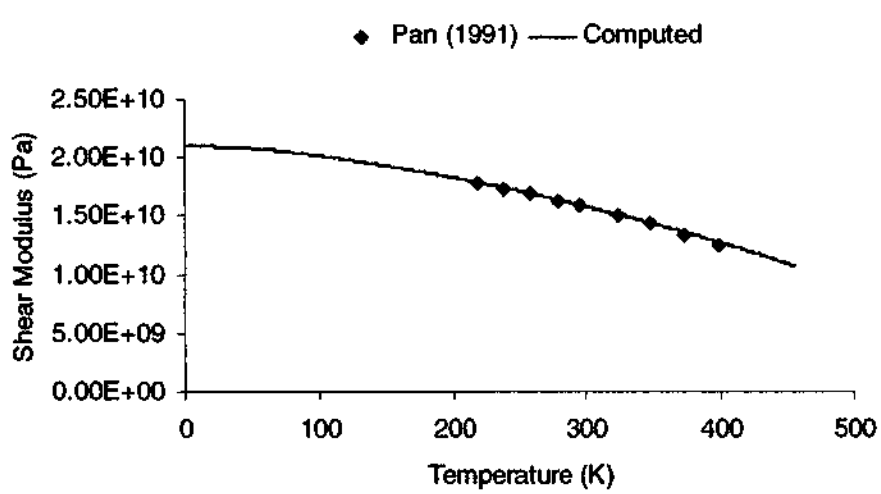

(d) Shear Modulus vs. Temperature (Modified U^L)

Figure 6.22 (continued)

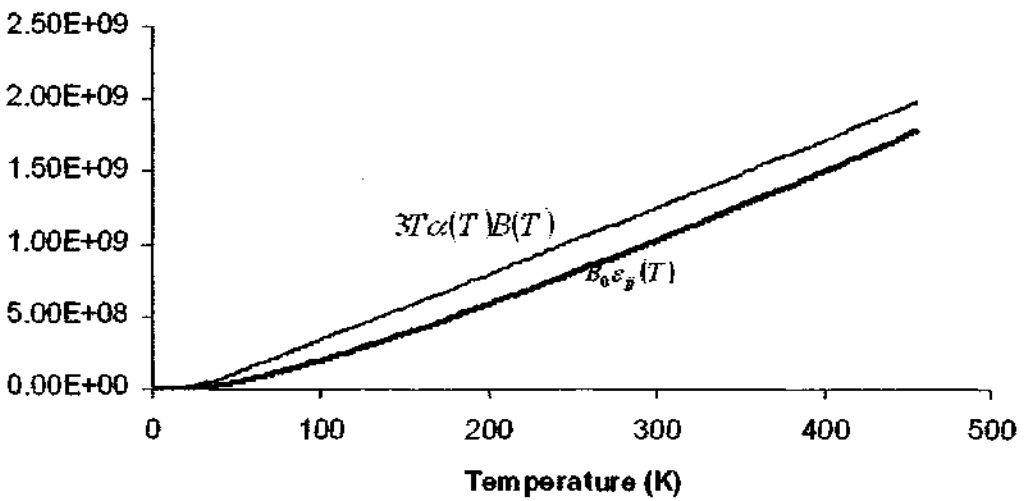

(e) Consistency with Second Law of Thermodynamics

Figure 6.22 (continued)

6.5.2 Plastic Deformations

For plastic deformations, consistent with the assumption that approximately 10% of the dissipated plastic work is absorbed in the crystal, while the rest is dissipated as heat, it may be assumed that

$$\alpha_h \approx 0.1$$

...(6.36)

Based on the modified U^L used for solder, the maximum shear stress that the material could withstand at –20°C and high strain rates, ignoring creep, is approximately 150 MPa, while the maximum value obtained for the testing of Wang et al. (2001) is approximately 45 MPa. Thus, based on Eq. (5.71),

$$\beta \approx 1150\alpha_h \approx 100$$

...(6.37)

The rate-independent elastoplastic curves for solder in the absence of creep for solder at various temperatures are as shown in Figure 6.23. For comparison, the RI curves at the highest strain-rate have been included. As expected, the effect of creep increases with temperature, causing larger deviations from the elastoplastic behavior.

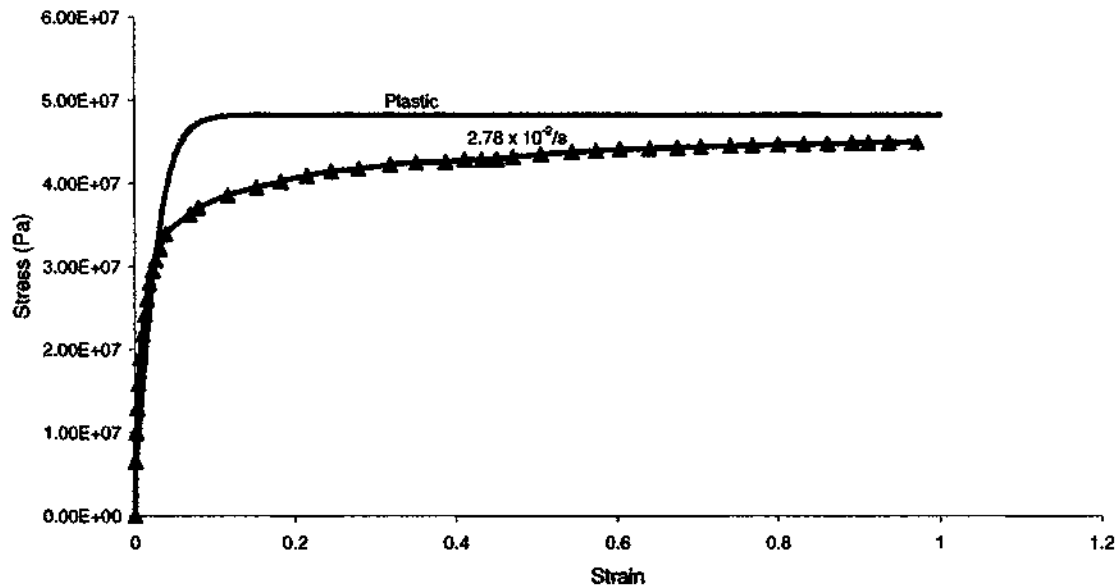

(a) T = -20°C

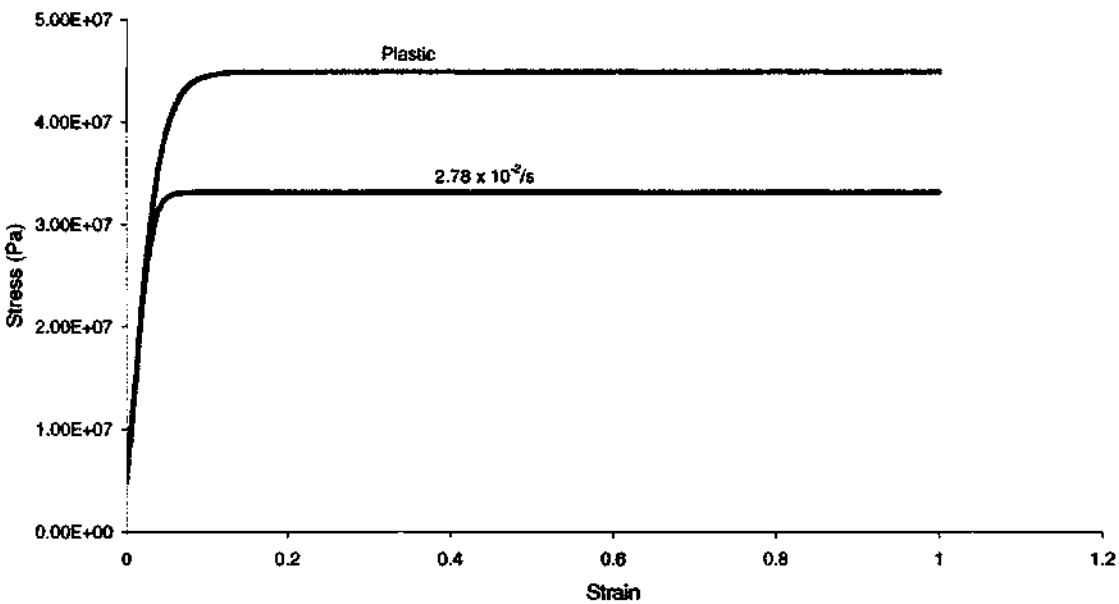

(b) T = 25°C

Figure 6.23 Instantaneous Plastic vs. Highest Rate Test RI Stress-Strain Response

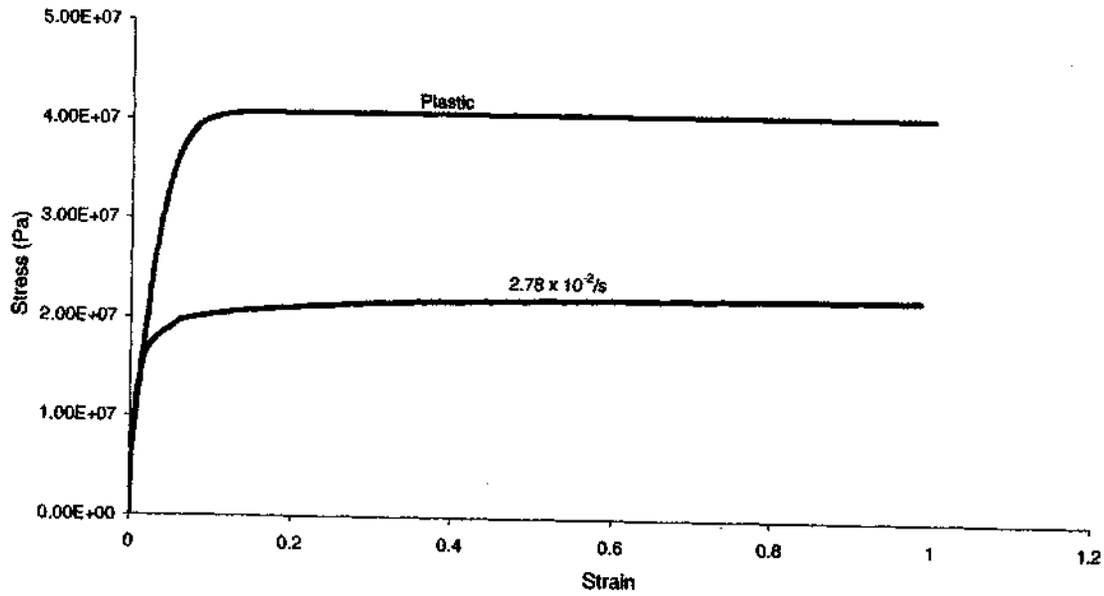

(c) T = 75°C

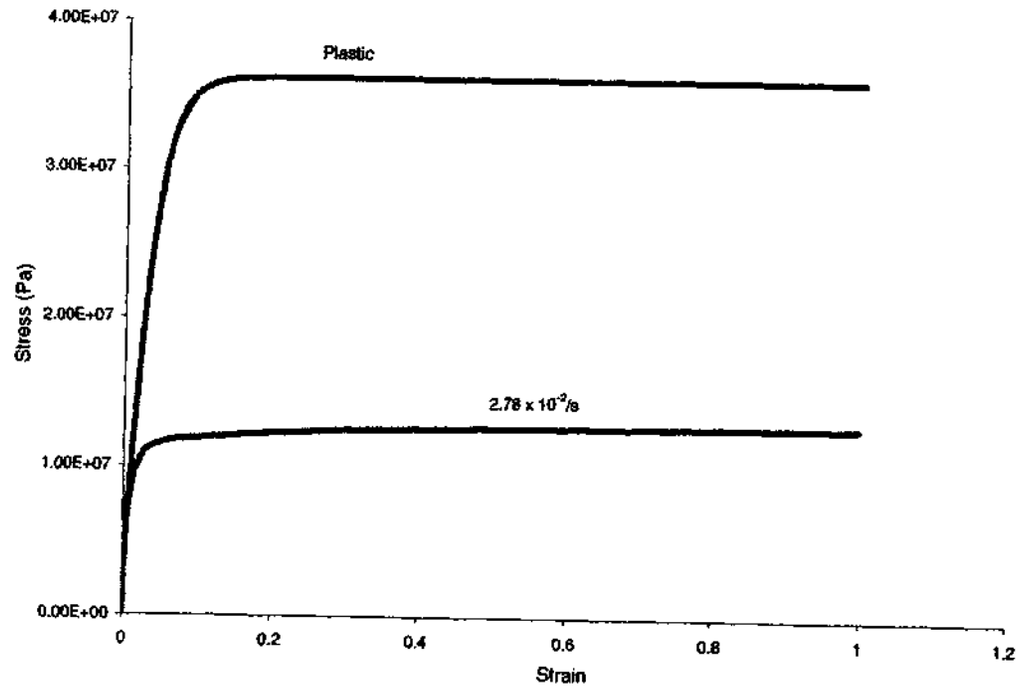

(d) T = 125°C

Figure 6.23 (continued)

6.5.3 Creep

For creep, three additional parameters, Γ_F, N and β_c need to be determined for Eq. (5.73). These parameters were determined by manually fitting all the twelve curves from the data of Wang (2001) simultaneously. The values obtained were

$$\Gamma_F = 2.5\times10^{-5} \qquad \ldots(6.38)$$

$$\beta_c = 7\times10^{-5} \qquad \ldots(6.39)$$

$$N = 4 \qquad \ldots(6.40)$$

Based on these values, the plots for all curves are shown in Figure 6.24. It may be noted that unlike the curves for Perzyna simulation, which were obtained for stress-controlled loading, the curves for this model are obtained under strain-controlled loading. Thus, the difference between test results and backpredictions is in the stress at any given value of the strain, unlike the Perzyna curves wherein the difference is in the strains at any given stress value.

At 125°C, especially for the lowest strain rate test, the predicted curve is substantially higher than the RI response from the test. This could potentially be due to a shift in the dominant creep mechanism.

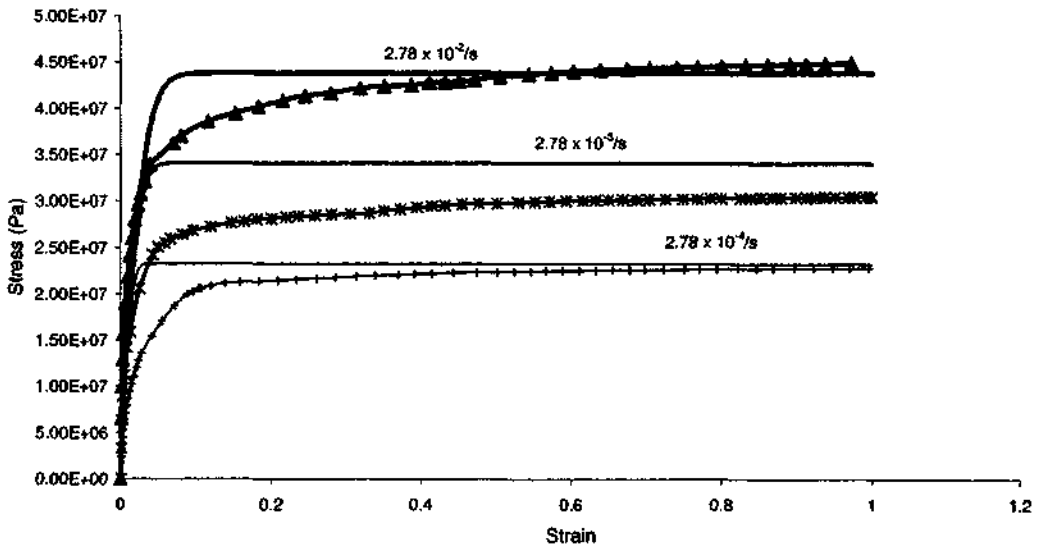

(a) T = -20°C

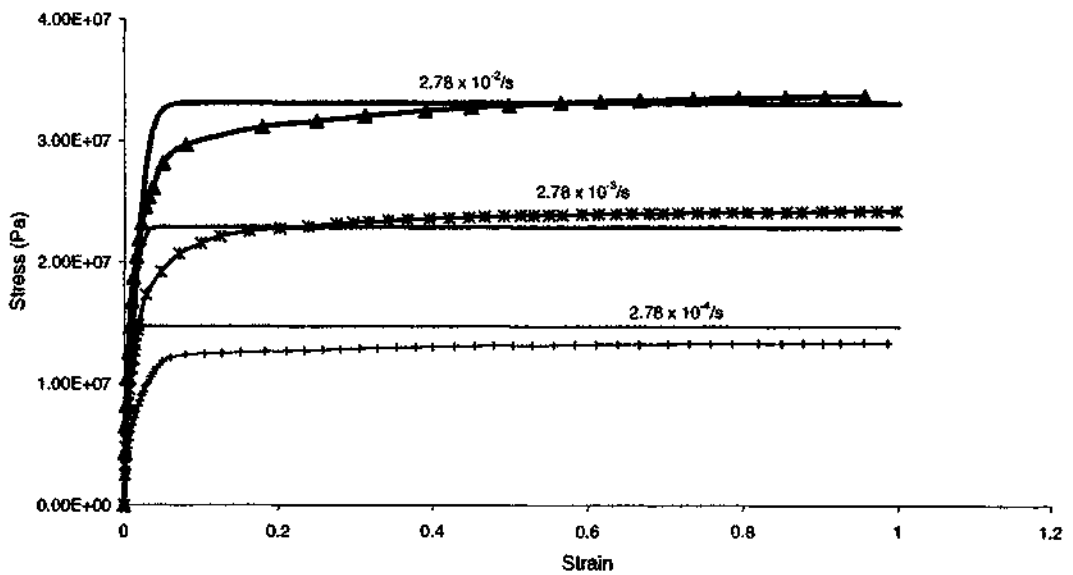

(b) T = 25°C

Figure 6.24 Creep Response

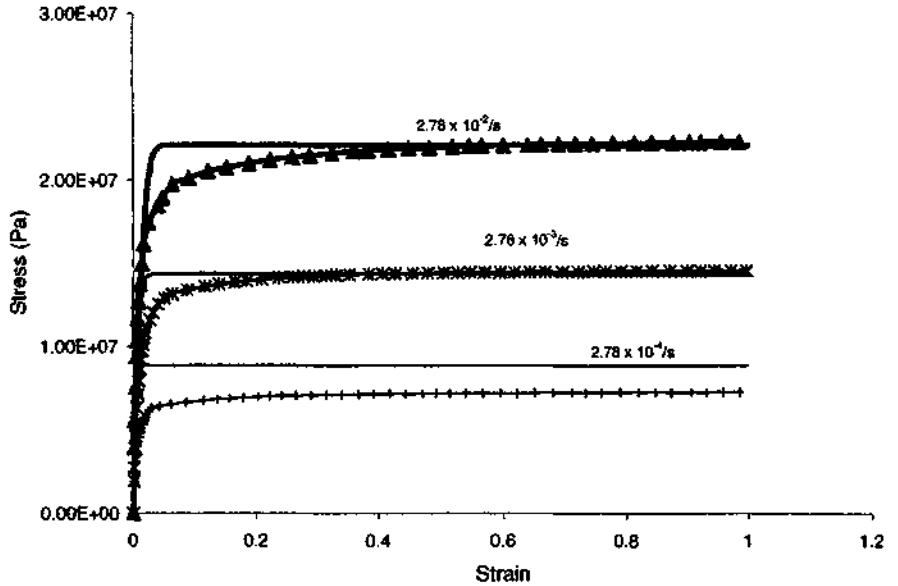

(c) T = 75°C

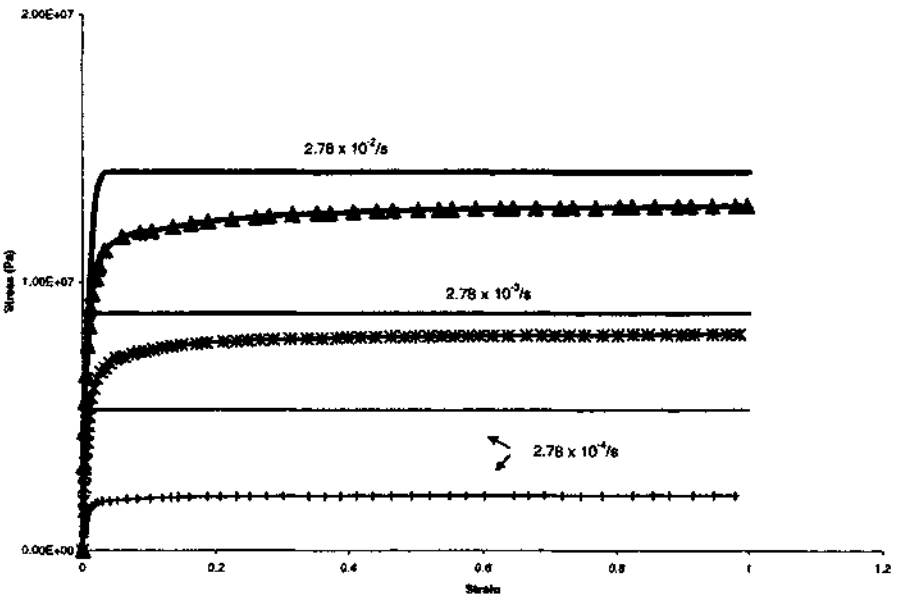

(d) T = 125°C

Figure 6.24 (continued)

7. CONCLUSIONS

This chapter presents a summary of the work and the conclusions based on the same.

7.1 Summary

A number of theoretical issues related to solder modeling were investigated in this work. Alternative schemes were developed for resolution of the issues and were validated primarily with respect to the test-data of Wang et al. (2001).

The simplified elastoplastic scheme was generalized and was found to be of limited validity for solder modeling. Generalizations included the incremental elastic and elastoplastic equations and the consistency condition for plastic strains. Solder parameters in prior literature were shown to require correction in the value of 3R. The corrected parameters permit Perzyna viscoplastic simulation, which is more appropriate than the elastoplastic scheme. Limitations of the Perzyna viscoplastic scheme were also discussed and results based on the test-data of Wang et al. (2001) confirmed that the fluidity parameter showed anomalous behavior with temperature when parameters are

obtained from constant strain-rate tests. The value at -20°C was higher than corresponding values at 25°C and 75°C.

A continuous-yield plasticity yield function was proposed to ensure temperature-independent zero initial plastic strain trajectory and an elastic initial matrix. The proposed function was shown to resolve the issues of discontinuous yield under tensile loads and spurious plastic strains under unconstrained heating and cooling, which were demonstrated for the HiSS-δ_0 yield function.

Additionally, simplified solutions were presented to ameliorate specific issues with the HiSS-δ_0 function. An iterative procedure was developed for the inconsistency in HiSS-δ_0 due to the presence of the nonzero initial plastic strain trajectory. Results for the test-data indicate consistent improvements for elastoplastic backpredictions using the parameters computed based on the iterative procedure as compared to the existing scheme. Further, replacing J_1 with $|J_1|$, was attempted to obtain continuous yield under both tensile and compressive loads, but resulted in increasing shear strength with tensile mean pressure.

The simple modifications did not address the issue of thermally-generated spurious plastic strains. Thermally-generated spurious plastic strains for solder were shown to be larger than the effects of thermal expansion and contraction, confirming the significance of the issue for solder modeling. Li (2002) has suggested treating the initial plastic strain trajectory, computed based on the iterative procedure developed here, as a material

parameter in a modified hardening function to resolve the problem of thermally-generated spurious plastic strains under HiSS-δ_0. However, the simplified solutions are problem-specific and do not treat all issues in the comprehensive manner of the proposed plasticity yield function.

For the shear test-data of Wang et al. (2001), results from the proposed yield function were similar to the improved HiSS-δ_0 results based on the iterative parameter determination scheme, as expected. The proposed yield function provides equivalent results to HiSS-δ_0 in cases where the HiSS-δ_0 function is applicable, while removing the problem of spurious plastic strains due to change in the initial plastic strain trajectory with temperature, providing continuous yield under both tension and compression, with an elastic initial tangent matrix.

The convexity condition for yield functions was seen to require modification to ensure that all yield surfaces possible for a material under zero stress included the origin. It was also shown that the tensor definition of the plastic strain trajectory was not equivalent to the vector definition employed in some prior literature. Apart from providing different numerical values for the plastic strain trajectory, and thus impacting parameter determination and simulations erroneously, the vector definition is not an invariant.

Vaynman et al. (1998) have shown that joints that exhibited larger plastic strains but had lower work-dissipated due to high ductility and low stresses failed later as compared to

joints with higher dissipated work but lower values of the plastic strain. At the suggestion of Desai (1998), a dissipated-work based DSC scheme was formulated. However lack of an explicit work balance in DSC due to simplifying assumptions regarding the equality strains in all phases along with the special assumption regarding unloading modulus was seen to lead to contradictory results. Results for the test-data of Wang et al. (2001) did not provide any improvement in parameters as regards to their variation with loading conditions, or any improvements in backpredictions. Thus, the formulation was not found to be of much utility for solder.

An issue of interest in material modeling is the expression of material parameters as functions of loading conditions such as temperature and strain-rate. This was not conducted for the elastoplastic formulation due to the limited utility of the formulation. To avoid curve fitting for Perzyna simulation, a scheme that used all available test-data at any strain-rate simultaneously to determine the viscoplastic parameters was presented and validated based on the test data. However, the anomalous behavior of the fluidity parameter with temperature, as predicted, precluded expression of the parameters as functions of temperature.

For direct comparison of the ability of one material model relative to another for predicting given material behavior, it is essential that parameters used be as accurate as feasible. Expressing parameters as functions of temperature shifts curve fitting from test

backpredictions to fitting functions for variation of parameters. Any additional error introduced due to this only contaminates the results for comparison of various models.

Instead of attempting expression of material parameters as functions of temperature, an integrated thermomechanical model was developed based on the concept of superposition of phases. The model was validated for aluminum, lead, tin and solder, and was shown to be inherently capable of providing the variation of the coefficient of thermal expansion and elastic parameters with temperature, based on the stress-strain-temperature relationships.

For the case of aluminum, which is an isotropic material that does not undergo phase change, only one empirical factor was required to obtain the variation of the coefficient of thermal expansion, bulk modulus and shear modulus with temperature. For lead, with marked anisotropy, the elastic constants B and C_{44} showed extremely close correlation between predictions and observed behavior. Further for lead, available values of the shear modulus G were quite close to $C_{44}/2$, and thus, for temperatures where this approximation holds, good predictions of G can be obtained directly. In other cases, existing relationships that average elastic constants across directions must be used. Even though the model is not meant for materials that undergo phase change, an empirical correction to the latent heat of fusion, in terms of a scaling factor, was shown to provide reasonable results for tin and solder.

This is useful for solder as determination of elastic parameters is difficult at high temperatures and any error in the elastic parameters contaminates subsequently determined parameters. As shown based on the static-surface results of Perzyna and the simplified rate-dependent elastoplastic backpredictions for the lowest strain-rate test curves, if the formulation is sufficiently complex, two different values of elastic parameters may be assumed and each may provide a corresponding set of plasticity parameters as well as reasonable backpredictions for the test.

The thermomechanical model was extended to plastic deformations and to schemes for modeling creep below the yield surface. Further work is required for development of the creep part of the model. However, a simple scheme was shown to be reasonable for fitting a number of solder test curves at different strain-rates at four temperatures ranging from –20°C to 125°C based on three temperature-independent creep parameters.

For experimental work[17], image acquisition was carried out for the testing of Wang et al. (2001). Results from the same helped prevent rocking of sample and undue compression, aiding development of test procedures that ensured correspondence between the nominal applied deformation, and that realized at the joints. The Digital Image Correlation approach was found to be substantially more amenable to application than speckle interferometry, although detailed strain-mapping for areas with a loss of discernible surface features during testing remains an issue. An improved technique for sample

[17] Testing related experimental work was conducted under the guidance of Dr. C. S. Desai.

making was also developed, so as to improve upon the procedure of Wang et al. (2001) and obtain samples without undue voids, dissolved copper, residual stresses from post-soldering machining as well as consistency with industrial processes. Test results based on the same for Ag/Sn solder are not presented here. Improvements (not reported) were also made towards the maintainability of the test device.

7.2 Conclusions

The work showed that simplified ad-hoc assumptions may lead to unanticipated inconsistencies under general loading conditions. Simple loading paths for elastic deformations demonstrated the need for generalization of incremental relationships and the limitations of the rate-dependent formulation. Limitations of the Perzyna scheme were also determined based on simple shear test data for solder. Uniaxial tension and unconstrained heating and cooling indicated issues with HiSS-δ_0 and the need for the proposed yield function developed here. Work-balance analysis for DSC demonstrated the approximation inherent in the assumption of strain compatibility.

The analyses demonstrated that the approach used in the work, that of studying existing material models and constitutive formulations under various simplified conditions, where the nature of the result is known *a priori*, provided much useful information regarding limitations of existing formulations and towards the development of appropriate

formulations such as the proposed yield function. This approach is obviously not a replacement for finite element simulations of field problems, but is recommended for use as an initial step to gain confidence in the material model selected, prior to solution of complex field problems. Literature indicates that finite element simulations based on complex material models and practical geometries and load conditions lead to cases where gross errors in the simulation may go undetected.

Dependence of material parameters on loading conditions, such as the strain-rate and temperature-dependent elastoplastic formulation developed here, complicated the overall formulation. Further, it is an indication that the formulation does not explain the observed behavior completely. Thus, rate-dependent parameters used for simplified elastoplastic simulations were not required for the viscoplastic simulations which inherently predicted rate-dependent behavior. The concept of superposition of phases was shown to lead to a comprehensive thermoelastic and elastoplastic model for materials, which is based on temperature-independent material parameters. A preliminary approach towards creep simulation provided promising results. Modifications (not reported) of the yield criterion were investigated to incorporate softening into the elastoplastic scheme for incorporation of damage, for materials where damage is restricted to regions of plastic deformation.

Visual monitoring of tests was determined to be extremely helpful in mitigating the effects of machine compliance as well as ensuring that the intended nominal deformation is actually realized within the test specimen.

APPENDIX I

HISTORY DEPENDENCE OF ELASTIC RELATIONSHIPS

I.1 Existing Formulation

The incremental relationship between stress and elastic strain in terms of the tangent stiffness matrix used in prior literature for solder modeling (Wang et al., 2001) is

$$d\sigma_{ij} = C^{e}_{ijkl}(p_1,..., p_n)d\varepsilon^{e}_{kl} \qquad ...(I.1)$$

where the p_i are loading parameters such as temperature, strain rate, stress and strain. Solder elastic parameters vary with temperature, and for the simplified elastoplastic formulation, with strain rate. For variable material parameters, the existing formulation does not provide a history-independent, one-to-one relationship between stress and elastic strain.

I.1.1 Temperature Dependence

Consider an elastic material block, with temperature-dependent properties, i.e.

$$G = G(T) \qquad ...(I.2)$$

Let the block be at the initial state of strain and temperature (0, T_i) as shown in Figure I.1. The block is loaded to a final state (γ, T_f) via two alternative paths.

Path 1

The block is first loaded to a shear strain γ isothermally, and the stress at state A is

$$\tau_A = G(T_A)\gamma$$

...(I.3)

Increasing the temperature while maintaining a constant shear stress ($d\gamma = 0$) to reach the final state provides for the final stress

$$\tau_f\big|_{Path1} = \tau_A + \int_A^f G(T)d\gamma = \tau_A = G(T_A)\gamma$$

...(I.4)

Path 2

The block is first heated under zero applied stresses to temperature T_f, to reach state A' (0, T_f) with no shear strain

$$\tau_{A'} = \int_i^{A'} G(T)d\gamma = 0$$

...(I.5)

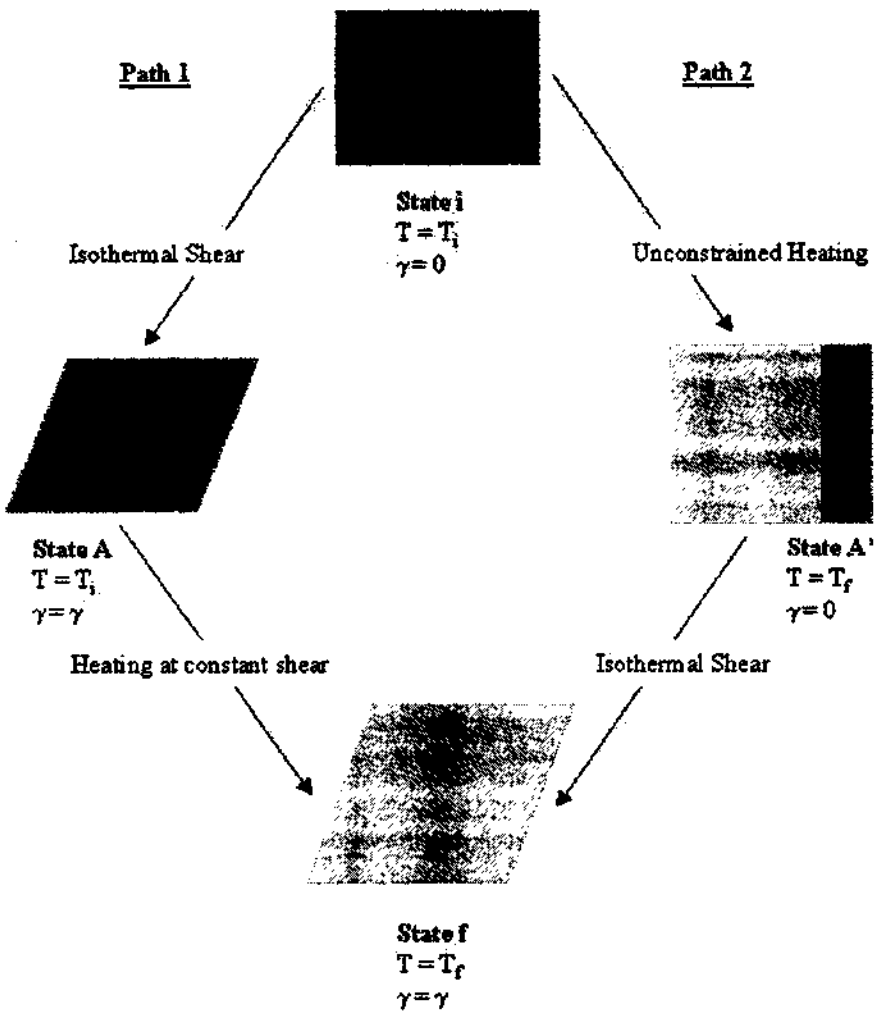

Figure I.1: Alternative Paths for (T_0, $\gamma_0 = 0$) to (T_f, γ_f)

The block is then sheared to the strain γ at temperature T_f, to provide

$$\tau_f\big|_{Path2} = G(T_f)\gamma$$

...(I.6)

Thus, starting from the same initial state (0, Ti) and ending at the same final state (γ, T_f) the stress at the final state is path-dependent. For the paths considered,

$$\tau_f\big|_{Path1} - \tau_f\big|_{Path2} = \left(G(T_i) - G(T_f)\right)\gamma$$

...(I.7)

I.1.2 Rate Dependence

Consider a block of material wherein the shear modulus is a function of the strain-rate.

$$G = G\left(\dot{\gamma}\right)$$

...(I.8)

The initial state (i) is the stress-free state. The final state (f) of the material is that of shear strain γ, held at a constant strain i.e. at zero strain rate. The loading is accomplished through two alternate paths as shown in Figure I.2. To remove interference from temperature effects, both paths are assumed to be isothermal.

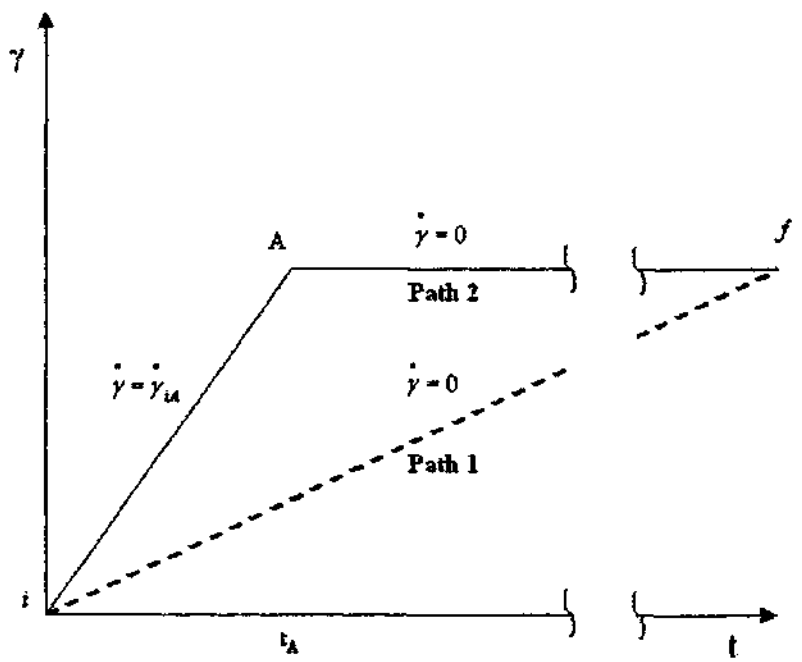

Figure I.2: Alternative Paths with Different Strain Rate History

Path 1

The material is loaded quasi-statically to the shear strain γ. The stress at this state is

$$\tau_f\big|_{Path1} = G(0)\gamma$$

...(I.9)

Path 2

The material is first loaded to the final strain γ at a finite strain rate $\dot{\gamma}_{iA}$, from state *i* to state A with

$$\tau_A = G\left(\dot{\gamma}_{iA}\right)\gamma$$

...(I.10)

The strain is then held constant thereafter (dγ = 0). Thus, at the final state,

$$\tau_f\big|_{Path2} = \tau_A + \int_A^f G d\gamma = G\left(\dot{\gamma}_{iA}\right)\gamma$$

...(I.11)

In this case

$$\tau_f\big|_{Path1} - \tau_f\big|_{Path2} = \left(G(0) - G\left(\dot{\gamma}_{iA}\right)\right)\gamma$$

...(I.12)

I.2 Generalized Elastic Formulation

The existing elastic formulation of Eq. (I.1) for both temperature and rate dependent elastic parameters has been shown to be inconsistent with the assumption that the relationship between stresses and elastic strains is history-independent.

If the generalized elastic relationship

$$\sigma_{ij} = C^{se}_{ijkl}(p_1,\ldots p_n)\varepsilon^e_{kl} \qquad \ldots(I.13)$$

$$\Rightarrow \qquad d\sigma_{ij} = C^{se}_{ijkl}(p_1,\ldots, p_n)d\varepsilon^e_{kl} + \left(\frac{\partial C^{se}_{ijkl}}{\partial p_i}\varepsilon^e_{kl}\right)dp_i \qquad \ldots(I.14)$$

is used instead, the final stress depends only on the strain and other relevant parameters such as temperature or strain-rate at that instant, and not on the history.

For a temperature-dependent material, the generalized incremental relationship is

$$d\sigma_{ij} = C^e_{ijkl}(T)d\varepsilon^e_{kl} + \left(\frac{\partial C^e_{ijkl}}{\partial T}\varepsilon^e_{kl}\right)dT \qquad \ldots(I.15)$$

Application of the generalized relationship modifies Eq. (I.4) for Path 1 of the temperature dependence problem to

$$\tau_f\big|_{Path1} = \tau_A + \int_A^f G(T)d\gamma + \gamma\int_A^f dG(T) = \tau_A + G(T_f)\gamma - G(T_A)\gamma = G(T_f)\gamma$$

...(I.16)

Thus, from Eqs. (I.6) and (I.16), both paths provide, as expected,

$$\tau_f = G(T_f)\gamma$$

...(I.17)

For the case of rate-dependent material parameters (Figure I.2) for Path 2, there is a discontinuity in the strain rate at point A. Application of the generalized formulation as

$$d\sigma_{ij} = C^e_{ijkl}\left(\dot{\gamma}\right)d\varepsilon^e_{kl} + \left(\frac{\partial C^e_{ijkl}}{\partial\dot{\gamma}}\varepsilon^e_{kl}\right)d\dot{\gamma}$$

...(I.18)

provides

$$\tau_A\big|_{1\to\left(\frac{\gamma}{\dot{\gamma}_{iA}}\right)^-} = G\left(\dot{\gamma}_{iA}\right)\gamma$$

...(I.19)

and

$$\tau_A\big|_{1\to\left(\frac{\gamma}{\dot{\gamma}_{iA}}\right)^+} = \tau_A\big|_{1\to\left(\frac{\gamma}{\dot{\gamma}_{iA}}\right)^-} + \left(G(0) - G\left(\dot{\gamma}_{iA}\right)\right)\gamma = G(0)\gamma$$

...(I.20)

Thus,

$$\tau_A\big|_{Path2} = \tau_A\big|_{t\to\left(\frac{\gamma}{\dot{\gamma}_{iA}}\right)^-} = G(0)\gamma$$

...(I.21)

and for both paths, Eqs. (I.9) and (I.21) provide the same value of the final stress (Figure I.3), given by

$$\tau_f = G(0)\gamma$$

...(I.22)

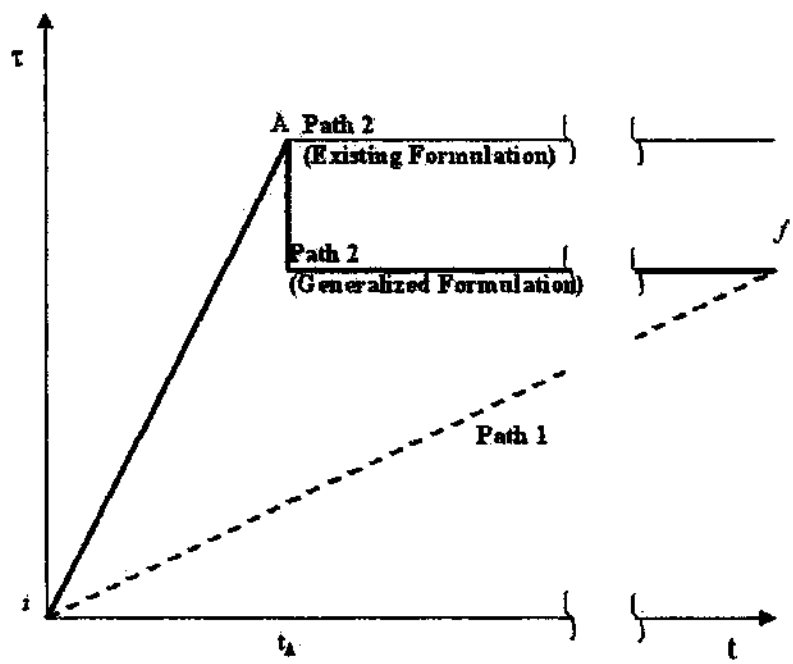

Figure I.3: Stress Response for Existing and Generalized Formulations

APPENDIX II

OVERLAY MODELS

Various overlay schemes, based on combinations of springs, dashpots and sliders can be used for modeling elastic, viscoelastic, elastoviscoplastic and viscoelastic-viscoplastic[18]. Examples include the Maxwell model, the Kelvin model, the standard solid model and their combinations and generalizations (Mase, 1970).

II.1 Viscoelastic Material

An overlay model for a viscoelastic material is shown in Figure II.1. The global equilibrium equation, where subscripts 1 and 2 refer to branches 1 and 2 respectively, is

$$\sigma = t_1\sigma_1 + t_2\sigma_2 \qquad \ldots(II.1)$$

while the global compatibility condition provides

$$\varepsilon_1 = \varepsilon_2 = \varepsilon \qquad \ldots(II.2)$$

[18] Overlay equations were derived in an unpublished report, as part of assistanship work at University of Arizona, in 2000.

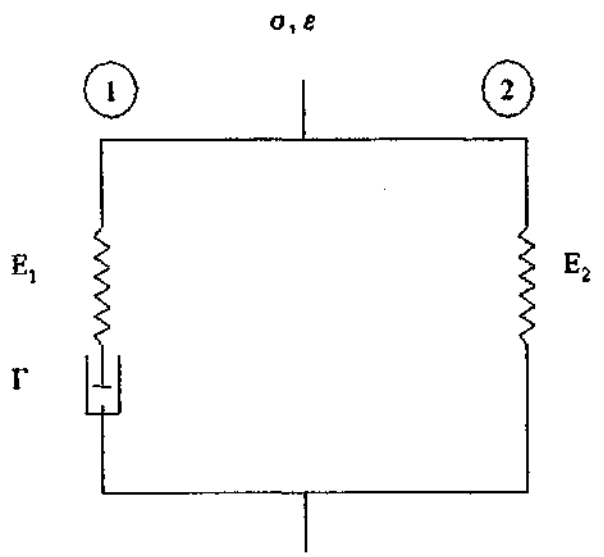

Figure II.1 Viscoelastic Overlay Model

For branch 2, the governing equation is

$$\sigma_2 = E_2 \varepsilon$$

...(II.3)

For branch 1, compatibility of strains requires

$$\varepsilon(t) = \varepsilon^E(t) + \varepsilon^{DP}(t)$$

...(II.4)

where E refers to the spring, and DP to the dashpot.

The equilibrium condition is

$$\sigma_1 = E_1 \varepsilon^E = \frac{1}{\Gamma} \frac{d\varepsilon^{DP}}{dt}$$

...(II.5)

If the strain applied to the material is known as a function of time, the stress can be determined by solving

$$\frac{1}{E_1 \Gamma} \frac{d\varepsilon^{DP}}{dt} + \varepsilon^{DP} = \varepsilon(t)$$

...(II.6)

for obtaining ε^{DP} as a function of time, followed by

$$\sigma(t) = t_1 E_1 \left(\varepsilon(t) - \varepsilon^{DP}(t)\right) + t_2 E_2 \varepsilon(t)$$

...(II.7)

If the stress is known as a function of time, the strain can be calculated using

$$\frac{1}{E_1\Gamma}(t_1E_1+t_2E_2)\frac{d\varepsilon(t)}{dt}+t_2E_2\varepsilon(t)=\frac{1}{E_1\Gamma}\frac{d\sigma(t)}{dt}+\sigma(t)$$

...(II.8)

For the viscoelastic overlay model, parameters may be determined from a constant stress test with stress σ_0 applied at t = 0, and held constant thereafter.

As the dashpot is inoperative at t = 0

$$\varepsilon(0)=\frac{\sigma_0}{E_1t_1+E_2t_2}$$

...(II.9)

$$\sigma_1(0)=\frac{E_1\sigma_0}{E_1t_1+E_2t_2}$$

...(II.10)

Differentiating Eq. (II.1) with respect to time provides

$$\frac{d\sigma_2}{dt}=-\frac{t_1}{t_2}\frac{d\sigma_1}{dt}$$

...(II.11)

Branch 2 provides

$$\varepsilon = \frac{\sigma_2}{E_2} \Rightarrow \frac{d\varepsilon}{dt} = -\frac{1}{E_2}\frac{t_1}{t_2}\frac{d\sigma_1}{dt}$$

...(II.12)

Branch 1 provides

$$\varepsilon = \varepsilon^e + \varepsilon^{DP}$$

...(II.13)

$$\Rightarrow \frac{d\varepsilon}{dt} = \frac{1}{E_1}\frac{d\sigma_1}{dt} + \Gamma\sigma_1$$

...(II.14)

Equating terms in Eqs. (II.13) and (II.14)

$$\Rightarrow \left(\frac{1}{E_1} + \frac{t_1}{t_2}\frac{1}{E_2}\right)\frac{d\sigma_1}{dt} + \Gamma\sigma_1 = 0$$

...(II.15)

$$\Rightarrow \sigma_1 = C_1 e^{\frac{-t\Gamma}{\left(\frac{1}{E_1} + \frac{t_1}{t_2}\frac{1}{E_2}\right)}}$$

...(II.16)

Using the initial condition of Eq. (II.10)

$$\Rightarrow \sigma_1 = \frac{E_1\sigma_0}{E_1t_1 + E_2t_2} e^{\frac{-t\Gamma}{\left(\frac{1}{E_1}+\frac{t_1}{t_2}\frac{1}{E_2}\right)}} = \frac{E_1\sigma_0}{E_1t_1 + E_2t_2} e^{\frac{-t\Gamma E_1E_2t_2}{(E_1t_1+E_2t_2)}}$$

...(II.17)

$$\Rightarrow \frac{d\sigma_1}{dt} = \frac{E_1\sigma_0}{E_1t_1 + E_2t_2} \frac{-\Gamma E_1E_2t_2}{(E_1t_1 + E_2t_2)} e^{\frac{-t\Gamma E_1E_2t_2}{(E_1t_1+E_2t_2)}} = -\frac{\Gamma E_1^2E_2t_2\sigma_0}{(E_1t_1 + E_2t_2)^2} e^{\frac{-t\Gamma E_1E_2t_2}{(E_1t_1+E_2t_2)}}$$

...(II.18)

$$\Rightarrow \frac{d\sigma_2}{dt} = \frac{\Gamma E_1^2E_2t_1\sigma_0}{(E_1t_1 + E_2t_2)^2} e^{\frac{-t\Gamma E_1E_2t_2}{(E_1t_1+E_2t_2)}}$$

...(II.19)

$$\Rightarrow \frac{d\varepsilon}{dt} = \frac{\Gamma E_1^2t_1\sigma_0}{(E_1t_1 + E_2t_2)^2} e^{\frac{-t\Gamma E_1E_2t_2}{(E_1t_1+E_2t_2)}}$$

...(II.20)

$$\Rightarrow \varepsilon = \frac{-\sigma_0}{E_1t_1 + E_2t_2} \frac{E_1t_1}{E_2t_2} e^{\frac{-t\Gamma E_1E_2t_2}{E_1t_1+E_2t_2}} + \frac{\sigma_0}{E_1t_1 + E_2t_2}\left[1 + \frac{E_1t_1}{E_2t_2}\right]$$

...(II.21)

As $t \rightarrow \infty$,

$$\varepsilon \rightarrow \frac{\sigma_0}{E_1t_1 + E_2t_2}\left[1 + \frac{E_1t_1}{E_2t_2}\right] = \frac{\sigma_0}{E_2t_2}$$

...(II.22)

Using the final observed value of strain in Eq. (II.22) provides E_2t_2, which substituted in Eq. (II.9) provides E_1t_1.

Additionally,

$$\left.\frac{d\varepsilon}{dt}\right|_{t=0} = \frac{\Gamma E_1^2 t_1 \sigma_0}{(E_1t_1 + E_2t_2)^2}$$

...(II.23)

which provides $E_1\Gamma$, thereby providing all the coefficients in Eqs. (II.6) – (II.8). The results also indicate that there is no loss of generality in assuming any t_1 and t_2, as long as their sum is unity.

II.2 Viscoelastic-Viscoplastic Material

Consider the model shown in Figure II.2. Let a constant stress, σ_0, be applied to the material. Deformations under the viscoelastic-viscoplastic model occur in two stages. When the stress in branch 2 is less than σ_y, the model is identical to the viscoelastic model. When the time reaches a time, t*, when $\sigma_2 = \sigma_y$, the slider starts to yield. During the initial viscoelastic phase,

$$\varepsilon = \frac{-\sigma_0}{E_1t_1 + E_2t_2}\frac{E_1t_1}{E_2t_2}e^{\frac{-t\Gamma_1E_1E_2t_2}{E_1t_1+E_2t_2}} + \frac{\sigma_0}{E_2t_2}$$

...(II.24)

If

$$\sigma_0 > t_2 \sigma_y$$

...(II.25)

the slider yields eventually. Let t* be the time at which the slider yields. Then, at that time, the strain provides

$$\sigma_y = E_2 \varepsilon^* = E_2 \left(\frac{-\sigma_0}{E_1 t_1 + E_2 t_2} \frac{E_1 t_1}{E_2 t_2} e^{\frac{-t^* \Gamma_1 E_1 E_2 t_2}{E_1 t_1 + E_2 t_2}} + \frac{\sigma_0}{E_2 t_2} \right)$$

...(II.26)

$$\Rightarrow \qquad t^* = -\frac{E_1 t_1 + E_2 t_2}{\Gamma_1 E_1 E_2 t_2} \ln \left(\frac{\frac{\sigma_y}{E_2} - \frac{\sigma_0}{E_2 t_2}}{\frac{-\sigma_0}{E_1 t_1 + E_2 t_2} \frac{E_1 t_1}{E_2 t_2}} \right)$$

...(II.27)

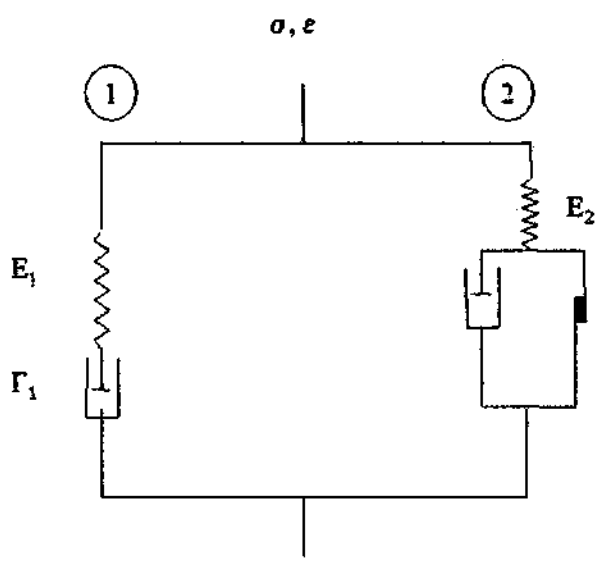

Figure II.2 Viscoelastic-Viscoplastic Overlay Model

Beyond this time, the viscoelastic-viscoplastic behavior is observed.

The total stress remains constant, and thus

$$\sigma_0 = t_1 E_1 \varepsilon_1^e(t) + t_2 E_2 \varepsilon_2^e(t) = const \qquad \text{...(II.28)}$$

$$\Rightarrow \varepsilon_2^e = \frac{\sigma_0 - E_1 t_1 \varepsilon_1^e}{E_2 t_2} \qquad \text{...(II.29)}$$

$$\Rightarrow \frac{d\varepsilon_2^e}{dt} = -\frac{E_1 t_1}{E_2 t_2}\frac{d\varepsilon_1^e}{dt} \qquad \text{...(II.30)}$$

For Branch 1, the total strain can be written as

$$\varepsilon = \varepsilon_1^e + \varepsilon_1^{DP} \qquad \text{...(II.31)}$$

$$\Rightarrow \quad \frac{d\varepsilon_1^e}{dt} = \frac{d\varepsilon}{dt} - \frac{d\varepsilon_1^{DP}}{dt} \qquad \text{...(II.32)}$$

The stresses across the spring and the dashpot are the same. Thus

$$\sigma_1 = E_1 \varepsilon_1^e = \frac{1}{\Gamma_1}\frac{d\varepsilon_1^{DP}}{dt} \qquad \text{...(II.33)}$$

$$\Rightarrow \frac{d\varepsilon_1^{DP}}{dt} = \Gamma_1 E_1 \varepsilon_1^e$$

...(II.34)

Substituting Eq. (II.34) into Eq. (II.32),

$$\frac{d\varepsilon_1^e}{dt} = \frac{d\varepsilon}{dt} - \Gamma_1 E_1 \varepsilon_1^e$$

...(II.35)

Substituting Eq. (II.35) in Eq. (II.30)

$$\frac{d\varepsilon_2^e}{dt} = \frac{E_1 t_1}{E_2 t_2}\left[\Gamma_1 E_1 \varepsilon_1^e - \frac{d\varepsilon}{dt}\right]$$

...(II.36)

For Branch 2, the total strain is

$$\varepsilon = \varepsilon_2^e + \varepsilon_2^{DP}$$

...(II.37)

Using Eq. (II.31)

$$\varepsilon_2^{DP} = \varepsilon - \frac{\sigma_0 - E_1 t_1 \varepsilon_1^e}{E_2 t_2}$$

...(II.38)

Using Eq. (II.35)

$$\Rightarrow \frac{d\varepsilon_2^{DP}}{dt} = \frac{d\varepsilon}{dt} - \frac{E_1 t_1}{E_2 t_2}\left[\Gamma_1 E_1 \varepsilon_1^e - \frac{d\varepsilon}{dt}\right] = \left(1 + \frac{E_1 t_1}{E_2 t_2}\right)\left[\frac{d\varepsilon_1^e}{dt}\right] - \frac{E_1 t_1}{E_2 t_2}\left(\Gamma_1 E_1 \varepsilon_1^e\right)$$

...(II.39)

While the slider is yielding,

$$\frac{d\varepsilon_2^{DP}}{dt} = \Gamma_2\left(E_2 \varepsilon_2^e - \sigma_y - H\varepsilon_2^{DP}\right)$$

...(II.40)

$$\Rightarrow \left(1 + \frac{E_1 t_1}{E_2 t_2}\right)\left[\frac{d\varepsilon_1^e}{dt}\right] - \frac{E_1 t_1}{E_2 t_2}\Gamma_1 E_1 \varepsilon_1^e = \Gamma_2\left[\frac{\sigma_0 - E_1 t_1 \varepsilon_1^e}{t_2} - \sigma_y - H\left(\varepsilon - \frac{\sigma_0 - E_1 t_1 \varepsilon_1^e}{E_2 t_2}\right)\right]$$

...(II.41)

$$\Rightarrow \varepsilon = \frac{-1}{\Gamma_2 H}\left[\left(1 + \frac{E_1 t_1}{E_2 t_2}\right)\frac{d\varepsilon_1^e}{dt} + \left[\frac{\Gamma_2 t_1 E_1}{t_2} + \frac{E_1 t_1 \Gamma_2 H}{E_2 t_2} - \frac{E_1^2 t_1 \Gamma_1}{E_2 t_2}\right]\varepsilon_1^e - \Gamma_2\left(\sigma_0\left(\frac{1}{t_2} + \frac{H}{E_2 t_2}\right) - \sigma_y\right)\right]$$

...(II.42)

Or, for simplicity,

$$\varepsilon = A\frac{d\varepsilon_1^e}{dt} + B\varepsilon_1^e + C$$

...(II.43)

where A, B and C are known constants. This gives

$$\frac{d\varepsilon}{dt} = A\frac{d^2\varepsilon_1^e}{dt^2} + B\frac{d\varepsilon_1^e}{dt}$$

...(II.44)

Rearranging Eq. (II.35) to give

$$\frac{d\varepsilon}{dt} = \frac{d\varepsilon_1^e}{dt} + \Gamma_1 E_1 \varepsilon_1^e$$

...(II.45)

$$\Rightarrow A\frac{d^2\varepsilon_1^e}{dt^2} + B\frac{d\varepsilon_1^e}{dt} = \frac{d\varepsilon_1^e}{dt} + \Gamma_1 E_1 \varepsilon_1^e$$

...(II.46)

$$\Rightarrow A\frac{d^2\varepsilon_1^e}{dt^2} + [B-1]\frac{d\varepsilon_1^e}{dt} - \Gamma_1 E_1 \varepsilon_1^e = 0$$

...(II.47)

The solution to the equation is

$$\varepsilon_1^e = C_1 e^{\lambda_1 t} + C_2 e^{\lambda_2 t}$$

...(II.48)

where

$$\lambda_{1,2} = \frac{1-B \pm \sqrt{[B-1]^2 + 4A\Gamma_1 E_1}}{2A}$$

...(II.49)

$$\Rightarrow \frac{d\varepsilon_1^e}{dt} = \lambda_1 C_1 e^{\lambda_1 t} + \lambda_2 C_2 e^{\lambda_2 t}$$

...(II.50)

Substituting in Eq. (II.43)

$$\Rightarrow \varepsilon = A\left(\lambda_1 C_1 e^{\lambda_1 t} + \lambda_2 C_2 e^{\lambda_2 t}\right) + B\left(C_1 e^{\lambda_1 t} + C_2 e^{\lambda_2 t}\right) + C$$

...(II.51)

The boundary conditions may be determined as follows.

At time t = t*, the total strain is given by

$$\varepsilon^* = \frac{\sigma_y}{E_2}$$

...(II.52)

Thus,

$$\Rightarrow \frac{\sigma_y}{E_2} = A\left(\lambda_1 C_1 e^{\lambda_1 t^*} + \lambda_2 C_2 e^{\lambda_2 t^*}\right) + B\left(C_1 e^{\lambda_1 t^*} + C_2 e^{\lambda_2 t^*}\right) + C$$

...(II.53)

Further, given that for t > t*

$$\varepsilon_1^e = C_1 e^{\lambda_1 t} + C_2 e^{\lambda_2 t}$$

...(II.54)

At t = t*,

$$t_1\sigma_1 = \sigma_0 - t_2\sigma_y$$

...(II.55)

Thus,

$$\varepsilon_1^e(t^*) = C_1 e^{\lambda_1 t^*} + C_2 e^{\lambda_2 t^*} = \frac{\sigma_0 - t_2\sigma_y}{E_1 t_1}$$

...(II.56)

Rewriting Eq. (II.53) as

$$(A\lambda_1 + B)e^{\lambda_1 t^*}C_1 + (A\lambda_2 + B)e^{\lambda_2 t^*}C_2 = \frac{\sigma_y}{E_2} - C$$

...(II.57)

the solutions are

$$C_2 = \frac{e^{-\lambda_2 t^*}}{A(\lambda_1 - \lambda_2)}\left((A\lambda_1 + B)\left[\frac{\sigma_0 - t_2\sigma_y}{E_1 t_1}\right] - \frac{\sigma_y}{E_2} + C\right)$$

...(II.58)

$$C_1 = \frac{e^{-\lambda_1 t^*}}{A(\lambda_2 - \lambda_1)}\left((A\lambda_2 + B)\left[\frac{\sigma_0 - t_2\sigma_y}{E_1 t_1}\right] - \frac{\sigma_y}{E_2} + C\right)$$

...(II.59)

APPENDIX III

DSC UNLOADING AND WORK BALANCE

III.I Unloading Modulus

A special assumption is required for unloading slope under DSC (Figure 3.4). Under the assumption of equal strains, when the material has been loaded to point A, the RI material is at the corresponding point A'. Removal of applied stresses results in elastic unloading of RI material. The RI material reaches point B'. The FA material, being a void, does not restrict the recovery of elastic strain. The observed unloading path should then be AB', with the observed unloading modulus being less than the RI modulus.

This would also be expected from the state of the material, where only a fraction of the material is the RI material, while the remainder has been converted into a void. During unloading, the plastic strain trajectory, and thus the disturbance, does not vary, allowing for a constant unloading slope which equals the RI elastic modulus times the fraction of the RI material, i.e. $1 - D$.

However, in order to match predictions to observations, a postulate that the observed unloading modulus equals the RI unloading modulus is required. Thus, unloading from A

takes the material to point B instead of B'. It is further assumed that reloading of the material to the original stress is also elastic.

III.2 Work Balance

As against the Gurson model where the equality of total dissipated work to the dissipated work in the intact phase is enforced, DSC in conjunction with the assumption of equality of strains does not maintain the equality of total dissipated work to the dissipated work in the RI and FA phases.

The observed stress is given by

$$\sigma_{ij}^{a} = (1-D)\sigma_{ij}^{i} + D\sigma_{ij}^{c} \qquad \ldots(\text{III.1})$$

The total incremental work done on the material is

$$dW = \sigma_{ij}^{a} d\varepsilon_{ij} = \left[(1-D)\sigma_{ij}^{i} + D\sigma_{ij}^{c}\right] d\varepsilon_{ij} \qquad \ldots(\text{III.2})$$

The observed strain increment can be decomposed into the elastic and inelastic components using

$$d\varepsilon_{ij} = \left(d\varepsilon_{ij}^{e}\right)^{a} + \left(d\varepsilon_{ij}^{p}\right)^{a}$$

...(III.3)

The observed plastic work may then be written as

$$\left(dW^{p}\right)^{a} = (1-D)\sigma_{ij}^{i}\left(d\varepsilon_{ij}^{p}\right)^{a} + D\sigma_{ij}^{c}\left(d\varepsilon_{ij}^{p}\right)^{a}$$

...(III.4)

Since the observed elastic modulus for unloading is assumed to be the elastic modulus of the intact material, the reversible strain is given by

$$\left(\varepsilon_{ij}^{e}\right)^{a} = \left[\left(C_{ijkl}^{e}\right)^{i}\right]^{-1}\sigma_{ij}^{a}$$

...(III.5)

For constant material parameters,

$$\left(d\varepsilon_{ij}^{e}\right)^{a} = \left[\left(C_{ijkl}^{e}\right)^{i}\right]^{-1} d\sigma_{ij}^{a}$$

...(III.6)

During post-peak softening, the observed recoverable strain increment is negative as the stress increment is negative.

For the RI material, the strain increment can be decomposed into elastic and plastic components. For the FA phase, all strains are irreversible. Thus, the total work done from Eq. (III.2) can also be written as

$$dW = (1-D)\sigma_{ij}^{i} d\varepsilon_{ij} + D\sigma_{ij}^{c} d\varepsilon_{ij} = (1-D)\sigma_{ij}^{i}\left(d\varepsilon_{ij}^{e}\right) + (1-D)\sigma_{ij}^{i}\left(d\varepsilon_{ij}^{p}\right) + D\sigma_{ij}^{c} d\varepsilon_{ij}$$

...(III.7)

The first two terms on the RHS represent the elastic and the plastic components of RI work respectively, while the last term is the FA plastic work.

Equating the total plastic work done from Eq. (III.4), to the total plastic work done on the phases,

$$dW^{p} = (1-D)\sigma_{ij}^{i}\left(d\varepsilon_{ij}^{p}\right) + D\sigma_{ij}^{c} d\varepsilon_{ij} = (1-D)\sigma_{ij}^{i}\left(d\varepsilon_{ij}^{p}\right)^{a} + D\sigma_{ij}^{c}\left(d\varepsilon_{ij}^{p}\right)^{a}$$

...(III.8)

Subtracting Eq. (III.8) for the incremental plastic work from Eq. (III.7) for the total incremental work provides for the elastic work,

$$dW - dW^{p} = (1-D)\sigma_{ij}^{i}\left(d\varepsilon_{ij} - \left(d\varepsilon_{ij}^{p}\right)\right) = (1-D)\sigma_{ij}^{i}\left(d\varepsilon_{ij} - \left(d\varepsilon_{ij}^{p}\right)^{a}\right) + D\sigma_{ij}^{c}\left(d\varepsilon_{ij} - \left(d\varepsilon_{ij}^{p}\right)^{a}\right)$$

...(III.9)

$$\Rightarrow \qquad (1-D)\sigma_{ij}^{i}\left(d\varepsilon_{ij}^{e}\right) = \sigma_{ij}^{a}\left(d\varepsilon_{ij}^{e}\right)^{a}$$

...(III.10)

This cannot be valid, as during the post-peak portion of the stress-strain curve, the observed elastic strain decreases while the RI elastic strain increment is non-negative. Further, if the FA material does not carry any stress, Eq. (III.10) provides

$$\left(d\underset{\sim}{\varepsilon}^{p}\right)^{*} = d\underset{\sim}{\varepsilon} - \left(\underset{\sim}{\sigma}^{a}\right)^{-1}(1-D)\underset{\sim}{\sigma}^{i}\left(d\underset{\sim}{\varepsilon} - \left(d\underset{\sim}{\varepsilon}^{p}\right)\right) = \left(d\underset{\sim}{\varepsilon}^{p}\right) \qquad \ldots(\text{III.11})$$

However, the observed plastic strain increment does not equal the RI plastic strain increment.

APPENDIX IV

YIELD FUNCTION ISSUES

IV.1 HISS-δ_0

The plastic strain trajectory, under an initial state of zero strain, is typically assumed to be zero as a material that has never been loaded has not undergone any plastic deformation. The HiSS-δ_0 function provides[19]

$$\alpha = \left[\gamma - \frac{J_{2D}}{(J+3R)_1^2(1-\beta S_r)^n}\right]\left(\frac{J_1+3R}{p_a}\right)^{2-n} \qquad \ldots(IV.1)$$

$$\Rightarrow \qquad \alpha_0 = \alpha\big|_{J_1=J_{2D}=0} = \gamma\left(\frac{3R}{p_a}\right)^{2-n} \qquad \ldots(IV.2)$$

$$\Rightarrow \qquad \xi_0 = \left(\frac{a_1}{\alpha_0}\right)^{\frac{1}{m}} \neq 0 \qquad \ldots(IV.3)$$

[19] It is assumed that $1-\beta S_r \neq 0$, even when $S_r = 0/0$ and is undefined. This is reasonable as for all possible stress states other than at the state of zero stress, S_r can be shown to vary between -1 to +1 (Li, 2002) while β is always less than 0.755923 from convexity considerations for the yield surface.

IV.1.1. Hardening Parameters

For the determination of hardening parameters, the value of the hardening parameter, α, at each data point is computed from the stress state using

$$\alpha = \left[\gamma - \frac{J_{2D}}{(J+3R)_1^2 (1-\beta S_r)^m}\right]\left(\frac{J_1+3R}{p_a}\right)^{2-n}$$

...(IV.4)

The plastic strain increment is computed using

$$d\varepsilon_{ij}^p = d\varepsilon_{ij} - d\varepsilon_{ij}^e = d\varepsilon_{ij} - \left[C_i^e\right]_{ijkl}^{-1} d\sigma_{kl}$$

...(IV.5)

which provides

$$\xi = \int \sqrt{d\varepsilon_{ij}^p d\varepsilon_{ij}^p}$$

...(IV.6)

The definition of α in terms of ξ provides

$$\ln(\alpha) = \ln(a1) - \eta 1 \ln(\xi)$$

...(IV.7)

Then for any test, the best fit line to the plot of α vs. ξ given by

$$\ln(\alpha) = C_1 \ln(\xi) + C_2$$

...(IV.8)

provides

$$a_1 = e^{C_1}$$

...(IV.9)

$$\eta_1 = -C_2$$

...(IV.10)

Since the integration of Eq. (IV.6) starts at the first increment of load, this implicitly assumes a value of zero for the initial plastic strain trajectory at zero stress, ξ_0, which is inconsistent with Eq. (IV.3). However ξ_0 cannot be determined using Eq. (IV.3) before a1 and η1 are known, while determination of a1 and η1 requires ξ_0.

IV.1.2 Thermal Loading

The consistency condition for plastic yielding is

$$dF = \frac{\partial F}{\partial \underset{\sim}{\sigma}} d\underset{\sim}{\sigma} + \frac{\partial F}{\partial \xi} d\xi + \frac{\partial F}{\partial T} dT = 0$$

...(IV.11)

If the material is subjected to unconstrained heating or cooling,

$$d\underset{\sim}{\sigma} = 0$$

...(IV.12)

$$\Rightarrow \qquad d\xi = -\left[\left(\frac{\partial F}{\partial T}\right)\Big/\left(\frac{\partial F}{\partial \xi}\right)\right]dT$$

...(IV.13)

A positive value of $d\xi_0$ implies that the material has undergone a plastic strain increment.

Assuming isotropic strains, the linear plastic strain increment can be obtained as

$$d\varepsilon_1^p = \frac{1}{\sqrt{3}}d\xi$$

...(IV.14)

For $d\xi$ to be zero, either

$$\left.\frac{\partial F}{\partial T}\right|_{\underline{\sigma}=0} = 0$$

...(IV.15)

or

$$\left.\frac{\partial F}{\partial \xi}\right|_{\underline{\sigma}=0} \to \infty$$

...(IV.16)

Now Eq. (IV.16) is satisfied only if $\xi \to 0$, and thus at zero stress,

$$\left.\frac{\partial F}{\partial \xi}\right|_{\sigma=0} = -a1\eta 1\left(\frac{3R}{p_a}\right)^n \frac{1}{\xi^{\eta 1+1}} \neq \infty(\forall \xi \neq 0)$$

...(IV.17)

Further, F(σ, ξ, T) may be written as

$$F = \frac{J_{2D}}{p_a^2} - \left(-\left(\frac{a1}{\xi^{\eta 1}}\right)\left(\frac{J_1 + 3R}{p_a}\right)^n + \gamma\left(\frac{J_1 + 3R}{p_a}\right)^2\right)(1 - \beta S_r)^{-0.5}$$

...(IV.18)

At zero stresses, assuming β = 0 without loss of generality in the proof, and for the case of metals,

$$\frac{\partial F}{\partial T} = \left[\frac{\partial}{\partial T}\left(\frac{a1}{\xi^{\eta 1}}\right)\right]\left(\frac{3R}{p_a}\right)^n + \left(\frac{a1}{\xi^{\eta 1}}\right)\frac{\partial}{\partial T}\left(\frac{3R}{p_a}\right)^n - \frac{\partial \gamma}{\partial T}\left(\frac{3R}{p_a}\right)^2 - \gamma\frac{1}{p_a^2}\frac{\partial}{\partial T}(3R)^2$$

...(IV.19)

$$\Rightarrow \frac{\partial F}{\partial T} = \left(\frac{1}{\xi^{\eta 1}}\right)\left(\frac{3R}{p_a}\right)^n \frac{\partial a1}{\partial T} + a1\left(\frac{3R}{p_a}\right)^n \frac{\partial}{\partial T}\left(\frac{1}{\xi^{\eta 1}}\right) + \left(\frac{a1}{\xi^{n1}}\right)\frac{\partial}{\partial T}\left(\frac{3R}{p_a}\right)^n$$
$$-\gamma\frac{\partial}{\partial T}\left(\frac{3R}{p_a}\right)^2 + n\left(\frac{a1}{\xi^{n1}}\right)\left(\frac{3R}{p_a}\right)^{n-1}\frac{\partial n}{\partial T} - \left(\frac{3R}{p_a}\right)^2\frac{\partial \gamma}{\partial T}$$

...(IV.20)

$$\Rightarrow \frac{\partial F}{\partial T}=\left[\left(\frac{1}{\xi^{\eta 1}}\right)\left(\frac{3R}{p_a}\right)^{n}\right]\frac{\partial a1}{\partial T}+\left[a1\eta 1\ln\xi\left(\frac{3R}{p_a}\right)^{n}\right]\frac{\partial \eta 1}{\partial T}+\left[R^{n-1}\left(\frac{a1}{\xi^{n1}}\right)\left(\frac{3}{p_a}\right)^{n}-\gamma R\left(\frac{3}{p_a}\right)^{2}\right]\frac{\partial R}{\partial T}$$
$$+n\left(\frac{a1}{\xi^{n1}}\right)\left(\frac{3R}{p_a}\right)^{n-1}\frac{\partial n}{\partial T}-\left(\frac{3R}{p_a}\right)^{2}\frac{\partial \gamma}{\partial T}$$

...(IV.21)

or using the constraint F = 0,

$$\frac{\partial F}{\partial T}=\left[\left(\frac{1}{\xi^{\eta 1}}\right)\left(\frac{3R}{p_a}\right)^{n}\right]\frac{\partial a1}{\partial T}+\left[a1\eta 1\ln\xi\left(\frac{3R}{p_a}\right)^{n}\right]\frac{\partial \eta 1}{\partial T}+n\left(\frac{a1}{\xi^{\eta 1}}\right)\left(\frac{3R}{p_a}\right)^{n-1}\frac{\partial n}{\partial T}-\left(\frac{3R}{p_a}\right)^{2}\frac{\partial \gamma}{\partial T}$$

...(IV.22)

None of the individual terms are zero, if all material parameters are temperature dependent. Thus, setting the derivative equal to zero involves an additional relationship between independent material parameters. For solders, the constraint may be simplified by assuming γ and n to be temperature independent following Wang et al. (2001). This provides,

$$\frac{\partial F}{\partial T}=\left(\frac{3R}{p_a}\right)^{n}\frac{\partial}{\partial T}\left[\left(\frac{a1}{\xi^{\eta 1}}\right)\right]$$

...(IV.23)

and, requiring $\partial F/\partial T \equiv 0$ implies, for nonzero 3R,

$$\frac{\partial}{\partial T}\left(\frac{a1}{\xi^{\eta 1}}\right)_{\xi=\xi_0(T)} \equiv 0$$

...(IV.24)

$$\Rightarrow \frac{\partial a1}{\partial T} = -\frac{[a1\eta 1 \ln \xi_0]}{\left(\frac{1}{\xi_0^{\eta 1}}\right)}\frac{\partial \eta 1}{\partial T}$$

...(IV.25)

$$\Rightarrow \frac{\partial a1}{\partial T} = -\frac{(a1)^2 p_a^{2-n}}{\gamma(3R)^{2-n}} \ln\left(\frac{a1 p_a^{2-n}}{\gamma(3R)^{2-n}}\right)\frac{\partial \eta 1}{\partial T}$$

...(IV.26)

This is a constraint between independent parameters, and cannot be satisfied in general. Thus, $d\xi$ is not zero in general for unconstrained heating or cooling.

While the consistency condition is the fundamental condition, Eq. (3.19), derived from the same used in computations. It provides identical results for thermally generated increments of plastic strain trajectory. The incremental plastic strains due to unconstrained temperature change, based on the consistency condition, are

$$d\varepsilon_{ij}^{p} = \frac{1}{\sqrt{3}}\delta_{ij}d\xi = -\frac{1}{\sqrt{3}}\delta_{ij}\frac{\left(\frac{\partial F}{\partial T}\right)}{\left(\frac{\partial F}{\partial \xi}\right)}dT$$

...(IV.27)

The same result is obtained directly using the basic incremental thermo-elastoplastic equation of Wang et al. (2001)

$$d\sigma = C^{EP} d\varepsilon + C^{T} dT$$

...(IV.28)

which is given by, assuming Q = F for the associated yield function HiSS-δ_0[20],

$$d\underset{\sim}{\sigma} = \underset{\sim}{C}^{e}\left[\underset{\sim}{I} - \frac{\frac{\partial F}{\partial \underset{\sim}{\sigma}}\left(\frac{\partial F}{\partial \underset{\sim}{\sigma}}\right)^{T}\underset{\sim}{C}^{e}}{\left(\frac{\partial F}{\partial \underset{\sim}{\sigma}}\right)^{T}\underset{\sim}{C}^{e}\frac{\partial F}{\partial \underset{\sim}{\sigma}} - \frac{\partial F}{\partial \xi}\left(\left(\frac{\partial F}{\partial \underset{\sim}{\sigma}}\right)^{T}\frac{\partial F}{\partial \underset{\sim}{\sigma}}\right)^{1/2}}\right] d\underset{\sim}{\varepsilon}$$

$$-\underset{\sim}{C}^{e}\left(\alpha_T \underset{\sim}{I} - \frac{\frac{\partial F}{\partial \underset{\sim}{\sigma}}\left(\left(\frac{\partial F}{\partial \underset{\sim}{\sigma}}\right)^{T}\underset{\sim}{C}^{e}\alpha_T \underset{\sim}{I} - \frac{\partial F}{\partial T}\right)}{\left(\frac{\partial F}{\partial \underset{\sim}{\sigma}}\right)^{T}\underset{\sim}{C}^{e}\frac{\partial F}{\partial \underset{\sim}{\sigma}} - \frac{\partial F}{\partial \xi}\left(\left(\frac{\partial F}{\partial \underset{\sim}{\sigma}}\right)^{T}\frac{\partial F}{\partial \underset{\sim}{\sigma}}\right)^{1/2}}\right) dT$$

...(IV.29)

where the total strain increment is assumed to be separable as elastic (e), plastic (p) and thermal (T) components respectively.

[20] It may be noted that since C^e is a 6x6 matrix, a column vector $\underline{I}^T$ = {111000} must be multiplied by α_T to get a column vector $\alpha_T \underline{I} dT$ in the second term, for proper matrix multiplication.

$$d\varepsilon = d\varepsilon^{e} + d\varepsilon^{p} + d\varepsilon^{T}$$

...(IV.30)

The thermal component of the strain is given by

$$d\varepsilon^{T} = \alpha_{T} dT$$

...(IV.31)

Eq. (IV.30) may be written for convenience, as the sum of a a thermal component and another components ($d\varepsilon^{s}$), which is the sum of the elastic and the plastic components, as

$$d\varepsilon = d\varepsilon^{e} + d\varepsilon^{p} + \alpha_{T}\, \underline{I}\, dT = d\varepsilon^{s} + \alpha_{T}\, \underline{I}\, dT$$

...(IV.32)

Substituting Eq. (IV.32) in Eq. (IV.29) provides, after cancellation,

$$d\underset{\sim}{\sigma} = \underset{\sim}{C}^{e}\left[d\underset{\sim}{\varepsilon}^{s} - \frac{\frac{\partial F}{\partial \underset{\sim}{\sigma}}\left(\frac{\partial F}{\partial \underset{\sim}{\sigma}}\right)^{T} \underset{\sim}{C}^{e}}{\left(\frac{\partial F}{\partial \underset{\sim}{\sigma}}\right)^{T} \underset{\sim}{C}^{e} \frac{\partial F}{\partial \underset{\sim}{\sigma}} - \frac{\partial F}{\partial \xi}\left(\left(\frac{\partial F}{\partial \underset{\sim}{\sigma}}\right)^{T} \frac{\partial F}{\partial \underset{\sim}{\sigma}}\right)^{1/2}} d\varepsilon^{s} - \frac{\frac{\partial F}{\partial \underset{\sim}{\sigma}}\left(\frac{\partial F}{\partial T}\right)}{\left(\frac{\partial F}{\partial \underset{\sim}{\sigma}}\right)^{T} \underset{\sim}{C}^{e} \frac{\partial F}{\partial \underset{\sim}{\sigma}} - \frac{\partial F}{\partial \xi}\left(\left(\frac{\partial F}{\partial \underset{\sim}{\sigma}}\right)^{T} \frac{\partial F}{\partial \underset{\sim}{\sigma}}\right)^{1/2}} dT \right]$$

...(IV.33)

For unconstrained heating and cooling, the stress remains constant at zero, and

$$d\underset{\sim}{\sigma} = 0$$

...(IV.34)

Thus, if the term in the bracket of Eq. (IV.33) is not an eigenvector for the elastic matrix,

$$d\underset{\sim}{\varepsilon}^s - \frac{\frac{\partial F}{\partial \underset{\sim}{\sigma}}\left(\frac{\partial F}{\partial \underset{\sim}{\sigma}}\right)^T \underset{\sim}{C}^e}{\left(\frac{\partial F}{\partial \underset{\sim}{\sigma}}\right)^T \underset{\sim}{C}^e \frac{\partial F}{\partial \underset{\sim}{\sigma}} - \frac{\partial F}{\partial \xi}\left(\left(\frac{\partial F}{\partial \underset{\sim}{\sigma}}\right)^T \frac{\partial F}{\partial \underset{\sim}{\sigma}}\right)^{1/2}} d\underset{\sim}{\varepsilon}^s - \frac{\frac{\partial F}{\partial \underset{\sim}{\sigma}}\left(\frac{\partial F}{\partial T}\right)}{\left(\frac{\partial F}{\partial \underset{\sim}{\sigma}}\right)^T \underset{\sim}{C}^e \frac{\partial F}{\partial \underset{\sim}{\sigma}} - \frac{\partial F}{\partial \xi}\left(\left(\frac{\partial F}{\partial \underset{\sim}{\sigma}}\right)^T \frac{\partial F}{\partial \underset{\sim}{\sigma}}\right)^{1/2}} dT = 0$$

...(IV.35)

Assuming the denominator term to be nonzero at zero stress, which holds for HiSS in general,

$$\left[\left(\frac{\partial F}{\partial \underset{\sim}{\sigma}}\right)^T \underset{\sim}{C}^e \frac{\partial F}{\partial \underset{\sim}{\sigma}} - \frac{\partial F}{\partial \xi}\left(\left(\frac{\partial F}{\partial \underset{\sim}{\sigma}}\right)^T \frac{\partial F}{\partial \underset{\sim}{\sigma}}\right)^{1/2}\right] d\underset{\sim}{\varepsilon}^s - \frac{\partial F}{\partial \underset{\sim}{\sigma}}\left(\frac{\partial F}{\partial \underset{\sim}{\sigma}}\right)^T \underset{\sim}{C}^e d\underset{\sim}{\varepsilon}^s = \frac{\partial F}{\partial \underset{\sim}{\sigma}}\left(\frac{\partial F}{\partial T}\right) dT$$

...(IV.36)

Under the unconstrained conditions, $J_1 = J_{2D} = 0$. Consider for simplicity, a material such as solder, with $\beta = 0$. Then at zero stress

$$\frac{\partial F}{\partial \underset{\sim}{\sigma}} = \frac{\partial F}{\partial J_1}\frac{\partial J_1}{\partial \underset{\sim}{\sigma}} + \frac{\partial F}{\partial J_{2D}}\frac{\partial J_{2D}}{\partial \underset{\sim}{\sigma}} = \frac{\partial F}{\partial J_1}\underset{\sim}{I} = (n-2)\gamma\left(\frac{3R}{p_a^2}\right)\underset{\sim}{I} = say, \Omega \underset{\sim}{I} \ (where\ \Omega\ is\ scalar)$$

...(IV.37)

Thus,

$$\Omega^2 \underset{\sim}{I}^T \underset{\sim}{C}^e \underset{\sim}{I}\, d\underset{\sim}{\varepsilon}^s - \Omega^2 \underset{\sim}{I}\underset{\sim}{I}^T \underset{\sim}{C}^e\, d\underset{\sim}{\varepsilon}^s - \sqrt{3}\Omega\frac{\partial F}{\partial \xi} d\underset{\sim}{\varepsilon}^s = \Omega \underset{\sim}{I}\left(\frac{\partial F}{\partial T}\right)dT$$

...(IV.38)

From the symmetry of the situation, since the shear components of $d\underset{\sim}{\varepsilon}^s$ can be assumed to be zero, and the axial strain assumed to be equal, for a material under zero stresses and no directional preference, Eq. (IV.38) then provides

$$-\sqrt{3}\Omega\frac{\partial F}{\partial \xi} d\underset{\sim}{\varepsilon}^s = \Omega \underset{\sim}{I}\left(\frac{\partial F}{\partial T}\right)dT$$

...(IV.39)

or, for the axial strain components,

$$d\varepsilon^s = -\frac{1}{\sqrt{3}}\frac{(\partial F/\partial T)}{\partial F/\partial \xi}dT$$

...(IV.40)

IV.1.3 Tensile Loading

The HiSS-δ_0 model assigns a positive value to compressive stresses. For simplicity, let a material with $\beta = 0$ be considered without loss of generality. Uniaxial tensile loading,

starting from a state of zero stress, causes the material to move from the initial yield surface to the inside of the surface. Under uniaxial loading,

$$J_1 = \sigma_1$$

...(IV.41)

$$J_{2D} = \frac{\sigma_1^2}{3}$$

...(IV.42)

The consistency condition provides

$$d\xi = -\frac{\partial F / \partial \sigma_1}{\partial F / \partial \xi} d\sigma_1$$

...(IV.43)

where

$$\frac{\partial F}{\partial \xi} = -a1\eta 1 \xi^{-\eta 1-1} \left(\frac{\sigma_1 + 3R}{p_a} \right)^n < 0$$

...(IV.44)

and at the beginning of loading, as n > 2 is required for convexity (Desai, 2001),

$$\frac{\partial F}{\partial \sigma_1} = (n-2)\gamma \left(\frac{R}{p_a^2} \right) > 0$$

...(IV.45)

Assuming compressive stresses to be positive,

$$d\sigma_1 > 0 \Rightarrow d\xi > 0 (loading)$$

...(IV.46)

$$d\sigma_1 < 0 \Rightarrow d\xi < 0 (unloading)$$

...(IV.47)

IV.2 Proposed Yield Function

Since the proposed yield function is a true continuous yield function, the state of zero stress is the transition between the elastic regime and the initiation of plasticity. The initial elastoplastic matrix for the proposed yield function is shown to be the elastic matrix in the limit of zero stress. Further, it is shown that in the limit of zero ξ, which holds true for the proposed yield function at zero stress, no spurious plastic strains are generated.

IV.2.1 General Derivatives

The yield function is

$$F = \frac{J_{2D}}{p_a^2} + \gamma \left((1-\alpha) \left(\frac{|J_1|}{p_a} \right)^n - \alpha \left(\frac{J_1 + 3R}{p_a} \right)^q \right) (1 - \beta S_r)^{-0.5} \equiv 0$$

...(IV.48)

Therefore, for the general case,

$$\frac{\partial F}{\partial J_1} = \gamma\left(\mathrm{sgn}(J_1)(1-\alpha)\frac{n}{p_a^n}(|J_1|)^{n-1} - \alpha\frac{q}{p_a^q}(J_1+3R)^{q-1} \right)(1-\beta S_r)^{-0.5}$$

...(IV.49)

$$\frac{\partial F}{\partial J_{2D}} = \left[\frac{1}{p_a^2} - \frac{3\sqrt{27}}{4}\beta\gamma\left[(1-\alpha)\frac{|J_1|^n}{p_a^n} - \frac{\alpha}{p_a^q}(J_1+3R)^q \right]\frac{J_{3D}J_{2D}^{-5/2}}{(1-\beta S_r)^{3/2}} \right]$$

...(IV.50)

$$\frac{\partial F}{\partial J_{3D}} = -\frac{3\sqrt{27}}{4}\beta\gamma\left[(1-\alpha)\frac{|J_1|^n}{p_a^n} - \frac{\alpha}{p_a^q}(J_1+3R)^q \right]\frac{J_{2D}^{-3/2}}{(1-\beta S_r)^{3/2}}$$

...(IV.51)

and

$$\frac{\partial F}{\partial \xi} = -\gamma(1-\beta S_r)^{-0.5}\left(\left(\frac{|J_1|}{p_a} \right)^n + \left(\frac{J_1+3R}{p_a} \right)^q \right)\frac{2a1\eta 1}{(a1+\xi^{\eta 1})^3}\xi^{2\eta 1-1}$$

...(IV.52)

For solder, since $\beta = 0$,

$$F = \frac{J_{2D}}{p_a^2} + \gamma\left((1-\alpha)\left(\frac{|J_1|}{p_a} \right)^n - \alpha\left(\frac{J_1+3R}{p_a} \right)^q \right) \equiv 0$$

...(IV.53)

$$\frac{\partial F}{\partial J_1} = \gamma\left(\operatorname{sgn}(J_1)(1-\alpha)\frac{n}{p_a^n}(|J_1|)^{n-1} - \alpha\frac{q}{p_a^q}(J_1+3R)^{q-1} \right)$$

...(IV.54)

$$\frac{\partial F}{\partial J_{2D}} = \frac{1}{p_a^2}$$

...(IV.55)

$$\frac{\partial F}{\partial J_{3D}} = 0$$

...(IV.56)

and

$$\frac{\partial F}{\partial \xi} = -\gamma\left(\left(\frac{|J_1|}{p_a}\right)^n + \left(\frac{J_1+3R}{p_a}\right)^q \right) \frac{2a1\eta 1}{(a1+\xi^{\eta 1})^3}\xi^{2\eta 1-1}$$

...(IV.57)

IV.2.2 Initial Elastoplastic Matrix

The elastoplastic matrix is given by

$$\underset{\sim}{C}^{ep} = \underset{\sim}{C}^{e} - \frac{\underset{\sim}{C}^{e}\left(\frac{\partial F}{\partial \underset{\sim}{\sigma}}\right)\left(\frac{\partial F}{\partial \underset{\sim}{\sigma}}\right)^T \underset{\sim}{C}^{e}}{\left(\frac{\partial F}{\partial \underset{\sim}{\sigma}}\right)^T \underset{\sim}{C}^{e}\left(\frac{\partial F}{\partial \underset{\sim}{\sigma}}\right) - \left(\frac{\partial F}{\partial \xi}\right)\left[\left(\frac{\partial F}{\partial \underset{\sim}{\sigma}}\right)^T\left(\frac{\partial F}{\partial \underset{\sim}{\sigma}}\right)\right]^{\frac{1}{2}}}$$

...(IV.58)

At the stress free-state,

$$\left(\frac{\partial F}{\partial \underset{\sim}{\sigma}}\right)=\left(\frac{\partial F}{\partial J_1}\right)\left(\frac{\partial J_1}{\partial \underset{\sim}{\sigma}}\right)+\left(\frac{\partial F}{\partial J_{2D}}\right)\left(\frac{\partial J_{2D}}{\partial \underset{\sim}{\sigma}}\right)+\left(\frac{\partial F}{\partial J_{3D}}\right)\left(\frac{\partial J_{3D}}{\partial \underset{\sim}{\sigma}}\right)=0$$

...(IV.59)

Further, since the initial value of the plastic strain trajectory is zero,

$$\left(\frac{\partial F}{\partial \xi}\right)=0$$

...(IV.60)

Thus, the second term on the RHS of Eq. (IV.58) is indeterminate. This is because the material transitions from elastic behavior to plastic yield at the state of zero stress.

In order to demonstrate that the initial material behavior approaches the elastic behavior at zero stress, the fundamental derivation of Eq. (IV.58), as provided in Desai (2001), is considered. The matrix-vector notation has been changed to the tensor form.

The basic consistency condition used for the derivation is

$$dF=\frac{\partial F}{\partial \sigma_{ij}}d\sigma_{ij}+\frac{\partial F}{\partial \xi}d\xi=0$$

..(IV.61)

The normality rule

$$d\varepsilon_{ij}^{p} = \lambda\left(\frac{\partial F}{\partial \sigma_{ij}}\right)$$

...(IV.62)

is used to express $d\xi$, which is defined in terms of the tensor notation, as

$$d\xi = \sqrt{d\varepsilon_{ij}^{p} d\varepsilon_{ij}^{p}} = \lambda\sqrt{\frac{\partial F}{\partial \sigma_{ij}}\frac{\partial F}{\partial \sigma_{ij}}}$$

...(IV.63)

which provides

$$\frac{\partial F}{\partial \sigma_{ij}} d\sigma_{ij} + \frac{\partial F}{\partial \xi}\left(\lambda\sqrt{\frac{\partial F}{\partial \sigma_{ij}}\frac{\partial F}{\partial \sigma_{ij}}}\right) = 0$$

...(IV.64)

Then, using

$$d\varepsilon_{ij} = d\varepsilon_{ij}^{e} + d\varepsilon_{ij}^{p}$$

...(IV.65)

$$d\sigma_{ij} = C_{ijkl}^{e}\left(d\varepsilon_{ij} - d\varepsilon_{ij}^{p}\right)$$

...(IV.66)

$$\frac{\partial F}{\partial \sigma_{ij}} C_{ijkl}^{e}\left(d\varepsilon_{ij} - d\varepsilon_{ij}^{p}\right) + \frac{\partial F}{\partial \xi}\left(\lambda\sqrt{\frac{\partial F}{\partial \sigma_{ij}}\frac{\partial F}{\partial \sigma_{ij}}}\right) = 0$$

...(IV.67)

or, using the normality rule,

$$\lambda = \frac{\dfrac{\partial F}{\partial \sigma_{ij}} C^{e}_{ijkl} d\varepsilon_{ij}}{\left[\dfrac{\partial F}{\partial \sigma_{ij}} C^{e}_{ijkl} \dfrac{\partial F}{\partial \sigma_{ij}} - \dfrac{\partial F}{\partial \xi}\left(\sqrt{\dfrac{\partial F}{\partial \sigma_{ij}} \dfrac{\partial F}{\partial \sigma_{ij}}}\right)\right]}$$

...(IV.68)

based on which Eq. (IV.58) is derived. However, this assumes that the coefficient of λ is nonzero.

Instead of obtaining the limiting value of the ratio of Eq. (IV.68), the basic consistency condition is used to obtain

$$d\xi = -\frac{\dfrac{\partial F}{\partial \sigma_{ij}}}{\dfrac{\partial F}{\partial \xi}} d\sigma_{ij}$$

...(IV.69)

Now

$$\frac{\partial F}{\partial \sigma_{ij}} = \frac{\partial F}{\partial J_1} \frac{dJ_1}{d\sigma_{ij}} + \frac{\partial F}{\partial J_{2D}} \frac{dJ_{2D}}{d\sigma_{ij}} + \frac{\partial F}{\partial J_{3D}} \frac{dJ_{3D}}{d\sigma_{ij}}$$

...(IV.70)

Since $\beta = 0$,

$$\frac{\partial F}{\partial \sigma_{ij}} = \gamma\left(\operatorname{sgn}(J_1)\frac{n}{p_a^n}\left(|J_1|\right)^{n-1} - \left(\frac{\xi^{\eta 1}}{a1+\xi^{\eta 1}}\right)\left(\frac{n^2}{p_a^n}\left(|J_1|\right)^{n-1} + \frac{q}{p_a^q}(J_1+3R)^{q-1}\right)\right)\delta_{ij} + \frac{s_{ij}}{p_a^2}$$

...(IV.71)

Thus,

$$d\xi = -\frac{\left(\operatorname{sgn}(J_1)\frac{n}{p_a^n}\left(|J_1|\right)^{n-1} - \left(\frac{\xi^{\eta 1}}{a1+\xi^{\eta 1}}\right)^2\left(\frac{n^2}{p_a^n}\left(|J_1|\right)^{n-1} + \frac{q}{p_a^q}(J_1+3R)^{q-1}\right)\right)\delta_{ij} + \frac{s_{ij}}{p_a^2}}{\left(\frac{n^2}{p_a^n}\left(|J_1|\right)^{n} + \frac{q}{p_a^q}(J_1+3R)^{q}\right)\frac{2a1\eta 1\xi^{2\eta-1}}{\left(a1+\xi^{\eta 1}\right)^3}} d\sigma_{ij}$$

...(IV.72)

The stress is first substituted to be equal to zero. This does not create any singularity, if stress and ξ are considered independent.

Then,

$$d\xi = \frac{\left(\frac{\xi^{\eta 1}}{a1+\xi^{\eta 1}}\right)^2 \frac{q}{p_a^q}(3R)^{q-1}\delta_{ij}}{\frac{q}{p_a^q}(3R)^{q}\frac{2a1\eta 1\xi^{2\eta-1}}{\left(a1+\xi^{\eta 1}\right)^3}} d\sigma_{ij} = \frac{1}{3R}\left(\frac{\xi^{\eta 1}}{a1+\xi^{\eta 1}}\right)^2 \frac{\left(a1+\xi^{\eta 1}\right)^3}{2a1\eta 1\xi^{2\eta-1}} d\sigma_{ij} = \frac{\xi\left(a1+\xi^{\eta 1}\right)}{6Ra1\eta 1} d\sigma_{ij}$$

...(IV.73)

As $\xi \rightarrow 0$,

$$d\xi \to 0$$

...(IV.74)

and

$$d\varepsilon_{ij}^{p} \to 0$$

...(IV.75)

Thus,

$$d\sigma_{ij} = C_{ijkl}^{e} d\varepsilon_{ij}^{e} = C_{ijkl}^{e} d\varepsilon_{ij}$$

...(IV.76)

This ensures that the initial constitutive matrix may be assumed to be the elastic matrix.

IV.2.3 Thermal Strains

The required condition for zero plastic strains under unconstrained heating and cooling is

$$\frac{\partial F}{\partial T} \Big/ \frac{\partial F}{\partial \xi} = 0$$

...(IV.77)

For this, the yield function

$$F = \frac{J_{2D}}{p_a^2} + \gamma\left(\left(1-\alpha\left(\frac{|J_1|}{p_a}\right)^n - \alpha\left(\frac{J_1+3R}{p_a}\right)^q\right)(1-\beta S_r)^{-0.5} \equiv 0\right)$$

...(IV.78)

must be expressed as F(σ, ξ, T), where the property dependence of material parameters is responsible for the variation of F with temperature. In this regard, partial differentiation with any variable implies that the other two are kept constant. Specifically, if the differentiation is with respect to T, then σ and ξ must be held constant.

Thus,

$$F = \frac{J_{2D}}{p_a^2} + \gamma\left(\left(1-\left(\frac{\xi^{\eta 1}}{a1+\xi^{\eta 1}}\right)^2\right)\left(\frac{|J_1|}{p_a}\right)^n - \left(\frac{\xi^{\eta 1}}{a1+\xi^{\eta 1}}\right)^2\left(\frac{J_1+3R}{p_a}\right)^q\right)(1-\beta S_r)^{-0.5} \equiv 0$$

...(IV.79)

All material parameters, other than β, are assumed to be temperature dependent. β is assumed to be zero without loss of generality for the proof, and also the case of metals. Since the term within the brackets is zero at zero stress, the coefficient of the differential of γ with respect to temperature is zero. Thus, from the product rule for differentiation,

$$\frac{\partial F}{\partial T}=\gamma\left(-\frac{\partial}{\partial T}\left[\left(\frac{\xi^{\eta 1}}{a1+\xi^{\eta 1}}\right)^{2}\right]\left[\left(\frac{|J_1|}{p_a}\right)^{n}+\left(\frac{J_1+3R}{p_a}\right)^{q}\right]-\left(\frac{\xi^{\eta 1}}{a1+\xi^{\eta 1}}\right)^{2}\frac{\partial}{\partial T}\left[\left(\frac{|J_1|}{p_a}\right)^{n}+\left(\frac{J_1+3R}{p_a}\right)^{q}\right]\right)$$

...(IV.80)

where it is noted that

$$\frac{\partial}{\partial T}\left(\frac{\xi^{\eta 1}}{a1+\xi^{\eta 1}}\right)^{2}=2\left(\frac{\xi^{\eta 1}}{a1+\xi^{\eta 1}}\right)\frac{a1\frac{\partial}{\partial T}\left(\xi^{\eta 1}\right)-\xi^{\eta 1}\frac{\partial a1}{\partial T}}{\left(a1+\xi^{\eta 1}\right)^{2}}$$

...(IV.81)

At fixed $\xi = 0$, with a1 and $\eta 1$ being functions of temperature,

$$\left(\frac{\xi^{\eta 1}}{a1+\xi^{\eta 1}}\right)^{2}=0$$

...(IV.82)

and

$$\frac{\partial}{\partial T}\left(\frac{\xi^{\eta 1}}{a1+\xi^{\eta 1}}\right)^{2}=0$$

...(IV.83)

as

$$\frac{\partial}{\partial T}\xi^{\eta 1}=\xi^{\eta 1}\ln\left(\xi^{\eta 1}\right)\frac{\partial \eta 1}{\partial T}\xrightarrow{\xi\to 0}0$$

...(IV.84)

Thus, even when parameters vary with temperature, as long as the rate of change of parameters with temperature is not infinite, for the modified yield function,

$$\left.\frac{\partial F}{\partial T}\right|_{\sigma=0} \equiv 0$$

...(IV.85)

The result is obtained because ξ_0 is zero at zero stresses for the proposed yield function, independent of temperature. However, at zero stress, we also have

$$\frac{\partial F}{\partial \xi} = -\gamma\left(\left(\frac{|J_1|}{p_a}\right)^n + \left(\frac{J_1+3R}{p_a}\right)^q\right)\frac{2a1\eta 1}{\left(a1+\xi^{\eta 1}\right)^3}\xi^{2\eta 1-1} = 0$$

...(IV.86)

This is expected as for a true continuous yield model, the state of zero stress is the transition between elastic behavior and plastic behavior. To determine the value of the ratio at the origin of the stress axes directly, it is noted that

$$\frac{\frac{\partial F}{\partial T}}{\frac{\partial F}{\partial \xi}} = \frac{\left(-\frac{\partial}{\partial T}\left[\left(\frac{\xi^{\eta 1}}{a1+\xi^{\eta 1}}\right)^2\right]\left[\left(\frac{|J_1|}{p_a}\right)^n + \left(\frac{J_1+3R}{p_a}\right)^q\right] - \left(\frac{\xi^{\eta 1}}{a1+\xi^{\eta 1}}\right)^2 \frac{\partial}{\partial T}\left[\left(\frac{|J_1|}{p_a}\right)^n + \left(\frac{J_1+3R}{p_a}\right)^q\right]\right)}{\left[\left(\frac{|J_1|}{p_a}\right)^n + \left(\frac{J_1+3R}{p_a}\right)^q\right]\frac{2a1\eta 1\xi^{2\eta 1-1}}{\left(a1+\xi^{\eta 1}\right)^3}}$$

...(IV.87)

which can be simplified to

$$\frac{\frac{\partial F}{\partial T}}{\frac{\partial F}{\partial \xi}} = -\frac{\frac{\partial}{\partial T}\left[\left(\frac{\xi^{\eta 1}}{a1+\xi^{\eta 1}}\right)^2\right]\frac{\left(a1+\xi^{\eta 1}\right)^3}{2a1\eta 1\xi^{2\eta 1-1}} - \left(\frac{\xi^{\eta 1}}{a1+\xi^{\eta 1}}\right)^2\frac{\left(a1+\xi^{\eta 1}\right)^3}{2a1\eta 1\xi^{2\eta 1-1}}\frac{\frac{\partial}{\partial T}\left[\left(\frac{|J_1|}{p_a}\right)^n+\left(\frac{J_1+3R}{p_a}\right)^q\right]}{\left[\left(\frac{|J_1|}{p_a}\right)^n+\left(\frac{J_1+3R}{p_a}\right)^q\right]}}{}$$

...(IV.88)

The first term on the RHS which can be written as

$$Term1 = \frac{a1\xi\ln(\xi)\frac{\partial \eta 1}{\partial T} - \xi\frac{\partial a1}{\partial T}}{a1\eta 1}$$

...(IV.89)

Since $\xi\ln(\xi)$ tends to zero as ξ tends to zero, Term1 → as $\xi \rightarrow 0$. Considering the second term, which may be written as

$$Term2 = -\frac{1}{\left[\left(\frac{|J_1|}{p_a}\right)^n+\left(\frac{J_1+3R}{p_a}\right)^q\right]}\frac{\xi\left(a1+\xi^{\eta 1}\right)}{2a1\eta 1}\frac{\partial}{\partial T}\left[\left(\frac{|J_1|}{p_a}\right)^n+\left(\frac{J_1+3R}{p_a}\right)^q\right]$$

...(IV.90)

The denominator approaches a positive, nonzero value if 3R is not zero. Thus, considering only the numerator,

$$Term2 = -\frac{\xi\left(a1+\xi^{\eta 1}\right)}{2a1\eta 1}\left[\frac{|J_1|}{p_a}\ln\left(\frac{|J_1|}{p_a}\right)\frac{\partial n}{\partial T}+\frac{J_1+3R}{p_a}\ln\left(\frac{J_1+3R}{p_a}\right)\frac{\partial q}{\partial T}\right]$$

...(IV.91)

If the rate of variation of parameters with temperature is finite, Term2 → 0 as $\xi \rightarrow 0$ and $J_1 \rightarrow 0$. Thus,

$$\frac{\partial F}{\partial T}\Big/\frac{\partial F}{\partial \xi}\Big|_{\lim_{\xi\to 0}} \rightarrow 0$$

...(IV.92)

APPENDIX V

PERZYNA FORMULATION

V.1 Asymptotic Behavior

Consider a constant strain – rate simple shear test at zero confining pressure. The parameter β may be assumed to be zero for simplicity, as is the case for solder.

Since the strain is unidirectional, the relevant shear component of the total strain tensor at any instant is given by

$$\varepsilon = \varepsilon^{e} + \varepsilon^{vp} \qquad \text{...(V.1)}$$

$$\Rightarrow \qquad \frac{d\varepsilon}{dt} = \frac{d\varepsilon^{e}}{dt} + \frac{d\varepsilon^{vp}}{dt} \qquad \text{...(V.2)}$$

where the LHS, dε/dt, is a constant for a given test.

Now

$$\frac{d\varepsilon^e}{dt} = \frac{1}{2G}\frac{d\tau}{dt}$$

...(V.3)

and

$$\frac{d\varepsilon^{vp}}{dt} = \Gamma\langle F\rangle^N \frac{\partial F}{\partial \tau}$$

...(V.4)

Further,

$$\xi = \xi_0 + \sqrt{2}\varepsilon^{vp}$$

...(V.5)

where ξ_0 is due to the potential for the presence of an initial nonzero plastic strain trajectory in functions such as HiSS.

Thus, for the constant strain-rate test,

$$\xi = \xi_0 + \sqrt{2}\left(t\frac{d\varepsilon}{dt} - \frac{\tau}{2G}\right)$$

...(V.6)

For the proposed yield function, for equations in terms of tensor strain components, using

$$F = \frac{\tau^2}{p_a^2} + \left(\frac{\xi^{\eta 1}}{a1 + \xi^{\eta 1}}\right)\gamma\left(\frac{3R}{p_a}\right)^2$$

...(V.7)

$$\frac{\partial F}{\partial \tau_{ij}} = \frac{\tau_{ij}}{p_a^2}$$

...(V.8)

$$\xi_0 = 0$$

...(V.9)

$$\frac{1}{2G}\frac{d\tau}{dt} + \Gamma\left\langle \frac{\tau^2}{p_a^2} - \left(\frac{\left(\sqrt{2}\left(t\frac{\partial \varepsilon}{\partial t} - \frac{\tau}{2G}\right)\right)^{\eta 1}}{a1 + \left(\sqrt{2}\left(t\frac{\partial \varepsilon}{\partial t} - \frac{\tau}{2G}\right)\right)^{\eta 1}} \right)^2 \gamma\left(\frac{3R}{p_a}\right)^2 \right\rangle^N \frac{\tau}{p_a^2} = \frac{\partial \varepsilon}{\partial t}$$

...(V.10)

As t $\rightarrow\infty$, and if τ is bounded and approaches a constant value τ_u,

$$\left(\frac{\left(\sqrt{2}\left(t\frac{\partial \varepsilon}{\partial t} - \frac{\tau}{2G}\right)\right)^{\eta 1}}{a1 + \left(\sqrt{2}\left(t\frac{\partial \varepsilon}{\partial t} - \frac{\tau}{2G}\right)\right)^{\eta 1}} \right)^2 \rightarrow 1$$

...(V.11)

and

$$\frac{d\tau}{dt} \rightarrow 0$$

...(V.12)

Thus, the final equation is

$$\Gamma\left\langle \frac{\tau_u^2}{p_a^2} - \gamma\left(\frac{3R}{p_a}\right)^2 \right\rangle^N \frac{\tau_u}{p_a^2} = \frac{\partial \varepsilon}{\partial t} = \frac{1}{2}\frac{\partial \gamma}{\partial t}$$

...(V.13)

For the HiSS-δ_0 model, for tensor strain components, using

$$F = \frac{\tau^2}{p_a^2} + \alpha\left(\frac{3R}{p_a}\right)^n - \gamma\left(\frac{3R}{p_a}\right)^2$$

...(V.14)

$$\Rightarrow \qquad \frac{\partial F}{\partial \tau_{ij}} = \frac{\tau_{ij}}{p_a^2}$$

...(V.15)

Using

$$\alpha = \frac{a1}{\xi^{\eta_1}}$$

...(V.16)

and

$$\alpha_0 = \gamma\left(\frac{3R}{p_a}\right)^{2-n}$$

...(V.17)

$$\Rightarrow \xi_0 = \left(\frac{a1}{\gamma \left(\frac{3R}{p_a} \right)^{2-n}} \right)^{\frac{1}{\eta 1}}$$

...(V.18)

Thus, the governing equation is

$$\frac{1}{2G}\frac{d\tau}{dt} + \Gamma \left\langle \frac{\tau^2}{p_a^2} - \frac{a1}{\left(\xi_0 + \sqrt{2}\left(t\frac{\partial \varepsilon}{\partial t} - \frac{\tau}{2G} \right) \right)^{\eta 1}} \left(\frac{3R}{p_a} \right)^n + \gamma \left(\frac{3R}{p_a} \right)^2 \right\rangle^N \frac{\tau}{p_a^2} = \frac{\partial \varepsilon}{\partial t}$$

...(V.19)

which provides, as $t \to \infty$, if τ is bounded and approaches a constant value τ_u,

$$\Gamma \left\langle \frac{\tau_u^2}{p_a^2} - \gamma \left(\frac{3R}{p_a} \right)^2 \right\rangle^N \frac{\tau_u}{p_a^2} = \frac{\partial \varepsilon}{\partial t} = \frac{1}{2}\frac{\partial \gamma}{\partial t}$$

...(V.20)

APPENDIX VI

ENERGY EXPRESSIONS FOR PHASES

VI.1 Configuration Energy

The stress-strain behavior for the asymptotic phase is at 0 K, which is not observed in practice. However the second and third laws of thermodynamics[21] suggest that elastic parameters should tend to a constant value in the limit of low temperatures. Further, it is assumed that no heat transfer is associated with deformations at this temperature. The analysis presented is only a conceptual scheme to obtain the form of the behavior of the hypothetical phase of the material at 0K and must be interpreted in that sense.

At 0 K, from a classical perspective, the material has no kinetic energy due to vibratory motion and behavior is governed solely by potential energy increments due to deformation. The depth of the potential well is the sum of the enthalpy of sublimation and ionization energy, and the energy, U, of a crystal may be given by an equation of the form (Cottrell, 1957)

$$U = Br^{-2} - Ar^{-1} \qquad \ldots(VI.1)$$

where B and A are constants, and r is the atomic radius.

Assuming interatomic force to depend only on the distance between atoms, the potential energy due to configuration of the material can be defined as the sum of the configuration energies of the individual bonds between atoms irrespective of the specific law of attraction (Langhaar, 1962). The number of atoms in a macroscopic specimen is extremely large and the interactions between the nearest neighbors dominate the force considerations[22], ensuring it is reasonable to assign a configuration energy to each atom (Feynman, 1989).

Rose et al. (1984) have shown that for metals at 0K and in the absence of phase change, the configuration energy per atom due to volumetric deformation $\Omega(r_w)$ can be expressed in terms of the sublimation enthalpy per atom under zero confining pressure, Ω_0, and the Wigner-Seitz radius, r_w, corresponding to the deformed state as

$$\Omega(r_w) = \Omega_0 e^{-a}\left(-1 - a - 0.05a^3\right) \qquad \ldots(\text{VI.2})$$

where

[21] These are applicable for equilibrium processes. Ericksen (1998) has stated that it is often implicitly assumed in literature that only volumetric deformations conform to this requirement.

[22] The absence of faulted close packed sequences in crystals, where FCC and HCP structures could alternate indicates that forces other than those due to the nearest neighbors are not entirely negligible (Cottrell, 1957)

$$a = \eta^* \left(\frac{r_w}{r_{w0}} - 1 \right)$$

...(VI.3)

with η^* an empirical factor related to the anharmonicity of the crystal, which determines the region over which Hooke's law is valid. It is estimated experimentally from the bulk modulus at 0K, B_0, using

$$\eta^* = \left(\frac{12\pi B_0 r_w^3}{\Omega_0} \right)^{1/2}$$

...(VI.4)

For small strains, a <<1, and the energy expression for a unit volume of material at 0K for volumetric strains from Eq. (VI.2) can be approximated by

$$U = -U_0 + \frac{1}{2} B_0 \varepsilon_v^2$$

...(VI.5)

Thus, the energy expression for small strains is equivalent to the engineering expression, and hence the stress-strain relationship at 0 K for volumetric strains may be assumed to be the usual elastic expression based on the Bulk Modulus at 0 K.

Shear distortions which do not change the volume still result in change in potential energy due to electrostatic energy of valence electrons, ion-ion interactions in metals, and in some metals and alloys, changes in the Fermi energy (Cottrell, 1957). Thus, in an

engineering sense, the potential energy due to shear deformations may be added to provide

$$U = -U_0 + \frac{1}{2} B_0 \varepsilon_{mm} \varepsilon_{nn} + G_0 \left(\varepsilon_{ij} \varepsilon_{ij} - \frac{1}{3} \varepsilon_{mm} \varepsilon_{nn} \right)$$

...(VI.6)

where the all strains are assumed to be elastic.

It is noted that the expression of Eq. (VI.6) is valid for small strains only, as the potential energy increases in an unbounded fashion with strain. This is in contradiction to the assumption that the energy is zero when the atoms are an infinite distance apart.

Further, changing the datum of energy does not change the increment of energy, which is the physically meaningful quantity. Thus, the potential energy may be written in the form

$$U = -\frac{U_0}{\eta} + \frac{1}{2} B_0 \varepsilon_{mm} \varepsilon_{nn} + G_0 \left(\varepsilon_{ij} \varepsilon_{ij} - \frac{1}{3} \varepsilon_{mm} \varepsilon_{nn} \right)$$

...(VI.7)

for expedience, as the small strain equation, used routinely in mechanics does not correspond to the datum of zero energy being at the state where atoms are infinitely apart. Here, η is a constant which is determined empirically.

VI.2 Debye Specific Heat

The Debye expression

$$C_v = \frac{36R}{x^3}\int_0^x \frac{y^3}{e^y - 1}dy - \frac{9xR}{e^x - 1}$$

...(VI.8)

where R is the universal gas constant and $x = T_D/T$, with T_D being the Debye temperature of the material, here assumed constant for a given material for simplicity, provides

$$\frac{dC_v}{dx} = \left(\frac{-3}{x}\right)\frac{36R}{x^3}\int_0^T \frac{y^3}{e^y - 1}dy + \frac{36R}{x^3}\frac{x^3}{e^x - 1} - 9R\frac{e^x - 1 - xe^x}{(e^x - 1)^2}$$

...(VI.9)

$$\Rightarrow \quad \frac{dC_v}{dx} = \left(\frac{-3}{x}\right)\left[\frac{36R}{x^3}\int_0^T \frac{y^3}{e^y - 1}dy - \frac{9Rx}{e^x - 1}\right] + \frac{9R}{e^x - 1} - 9R\frac{e^x - 1 - xe^x}{(e^x - 1)^2}$$

...(VI.10)

$$\Rightarrow \quad \frac{dC_v}{dx} = \left(\frac{-3}{x}\right)C_v + \frac{9Rxe^x}{(e^x - 1)^2}$$

...(VI.11)

$$\Rightarrow \quad \frac{dC_v}{dT} = \left(\frac{3}{T}\right)C_v - \left(\frac{T_D^2}{T^3}\right)\frac{9R(e^{(T_D/T)})}{(e^{(T_D/T)} - 1)^2}$$

...(VI.12)

This expression can be integrated numerically. The Adams-Moulton predictor-corrector scheme (Kreyszig, 1983) was used, with the Adams-Bashford method as the initial predictor. The starting values may be obtained based on the low-temperature approximation (Reed and Clark, 1984)

$$C_v(T)=\frac{12}{5}R\pi^4\left(\frac{T}{T_D}\right)^3$$

...(VI.13)

VI.3 Loading Sequence

For the sequence of loading where the material is first loaded with the deviatoric components of the strain, followed by the volumetric components, the configuration energy at the end of the loading is given by Eq. (VI.7). All strains are assumed elastic.

An alternative loading sequence may be considered wherein the volumetric component of the stress is applied first, followed by the deviatoric components. For the volumetric loading, the bulk modulus does not change, and the energy subsequent to the loading is

$$U=-\frac{U_0}{\eta}+\frac{1}{2}B_0\varepsilon_{mm}\varepsilon_{nn}$$

...(VI.14)

Since the fraction of the liquid is

$$F_L = \frac{1}{2}\frac{B_0\varepsilon_{mm}\varepsilon_{nn}}{U^L - G_0\left(\varepsilon_{ij}\varepsilon_{ij} - \frac{1}{3}\varepsilon_{mm}\varepsilon_{nn}\right)}$$

...(VI.15)

the deviatoric stress for the loading is then given in terms of the deviatoric components of the strain by

$$s_{ij} = G_0\left[1 - \frac{1}{2}\frac{B_0\varepsilon_{mm}\varepsilon_{nn}}{U^L - G_0\left(\varepsilon_{ij}\varepsilon_{ij} - \frac{1}{3}\varepsilon_{mm}\varepsilon_{nn}\right)}\right]e_{ij}$$

...(VI.16)

The change in potential energy due to the loading is then

$$\int_0^{e_{ij}} s_{ij}\,de_{ij} = G_0 e_{ij}e_{ij} - G_0\int_0^{e_{ij}}\left[\frac{1}{2}\frac{B_0\varepsilon_{mm}\varepsilon_{nn}}{U^L - G_0\left(\varepsilon_{ij}\varepsilon_{ij} - \frac{1}{3}\varepsilon_{mm}\varepsilon_{nn}\right)}\right]e_{ij}\,de_{ij}$$

...(VI.17)

The second term results in the difference of work done between the paths. However, if the strains are small enough that the volumetric and deviatoric strain energies are small compared to the latent heat of fusion, it may be assumed that

$$\frac{1}{2}B_0\varepsilon_{mm}\varepsilon_{mm} \sim G_0 e_{ij}e_{ij} \sim hU^L$$

...(VI.18)

where

$$h \ll 1$$

...(VI.19)

providing,

$$\frac{G_0}{2}\int_0^{e_{ij}}\left[\frac{B_0\varepsilon_{mm}\varepsilon_{nn}}{U^L - G_0\left(\varepsilon_{ij}\varepsilon_{ij} - \frac{1}{3}\varepsilon_{mm}\varepsilon_{nn}\right)}\right]e_{ij}de_{ij} \sim \frac{1}{2}\left[\frac{hU^L}{(1-h)U^L}\right]\frac{1}{2}\left(G_0 e_{ij}e_{ij}\right) \sim h\left(\frac{1}{2}G_0 e_{ij}e_{ij}\right)$$

...(VI.20)

indicating that the difference is of a higher order than the shear work done for the loading sequence wherein the deviatoric strains were applied first.

REFERENCES

1. Andersen, I., Guven, I., Madenci, E., Gustaffson, G., "The Necessity of Reexamining Previous Life Prediction Analyses of Solder Joints in Electronic Packages", *IEEE Trans Comp and Pckgng Tech*, vol 23 no 3, Sept 2000, pp 516 – 520.

2. Attarwala, A.I., Tien, J.K., Masada, G.Y., Dody G., "Confirmation of Creep and Fatigue Damage in Pb/Sn Solder Joints", *ASME Jour. Elect. Packaging*, vol 114, June 1992, pp. 109 – 111.

3. Basaran, C., *Finite Element Thermomechanical Analysis of Electronic Packaging Problems using Disturbed State Constitutive Models*, Ph.D. Dissertation, Dept. of Civil Eng. and Engineering Mechanics, University of Arizona, Tucson AZ 85721, 1994.

4. Barker, D., Vodzak, J., Dasgupta, A., Pecht M., "Combined Vibrational and Thermal Solder Joint Fatigue – A Generalized Strain versus Life Approach", *ASME Jour. Elect. Packaging*, vol 112, June 1990, pp. 129 – 134.

5. Bonda and Noyan, "Effect of Specimen Size in Predicting the Mechanical Properties of PbSn Solder Alloys", *IEEE Trans CPMT – Part A*, v 19 n 2., June 1996, pp. 208 – 212.

6. Cadek, J.A., *Creep in Metallic Materials*, Elsevier, Amsterdam, The Netherlands, 1988.

7. Caglioti, A., and Milone, A.F., eds., Mechanical and Thermal Behavior of Engineering Materials, Lecture LXXXII, Proceedings of the International School of Physics, Italian Physical Society, North Holland Publishing Company, NY, 1982.

8. Chan, Y.C., Tu, P.L., So, A.C.K., Lai, J.K.L., "Effect of Intermetallic Compounds on the Shear Fatigue of Cu/63Sn-37Pb Solder Joints", *IEEE Trans CPMT – Part B*, v 20 n 4., Nov 1997, pp. 463 – 469.

9. Chen, J.Y., *Optimization in the Disturbed State Concept Constitutive Modeling and Application in Finite Element Analysis*, Ph.D. Dissertation, Dept. of Civil Eng. and Engineering Mechanics, University of Arizona, Tucson AZ 85721, 1997.

10. Chia, J.H., *Constitutive Modeling of Thermomechanical Response of Materials in Semiconductor Devices with Emphasis on Interface Behavior*, Ph.D. Dissertation, Dept. of Civil Eng. and Engineering Mechanics, University of Arizona, Tucson AZ 85721, 1994.

11. Choi, S., Bieler, T.R., Lucas, J.P., Subramaniam, K.N., "Characterization of the Growth of Intermetallic Interfacial Layers of Sn-Ag and Sn-Pb Eutectic Solders and Their Composite Solders on Cu Substrate During Isothermal Long-Term Aging", *Journal of Electronic Materials*, vol 28 no 11, 1999, pp. 1209 – 1215.

12. Coffin, L.F., "Fatigue at High Temperature", *ASTM STP 520*, PA, 1973.

13. Conrad, H., Guo, Z., Fahmy, Y., and Yang, D., "Influence of Microstructure Size on the Plastic Deformation Kinetics, Fatigue Crack Growth Rate, and Low-Cycle Fatigue of Solder Joints", *Journal of Electronic Materials*, vol 28, No. 9, 1999, pp. 1062 – 1070.

14. Constable, J.H., and Lizzul, C., "An Investigation of Solder Joint Fatigue Using Electrical Resistance Spectroscopy", *IEEE Trans. CPMT – Part A*, v 18 n1, March 1995, pp 142 – 152.

15. Cook, R.D., Malkus, D.S., Plesha, M.E., *Concepts and Applications of Finite Element Analysis*, Wiley, 1989.

16. Cottrell, A.H., *Theoretical Structural Metallurgy*, 2nd ed. Edward Arnold (Publishers) Ltd., London, 1957.

17. Cutiongco, E.C., Vaynman, S., Fine, M.W., Jeonette, D.A., "Isothermal Fatigue of 63Sn-37Pb Solder", *ASME Jour. Elect. Packaging*, vol 112, June 1990, pp. 110 – 114.

18. Darveaux, R., Banerji, K., "Constitutive Relations for Tin-Based Solders", *IEEE Trans. CHMT*, v15 no. 6, Dec 1992, pp 1013 – 1024.

19. Dascher, D., "Measuring Parasitic Capacitance and Inductance using TDR", *Hewlett – Packard Journal*, April 1996.

20. Dasgupta, A., Oyan, C., Barker, D., Pecht, M., "Solder Creep-Fatigue Analysis by an Energy Partitioning Approach", *ASME Jour. Elect. Packaging*, vol 114, June 1992, pp. 152 – 159.

21. Desai, C.S., *Private communication suggesting investigation of dissipated-work based DSC*, 1998.

22. Desai, C.S., *Private communications suggesting use of image acquisition for solder testing*, 1998.

23. Desai, C. S., *Mechanics of Materials and Interfaces: The Disturbed State Concept*, CRC Press, Boca Raton, FL, 2001.

24. Desai, C.S., Whitenack, R., "Review of Models and the Disturbed State Concept for Thermomechanical Analysis in Electronic Packaging", *ASME Jour. Elect. Packaging*, vol 123, March 2001, pp. 19 – 33.

25. Desai, C.S., Wang Z., Dube, M., "New Thermomechanical Device and Testing Towards Modeling Behavior of Joining Materials, *Proc. IPAC'01 The Pacific Rim/ASME International Electronic Packaging Technical Conference and Exhibition*, July 8-13,2001, Kauai, Hawaii, USA.

26. Desai, C.S., *Private communication regarding development of approximate procedure for curved ultimate envelope*, 2002.

27. Dieter, G.E., *Mechanical Metallurgy*, McGraw Hill Inc., 1961.

28. Dishongh, T.J., *The Disturbed State Concept for Material and Interfaces with Applications in Electronic Packaging*, Ph.D. Dissertation, Dept. of Civil Eng. and Engineering Mechanics, University of Arizona, Tucson AZ 85721, 1997.

29. Dowling, N.E., *Mechanical Behavior of Materials*, Prentice Hall, Englewood Cliffs, New Jersey, 1993.

30. Dube, M., "Implications of Cannot Duplicate", *MFPT Conference*, Virginia Beach, VA, March 30 – April 13, 1998.

31. Dube, M., and Sahay, C., "Uniform Entry Flow at Low Reynolds Numbers", *ASME Intl. Mech. Eng. Conf and Exp*, Atlanta, GA, Nov 17-22, 1996.

32. Ericksen, J.L., *Introduction to the Thermodynamics of Solids*, Rev. Ed., Springer – Verlag NY Inc., NY, 1998.

33. Engelmaier, W., "Functional Cycles and Surface Mounting Attachment Reliability", ISHM Technical Monograph Series 6984 – 002, ISHM, Silver Spring, MD, Oct. 1984, pp. 87 – 114.

34. Feynman, R.P., Leighton, R.B., Sands, M.L., The Feynman Lectures on Physics, vII, Addison-Wesley, Redwood City CA, 1989

35. Frear, D.R., Sorensen, N.R., Martens, J.S., "Test Methodologies to Perform Valid Accelerated Thermomechanical Fatigue Tests of Solder Joints", *Fatigue of Electronic Materials*, ASTM STP 1153, S.A. Schroeder and M.R. Mitchell, Eds., ASTM, Philadelphia, PA, 1994, pp. 95 – 109.

36. Frost, N.E., Marsh, K.J., and Pook, L.P., *Metal Fatigue*, Dover Publications Inc., Mineola NY, 1999.

37. Gittus, J., *Creep, Viscoelasticity and Creep Fracture in Solids*, Applied Science Publishers Ltd., London, 1975.

38. Guo, Y., Woychik, C.G., "Thermal Strain Measurements of Solder Joints in Second Level Interconnections using Moiré Interferometry", *ASME Jour. Elect. Packaging*, vol 114, March 1992, pp. 88 – 92.

39. Guo, Z., Sprecher, A.F., Conrad, H., "Plastic Deformation Kinetics of Eutectic Pb-Sn Solder Joints in Monotonic Loading and Low Cycle Fatigue", *ASME Jour. Elect. Packaging*, vol 114, June 1992, pp. 112 – 117.

40. Gurson, A.L., "Continuum Theory of Ductile Rupture by Void Nucleation and Growth", *J. Eng. Mat. Tech.*, Paper No. 76-Mat-CC, 1977.

41. Hacke, P.L., Sprecher, A.F., Conrad, H., "Microstructure Coarsening During Thermo-Mechanical Fatigue of Pb-Sn Solder Joints", *Journal of Electronic Materials*, v 26, n 7, 1997, pp 774 – 782.

42. Hacke, P.L., Fahmy, Y., Conrad, H., "Phase Coarsening and Crack Growth Rate during Thermo-Mechanical Cycling of 63Sn37Pb Solder Joints", *Journal of Electronic Materials*, v 27, n 8, 1998, pp 941 – 947.

43. Hare, E.W., and Stang, R.G., "Stress Relaxation Behavior of Eutectic Tin-Lead Solder", *Journal of Electronic Materials*, v 24, n 10, 1995, pp 1473 – 1484.

44. Harper, C.A., ed., *Electronic Packaging and Interconnection Handbook*, 3rd ed., McGraw Hill, 2001.

45. Hill, R., *The Mathematical Theory of Plasticity*, The Oxford Engineering Science Series, Clarendon Press, Oxford, U.K., 1950, reprinted 1998.

46. Hirsch, P.B., ed., *The Physics of Metals 2. Defects*, Cambridge University Press, Cambridge UK, 1975.

47. Igoshev, V.I., and Kleiman, J.I., "Creep Phenomena in Lead – Free Solders", *Journal of Electronic Materials*, v 29, n 2, 2000, pp 244 – 250.

48. Jackson, K.A., *Private Communication*, 2002.

49. Ju, S.H., Kuskowski, S., Sandor, B.I., and Plesha, M.E. , "Creep-fatigue damage analysis of solder joints", *Fatigue of Electronic Materials*, S.A. Schroeder and M.R. Mitchell, Eds., ASTM Special Technical Publication, n 1153, 1994, p 1-21.

50. Ju, S. H., Sandor, B. I., and Plesha, M. E., "Life Prediction of Solder Joints by Damage and Fracture Mechanics," *ASME Jour. Elect. Packaging.*, vol 118, Dec 1996, pp. 193–200.

51. Kachanov, L.M., *Theory of Creep*, Kennedy A.J. (Translator), National Lending Library, Boston, MA 1958.

52. Kachanov, L.M., *Introduction to Continuum Damage Mechanics*, Martinus Nijhoft Publishers, Dordrecht, The Netherlands, 1986.

53. Kachanov, L.M., *Foundations of the Theory of Plasticity*, North-Holland Publishing Co., 1971.

54. Kelkar, N, Dasgupta, A., Pecht, M., Knowles, I., Hawley, M., Jennings, D., "Smart Electronic Systems for Condition Based Health Management", *Qual. and Rel. Intl*, v. 12, 1996, pp. 1- 6.

55. Kennedy, A.J., *Processes of Creep and Fatigue in Metals*, Edinburgh, Oliver and Boyd, 1962.

56. Knecht, S., and Fox, L., "Integrated matrix creep: Application to accelerated testing and lifetime prediction", in *Solder Joint Reliability: Theory in Application*, J. H. Lau, Ed. New York: Van Nostrand Reinhold, 1991, ch. 16.

57. Konetzki, R.A., Zhang, M.X., Sluzewski, D.A., Chang, Y.A., "Oxidation of (Pb, Sn) and (Pb, In) Alloys", *ASME Jour. Elect. Packaging*, vol 112, June 1990, pp. 175 – 178.

58. Kreyszig, E., *Advanced Engineering Mathematics*, John Wiley & Sons, NY, 1983.

59. Lau, J. H., and Pao, Y-H., *Solder Joint Reliability of BGA, CSP, Flip Chip, and Fine Pitch SMT Assemblies*, McGraw-Hill, 1997.

60. Lau, J.H., Ed., *Solder Joint Reliability: Theory and Applications*, van Nostrand Reinhold, NY, 1991.

61. Langhaar, H.L., *Energy Methods in Applied Mechanics*, John Wiley & Sons Inc., NY, 1961.

62. Lee, S-M., Stone, D.S., "Deformation and Fracture of Pb-Sn – Eutectic Under Tensile and Fatigue Loading", *ASME Jour. Elect. Packaging*, vol 114, June 1992, pp. 118 – 121.

63. Lee, W.W., Nguyen, L.T., Selvaduray, G.S., "Solder joint fatigue models: review and applicability to chip scale packages", *Microelectronics Reliability*, 40, 2000, pp. 231 – 244.

64. Li, H., *Private Communication*, 2002.

65. Marder, M.P., *Condensed Matter Physics,* John Wiley, NY, 2000.

66. Mase, G.E., *Theory and Problems of Continuum Mechanics*, Schaum's Outline Series, Mc. Graw Hill Inc., 1970.

67. Mei, Z., Morris, J.W., Shine, M.C., "Superplastic Creep of Eutectic Tin-Lead Solders", *ASME Jour. Elect. Packaging*, vol 113, June 1991, pp. 109 – 113.

68. Mei, Z., Morris, J.W., "Fatigue Lives on 60/40 Solder Joints Made with Different Cooling Rates", *ASME Jour. Elect. Packaging*, vol 114, June 1992, pp. 104 – 108.

69. Natishan, M., Dube, M., "Health Monitoring of Electronics Systems", *Proc. Predictive Technology Symp.*, Alexandria, VA, Nov 6-7, 1997.

70. Needleman, A., Tvergaard, V., "An Analysis of Ductile Rupture in Notched Bars", *J. Mech. Phys. Solids*, vol. 32, no. 6, Pergamon Press, 1984.

71. Novacki, W., *Thermoelasticity,* 2nd ed., Pergamon Press, Polish Scientific Publishers, Warszawa, 1986.

72. Oyan, C., Dasgupta, A., Pecht, M., Barker, D., "Role of Strain – Partitioning Analysis in Solder Life Prediction", The International Journal for Hybrid Microelectronics, vol 14 no 2, June 1991, pp 37 - 47.

73. Pan, T-Y., "Thermal Cycling Induced Plastic Deformation in Solder Joints – Part I: Accumulated Deformation in Surface Mount Joints", *ASME Jour. Elect. Packaging*, vol 113, March 1991, pp. 8 – 15.

74. Pang, J.H.L., Tan, K.H., Shi, X., Wang, Z., "Thermal Cycling Aging Effects on Microstructural and Mechanical Properties of a Single PBGA Solder Joint Specimen", *IEEE Trans. Compts. Packgng. Tech.*, v24 no. 1, March 2001, pp 10 – 16.

75. Pecht, M., Dube, M., Natishan, M., Williams, R., Banner, J., Knowles, I., "Evaluation of Built-in Test", *IEEE Trans Aero. and Electron. Sys.*, vol 37, n 1, Jan 2001, pp. 266 – 271.

76. Pecht, M., and Ramappan, V., "Are Components Still the Major Problem: A Review of Electronic System and Device Field Failure Returns", *IEEE Trans. CHMT*, v15 no. 6, Dec 1992, pp 1160 – 1164.

77. Perzyna, P., "Fundamental Problems in Viscoplasticity", *Advances in Applied Mechanics*, v 9, 1966, pp 243 – 377.

78. Planicka, F., Rehounek, L., Vack, V, Zlabeck, P., Double Leaf Spring Gauge for the Continuous Measurement of the Diameter Change", Experimental Stress Analysis 2001, Tabor, Czech Republic, June 4 – 8, 2001.

79. Qian, Z., Ren, W., Liu, S., "A Damage Coupling Framework of Unified Viscoplasticity for the Fatigue of Solder Alloys", *ASME Jour. Elect. Packaging*, vol 121, Sept 1999, pp. 162 – 168.

80. Rafanelli, A.J., "Ramberg-Osgood Parameters for 63-37 Sn-Pb Solder", *ASME Jour. Elect. Packaging*, vol 114, June 1992, pp. 234 – 238.

81. Reed, R.P and Clark, A.F., eds., *Materials at Low Temperatures*, American Society for Metals, Metals Park, Ohio 44073, 1983.

82. Rose, J.H., Smith., J.R., Guinea, F., and Ferrante, J., "Universal Features of the Equation of State of Metals", *Physical Review B*, The American Physical Society, March 1984, pp. 2963 – 2969.

83. Ross, R.G., "A Systems Approach to Solder Joint Fatigue in Spacecraft Electronic Packaging", *ASME Jour. Elect. Packaging*, vol 113, June 1991, pp. 121 – 128.

84. Shao, C., *Implementation of DSC Model for Dynamic Analysis of Soil-Structure Interaction Problems*, Ph.D. Dissertation, Dept. of Civil Eng. and Engineering Mechanics, University of Arizona, Tucson AZ 85721, 1998.

85. Shen, Y-L., Li, W., Fang, H.E., "Phase Structure and Cyclic Deformation in Eutectic Tin-Lead Alloy: A numerical analysis", ASME *Jour. Elect. Packaging*, vol 121, March, 2001, pp 74 - 78.

86. Shi, X.Q., Zhou. W., Pang, H.L.J., Wang, Z.P., "Effect of Temperature and Strain Rate on the Mechanical Properties of 63Sn/37Pb Solder Alloy", ASME *Jour. Elect. Packaging*, vol 121, Sept, 1999, pp 179 - 185.

87. So, A.C.K., Chan, Y.C., Lai, J.K.L., "Reliability Studies of Surface Mount Solder Joints – Effect of Cu-Sn Intermetallic Compounds", Proc. 45th Electron. Comp. Conf., 1995, pp 1073 – 1080.

88. Solomon, H.D., "Low Cycle Fatigue of 60/40 Solder – Plastic Strain Limited vs. Displacement Limited Testing", *Electronic Packaging: Materials and Processes*, ed. J.A. Sartell, ASM.

89. Solomon, H.D., "Strain-Life Behavior in 60/40 Solder", ASME *Jour. of Electr. Packaging*, vol 111, June, 1989, pp 75 - 82.

90. Stephens, J.J., Frear D.R., "Time-dependent deformation behavior of near-eutectic 60Sn-40Pb solder" *Metallurgical and Materials Transactions A*: Physical Metallurgy and Materials Science, v 30 Issue number: n 5, 1999, p 1301-1313.

91. Stone, D.S., "The Creep-Fatigue Interaction in Solders and Solder Joints", *ASME Jour. Elect. Packaging*, vol 112, June 1990, pp. 100 – 103.

92. Summers, T.S.E, Morris, J.W, "Isothermal Fatigue Behavior of Sn-Pb Solder Joints", ASME *Jour. Electr. Packaging*, vol 112, June, 1990, pp 94 - 99.

93. Swalin, R.A., *Thermodynamics of Solids*, 2nd ed., John Wiley & Sons, NY 1992.

94. Syed A., Panczak, T., Darveaux, R., Lee, S., Lee, C., Partridge, J., "Solder Joint Reliability of Chip Array BGA", *Pan Pacific Microelectronics Symposium*, Maui, 1998.

95. Tien, J.K., Hendrix, B.C., Attarwala, A.J., "Understanding the Cyclic Mechanical Behavior of Lead/Tin Solder", *ASME Jour. Elect. Packaging*, vol 113, June 1991, pp. 115 – 120.

96. Tribula, D., Grivas, D., Frear, D.R., Morris, J.W., "Observations on the Mechanisms of Fatigue in Eutectic Pb-Sn Solder Joints", *ASME Jour. Elect. Packaging*, vol 111, June 1989, pp. 83 – 89.

97. Tribula, D., Morris, J.W., "Creep in Shear of Experimental Solder Joints", *ASME Jour. Elect. Packaging*, vol 112, June 1990, pp. 88 – 93.

98. Vaynman, S., Ghosh, G., Fine, M.E., "Effects of Palladium and Solder Aging on Mechanical and Fatigue Properties of Tin-Lead Eutectic Solder", *Journal of Electronic Materials*, v 27, n 11, 1998, pp. 1223 – 1228.

99. Vianco, P.T., Burchett, S.N., Neilsen, M.K., Rejent, J.A., Frear, D.R., "Coarsening of the Sn-Pb Solder Microstructure in Constitutive Model-Based Predictions of Solder

Joint Thermal Mechanical Fatigue", *Journal of Electronic Materials*, v 28, n 11, 1999, pp. 1290 – 1298.

100. Wang, Z., Disturbed State Constitutive Modeling and Testing of Solders in Electronic Packaging, Ph.D. Dissertation, Dept. of Civil Eng. and Engineering Mechanics, University of Arizona, Tucson AZ 85721, 2001.

101. Wang, Z., Desai, C.S., and Kundu, T., *Disturbed State Constitutive Modeling and Testing of Joining Materials in Electronics Packaging*, Report to NSF, Dept. of Civil Eng. and Eng. Mechanics, University of Arizona, Tucson, AZ, April 2001.

102. Wilcox, J.R., Subrahmanyan, R., Li, C-Y., "Assembly Stiffness and Failure Criterion Considerations in Solder Joint Fatigue", *ASME Jour. Elect. Packaging*, vol 112, June 1990, pp. 115 – 122.

103. Wild, R.N., "Some Fatigue Properties of Solders and Solder Joints", *INTERNEPCON*, Brighton, England, Oct. 1975.

104. Williams, R., Banner, J., Knowles, I., Dube, M., Natishan, M., Pecht, M., "An Investigation of Cannot Duplicate Failures", *Qual. Reliab. Engng. Int.*, 14, 1998, pp. 331 – 347.

105. Wong B., Helling, D.E., "A Mechanistic Model for Solder Joint Failure Prediction under Thermal Cycling", *ASME Jour. Elect. Packaging*, vol 112, June 1990, pp. 104 – 109.

106. Yamada, S.E., "A Bonded Joint Analysis for Surface Mount Components", *ASME Jour. Elect. Packaging*, vol 114, March 1992, pp. 1 – 7.

107. Yang, W., Messler, R.W., Felton, L.E., "Microstructure Evolution of Eutectic Sn-Ag/ Solder Joints, *Journal of Electronic Materials*, Vol 23, No 8, 1994 pp 765 – 772.

108. Yang, W., Felton, L.E., Messler, R.W., "The Effect of Soldering Process Variables on the Microstructural and Mechanical Properties of Eutectic Sn – Ag/ Cu Joints, *Journal of Electronic Materials*, Vol 24, No 10, 1995 pp 1465 – 1472.

109. Yu. Q., Shiratori, M., "Fatigue – Strength Prediction of Microelectronics Solder Joints under Thermal Cyclic Loading", *IEEE Trans CPMT – A*, v20 no. 3, Sept. 1997, pp 266 – 273.

110. Zhang, X., Lee, S-W. R., Pao, Y-H., "A Damage Evolution Model for Thermal Fatigue Analysis of Solder Joints", *ASME Jour. Elect. Packaging*, vol 122, Sept 2000, pp. 200 – 206.

111. Zinovev, V.W., Handbook of Thermophysical Properties of Metals at High Temperatures, Nova Science Publishers Inc., NY, 1996.

112. Zubelewicz, A., Berriche, R., Keer, L.M., Fine, M.E., "Lifetime Prediction of Solder Materials", *ASME Jour. Elect. Packaging*, vol 111, Sept 1989, pp. 179 – 182.